PB82-249178

Mass Spectrometric Analysis of Involatile Samples

Utah Univ.
Salt Lake City

Prepared for

Environmental Research Lab.
Athens, GA

May 82

U.S. Department of Commerce
National Technical Information Service
NTIS.

BEGIN FIRST LINE OF TEXT HERE
CENTER OF PAGE
TOP OF IMAGE AREA

EPA 600/3-82-061
May 1982

PB82-249178

DROPPED HEAD BEGIN SECTIONS HERE

MASS SPECTROMETRIC ANALYSIS OF INVOLATILE SAMPLES

by

Jean H. Futrell, Austin L. Wahrhaftig and Lenore G. Randall
Department of Chemistry
University of Utah
Salt Lake City, Utah 84112

6-1/2"
9-1/4"

Grant No. R804335010

Project Officer

John M. McGuire
Analytical Chemistry Branch
Environmental Research Laboratory
Athens, Georgia 30613

ENVIRONMENTAL RESEARCH LABORATORY
OFFICE OF RESEARCH AND DEVELOPMENT
U.S. ENVIRONMENTAL PROTECTION AGENCY
ATHENS, GEORGIA 30613

BEGIN LAST LINE OF TEXT
3/8"
BOTTOM OF IMAGE AREA, OUTSIDE DIMENSION FOR TABLES AND ILLUSTRATIONS

REPRODUCED BY
NATIONAL TECHNICAL
INFORMATION SERVICE
U.S. DEPARTMENT OF COMMERCE
SPRINGFIELD, VA. 22161

EPA Form 2350-6 (4-80)

TYPING GUIDE SHEET

TECHNICAL REPORT DATA

(Please read Instructions on the reverse before completing)

1. REPORT NO. EPA-600/3-82-061	2. ORD Report	3. RECIPIENT'S ACCESSION NO. PB82 249178
4. TITLE AND SUBTITLE Mass Spectrometric Analysis of Involatile Samples		5. REPORT DATE May 1982
		6. PERFORMING ORGANIZATION CODE
7. AUTHOR(S) Jean H. Futrell, Austil L. Wahrhaftig, and Lenore G. Randall		8. PERFORMING ORGANIZATION REPORT NO.
9. PERFORMING ORGANIZATION NAME AND ADDRESS Department of Chemistry University of Utah Salt Lake City, Utah 84112		10. PROGRAM ELEMENT NO. ABNC1A
		11. CONTRACT/GRANT NO. R804335010
12. SPONSORING AGENCY NAME AND ADDRESS Environmental Research Laboratory--Athens GA Office of Research and Development U.S. Environmental Protection Agency Athens, Georgia 30613		13. TYPE OF REPORT AND PERIOD COVERED Final, 7/76-11/78
		14. SPONSORING AGENCY CODE EPA/600/01

15. SUPPLEMENTARY NOTES

16. ABSTRACT

Almost every phase of environmental protection depends on the ability to detect and analyze specific chemical pollutants. Gas chromatography/mass spectrometry (GC/MS) has been shown to be widely applicable for separation and analysis of volatile organics, whereas liquid chromatography has been found to be useful in separating, but not analyzing, non-volatile organics. This study investigated two approaches to developing an LC/MS system that would provide the same ease and reliability for non-volatile analysis that GC/MS does for volatile analysis. In one, the chromatographic system was a high pressure liquid chromatograph (HPLC) with ultrasonic nebulization and the other, a dense (supercritical) gas chromatograph. Neither an ultrasonic vaporization LC/MS nor a dense gas chromatograph/mass spectrometer system provided the required capabilities.

17. KEY WORDS AND DOCUMENT ANALYSIS

a. DESCRIPTORS	b. IDENTIFIERS/OPEN ENDED TERMS	c. COSATI Field/Group
Mass spectrometers 1402 Measuring instruments 1402 Chromatography 0704	Liquid chromatography/ mass spectrometry LC/MS DGC/MS HPLC/MS Dense gas chromatography/ mass spectrometry Supercritical GC/MS Ultrasonic nebulization	Water pollution & control 68D Analytical chemistry 99A Physical chemistry 99F

18. DISTRIBUTION STATEMENT RELEASE TO PUBLIC	19. SECURITY CLASS *(This Report)* UNCLASSIFIED	21. NO. OF PAGES 214
	20. SECURITY CLASS *(This page)* UNCLASSIFIED	22. PRICE

EPA Form 2220-1 (9-73)

NOTICE

Mention of trade names or commercial products does not consititute endorsement or recommendation for use.

FOREWORD

Nearly every phase of environmental protection depends on a capability to identify and measure chemical pollutants in the environment. The Analytical Chemistry Branch of the Athens Environmental Research Laboratory develops techniques for identifying and measuring chemical pollutants in water and soil.

Gas chromatography/mass spectrometry has been shown to be widely applicable for separation and analysis of volatile organics, whereas liquid chromatography has been found to be useful in separating, but not analyzing, non-volatile organics. This report describes a study of the feasibility of two of several possible methods of directly coupling a high performance liquid chromatograph to a mass spectrometer to improve analysis of non-volatiles.

David W. Duttweiler
Director
Environmental Research Laboratory
Athens, Georgia

EPA Form 2350-4 (4-80)
TYPING GUIDE SHEET

PREFACE

High-speed liquid chromatography has become established as a powerful new separation technique which is especially important for the analysis of polar, involatile and thermally unstable compounds which are not amenable to separation by gas chromatography. The most serious limitation to widespread application of this method, particularly in trace analysis, is the lack of a versatile, sensitive and compound-selective detector. The present status of liquid chromatography is quite analogous to gas chromatography before the development of GC/MS systems during the past decade. Since these involatile samples may comprise as much as 80 percent of all the chemical substances of interest in analytical problems, the development of a suitable detector, such as the mass spectrometer, is obviously an extremely important objective. The purpose of the study described in the following pages was to investigate the feasibility of several possible methods to couple directly a high performance liquid chromatograph, or equivalent, to a mass spectrometer and so permit the analysis of involatile samples with the same ease and speed now possible for volatile samples using GC/MS.

Two of the methods proposed involve the coupling of a conventional HPLC to a mass spectrometer. The first of these, using a laser to rapidly vaporize the liquid chromatograph effluent, was to be under the direction of Dr. Marvin L. Vestal. Dr. Vestal left the University of Utah to accept a position at the University of Houston at Houston, Texas, very shortly before the initiation of the subject grant and pursued that investigation at the University of Houston with NIH support. That research is not covered in this Report. An alternative method for a HPLC/MS instrument involved the use of ultrasonic atomization with conventional heating. The work on this phase of the research, under the direction of Professor Jean H. Futrell, is described in Section 4 of this Report.

The third portion of the research, under the direction of Professor Austin L. Wahrhaftig, involved the study of coupling a dense gas chromatograph--a chromatograph in which the moving phase is a gas at temperatures and pressures such that its density approaches that of a liquid--to a mass spectrometer. While there have been relatively few studies of separations by dense gas chromatography, the literature does indicate that the method is applicable to involatile and thermally labile compounds with some unique features that might well aid the separation of substances difficult to separate by HPLC. However, studies of mixtures by DGC have been hindered greatly by the lack of any highly sensitive, general purpose detector. The studies on DGC/MS in this proposal are described in Section 3 of this Report.

ABSTRACT

Two approaches, both using molecular beam forming interfaces between a chromatograph and a mass spectrometer, have been investigated for involatile and/or thermally labile compound analysis. In one, the chromatographic system was a high pressure liquid chromatograph (HPLC) and in the other, a dense (supercritical) gas chromatograph (DGC).

To date the LC/MS approach has not succeeded in stripping of polar solvents from truly involatile solutes in a single step with useful efficiency. However, the method of ultrasonic nebulization has been shown to be useful in promoting rapid volatization and it was demonstrated that the molecular beam method efficiently transfers micro-droplets into a high vacuum chamber. Effective means for coupling ultrasonic energy to a liquid were developed. A promising design for an LC/MS interface, consisting of an ultrasonic horn and a nozzle-skimmer-pump assembly connected to a discharge ion source spectrometer, is described and alternative LC/MS approaches are discussed.

The aim of the DGC/MS research was to design, construct, and test a DGC/MS combination as an alternative to HPLC/MS. DGC has the usual advantages of GC, rapid separations and sharp peaks; it is similar to HPLC in that the dense gas will dissolve involatile compounds but has increased separating ability from pressure programming. Because the "solvent" in DGC is already a gas, the major problem of an LC interface--providing the required enthalpy of vaporization to all solvent molecules--is effectively by-passed.

In this Report, prior work on dense gases as solvents and DGC and some notes on molecular beams are presented. The basic design of the DGC and interface is discussed, and results are presented for C_2H_4, C_2H_6, CO_2 and N_2O as solvent gases at temperatures between 10 and 60°C and at pressures between 60 and 270 atm with 12.5 and 5 μm nozzle orifices. Data has been obtained on solubilities of anthracene and triphenylbenzene in dense CO_2 and on capacity ratios on a Permaphase ODS packed column for anthracene and pyrene in dense CO_2 and for anthracene, fluoranthene, and pyrene in dense N_2O. A chromatographic separation of the latter three solutes on a Permaphase ODS column was attained. Caffeine has been dissolved, eluted, and detected. Some questionable evidence has been obtained for the transport of the involatile compounds, inosine and ℓ-histidine.

It is concluded that the feasibility of a DGC/MS system has been demonstrated but further development is required. Recommended additional studies are described.

This Report was submitted in fulfillment of Grant No. R-804335010 by the University of Utah under the sponsorship of the U.S. Environmental Protection Agency. This Report covers a period from 21 July 1976 to 20 November 1978, and work was completed as of 27 November 1978.

CONTENTS

Foreword iii
Preface iv
Abstract v
Figures ix
Tables xiii
Acknowledgement xiv

1. Introduction 1
2. Conclusions and Recommendations 4
3. The Direct Coupling of a Dense Gas Chromatograph to a Mass Spectrometer by a Supersonic Molecular Beam Interface (Austin L. Wahrhaftig and Lenore G. Randall) 7
   - 3.1 Dense Gases as Solvents 7
   - 3.2 Prior Dense Gas Chromatography Studies 8
   - 3.3 Formation and Properties of Molecular Beams: Application to the DGC/MS Interface Problem 13
   - 3.4 Design and Development of the DGC/MS Apparatus 25
     - 3.4.1 Prior Work 25
     - 3.4.2 General Outline of the Development 28
     - 3.4.3 Molecular Beam System 29
     - 3.4.4 Mass Spectrometer 47
     - 3.4.5 Dense Gas Supply 53
     - 3.4.6 Dense Gas Chromatograph 55
   - 3.5 Experimental Procedures and Results 69
     - 3.5.1 Formation and Detection of the Supersonic Beam 70
     - 3.5.2 Improvements 71
     - 3.5.3 Initial Solute and Cluster Experiments 80
     - 3.5.4 DGC Construction with Temperature Control 84
     - 3.5.5 Chromatographic Survey 89
     - 3.5.6 Brief Summary of Experimental Observations, Results and Conclusions 111
     - 3.5.7 Suggested Future Improvements and Experimentation 116

4. The Direct Coupling of a High Pressure Liquid Chromatograph to a Mass Spectrometer by a Supersonic Molecular Beam Interface Utilizing Ultrasonic Atomization (Jean H. Futrell) 119
    4.1 Prior HPLC/MS Interfaces 119
    4.2 Molecular Beam LC/MS Studies 121
        4.2.1 Apparatus 121
        4.2.2 Ultrasonic Vaporization Studies 132
        4.2.3 Laser Vaporization 141
        4.2.4 Surface Desorption 142
        4.2.5 Discharge Ion Source Studies 142

References 154
Appendices
A. Abbreviated Compilation of Previous Dense Gas Chromatography and Dense Gas Extraction Work 164

B. Electric Circuits Designed for DGC/MS Instrument 178

C. Centering, Mounting, and Testing of the Nozzle Pinhole 185

FIGURES

Number | Page

1. Reduced density as a function of reduced pressure for three gases at reduced temperatures close to 1 10
2. Sample chromatograms from prior DGC work 14-17
3. Free jet structure 19
4. Skimmer placement within the expanding jet 21
5. First trial design for a molecular beam/mass spectrometer interface 26
6. Cross section of the present molecular beam system and the mass spectrometer 30
7. Skimmer design 34
8. Collimator designs 35
9. Exploded view of the nozzle assembly 38
10. Cross section of a laser-drilled pinhole, according to the supplier 39
11. Nozzle assembly as seen from skimmer 40
12. Nozzle assembly water manifold cross section 42
13. Nozzle assembly 43
14. Nozzle tip and assembly heaters 45
15. Thermocouples and heaters of the molecular beam system 46
16. Cross sections of ionization chamber designs 49
17. Ion source and electric sector electrodes 51
18. Block diagram of system for full-time monitoring/ part-time recording of mass spectra 52

Figures (continued)

Number Page

19. Dense gas supply 54

20. Circulation of water from the DGC thermostatted bath 57

21. Top view of the DGC suspended panel. 59

22. Initial sample introduction system 60

23. General design of the DGC/MS 62

24. Comparison of useful filter areas. 63

25. Operation of the HPLC sampling valve 64

26. Sample loop configurations studied in this work 66

27. Assembly for sample loop pressurization 67

28. Typical placement of DGC components within the water bath 68

29. Region pressure vs. nozzle-skimmer separation for four regions of the molecular beam-mass spectrometer system 72

30. Molecular beam intensity vs. nozzle-skimmer separation for N_2 and CO_2 with the original ion source configuration. 73

31. Molecular beam intensity vs. nozzle-skimmer separation for two potential settings of the modified ion source . . . 76

32. Calculated equipotentials and ion trajectories of ions for the original ion source configuration. 78

33. Calculated equipotentials and ion trajectories of ions for the two electrode configuration 79

34. CO_2 cluster intensities as a function of nozzle-skimmer separation 82

35. Effect of adjusting ion source potentials to maximize a cluster ion intensity 85

36. Solvent gas cluster intensities as a function of expansion chamber pressures for four stagnation pressures of ethane 87

Figures (continued)

Number Page

37. Pressure drop across a packed chromatograph column 100

38. k' as a function of temperature or pressure for anthracene and pyrene for the dense CO_2/Permaphase ODS system 102

39. k' as a function of temperature or pressure for anthracene, fluoranthene, and pyrene for the dense N_2O/Permaphase ODS system. 103

40. Separation of anthracene, fluoranthene, and pyrene 105,106

41. Elution of caffeine by dense N_2O with a Permaphase column 110

42. Elution of caffeine by dense N_2O with a capillary column 112

43. Functional illustration of liquid chromatograph/mass spectrometer interface 122

44. Schematic of the LC/MS 123

45. Scale sectional drawing of the LC/MS interface of Figures 1 and 2. 124,125

46. Approximately-to-scale drawing of the critical liquid jet, supersonic expansion and crossed-beam ionizer section of the LC/MS interface 126

47. Intensity of CO_2^+ as a function of nozzle-skimmer distance 128,129

48. Schematic illustrations for three configurations of the ultrasonic nebulizer tested. 134,135

49. Comparison of electron impact spectrum of naphthalene obtained with the LC/MS interface with a library reference spectrum 137,138

50. Comparison of molecular ion (m/e 128) trace with the UV detector trace for naphthalene injected into the liquid chromatograph 140

51. Characteristic curve of a self-limited glow discharge. 144

52. Diagram of the glow discharge ion source evaluated in this research. 145

Figures (continued)

Number Page

53. Circuitry utilized to evaluate performance characteristics of the glow discharge ion source 146

54. Characteristic curves of established glow discharges for a series of pressures, obtained for a 4.0 mm electrode spacing for positive ions 149

55. Characteristic curves for established glow discharges for a series of pressures obtained for 4.0 mm electrode spacing for negative ions 150

56. Ion energy distribution for positive ions for a series of source pressures 151

57. Ion energy distribution for negative ions for a series of source pressures 152

B1. Baratron output circuit 179

B2. Current detector circuit 180

B3. Typical circuit used to amplify and display thermocouple voltage as temperature 181

B4. Oscilloscope drive amplifier 182

B5. Heater and fan control circuits for dense gas reservoir housing 183

B6. Water bath heater control 184

C1. Punch/centering jig for mounting nozzle orifices 186

C2. Parts requiring special finish-machining prior to use 187

C3. Volumetric flow rate vs. pinhole diameter squared for flow through nozzle orifices 192

C4. Volumetric flow rate vs. gauge pressure for N_2 flow through a typical 12.5 μm nozzle diameter 196

C5. Volumetric flow rate vs. gauge pressure for N_2 flow through DGC system excluding the nozzle sub-assembly 197

TABLES

Number Page

1. Vacuum System for Present DGC/MS 33

2. Summary of Studies by DGC/MS Listing Solutes and Dense Solvent Gases 90

3. The Relative Abundance of the Ten Most Intense Fragment Ions of Selected Compounds 94

4. Sensitivity Estimates for Ultrasonic Vaporization by LC/MS Interface Using Hexane Solvent 139

A1. Some Previous Work in Dense Gas Chromatography and Dense Gas Extraction 165

C1. Experimental and Calculated Flow Rates for Several Nozzle Diameters 194

ACKNOWLEDGEMENTS

We wish to acknowledge the invaluable help of Mr. William Wilcox and Mr. Jack Pitts in the construction of the DGC/MS instrument; of Mr. A.K. Praggrastis and Mr. Edwin Grimm in the electronics design and implementation; and of Ms. Cindy Welsh, Ms. Pamela Donaldson and Ms. Sharon Chase in the writing of this Report.

SECTION 1

INTRODUCTION

The great ability of liquid and gas chromatographies to separate complex mixtures into their constituents is well known and has been used extensively in recent years. Gas chromatography (GC) has been especially useful when combined with a mass spectrometer because the mass spectra of the separated compounds are determined directly upon elution from the column. With mixtures of known compounds and carefully prepared columns, substances separated by GC or HPLC (high performance liquid chromatography) can be identified by retention times; GC/MS permits positive identification of unknown compounds by comparison of the mass spectra with a library collection and also provides qualitative identification for constituents for which authentic spectra are unavailable.

Gas chromatography is limited, however, to substances which have at least some slight volatility (a few torr) without decomposition. Hence, many compounds can only be separated by HPLC. Unfortunately, such substances are also not easily studied by mass spectrometry. The techniques used--derivatization, flash evaporation, pyrolysis, etc.--all have manipulative disadvantages which have relegated these techniques to batch rather than continuous processes. However, the incentives for achieving a continuous LC/MS interface for handling involatile substances are so great that a substantial research effort to achieve this goal is easily justified. This report describes two approaches for such an interface: 1) a dense gas chromatograph/mass spectrometer (DGC/MS) interface utilizing a supersonic molecular beam system and 2) a high pressure liquid chromatograph/mass spectrometer interface (HPLC/MS) utilizing ultrasonic atomization and a supersonic molecular beam.

Since the HPLC/MS and DGC/MS experimental approaches to the problem of obtaining mass spectra of involatile compounds required completely different procedures for dealing with the respective samples, the two studies proceeded essentially independently. Consequently it is convenient to describe the work separately: DGC/MS in Section 3 and HPLC/MS in Section 4. Construction blueprints of the instruments developed at the University of Utah have been filed with the Athens Environmental Research Laboratory (AERL).

DGC/MS. The use of a dense (supercritical) gas as the mobile phase is an alternative to and, in some respects, a combination of GC and HPLC. The solvent power of a dense gas, a substance at temperatures somewhat above critical and at pressures yielding liquid-like densities, has been known for many years. Selected applications of dense gases as solvents are given in Section 3.1. Since 1962, dense gas chromatography (DGC) studies have been undertaken by several research groups. While these studies must all be considered preliminary relative to the extensive developments in GC and HPLC, they do indicate that DGC combines the GC advantages of low viscosity and high diffusivity with the LC advantage of a large range of solvent properties with a (unique) DGC advantage of a density dependent solvent power. An overview of DGC is presented in Section 3.2. A compilation of prior DGC studies including some related dense gas extraction studies is given in Appendix A. The discussions in Sections 3.1 and 3.2 and Table A1 illustrate the many areas in which DGC is and may be useful--thereby indicating the broad analytical potential of a DGC/MS instrument.

Studies were first initiated at the Chemistry Department, University of Utah in 1970 on the direct coupling of a DGC to a mass spectrometer. As noted above, the DGC/MS coupling is accomplished by using a supersonic molecular beam system in which the dense solvent gas/solute mixture at a high pressure, generally 60 to 300 atm, expands through a nozzle and travels without collision as a supersonic beam directly into the mass spectrometer ionization chamber. The basic theory as it specifically applies to this problem is given in Section 3.3. Many studies and applications of (supersonic) molecular beams may be found in the literature. However, none of these approach the extremely wide pressure range, low flow rate, and low final pressure required in this application.

The design of our present apparatus, constructed at minimal cost by adding an interface to an available mass spectrometer, is presented in Section 3.4. The experimental procedures and results are described in Section 3.5. Brief reference to the solvent gases and solutes studied along with our conclusions and recommendations is made in the next section, Section 2.

The development of DGC/MS provides the power and speed of mass spectrometry as an on-line analytical method combined with the separation power of HPLC for materials not amenable to GC/MS study. In addition, while the evidence is not conclusive, it appears that dense gases may be used to solvate substances not normally soluble even in the customary liquid solvents. The work to date on pressure programming and on the use of gas mixtures as the solvent indicates that DGC/MS may have advantages over LC/MS in specific cases. The use of DGC/MS to sample high pressure reaction vessels, often used in industrial processes including those proposed for liquefaction or gasification of coal and shale oil, is another important application of the technique. Progress in the health related areas, in energy development, and in pollution control will be aided by the development of DGC/MS.

HPLC/MS. There are formidable problems associated with the molecular flux required by HPLC and with the vacuum requirements of the mass spectrometer that are difficult to satisfy simultaneously--much more so than in GC/MS. A brief survey of the prior work in HPLC/MS interfaces is given in Section 4.1. Since most of these approaches have been variations of previously successful GC/MS interface techniques, it appeared that a markedly different approach should be investigated.

Accordingly, we proposed the exploration of molecular beam techniques as the basis of an LC/MS interface. The fundamental rationale is that molecular beam techniques are now relatively well established for the study of unstable species (free radicals or excited states) in the gas phase. One might consider an involatile molecule to be an analogously unstable species since it is intolerant to collisions with solid surfaces. In any HPLC/MS interface a liquid solution must be expanded into vacuum. One expects that liquid droplets will be formed rather than isolated solute and solvent molecules. Hence, energy--sufficient for vaporization and insufficient for decomposition--must be supplied to the expanding solution so that solute molecules can be vaporized from solutions intact without fragmentation. Provided precise control of energy input to the solution is achieved and provided the sampled beam portion of the solute molecules do not collide with any surface, such an approach will relax the volatility constraints of present systems. Two techniques have been investigated, both relying upon closely related molecular-beam-forming pumping systems. Vestal and coworkers have investigated laser vaporization at the University of Houston. Their results are reviewed briefly in Section 4.2.3. A second, related approach utilizing ultrasonic excitation to create microscopic droplets of the effluent and conventional thermal heating of the jet is described in Section 4.2.2. A discharge chemical ionization ion source was investigated as a means for final-state heating of the gas and ionizing the constituents of interest. This is described in Section 4.2.5.

SECTION 2

CONCLUSIONS AND RECOMMENDATIONS

2.1 DGC/MS

The first DGC/MS results demonstrate that this instrument is feasible and indicate that it should have its expected unique advantages. No insurmountable problems have been encountered and further development is strongly indicated.

Several solutes have been dissolved and transported to the mass spectrometer ion source: naphthalene, azobenzene, 1,3,5-triphenylbenzene, phenanthrene, anthracene, fluoranthene, pyrene, and caffeine. Anthraquinone has been detected in small amounts. There is some questionable evidence that inosine and ℓ-histidine were detected. The solvent dense gases studied were ethylene, ethane, carbon dioxide and nitrous oxide. Chromatographic capacity ratios as a function of temperature and pressure for two systems have been studied. Some simple separations have been achieved, along with obvious but incomplete separation of pairs of very similar compounds. The experimental work, results, and discussion are presented in Section 3.5 with a summarizing discussion of the results in Part 3.5.6 of that section.

The heart of the instrument is the nozzle, a small laser drilled pinhole. The small size of the orifice and the mounting design, which allows relatively easy replacement, not only make the interface between pressure extremes possible but also feasible for a somewhat general laboratory usage. The orifice size must be selected to limit the flow to within the gas-handling capacity of the pumps at the highest pressure to be used, yet give an adequate flow rate for effective chromatographic compound separation at as low a pressure as possible. This imposes conditions on the column and the entire system not found in DGC, HPLC, GC, and GC/MS instruments and limited the use of the present instrument with any one pinhole to a relatively narrow pressure range. The problem of nozzle plugging was far harder to eliminate than expected. Plugging by foreign material seems to have been solved by the present system of filters. Plugging by sample has been greatly reduced by the present temperature control system and should be eliminated by a more complete system.

Further DGC/MS studies are recommended, with emphasis on the following ten experimental or instrumental developments. The present apparatus, with minor modifications, is suitable for initial studies of the first seven points. Full exploitation of DGC/MS will require the incorporation of the major instrumental improvements, 8, 9, and 10, in a completely new instrument that also would include the changes noted in points 1 through 7.

1. Precise temperature control. Careful temperature control of the dense gas/solute mixture is of the utmost importance. Independent control of four regions is indicated: sample loop, chromatograph column, nozzle assembly, supply tubing and the nozzle tip.

2. Sampling. The sampling procedure influences chromatograph peak width strongly. A high pressure sampling system with minimum dead volume which permits equilibration of the sample with the dense gas without disturbing flow through the column must be devised. It must accept solid samples as well as solutions, since many substances of interest are not soluble in a convenient volatile solvent.

3. Column packings. The prior DGC work summarized in Table A1 in Appendix A indicates coated stationary supports will be of little use in this research. It seemed that the ideal column packings would be those commonly used in HPLC. From our limited experience with Permaphase ODS® by Du Pont, it now appears that such packings may not be suitable. More experimentation is needed to arrive at definite conclusions. The type of packing decomposition that appears to have occurred may be common but just never detected in other applications. This particular application is more demanding than most.

4. Higher solvent gas pressure. The present system can be used at the much higher pressures required to dissolve more involatile samples, but there was no time for such experimentation.

5. Solvent gas density or pressure programming. Such programming must be added to the instrument since other studies have shown that it is a powerful advantage of DGC.

6. Solvent gas mixtures. The dense gas supply should be constructed so that solvent mixtures can be conveniently and reproducibly made.

7. Data handling. The analysis of several m/e intensities in a chromatographic separation produces enormous amounts of raw data that is laborious to reduce by hand and expensive to record with the present oscillographic recorder.

8. Improved expansion chamber pumping. The nozzle orifice limits the flow rate. In order to avoid frequent orifice changes during pressure studies and in order to use larger orifice diameters to give good chromatographic resolution at low pressures and yet operate at pressures high enough to volatilize involatile samples while using density programming, a pumping speed several times higher than that presently used (2400 ℓ/sec) is required.

9. Increased temperature range. The nozzle assembly must be thermally isolated and the remainder of the chromatographic system modified to permit operation at temperatures as high as 250°C in order to use solvent gases and gas mixtures other workers have found effective. The present system is limited to a maximum temperature of approximately 60°C.

10. Improved mass spectrometer. The Perkin-Elmer Model 270 is unsuitable for this application. Part of the problem is inherent and part of it

stems from the prior abuse it received. A mass spectrometer with higher ionization efficiency, faster scanning, easily selected scan ranges, selected peak monitoring capability, more stable electronics, a higher resolution and a higher sensitivity is needed.

The primary aim of this part of the supported research project, the determination of the advantages and limitations of DGC/MS in the analysis of involatile compounds, should be continued by studying the conditions for migration and separation of such compounds. This would permit further evaluation of the technique along with the instrumental development.

2.2 HPLC/MS

The instrumental problems encountered in the HPLC/MS phase of the project were extensive and a satisfactory working model was not achieved. In the ultrasonic vaporization studies the physical coupling of the LC capillary end (through which the mixture expands) to the ultrasonic horn was exceedingly difficult. Several approaches and configurations have been attempted. A "best" design was finally attained which gives proper attention to coupling of the LC at a node of the oscillator and which avoids shear stress in the horn itself by utilizing a single metal (aluminum) of moderate tensile and compressive strength. However, further testing with a similar model constructed from Titanium (for corrosion resistance and inertness) will be required.

Besides the final derived design, the experiments also showed that coaxial alignment of the ultrasonic horn and the capillary is essential and that the placement of the capillary orifice (within the molecular beam forming system) and the tilt of the horn critically influence sensitivity of the apparatus to LC effluent. While EI mass spectra of various solutes and LC solvents were obtained with the ultrasonic vaporization configuration, no chemical ionization (CI) spectra were generated with the crossed molecular and electron beams. Hence, a discharge ion source for CI studies was designed for the LC/MS instrument. Ion currents that were orders of magnitude greater than those available in conventional CI sources were observed. Also, the discharge ion source can be suitably used with quadrupole and magnetic mass filters. Further experimentation to determine the dependence of positive and negative ion CI spectra on the discharge source pressure, temperature and electrode spacings should be conducted prior to the testing of this source as a CI/MS detector for HPLC.

A conceptual design for a second-generation LC/MS interface utilizing ultrasonic nebulization is advanced. With proper design and alignment of the horn, pumping section, and beam-forming apertures, this technique appears capable of coupling a molecular jet into the low pressure region. A heated, discharge CI source and stagnation chamber is suggested for stripping the final solvent molecules and ionizing the enriched LC effluent stream. Both positive and negative ion CI spectra should be investigated, utilizing compounds of particular relevance to the EPA's primary pollutant program.

SECTION 3

THE DIRECT COUPLING OF A DENSE GAS CHROMATOGRAPH TO A MASS SPECTROMETER BY A SUPERSONIC MOLECULAR BEAM INTERFACE

Austin L. Wahrhaftig and Lenore G. Randall

3.1. DENSE GASES AS SOLVENTS

It was realized over 100 years ago that the nature of the transition at the critical point implied that supercritical gases should have solvent properties analogous to those of a liquid.[1] Within the last ten years there has been intense interest in fluid mixtures at high pressures,[2-9] especially in the food, pharmaceutical, and coal industries. Natural gas at pressures above 68 atm and temperatures up to 200°C has been used to separate liquid hydrocarbon mixtures.[10] T.P. Zhuze et al. have used supercritical gases for the de-asphalting and deresination of petroleum, the extraction of lanolin from wool grease, and the extraction of ozocerite from its ores.[11-13] Desalination of water has been accomplished using liquid organic solvents at elevated temperatures (often just below critical) pressures.[11,14] Zosel has patented a process for the separation of mixtures of aluminum trialkyls having alkyl groups of different chain lengths using supercritical ethane or ethylene.[15] Several other processes patented by Zosel are important to the food industry: deoderization of plant oils (soybean, palm and peanut) with simultaneous removal of free fatty acids[16] using CO_2; oil extraction from soybean flakes, corn, and bones using propane, ethane, CO_2, or N_2O;[17] simultaneous hydrogenation and deoderization of fats and/or oils with a CO_2/H_2 gas mixture;[18] and decaffeination of coffee with supercritical CO_2[19] and supercritical humid CO_2.[20] O. Vitzthum et al. have also patented similar extractions: fats and oils from plant seeds with subcritical gases (CO_2, SF_6, $CCLF_3$ (?), CHF_2Cl, CF_3Cl, CF_2CH_2, C_3F_8, N_2O, C_2H_6, C_2H_4 and various mixtures of these gases);[21] hops extraction with supercritical CO_2;[22] cocoa butter and aroma components (with identification) from cocoa beans with CO_2;[23,24] spice (black pepper) extraction with CO_2;[25] oil (containing flavor components) and caffeine from coffee with CO_2;[26-28] and nicotine from tobacco using CO_2, N_2O, Ar, SF_6 or halogenated hydrocarbons.[29,30] They have also extracted black tea aroma constituents with supercritical CO_2 and then identified the volatile components of the extract using GC/MS.[31]

Several authors,[32-36] particularly Gangoli and Thodos,[37] have discussed the very real advantages of supercritical extraction of coal to liquid fractions, a hydrogen-rich, mineral-free solid, and a porous non-caking char residue which may be subsequently gasified.

Dense gas extraction could be used to good advantage in geological studies of rock composition. For example, Petersilie and Sörensen[38] describe first the separation and GC analysis of entrained hydrocarbon gases followed by the liquid solvent extraction and IR analysis of bituminous substances in their samples. Dense gas extraction with on-line analysis would considerably simplify the process. This type of extraction/analysis procedure would be particularly helpful in oil-shale sample characterization (typical procedure in reference 39). Geologists are not only interested in sample analysis but also in simulating formation-reaction conditions[40,41]--often at elevated pressures and temperatures.

These geological interests then are analogous to high pressure chemical reaction studies, many of which have industrial applications: polymerization, hydrogenation, cracking, and aldehyde, acid and alcohol production. However, Weale[42] has pointed out that utilization of high pressure reactions has been hampered by the lack of detailed studies of reaction kinetics and mechanisms and thermodynamic data at those high pressures. Reactions are studied in different ways: 1) removal of a sample after some definite reaction time, 2) continuous removal of a sample during a reaction (difficult at high pressures) and 3) continuous monitoring of parameters such as volume change, electrical conductivity, and spectrophotometric (useful only with well-characterized reactions, which are rarely found). In addition to being difficult, sample removal for monitoring in small-scale research studies may constitute removal of an appreciable amount of the reaction species and thereby disrupt the system under study.[43] Young has discussed experimental methods for studying phase behavior of mixtures at high temperatures and pressures and also mentioned sampling difficulties.[44]

In many of the briefly outlined extraction and kinetics applications of dense gases, a DGC/MS instrument as described in the following sections could be used to identify and to monitor continuously the various species in the dense gas phase at high pressures, eliminating the decompression followed by extra sample handling for analysis by GC, HPLC, IR, etc. Hence, such an instrument is potentially a powerful analytical tool in a large number of areas and its development is quite timely, particularly in the light of the recent, active work[45-67] in the area of dense gas extraction.

3.2. PRIOR DENSE GAS CHROMATOGRAPHY STUDIES

The remarkable ability of a modern gas chromatograph/mass spectrometer/computer system to separate complex mixtures, perform on-line mass analysis, and usually determine the composition by searching files, all in perhaps half an hour, has tremendously aided research in a wide variety of fields, including the areas of health, pollution, and synthetic fuel development. However, GC/MS can be used only with substances having some volatility without thermal decomposition. While derivatization of involatile or thermally labile compounds often permits their analysis by GC/MS, this technique is very difficult to apply to a mixture of compounds of unknown composition and structure.

Modern HPLC separates many mixtures inseparable by GC because the moving phase serves two purposes: solvation and zone movement. However, interfaces of liquid chromatographs with mass spectrometers (see reference 68 for a short review) must typically use high vaporization temperatures for both the solute and solvent,[69,70] eluent splitting techniques which decrease sensitivity,[71] high pressure chemical ionization techniques which may have a variable chemical ionization agent due to solvent gradient elution,[72-75] a silicone rubber membrane separator which enriches the eluent in solute but limits the type solvents used,[76] or high temperature hydrogenation of solutes which may result in complex mass spectra.[77]

These HPLC/MS interfaces are not yet commonly used because of the indicated problems. Usually the sample mixture is separated by HPLC, collected, dried, and then analyzed mass spectrometrically by introduction via the solids probe[78-83] thus requiring some slight volatility of the compounds. Alternatively the solute eluted by HPLC is derivatized and then identified by GC/MS[84]--a laborious, slow procedure which requires extra work on each separated compound and is particularly difficult with unknown compounds.

An alternate procedure to HPLC is dense gas chromatography (DGC) where the moving phase is a supercritical fluid. The possibility that a direct coupling of a mass spectrometer to a dense gas chromatograph would yield an instrument combining the advantages of GC/MS and HPLC was first discussed by Giddings, Myers and Wahrhaftig in 1970.[85] Since a dense gas solution becomes unstable upon pressure reduction, the only interface likely to succeed entailed the very rapid expansion of the solution into a vacuum to form a supersonic molecular beam which would carry solute directly, with minimal collision, into the mass spectrometer ion source. Elementary calculations indicated that while solute aggregation might be too fast for detection of isolated solute, several nonequilibrium effects, difficult even to estimate, might well make the rate of aggregation slow enough so that the coupling would be feasible. While the use of supersonic molecular beams has become very widespread in recent years, this application is unique in the conditions imposed on the beam system, as discussed in Section 3.3.

A dense gas (also referred[*] to as a supercritical fluid, high pressure gas, hyperpressure gas, ultra high pressure gas) is a gas at temperatures and pressures such that its density is comparable to normal liquid densities of the substance. As shown in Figure 1, for a gas at a temperature just above the critical temperature of the substance, liquid-like densities are rapidly approached with modest increases in pressure in the range of 0.7 to

---

[*] The various terms are used in different areas by different authors with some effort to define pressure regions, but there is no terminology that seems to have general acceptance. We prefer the term "dense gas" in order to emphasize the fact that the most important parameter in the work to be described is the density and not either the absolute pressure or temperature alone.

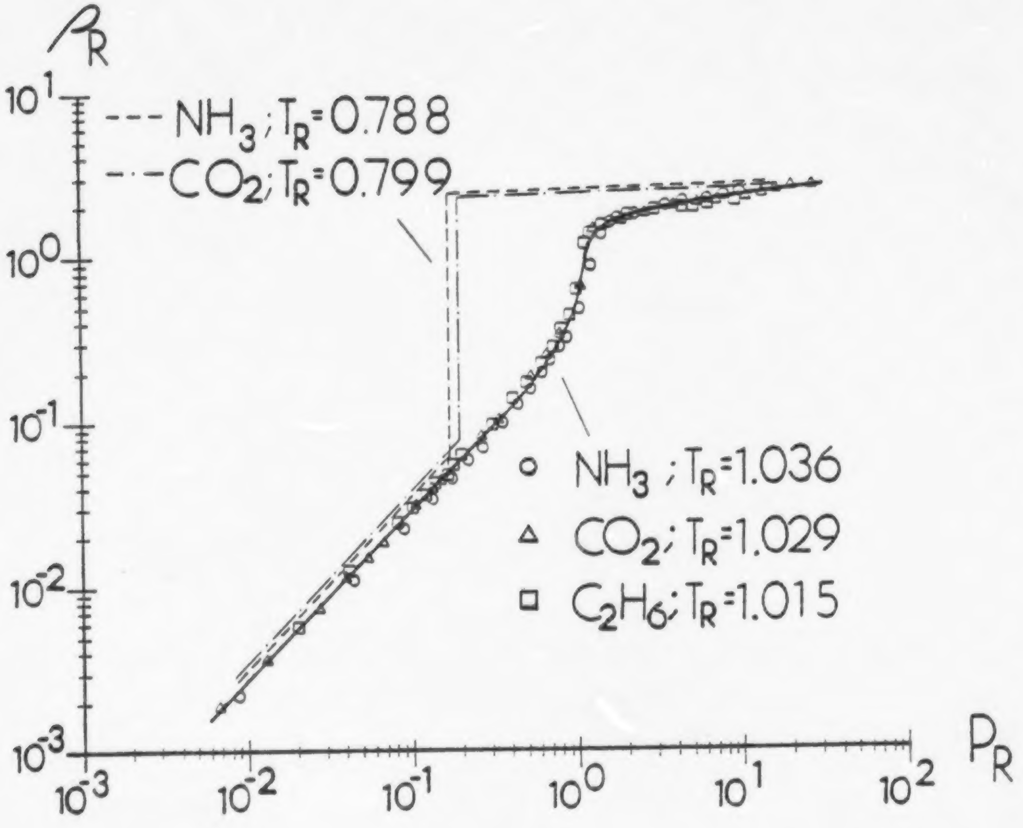

Figure 1. Reduced density (ρ_R) as a function of reduced pressure (P_R) for three gases at reduced temperatures (T_R) close to 1. Reduced data for ethylene, methane, nitrogen, acetylene, carbon monoxide, propane, and argon for $1.000 \leq T_R \leq 1.049$ also fall very close to the solid line curve. Reduced isotherms for carbon dioxide (T_R = 0.799) and ammonia (T_R = 0.788) show density as a function of pressure for subcritical gas and liquid phases. (Data for curves and for gases not specifically shown from references 86 and 87.)

2 times the critical pressure. Higher pressures are required to attain liquid-like densities for temperatures further above critical. The nearly liquid densities result in enhanced solubilities of solutes in the gas[1,2,88]--the basis of dense gas chromatography.

Four reviews of the work in DGC detail the theory, instrumentation, chromatographic materials and performance, analytical and physicochemical applications of DGC.[89-92] Much of the DGC work done to date, as well as some related dense gas extractions, is summarized in Table A1 in Appendix A. This compilation serves two purposes. First, it is an informative summary of compounds for which DGC is usable: biologically interesting molecules (e.g., amino acids, nucleosides, sterols, sugars, lipids), polynuclear aromatics (e.g., from automobile exhaust), food and pharmaceutical applications (e.g., gingerone, piperone, humulon, brucine, vitamins), polymers, and organometallic compounds. The broad analytical applications of DGC (and, hence, a DGC/MS instrument) are readily apparent. Second, it is an outline of experimental conditions for solubility of solutes in dense solvent gases and should be useful for planning laboratory work. A more extensive compilation is presented in reference 93. The rest of this section is devoted to a brief overview of DGC.

DGC combines characteristics of both gas and liquid chromatographies. A GC-type advantage is the speed of separation due to the low viscosity and high diffusivity of the gas. As in LC, DGC may be used to elute high molecular weight compounds, polymers, biological molecules, and thermally unstable molecules. Not only is the solvent power a function of the particular solvent gas used (i.e., its chemical effect from solute/solvent interaction) as in LC solvents, but also it is a function of the density of the gas (state effect). Additionally, Giddings *et al.*[94,95] and Klesper *et al.*[96] have shown that there is a threshold pressure of the dense gas above which it will solvate a particular solute. Thus, the solvent power may be quickly varied by density[94,95,97] (pressure)[82,98-103] programming as well as by the usual GC temperature programming.

For example, Bartmann[102] has published chromatograms of n-alkanes (n = 5 to 20) and cyclic hydrocarbons at 40 and 55°C for various column packings and CO_2 pressure programming in the range of 51 to 134 atm. He notes that the pressure-dependent solvent power of the mobile phase is the decisive factor in determining the migration rate and resolution. Nieman and Rogers[103] have found that there is an optimum temperature which depends upon the molecular weight range when linear pressure programming is applied to separating the oligomers of the silicone polymer, DC-710, with n-pentane as the mobile phase. Klesper and Hartmann[82] have studied the effect of pressure programming of various mixtures of n-pentane and methanol mobile phase upon the resolution of styrene oligomers for analytical and preparative scale DGC. Jentoft and Gouw[98] note that the pressure programming elution time (95% n-pentane/methanol) of coronene is one-third that of the isobaric conditions. Their studies show that polystyrene oligomer elution times are also up to three times as long with isobaric conditions as with pressure programming. Finally, work conducted here at the University of Utah by Bowman[97] indicates that linear density programming is superior to linear pressure programming because of the large change in density caused by a small change in pressure near the critical temperature (see Figure 1).

Sie and Rijnders[104,105] first noted the strong temperature dependence of the capacity ratio, a modified partition coefficient (stationary phase solute/gas phase solute), in the region close to and above the critical temperature of the gas. Here, because of the strong intermolecular forces of the dense solvent gas, more solute is dissolved resulting in a low value for this coefficient. As the temperature is increased, the density of the gas decreases with a simultaneous lessening of its solvent power so more solute is partitioned in the stationary phase and the partition coefficient increases. At even higher temperatures the partition coefficient may remain essentially constant or decrease again. Beyond this maximum (or leveling point) in the partition coefficient-temperature dependence the behavior is determined by the temperature-dependent volatility of the solute as in conventional GC. Nieman and Rogers[103] note the same temperature-dependent capacity ratio behavior in their experiments which include mixed solvents.

Since dense gases are such powerful solvents for large involatile molecules, the stationary phase in dense gas-liquid chromatography must be chosen with care.[89] However, this problem appears to have been alleviated by the new bonded phase packings developed for HPLC. The bonded phase packings and the pellicular or superficially porous glass beads seem to be well-suited for DGC: the small particle diameters (in narrow ranges) yield lower theoretical plate heights[106-108] as shown in GC and HPLC; however, the lower viscosity of a dense gas (compared to liquids) causes a lower pressure drop across the column than in HPLC.[106]

In the above discussion, no differentiation has been made between liquid and solid stationary phases. In dense gas-solid chromatography[105] the dense gas is adsorbed onto the solid adsorbent modifying it in situ, thereby eliminating the need for the usual deactivation treatments. The solute peaks are sharp and symmetrical with none of the typical GSC tailing. It has been proposed that the dense fluid coats the solid surface so that the mechanism is actually a fluid-liquid partition. In typical GSC the operating temperatures are 100-300°C above the boiling points of the solutes to be separated, far higher than is required for the same solutes in GLC where a temperature giving a vapor pressure on the order of 10 torr[109] may be used. Dense gas-solid and -liquid chromatographies effect separations at significantly lower temperatures since the minimum operating temperature is determined only by the critical temperature of the solvent dense gas. Advantages of dense gas-solid chromatography are the easier separations of close-boiling isomeric hydrocarbons than with dense gas-liquid chromatography and the faster separations than with liquid-solid chromatography.[105]

Selectivity in DGC is determined not just by the choice of the solvent gas (and its temperature and pressure) alone but by the combination of the solvent gas and the column packing.[89] In dense gas-solid chromatography, type selectivity is achieved with a polar support and a non-polar dense gas while light/heavy selectivity is achieved with a polar support and a polar gas.[105] In dense gas-liquid chromatography, type selectivity is similarly best obtained with a polar stationary phase and a non-polar dense gas, but better light/heavy selectivity is obtained with a non-polar stationary phase and a polar dense gas.[100,104] The parabolic solute solubility-solvent density relationship affects the selectivity. Lower densities may show typical GC boiling point selectivity with a non-polar dense gas and a polar stationary phase while increasing the density results in type selectivity.[89]

Figure 2a shows sample chromatograms for previous DGC work with specific conditions noted in the figure legend. Chromatogram A[105] is an example of dense-gas solid chromatography showing the fast (< 1 minute) separation of four aromatic compounds at a low temperature (213°C) with symmetrical peak shapes on untreated alumina. Chromatogram B[102] emphasizes the large effect of pressure programming and temperature upon separation. Separation of metallorganic compounds, unstable at elevated GC temperatures, is shown in Chromatogram C[110] while Chromatogram D[83] shows the large molecular weight compounds (polystyrene oligomer) which can be eluted with DGC. The usefulness of DGC is further demonstrated by Figure 2b: the separation of fat-soluble vitamins (A, E_1, and K_1) in Chromatogram E;[111] the separation of aspirin, phenacetin and caffeine in Chromatogram F;[111] and the extraction and separation of several aromatic hydrocarbons from coal tar in Chromatogram G.[105]

While these examples and those cited in Table A1, Appendix A clearly show the wide range of possible analytical applications of DGC, progress in this area has been hampered by the lack of a sensitive and selective detector even though some attempts have been made to overcome detection problems.[112,113] Ultraviolet detection limits the solute class, flame ionization detection limits the solvent gas, and thermal conductivity detection as well as the first two methods lacks specificity. This research was initiated in view of the demonstrated possibilities of DGC and the great extensions of DGC that would be possible if a DGC/MS system could be constructed with the mass spectrometer serving as a highly sensitive and selective detector as in modern GC/MS.

3.3. FORMATION AND PROPERTIES OF MOLECULAR BEAMS: APPLICATION TO THE DGC/MS INTERFACE PROBLEM

High solvent gas pressures can increase the volatility of a solute (i.e., the amount of solute in the gas phase) by a factor of 10^3 to over 10^{10},[52] presumably due to solvation of the solute molecules at the high pressure. With reduction in pressure, solvation will decrease and solute molecules will tend to aggregate. Thus, to obtain significant numbers of isolated solute molecules for ionization in a mass spectrometer, one must have the dense gas expand so that the solute molecules are transported as rapidly as possible with a minimal number of intermolecular collisions into the ionization region of the mass spectrometer. An obvious method of transportation and the only satisfactory method known to us is by means of a supersonic molecular beam.[85] Here a gas at some upstream or stagnation pressure, P_0, expands into a region at a lower pressure, P_1, ideally through a properly shaped converging-diverging nozzle. Under the assumption of isentropic, one-dimensional, steady flow, a pressure ratio P_0/P_1 greater than 1.9 will result in

Figure 2a. Sample chromatograms from previous DGC work.

A. Compounds - polynuclear aromatics
Dense solvent gas - n-pentane
Temperature - 213°C
Pressure - 50 kg/cm^2 (52 atm)
Column - alumina (120/140 mesh), 1 m long X 6 mm I.D.
Detector - UV
Sie and Rijnders (Reference 105. Reprinted from Separation Science 2 (1967), p. 768 by courtesy of Marcel Dekker, Inc.)

B. Compounds - n-alkanes (n = 5 to 22)
Dense solvent gas - CO_2
Temperature - upper chromatogram, 40°C; lower chromatogram, 55°C
Pressure - upper chromatogram: 55 atm initial, 101 atm final
1.00 ℓ/min program
lower chromatogram: 51 atm initial, 115 atm final
2.00 ℓ/min program
(Flow rate after expansion to atmospheric conditions is programmed to obtain pressure change.)
Column - Carbowax 400/Porasil C, 3 m long X 1.7 mm I.D.
Detector - modified flame ionization
Bartmann (Reference 102. Reprinted from Berichte der Bunsen-Gesellschaft für Physikalische Chemie 76 (1972), p. 337 by courtesy of Verlag Chemie GmbH.)

C. Compounds - metallorganics
Dense solvent gas - CO_2
Temperature - 33°C
Pressure - 1000 psi (68 atm) initial for 30 minutes
3000 psi (204 atm) final
130 psi/min program
Column - Carbowax 400 on Porasil F (100/120 mesh), 1 m long X 3 mm O.D.
Detector - high pressure UV detector cell
Jentoft and Gouw (Reference 110. Reprinted with permission from Analytical Chemistry 44 (1972), p. 685. Copyright by the American Chemical Society.)

D. Compounds - polystyrene oligomers
Dense solvent gas - 5% methanol in n-pentane
Temperature - 205°C
Pressure - 600 psi (41 atm) initial for 8 minutes
900 psi (61 atm) final
6 psi/min program
Column - Porasil C with bonded n-octyl groups (120/150 mesh), 4 m long X 3 mm O.D.
Detector - UV
Jentoft and Gouw (Reference 83. Reprinted from Journal of Polymer Science, Part B 7 (1969), p. 812 by permission of John Wiley and Sons, Inc.)

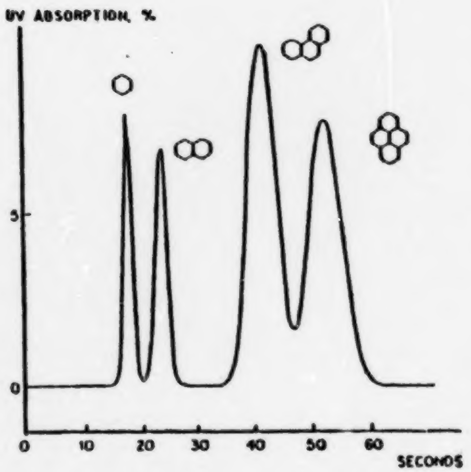
UV ABSORPTION, %
5
0
0
10
20
30
40
50
60
SECONDS

A

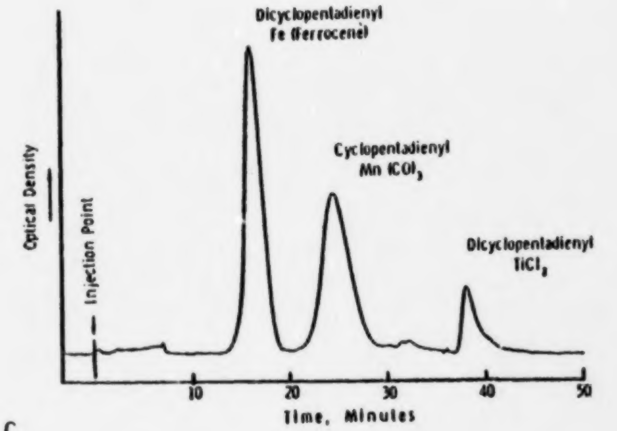
Optical Density
Injection Point
Dicyclopentadienyl
Fe (Ferrocene)
Cyclopentadienyl
Mn (CO)$_3$
Dicyclopentadienyl
TiCl$_2$
10
20
30
40
50
Time, Minutes

C

B

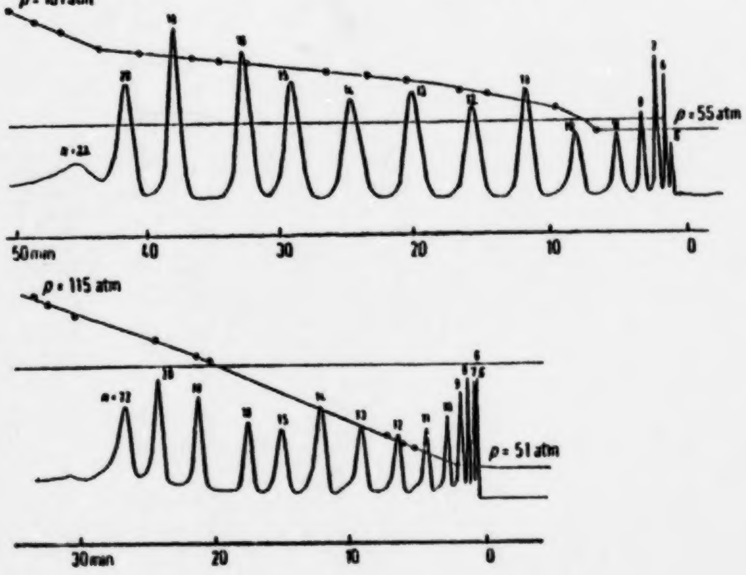
p = 101 atm
p = 55 atm
n = 22
20
19
18
15
14
13
12
11
10
9
8
7
6
5
50 min
40
30
20
10
0
p = 115 atm
p = 51 atm
n = 22
20
18
15
14
13
12
11
10
9
8
7
6
30 min
20
10
0

D

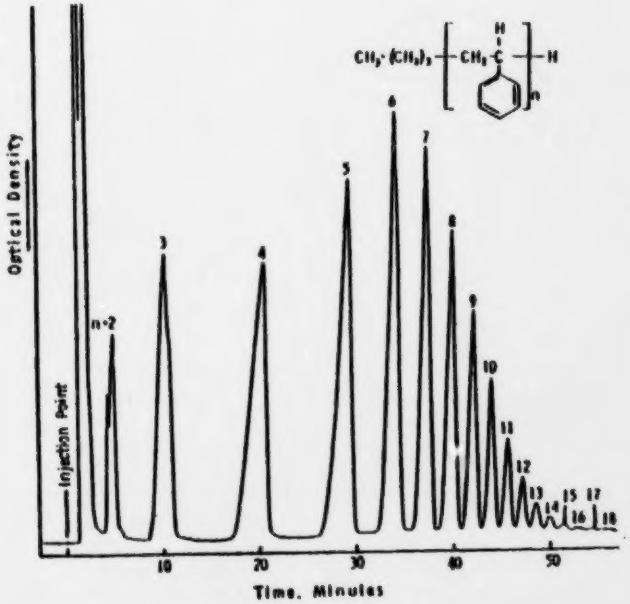
Optical Density
Injection Point
CH$_3$-(CH$_2$)$_3$-[CH$_2$-CH(C$_6$H$_5$)]$_n$-H
n = 2
3
4
5
6
7
8
9
10
11
12
13
14
15
16
17
18
10
20
30
40
50
Time, Minutes

Figure 2b. Sample chromatograms from previous DGC work.

E. Compounds - vitamins
Dense solvent gas - n-pentane
Temperature - 210°C
Pressure - 48 kg/cm^2 (50 atm)
Column - Porapak Q (100/120 mesh), 6 m long X 3 mm I.D.
Detector - UV
Sie and Rijnders (Reference 111. Reprinted with permission of authors.

F. Compounds - aspirin, phenacetin, caffeine
Dense solvent gas - diethyl ether
Temperature - 200°C
Pressure - 43 kg/cm^2 (44 atm)
Column - Porapak Q (100/120 mesh), 1 m long X 5 mm I.D.
Detector - UV
Sie and Rijnders (Reference 111. Reprinted with permission of authors.

G. Compounds - polynuclear aromatics from coal tar
Dense solvent gas - isopropanol
Temperature - 245°C
Pressure - 45 kg/cm^2 (46 atm)
Column - alumina (120/140 mesh), 1 m long X 6 mm I.D.
Detector - UV
Sie and Rijnders (Reference 105. Reprinted from Separation Science 2 (1967), p. 774 by courtesy of Marcel Dekker, Inc.

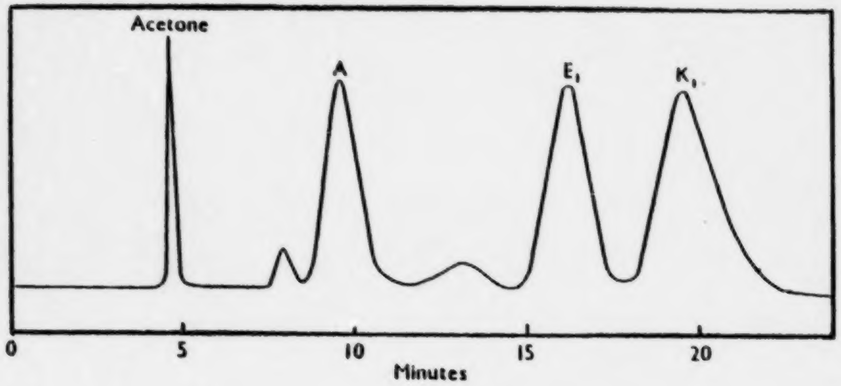
Acetone
A
E₁
K₁
0
5
10
15
20
Minutes

E

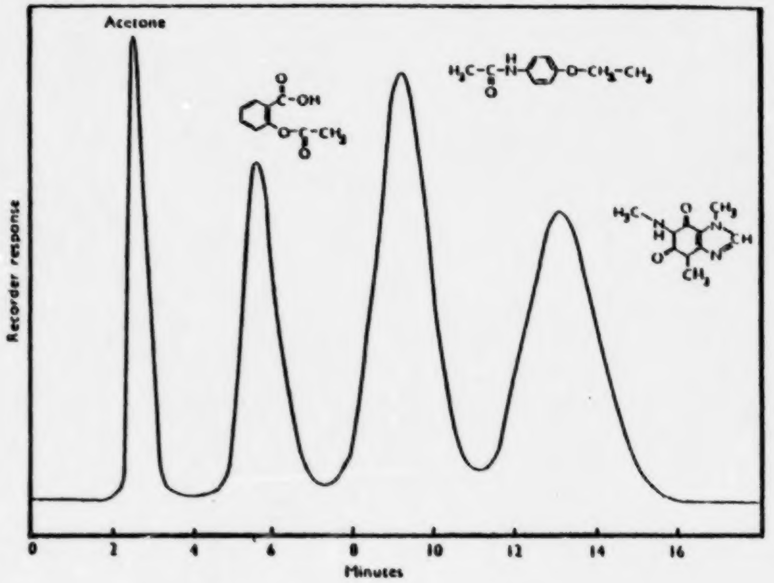
Acetone
Recorder response
0
2
4
6
8
10
12
14
16
Minutes

F

G

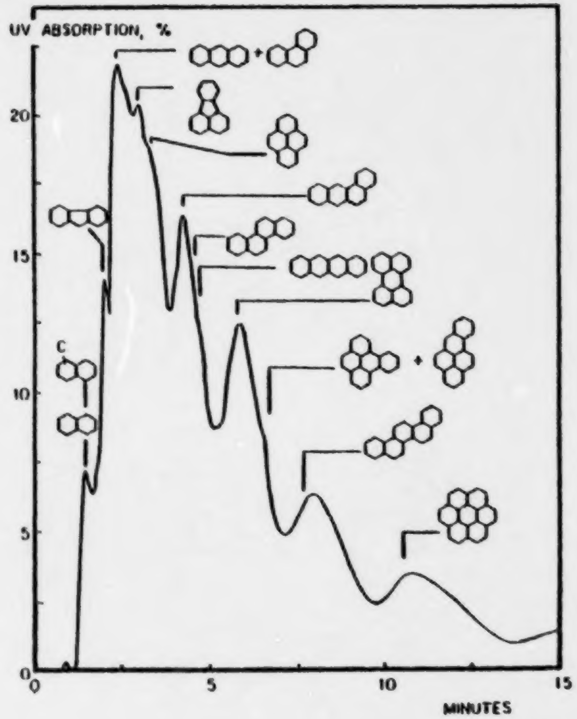
UV ABSORPTION, %
0
5
10
15
20
MINUTES
C

supersonic flow velocities. The central core of the free jet is then extracted by a skimmer to form a supersonic molecular beam.

Supersonic nozzle free jets and molecular beams are commonly used in a variety of experiments. They have become so familiar that the term "molecular beams" now refers to beams formed from nozzle sources as well as those from effusive oven sources. A computer search of "Chemical Abstracts" lists over 600 entries for molecular jets or beams from 1975 through June 1978. Over 180 of these entries are for 1977 and 1978. Spot-checking the references shows that half of them refer to supersonic molecular beams--they have become a commonplace laboratory tool.

In our literature searches we have yet to find any work which involves extracting a supersonic molecular beam from a free jet expansion at the large pressure ratios necessarily entailed by the coupling of a dense gas chromatograph to a mass spectrometer (if $P_0 = 270$ atm and $P_1 = 10^{-3}$ torr, $P_0/P_1 \approx 2 \times 10^8$). However, the prior experimental and theoretical work in molecular beams does indicate factors to be considered in designing the interface: the expansion structure and process, skimmer interaction with the free jet, the beam intensity as a function of nozzle-skimmer interaction, mixture component separation, appropriate background pressures, temperature distributions, and condensation kinetics.

Expansion structure and process. The shock wave system associated with a supersonic free jet system with no skimmer interaction is shown in Figure 3. The gas at pressure P_0 expands through the nozzle, diameter D_n, along streamlines, S, emanating from an apparent source, O. Interaction with the finite expansion chamber background pressure, P_1, produces the barrel shock wave, B, the reflected shock waves, R, and the normal shock wave, M--the Mach disk, after which the flow is subsonic. J is the jet boundary. The inner core of expanding gas is unaffected by pressure changes along the boundary. The expansion is isentropic at first, then passes through a transition region where there are fewer intermolecular collisions, and finally is molecular with no collisions,[114] provided the distance to the Mach disk is sufficient. A useful independent variable for describing the jet is the Mach number, the ratio of the velocity of the gas flow at a point in the jet to the velocity of sound in the gas at the temperature and pressure existing at that point. For isentropically expanding supersonic jets, the centerline Mach number depends only on the nozzle diameter and the distance from the nozzle exit plane and can be determined by the fitting formula of Ashkenas and Sherman[115] or by the source flow expansion model.[114] With this Mach number and the stagnation conditions, one may calculate the local temperature, pressure, density, and bulk mass velocity at any point along the centerline. As the gas expands and becomes more rarefied, nonequilibrium among the translational, rotational, and vibrational degrees of freedom results. The axial Mach number approaches a limiting (terminal) value determined by the stagnation conditions and the nozzle diameter (nozzle Knudsen number). There have been several theoretical treatments of transition flow.[115-118]

Flow after the Mach disk is subsonic and collision dominated following the destruction of the highly directed supersonic flow in this shock wave.

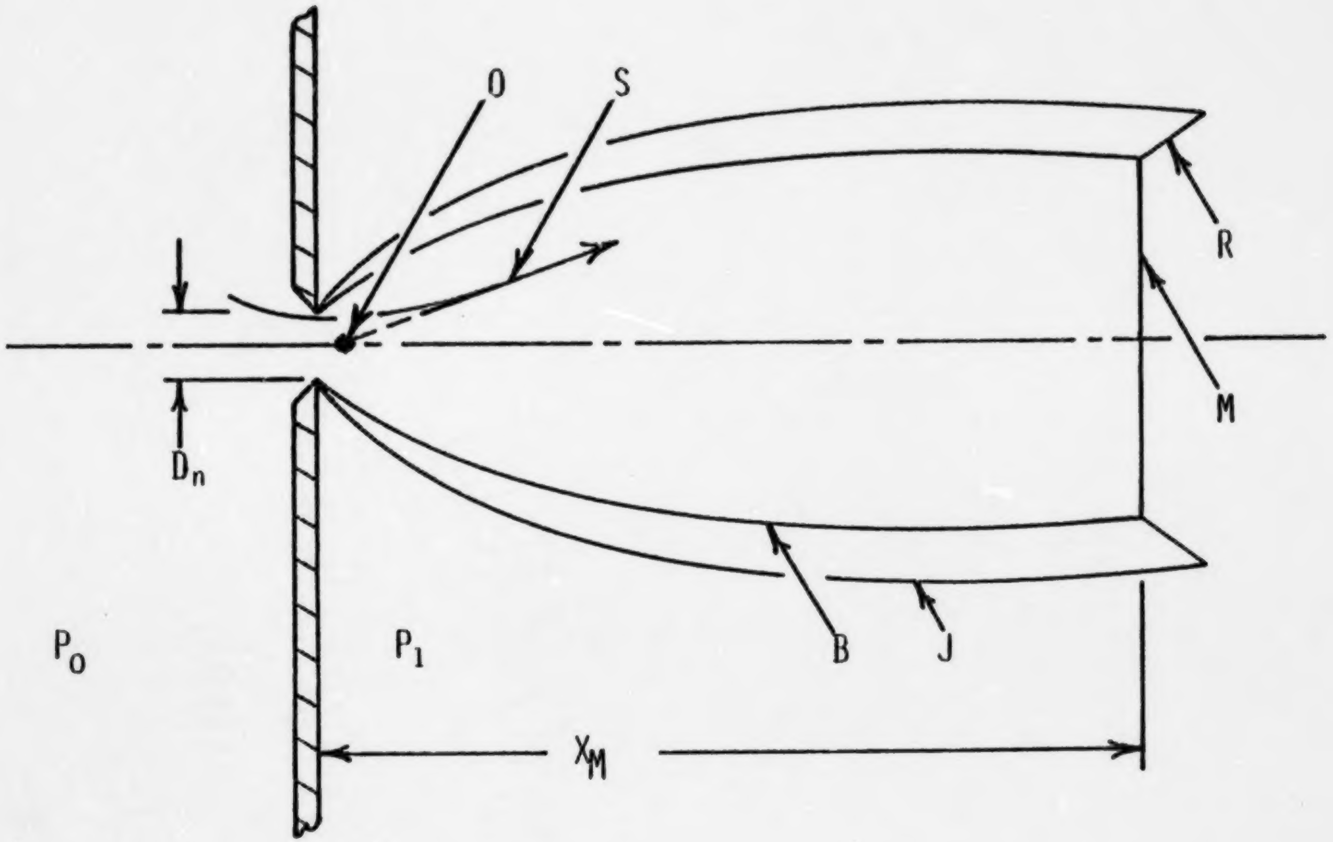
O
S
R
M
D_n
P_o
P_1
B
J
X_M

Figure 3. Free jet structure.

Hence, for proper extraction of the supersonic jet core, the skimmer must be placed in the jet upstream from the Mach disk. One then must estimate the distance from the nozzle exit plane to the Mach disk. This distance, X_M, has been found experimentally[115] to be

$$X_M = 0.67\, D_n\, (P_0/P_1)^{0.5}$$

for $15 \leq P_0/P_1 \leq 17{,}000$.

Skimmer interaction with the free jet. The next consideration is skimmer interaction with the free jet shock structure and with the inner core of supersonic molecules. It has been well established that there exists an intensity-attenuating interference of the skimmer with the flow.[119-122] The interference occurs for several reasons and requires careful design of the skimmer with respect to external and internal angles, length, and lip thickness. For an appropriately small external angle, an oblique shock wave will be attached to the skimmer edge (Figure 4). Too large an external angle causes detachment of the shock wave and changes its location to upstream of the skimmer opening. For denser flows that are isentropic to the skimmer, viscous effects, flow turbulence, and interaction with the internal skimmer surface may produce shock waves downstream of the skimmer opening. Hence, the internal angle should be as large as possible. Rebounding molecules from collisions at the base of the skimmer interfere with the flowstream molecules and so it has been found that longer skimmers lead to less intensity attenuation. A thick orifice edge produces a scattering viscous layer; consequently, the edge should be as sharp as possible.

Beam intensity as a function of nozzle-skimmer interaction. The beam intensity attenuating effect of the skimmer shows that the Mach disk distance is not the only factor to be considered for proper skimmer placement. At smaller nozzle-skimmer distances, the higher beam density and the resultant increase in density in front of the skimmer due to skimmer interference is controlling and gives an intensity *increasing* with increase in nozzle-skimmer separation. At larger separations, interaction with background density yields an intensity variation that is approximately a negative exponential function of the product of background pressure and nozzle-skimmer separation.[123-125] Hence, the intensity function is the product of the two terms with opposite trends resulting in a maximum in the relationship of beam intensity to nozzle-skimmer separation.

LeRoy[118,122] proposed a model for evaluating the skimmer interference term, combined it with the Beer's Law relation proposed by others for the background interference, and obtained the following expression for S_{max},

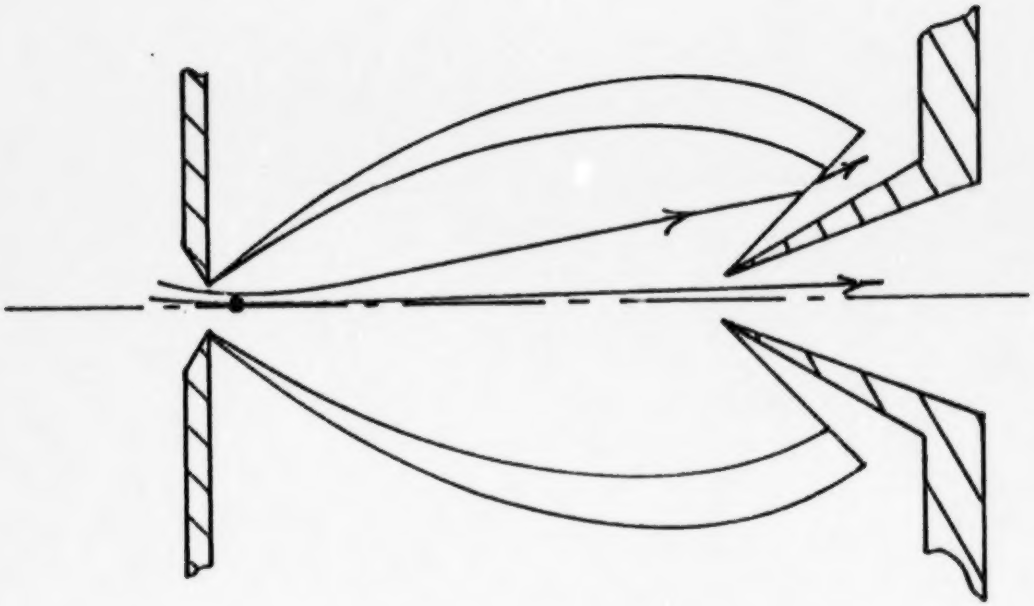

Figure 4. Skimmer placement within the expanding jet. Shock wave with transition to subsonic flow attached to skimmer surface.

the nozzle-skimmer separation for maximum intensity:

$$S_{max} \propto P_o^{0.37}/P_1^{0.17}T_o^{0.28}$$

where T_o is the stagnation temperature. This expression agrees quite well with his experimental data. Hagene and Pasquerault[123] proposed that

$$S_{max} \propto M_t/P_1^{0.5}$$

where M_t is the terminal Mach number which they calculated semi-empirically. While the calculated location of the intensity maximum agreed with experimental results, their expression for intensity agreed only qualitatively with experiment. These expressions are not necessarily contradictory since the experiments were run under different conditions: LeRoy used $P_o \approx 16$ to 180 torr and $P_1 \approx 2 \times 10^{-4}$ to 7×10^{-3} torr (therefore, P_o/P_1 was about 10^4) and Hagene and Pasquerault used $P_o \approx 12$ to 30 torr and $P_1 \approx 1 \times 10^{-2}$ to 8×10^{-2} torr (with P_o/P_1 about 10^3). Both expressions for S_{max} show that because it is a function of variable stagnation conditions, a variable nozzle-skimmer separation will be necessary in the DGC/MS molecular beam interface if it is to operate over a very wide stagnation pressure range.

Mixture component separation. Background pressure also has a major effect upon component separation in mixtures, where the components may come either from the initial beam or from the background gas. Campargue and Breton[126] specifically studied this effect with expansion chamber pressures between 10^{-2} and 1 torr after noting that higher pressure work had been done by Bier and Hagena (P_o = 40 atm, P_1 = 1 atm) and lower pressure work had been done by Fenn and Anderson and Brown and Heald ($P_1 = 10^{-4}$ to 10^{-2} torr). Earlier work by Campargue[127] had shown that the composition of a beam included both molecules from the expanding gas and background molecules so that the molecular flux through the skimmer was higher than expected. He stated that if either the background gas or the carrier gas were a light/heavy mixture with the expansion chamber pressure between 10^{-2} and 1 torr, light component enrichment caused by background invasion could occur. However, other experiments had indicated heavy component centerline enrichment. Campargue concluded that, in the absence of sampling probe interference, the observed separation is a superposition of two opposite effects: background invasion and pressure diffusion. With sufficiently low expansion chamber pressures or with increased stagnation pressure (even if the background pressure increases proportionately) background-molecule invasion is diminished[126,127] so that heavy species enrichment dominates. This centerline heavy-species enrichment, due to the pressure diffusion mechanism and discussed in several papers,[114,128,129] is highly desirable in our application to dense gas chromatography where heavy solute molecules are dissolved in lighter solvent gases.

Appropriate background pressure. While this aspect of expansion certainly suggests that an expansion chamber pressure of about 10^{-3} torr or less will be necessary for our application, it is instructive to set forth another argument. A 12.5 μm nozzle diameter has given satisfactory DGC flow rates with dense gas pressures up to 120 atm. Expansion into 1 atm pressure would place the Mach disk about 0.1 mm (≈0.004 inch) from the nozzle orifice. Construction and placement of a properly designed skimmer in that small distance appears to us to be impossible and, in addition, one is still left with the differential pumping problem of interfacing this high pressure expansion chamber with the low pressure mass spectrometer region. At $P_1 \approx 10^{-3}$ torr, the distance is increased by a factor of about 1000.

Temperature distributions. As previously described, flow from a converging nozzle or an orifice is along radial streamlines which appear to emanate from a point downstream of the exit. Pressure gradients along these streamlines result in a directed velocity with narrow, non-Maxwellian, anisotropic velocity distributions. Through collisions, rotational-translational and some vibrational-translational energy transfer takes place. The net result is a conversion of internal and random translational energy to directed translational energy. Several models have been proposed to calculate various parameters during the isentropic expansion, transition, and the molecular flow region in which there is a "freezing" of energy in the various degrees of freedom.[114,116,130] Consider an isentropic expansion of a monatomic gas starting with a stagnation temperature of 300°K. The temperature at that point where the Mach number is 10 will be about 9°K. Experimental translational, rotational, and vibrational temperatures of beam molecules have been measured. Klemperer has produced a beam of HCN in which the effective beam translational temperature is 4°K and has estimated an effective rotational temperature of about 10°K for the van der Waals complex ArHCl.[131] Smalley et al. expanded a dilute mixture of NO_2 in helium (100 atm) to form a supersonic jet in which the effective rotational temperature of NO_2 was ≈0.7°K and its effective vibrational temperature was 150°K.[132] The equilibrium form of NO_2 below 262°K is the solid, so at the low temperatures attained in an isentropic expansion and while the collision frequency remains relatively high, the molecules should form clusters of molecules and, at equilibrium, large solid particles.

Condensation kinetics. Clustering is often observed in molecular beams. Several studies have been directed toward the production both of nozzle beams without clusters and of cluster beams in which the cluster size ranges from dimers up to particles with millions of molecules in order to learn about the kinetics of cluster formation. A good review has been given by Hagena.[133] There have been many attempts to predict clustering behavior.[133-138] All agree that the extent of clustering depends upon the stagnation conditions (P_0,T_0) and the nozzle diameter and shape.

Current theories are inadequate to predict condensation conditions--hence, Hagena and Obert[136] developed a method of "corresponding jets" in which parameters are scaled. Farges et al.[138] used this method to compare their data for argon clusters with that of Hagena and Obert--even though the cluster size range, the detection method and the nozzle diameter were different. The actual average number of molecules in a cluster ($\bar{N}$) for the conditions of Farges et al. was fairly well predicted by the scaling rules of Hagena and Obert. Applying the same procedure to the data of Hagena and Obert for CO_2 assuming a sonic nozzle, we obtain the empirical equation (with P_0 in torr, T_0 in °K, and D in mm)

$$N = (6 \times 10^{11}) P_0^{1.44} D^{0.86} T_0^{-3.4}$$

With typical conditions for the DGC/MS of $P_0 = 120$ atm, $T_0 = 305$°K and $D = 12.5$ µm, the above relationship yields $\bar{N} \simeq 10^4$ molecules in an average cluster. A calculation using the density of solid CO_2 indicates that the size of a cubic particle with 10^4 molecules would be about 8 nm on an edge. If one uses the approximation suggested by Hagena[133] that the cluster velocity is equal to the limiting velocity in an isentropic expansion of the gas, the kinetic energy of such a cluster is 1 KeV. (Even if one neglects the internal degrees of freedom and the expansion work and assumes that all the translational energy is converted to directed kinetic energy, the cluster kinetic energy is still quite high at about 400 eV.) Hagena and Obert note that this correlation procedure is not valid for the comparison of different gases for which internal energy modes must be considered. The above expression for $\bar{N}$ does fit their data for CO_2 for constant nozzle diameter and shape and cluster size at different stagnation temperatures and pressures. However, Hagena and Obert do not consider extrapolations to the extreme conditions of the DGC/MS system.

Condensation is a function of the nozzle shape (sonic, laval, conical) as well as the diameter. Wegener[137] points out that condensation is delayed until the diverging part of a supersonic nozzle. He further states that when a simple hole replaces a regular nozzle, the expansion rate is so much faster that it has been impossible to determine the point of supersaturation, the onset of condensation and the nucleation rate. Hence, for the conditions of the DGC/MS (pressures higher than usual and temperatures not far above T_C--both favoring clusters, but very small nozzle diameters--opposing cluster formation) clustering behavior is not predictable, yet it is obvious that this behavior will crucially determine whether solute-solute and solute-solvent clusters will interfere with accurate solute analysis.

It is possible that solute-solvent clusters will be detected in the beam even if condensation is negligible. The existence of an apparent threshold pressure for large solute molecule will be encased in at least a monolayer of solvent molecules. The solute may remain highly solvated throughout the expansion, so that the mass spectrum will be that of the mixed species $[Su(Sv)_n]^+$ and its dissociation products, where fragmentation may result in loss of parts of solvent molecules, Sv, as well as parts of the solute molecules, Su. Calculation by Giddings et al.[85] indicated that there would be enough internal energy in a large solute molecule to "shake off" a solvent monolayer, but that the kinetics would have to be determined by experiment.

The molecular beam generating system designed with consideration of the above factors as well as all other components (dense gas supply, DGC, and mass spectrometer) of the DGC/MS instrument, is described in the next subsection of this Report.

3.4. DESIGN AND DEVELOPMENT OF THE DGC/MS APPARATUS

3.4.1. Prior Work

The feasibility of the DGC/MS instrument and some preliminary results were discussed in a paper by Giddings, Myers and Wahrhaftig[85] in 1970. Design work on a very simple instrument was started at that time, but was soon halted and not resumed until Autumn, 1973, when a Perkin-Elmer Model 270 mass spectrometer was made available for modification. The first trial design, which involved only minor changes to the mass spectrometer, was assembled in the Summer of 1974. By March, 1975, experiments had shown that a more elaborate design was necessary. Work was started on the new design, which was half-completed by the Summer of 1975 when the joint proposal to the EPA was submitted and favorably received. Part of the initial design was changed to allow a larger pump on the nozzle-skimmer chamber. The design of the molecular beam system and its interface to the mass spectrometer was completed by the Fall of 1975. Extensive alignment and tuning of the mass spectrometer was then undertaken while some parts for the interface were assembled and the machining job was given to the Chemistry Department Machine Shop. EPA support funds were not received until July 1976 at which time the major equipment items (high vacuum pumps, valves, pressure gauges, etc.) were ordered. Shipping errors and delays in machining postponed the first assembling of the molecular beam system until the last two weeks in November, 1976. Subsequent experimental work has led to the design and incorporation of many modifications to the instrument, particularly to improve sensitivity and temperature measurement and control, but there have been no changes to the basic molecular beam system.

Figure 5 is a scale diagram of the first trial design for a molecular beam/mass spectrometer interface, which was constructed and tested before EPA support was requested. This design, based upon the idea that a relatively high value of P_1 could be tolerated if P_0/P_1 (P_0, stagnation pressure; P_1, expansion chamber pressure) were large, utilized the solids inlet assembly already existing on the mass spectrometer. The molecular beam components were mounted and aligned within a cylindrical probe (P), the outer dimensions of which were the same as the original solids probe.

The nozzle-skimmer distance could be varied by 8.9 mm (0.35") with the closest approach of the nozzle orifice to the skimmer tip being 0.13 mm (0.005"). The skimmer (S) was stationary with the nozzle assembly (N) movable by a threaded nut. This design made no provision for estimating the nozzle-skimmer distance except by observing the turns of the controlling nut.

Details of the nozzle assembly are not shown. However, the nozzle orifice clamping design is the same as that presently used and will be detailed later. The major difference in the nozzle assemblies of the two designs is the outer aligning parts. This nozzle assembly uses three carefully machined, thin fins to align the assembly within the I.D. of the probe. The nozzle-skimmer region was evacuated by a 160 ℓ/min mechanical pump.

That part labeled M is the vertical cross section of the original electron beam collimating magnet. The placement of the filament (FL), the

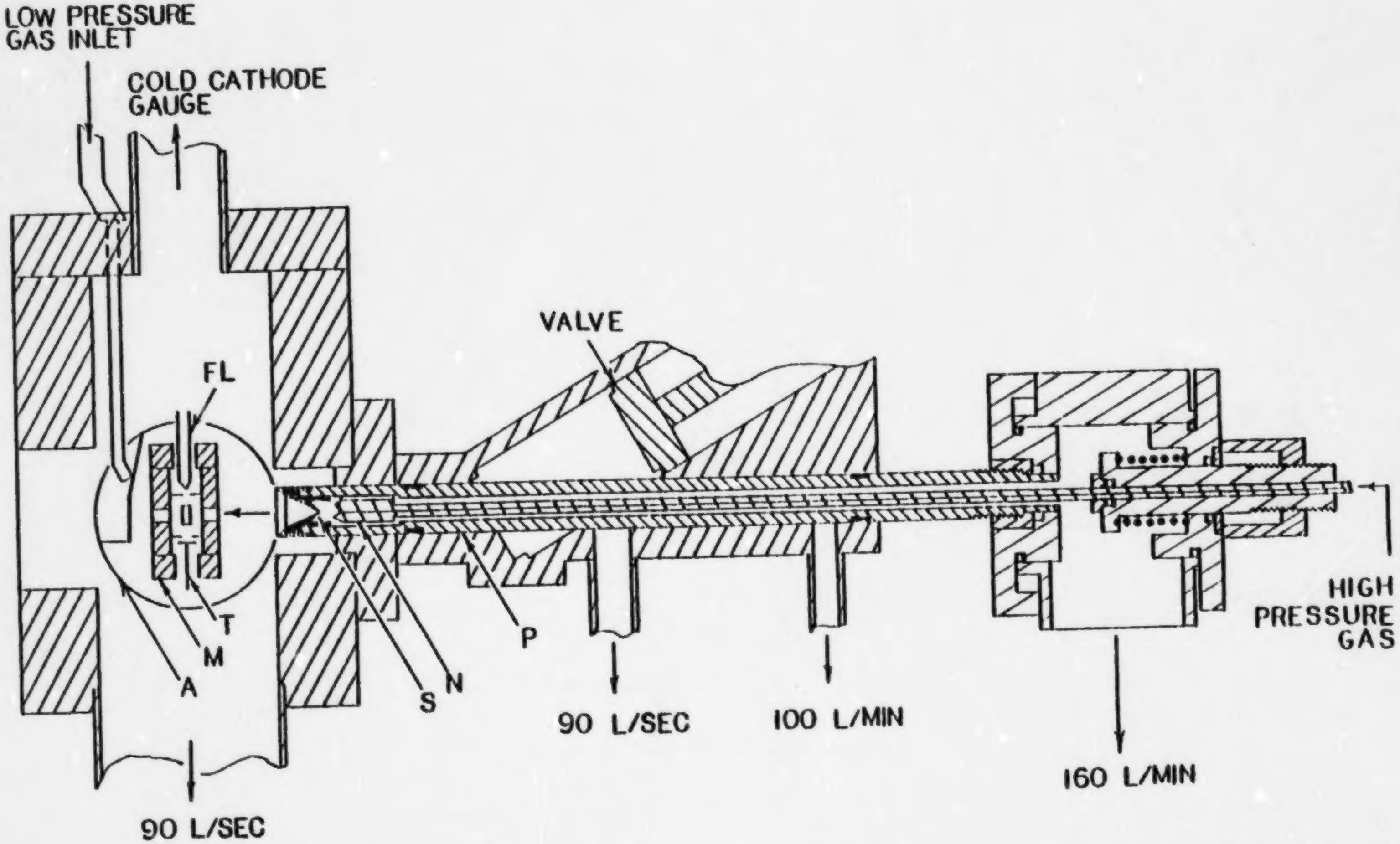
LOW PRESSURE GAS INLET
COLD CATHODE GAUGE
FL
VALVE
A
M
T
S
N
P
HIGH PRESSURE GAS
90 L/SEC
90 L/SEC
100 L/MIN
160 L/MIN

Figure 5. First trial design for a molecular beam/mass spectrometer interface. S-skimmer; N-nozzle assembly, centered in P by three thin fins; P-molecular beam probe replacing the customary solids inlet probe; FL-ion source filament; T-electron beam trap; M-ionization chamber including electron beam collimating magnets; and A-aligning circumference for ion source in the housing.

electron trap (T), the ionization chamber exit slit, and the filament and trap collimating orifices are accurately depicted. The ion source, particularly the magnet, was redesigned in later experiments with the present DGC/MS; however, the relative placement of all components remains the same.

The cold cathode gauge tube was moved from its original placement just above the diffusion pump water-cooled baffle to its present position indicated here, i.e., about 60 cm above the source housing. That large distance was chosen to avoid interference of the gauge tube magnetic field with the ion source or the electric sector. The low pressure gas inlet from a gas rack system added by earlier operators of the mass spectrometer was changed to that shown in this diagram and remains so located at this time. High vacuum valves which severely restricted the pumping speed on the ionization chamber and sector housings were replaced by direct, full pump diameter (5 cm flange I.D.) tubing connections.

The experiments with this design were conducted with nozzle orifices of 5 and 10 μm and various gases--nitrogen, cyclopropane, and propylene--at pressures from 1 to 11 atm at room temperature. The usual variation of molecular beam intensity (from ion current at the appropriate m/e) with nozzle-skimmer distance was never obtained.

A pressure ratio of about 10^4 was probably maintained (there was no pressure gauge in the nozzle-skimmer region) with 11 atm N_2 expanding through the 10 μm nozzle diameter. That would place the Mach disk (see subsection 3.3 for the empirical relation) about 0.67 mm (0.026") from the nozzle orifice exit plane. The distance[122] to the "bulge" in the shock structure, X_B, is given by a similar relation (with D_n, the nozzle diameter),

$$X_B = 0.45\ (P_o/P_1)^{0.5}D_n$$

so that distance for these conditions is 0.45 mm (0.018"). According to Bier and Hagena,[119] this distance is approximately the nozzle-skimmer separation at which detachment of the oblique shock wave from the skimmer surface occurs. Hence, at longer distances the beam will be destroyed by the detached shock wave in front of the skimmer. However, for this design at distances less than or equal to X_B, the skimmer tip would be inside the conical exit region of the clamp holding the nozzle orifice (basically the same as shown in Figures 9 and 13). Hence, the effective nozzle-skimmer background pressure would be greatly increased resulting in destruction of the supersonic beam. Even if the nozzle orifice clamping system had been redesigned to eliminate the conical exit volume, the distance of 0.45 mm (corresponding to only 0.7 turns of the control nut) is a very small region in which to obtain and use beam intensity profiles. Furthermore, a skimmer with a much smaller opening, sharper edge, and more precisely adjusted distance to nozzle would be required.

Raising the pressure ratio by a factor of at least 10, but preferably over 100, would permit larger nozzle-skimmer separations to be used and thereby eliminate both the local pressure build-up within the nozzle clamp cone with that design and the difficulty of operation in that small separation. However, the pumping speed on the nozzle region was not limited by the pump (Welch 1402 Duoseal mechanical pump) but by the small conductance around the aligning spider of the nozzle assembly within the I.D. of the cylindrical probe so that a much higher pressure ratio was not obtainable since increasing P_0 would also increase P_1, whereas decreasing D_n to decrease P_1 would also decrease X_B.

The diameter of the Mach disk can be approximated[114] by 0.48 X_M and would be about 0.32 mm (0.012"). The largest diameter of the shock tube would be at least this large. The inner diameter of the outer cylindrical portion of the skimmer is about 4.8 mm (0.314") so there was probably little interference with the shock structure by that I.D.

It was clear that a new design which incorporated better pumping conductances, maintained a much lower nozzle-skimmer chamber pressure, allowed a larger, more easily controlled nozzle-skimmer separation, and permitted use of the much higher stagnation pressures required for DGC was necessary. Therefore, the design of the present instrument was begun.

3.4.2. General Outline of the Development

The successful coupling of a dense gas chromatograph to a mass spectrometer required the design and construction not only of the supersonic molecular beam interface and its pumping system but also the dense gas supply, the dense gas chromatograph, and modifications to the detecting mass spectrometer. Experimental studies were conducted at each stage of assembly to provide direction for further development.

The first step was to design the molecular beam generating system and test it at stagnation pressures ranging from 1 atm to tank pressures of various gases. In the initial experiments with the present beam system, difficulties in detecting the molecular beam with the mass spectrometer led to the addition of two electrodes in the mass spectrometer ion source and also the construction of a separate in-line detection electrode. At the same time heaters and thermocouples were installed throughout the molecular beam system for improved monitoring and control of the beam formation.

Subsequent results showed that a molecular beam was being generated and detected by the mass spectrometer. Volatile compounds were dissolved in ethylene at room temperature and tank pressures (7 atm max.) and detected. The dense gas supply system was then constructed to allow use of the higher solvent gas pressures required to dissolve less volatile compounds. At this point the whole system operated at room temperature, thus limiting the choice of solvent gases to those with critical temperatures below room temperature. This solvent gas limitation plus solute deposition at various parts in the system due to the large solubility dependence upon temperature underscored the need for precise temperature control of the system from the sampling chamber to the nozzle tip. Therefore, the thermostatted dense gas chromatograph (DGC) was designed and temperature controls were added to the dense gas supply. A heater was added to the nozzle tip so that the tip temperature could be controlled separately from the rest of the nozzle assembly and the thermostatted system. Once solutes dissolved in gases at high pressures and introduced to the mass spectrometer via the molecular beam system had been detected, efforts were directed at minimizing nozzle plugging, increasing sensitivity, and testing the system with compounds of decreasing volatility.

Experimentation since the assembly of the thermostatted DGC has involved temperature and pressure studies, different column parameters, different injection configurations and procedures, a new ion source design, various solutes and solvent gases, and dead volume considerations. Important details of the several parts of the apparatus are described in the following subsections. A set of construction blueprints of various components of the DGC/MS instrument has been filed with Athens Environmental Research Laboratory, (AERL); those drawings contain many more details than can be feasibly presented in this report. The experimental results which, in many cases, led to the various apparatus modifications are described in the next subsection, 3.5.

3.4.3. Molecular Beam System

Originally, the conventional gas chromatograph supplied with the PE-270 mass spectrometer was mounted on the side of the ion source block opposite the solids probe inlet port. This was removed and replaced by the molecular beam system. The solids inlet port vacuum lock assembly also was replaced by a pumping cross which supports the present molecular beam detector (current detector assembly and ionization gauge tube) and the pumping connection to an added diffusion pump.

Figure 6 is a scale diagram of the molecular beam system and part of the mass spectrometer. References will be made to it throughout the following discussion. The essential elements for beam formation--nozzle assembly (1), skimmer (2) and collimator (3)--are mounted on and precisely aligned by the aligning assembly (4). The brass assembly structure is cagelike, with two sets of six symmetrically placed 3/8" D rods silver brazed to three mounting flanges, and forms a large open pumping area. The critical inner surfaces of the aligning rods and all other aligning and sealing surfaces on this cage structure were finish-machined after all brazing operations to assure the alignment of nozzle, skimmer, and collimator with the ion source. Easy interchange of various shaped skimmers and collimators is possible. The whole nozzle assembly is moved within the aligning assembly by means of the large separation-control nut (5) which engages a long threaded section of the nozzle assembly. The distance between the nozzle tip and the skimmer tip can be varied from essentially zero to greater than 70 mm. This distance is read to 0.025 mm by a geared turn-counter (The Veeder Mfg. Co., Hartford, CT) on the separation-control nut with accuracy limited by backlash of the system to approximately 0.1 mm. If the relationship for the distance from the nozzle to the Mach disk given in subsection 3.3 (for $15 \leq P_0/P_1 \leq 17,000$) still applies for a ratio approaching 10^8, then with $P_0 = 100$ atm, $P_1 = 10^{-3}$ torr, and $D_n = 12.5$ μm, $X_M = (0.67)D_n(P_0/P_1)^{0.5} = 73$ mm. Therefore, at stagnation pressures less than 100 atm the nozzle-skimmer distance may be varied so as to pass through the Mach discontinuity. At all pressures of interest the skimmer can be located within the supersonic expansion region.

Differentially pumped nozzle-skimmer (6) and skimmer-collimator (7) chambers are achieved by o-ring seals of the aligning assembly mounting

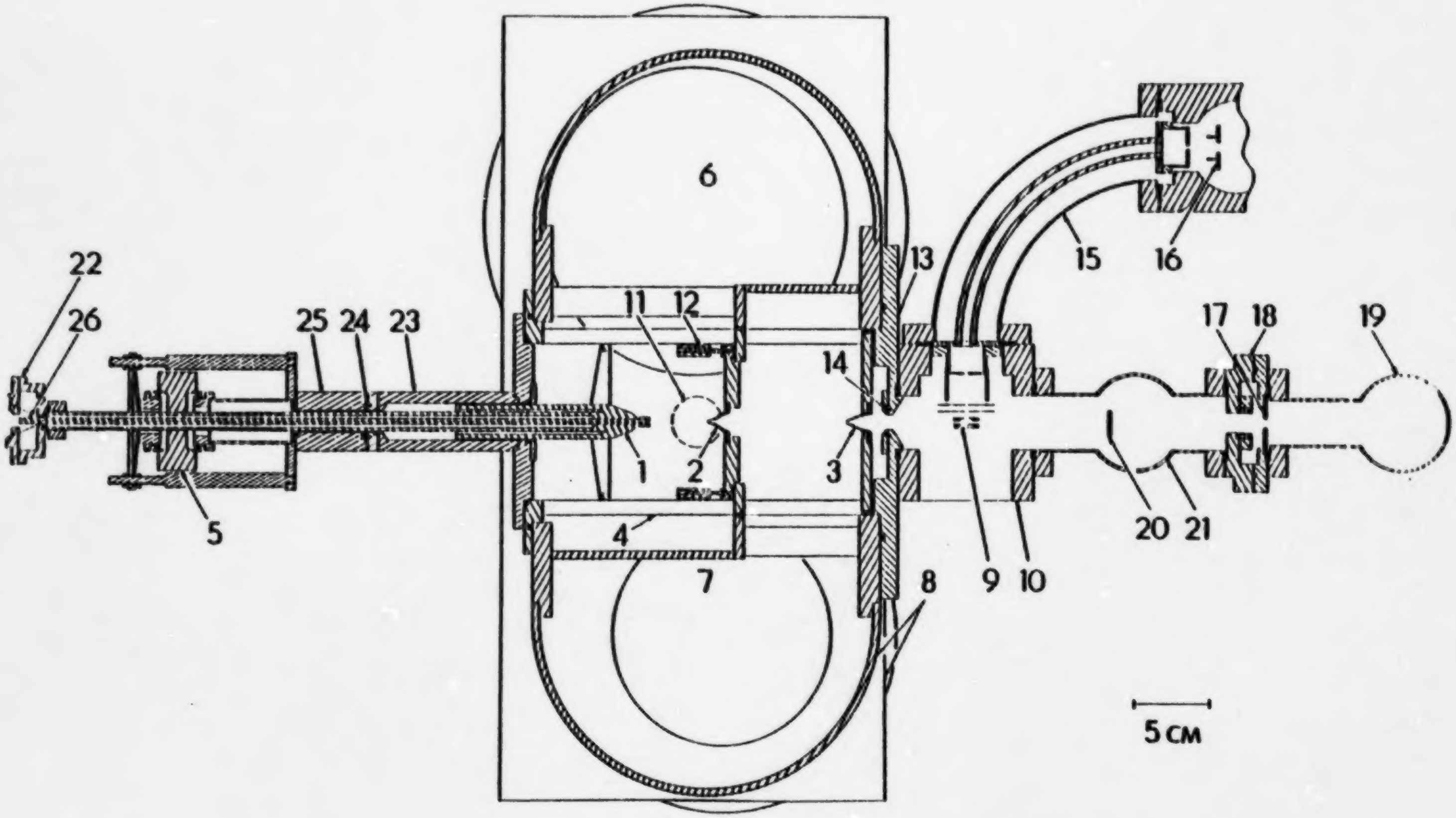
6
22
26
25
24
23
11
12
13
15
16
17
18
19
14
1
2
3
9
10
20
21
5
4
7
8
5 CM

Figure 6. Cross section of the present molecular beam system and the mass spectrometer.

flange, the skimmer mounting flange and the collimator mounting flange to the brass vacuum housing (8) which serves several purposes: structural attachment to the mass spectrometer while maintaining the integrity of the entire interface vacuum; complete separation of the nozzle-skimmer, skimmer-collimator and mass spectrometer ionization (9) chambers; precise alignment of the molecular beam aligning assembly with the mass spectrometer optics; and a mounting for valves, diffusion pumps and pressure gauges. The design of the brass vacuum housing permits close, side-by-side placement of the nozzle-skimmer and skimmer-collimator chamber diffusion pumps, thus allowing large cross-sectional pumping areas while minimizing the nozzle-skimmer, skimmer-collimator, and collimator-ion source distances. Special care was taken to design the internal structure to withstand deformation under vacuum. The accurate alignment required to couple the molecular beam aligning assembly with the mass spectrometer was obtained by first silver brazing and welding the rough-machined components followed by precise machining of all appropriate surfaces of the assembled housing.

The entire vacuum housing, including gate valves and diffusion pumps, is supported by three adjustable legs whose nylon pads slide on teflon-coated aluminum runners that have been incorporated into the mass spectrometer frame. The assemblage of the vacuum housing, the aligning assembly, and the vacuum components can be moved back from the ion source block (10) as far as 10 cm (when the interface is not under vacuum) to allow routine maintenance of seals. Four heating tapes, 96 watts each, have been wound about the outside of the vacuum housing. Two short pump leads were required to offset the diffusion pumps for clearance with the mass spectrometer steel frame; they were designed for maximum pumping speed with minimum distance between the chambers and the gate valves associated with the diffusion pumps. Both heating tapes and water cooling coils are wound about the pump leads; the heating tapes are 192 and 96 watts respectively and both cooling coils are of 3/16" O.D. copper refrigeration tubing.

The choice of diffusion pumps was a compromise between the financial cost and the minimum pumping speed necessary for initial instrument development. In order to minimize beam-skimmer interactions, beam intensity loss due to scattering and beam contamination by background gas and to obtain a nozzle-to-Mach disk distance convenient for construction, a pressure of 10^{-3} or less is required in the nozzle-skimmer region. Since 10^{-3} torr is just slightly below the pressure for maximum throughput of gas for most large diffusion pumps, the pumping system was designed to hold that pressure with the minimum gas flow adequate for feasibility studies. An assumed linear flow rate of 10 cm/sec of dense gas in a 0.5 mm I.D. tube corresponds to a flow of 2×10^{-5} ℓ/sec. The volume will increase by a factor of about 10^{8} if a gas at 40°C expands from 100 atm to 10^{-3} torr, requiring a pumping speed of at least 2000 ℓ/sec. Thus, the nozzle-skimmer chamber (6) is pumped by a Varian VHS-6 diffusion pump (2400 ℓ/sec) with a Welch 1374 duoseal mechanical pump (650 ℓ/min). A 6" VRC Hyvac gate valve with both inner diameters enlarged by the company to 20.0 cm separates the diffusion pump from the chamber pumping lead. Chamber pressure is measured by a Varian 801 thermocouple gauge (10^{-3} to 1 torr), a Varian 860 cold cathode gauge (10^{-7} to 10^{-2} torr) and an electronic manometer, the Type 220 Baratron® (10^{-4} to 1 torr) from MKS Instruments, Inc. The Type 220 Baratron was purchased inexpensively without a readout unit; the pressure display circuit, designed and constructed here, is shown in Figure B1, Appendix B. Both the cold cathode gauge tube and the Type 220 Baratron as well as the illuminated viewing port are mounted on a tubing cross on top of the housing just above the skimmer tip. The dashed circle in Figure 6 (11) indicates the viewing port placement. A second Varian 801 thermocouple gauge measures the roughing pressure between the mechanical pump and the diffusion pump.

In order to be able to remove up to 10% of the nozzle flow in the skimmer-collimator section, an oversize 4" (1200 ℓ/sec) diffusion pump, a Varian VHS-4 backed by a Welch 1376 mechanical pump (300 ℓ/min), was selected for a maximum operating pressure of 2×10^{-4} torr. A 4" VRC Hyvac gate valve with both inner diameters enlarged by the company to 14.9 cm separates the diffusion pump from the chamber pumping lead. This chamber pressure is also monitored by two Varian gauges: a 801 thermocouple gauge and a 860 cold cathode gauge, both mounted on the top of the housing. The roughing pressure between the mechanical and diffusion pumps is again measured by another Varian 801 thermocouple gauge. The vacuum system components for both the molecular beam system and the mass spectrometer are listed in Table 1.

The molecular beam is formed by skimming the central core of the free jet expanding from the nozzle orifice with a skimmer (2). As discussed in subsection 3.3, particular care must be taken in the skimmer design. Figure 7 is a detailed drawing of the present skimmer. Beryllium copper was chosen for the skimmer material because of its ease of machining.[139] A very fine chromel/alumel thermocouple junction (0.002" wire, Omega Engineering, Inc.) has been cemented with Varian Torr Seal® epoxy to the junction of the two outer conical sections. A low voltage heater made from 24 gauge nichrome wire (10 watts max.) has been clamped to the downstream side of the skimmer mounting flange and is used to heat the skimmer when desired; the location avoids any surface irregularities close to the skimmer base. A second chromel/alumel thermocouple junction (0.010" wire, Omega Engineering, Inc.) is clamped to the heater surface. It is thus possible to measure the effect of the molecular beam upon the skimmer temperature. Two adjustable posts (part 12, Figure 6) are also mounted on this flange. They determine the minimum nozzle-skimmer distance (from zero to about 1.5 cm). This minimum distance can be set by placing a special, flat-tipped dummy skimmer in the skimmer mounting flange and moving the nozzle assembly until the nozzle tip is the desired distance from the skimmer tip as determined by a feeler gauge and then adjusting the post to touch the large aligning ring of the nozzle assembly.

The molecular beam passing through the skimmer is further defined by the collimator (part 3, Figure 6). The first collimator was designed as shown in Figure 8a. Later it was decided to increase the flux into the mass spectrometer by using a large diameter orifice; it was evident from the typical low operating pressure of the skimmer-collimator chamber (10^{-5} to 10^{-4} torr) that the conical shape was not necessary at this point. Figure 8b shows the flat, large diameter collimator presently used. Both collimators were made from beryllium copper. A 24 gauge nichrome wire low voltage heater (12.4 watts max.), clamped to the upstream side of the collimator mounting flange, circles the collimator at a radius of about 3 cm. A chromel/alumel thermocouple junction (0.005" wire, Omega Engineering, Inc.) cemented with Torr Seal® epoxy 5 mm back from the tip of the cone monitored the temperature of the first collimator. With the present flat disk design, a 0.010" wire chromel/alumel thermocouple

TABLE 1. VACUUM SYSTEM FOR PRESENT DGC/MS

Region	Operating Pressure	Diffusion Pump*	Mechanical Pump*
Nozzle-Skimmer Chamber	5×10^{-4} to 10^{-2} (no beam, 2×10^{-7}) torr	Varian VHS-6 with slide valve Pump speed 2400 ℓ/sec Gauges: CC-1, BA-4, TC-1	Welch 1374 (650 ℓ/min) Gauge: TC-1
Skimmer-Collimator Chamber	10^{-5} to 5×10^{-4} (no beam, 2×10^{-7}) torr	Varian VHS-4 with slide valve Pump speed 1200 ℓ/sec Gauges: CC-1, TC-1	Welch 1376 (300 ℓ/min) Gauge: TC-1
Ionization Chamber (PE 270)	5×10^{-6} to 3×10^{-5} (no beam, 10^{-7}) torr	Veeco EP2W with baffle Pump speed 90 ℓ/sec Gauge: CC-2	Hitachi 4VP-C (100 ℓ/min) or Welch 1402 (160 ℓ/min) Gauge: TC-2
Molecular Beam Detector/Trap	10^{-5} to 5×10^{-4} (no beam, 10^{-7}) torr	CVC MCF-300 with baffle Pump speed 300 ℓ/sec Gauge: IO-1	Hitachi 4VP-C (100 ℓ/min) or Welch 1376 (300 ℓ/min) Gauge: TC-1
Analyzer (electric, magnetic sectors; electron multiplier of PE 270)	10^{-7} to 10^{-6} (no beam, $<10^{-7}$) torr	Veeco EP2W with baffle Pump speed 90 ℓ/sec Gauge: CC-2	Hitachi 3VP-C (50 ℓ/min) Gauge: TC-2
Vacuum Lock II	30 mtorr ($<10^{-3}$ with diffusion pump)	CEC VMF-80 (obsolete, part-time) Pump speed 60 ℓ/sec Gauge: CC-1	Welch 1405 (60 ℓ/min) Gauge: TC-1
DGC and Nozzle Assembly	30 mtorr during roughing operations	None	Welch 1402 (160 ℓ/min) Gauge: TC-1
Sample System for Reference Gas Introduction	<5 mtorr at vacuum; 1000 mtorr for sample introduction	CVC VMF-10 Pump speed 12.5 ℓ/sec Gauge: TC-3	Cenco Hyvac 2 Gauge: None

*Pressure gauges: CC-cold cathode, IO-ionization, BA-baratron, TC-thermocouple, 1-Varian NRC, 2-original equipment Televac, 3-Bendix Scientific Instruments, 4-MKS Instruments, Inc.

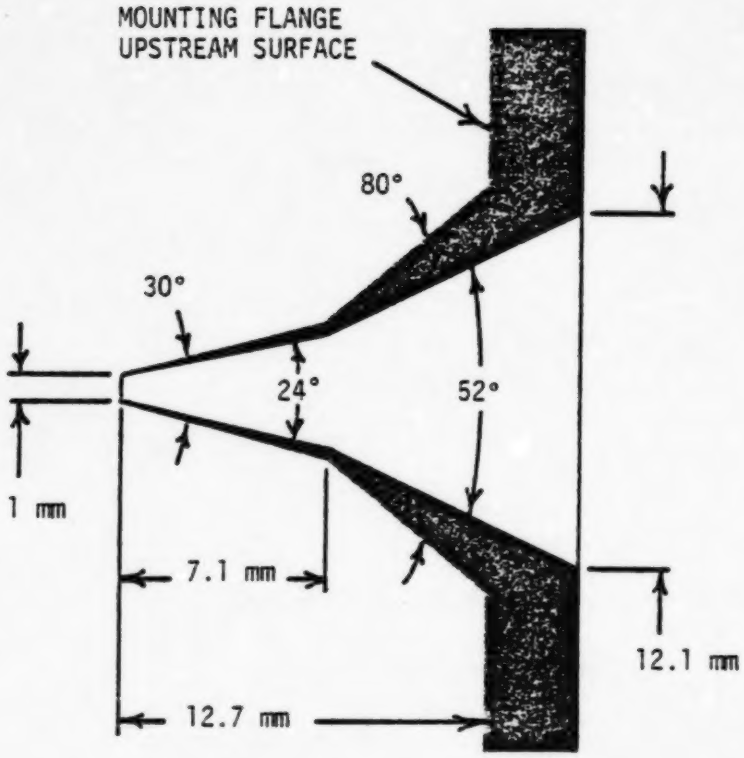
MOUNTING FLANGE
UPSTREAM SURFACE
80°
30°
24°
52°
1 mm
7.1 mm
12.1 mm
12.7 mm

Figure 7. Skimmer design.

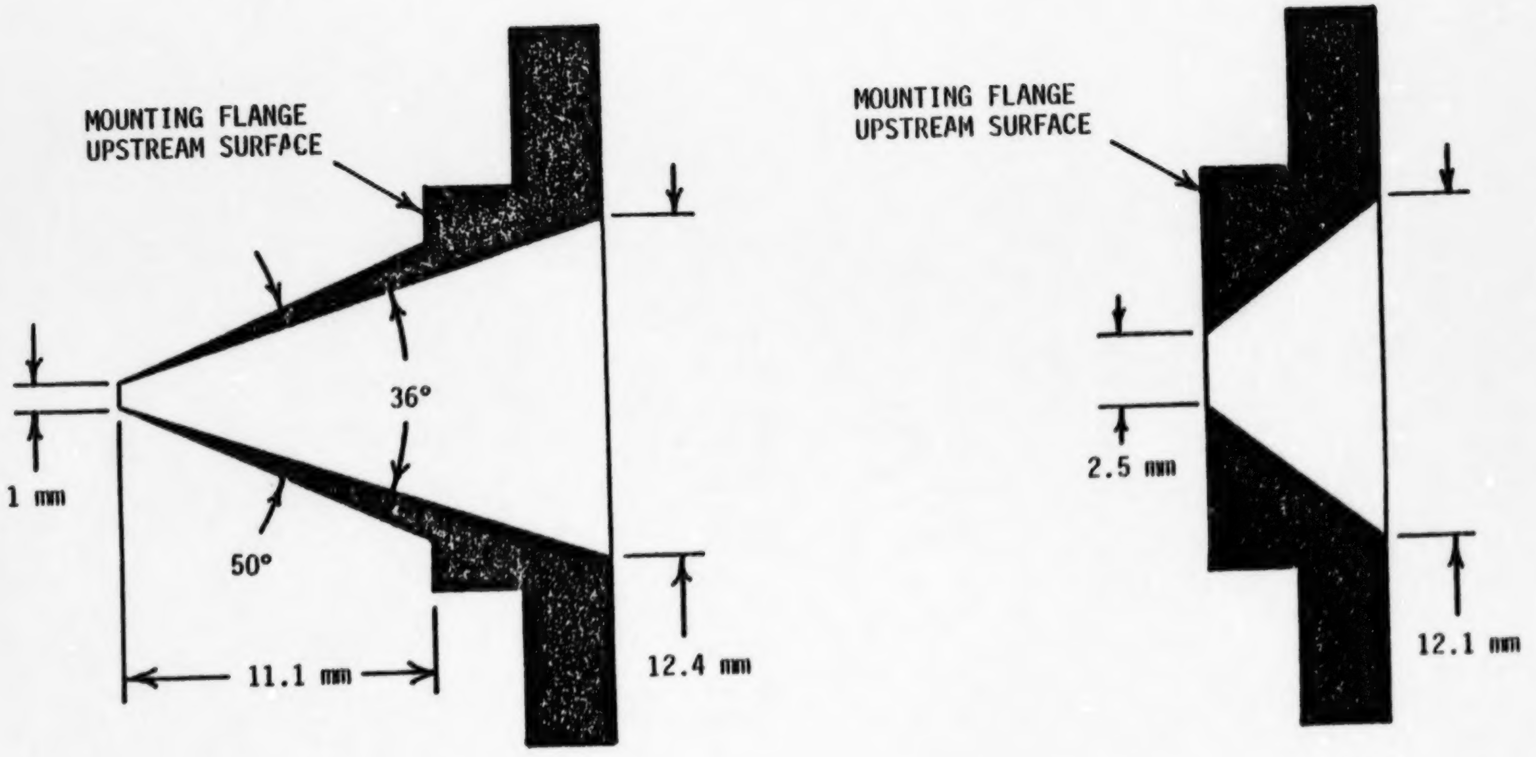
MOUNTING FLANGE UPSTREAM SURFACE
1 mm
36°
50°
11.1 mm
12.4 mm
MOUNTING FLANGE UPSTREAM SURFACE
2.5 mm
12.1 mm

a.

b.

Figure 8. Collimator designs.

junction is clamped against the outer upstream edge of the beryllium copper piece. The distance between the upstream surfaces of the skimmer and collimator mounting flanges is 90.5 mm.

A large (23 cm O.D.) stainless steel flange (part 13, Figure 6) which bolts to both the vacuum housing (8) and the ion source block (10) provides aligning and sealing surfaces or o-ring and copper gasket seals. A one-sided slide valve (14) within the flange allows the skimmer-collimator chamber to be isolated from the mass spectrometer ionization chamber. The valve aperture when open is 1.0 cm. In the closed position the ionization chamber pressure can be maintained at less than 10^{-7} torr with the skimmer-collimator chamber at atmospheric pressure.

The molecular beam passes through the slide valve into the ionization chamber where it intersects the ionizing electron beam of the Perkin-Elmer 270 mass spectrometer; the distance between the upstream surface of the collimator flange and the center of the electron beam is 6.8 cm. Ionized beam molecules are accelerated orthogonal to the intersection plane into the electrostatic sector (part 15, Figure 6), through an electrode (part 16, Figure 6) which measures total ion current by clipping the top and bottom from the ion beam, and then into the magnetic sector. Figure 6 shows the cross section of the original ion source magnet, the focus plates, the exit slit, and the electrostatic sector. The molecular beam entrance and exit holes are 2.5 mm diameter. The mass spectrometer is discussed more fully in the next subsection (3.4.4.). The ionization chamber is pumped by a two inch Veeco diffusion pump (type EP2W, 90 ℓ/sec) with either a Hitachi Model 4VP-C5 (100 ℓ/min) or a Welch Model 1402 (160 ℓ/min) roughing pump. A Televac-7A cold cathode gauge, located about 69 cm above the plane of the drawing (Figure 6), is attached to the top plate of the ionization chamber by 2.2 cm I.D. tubing. A Televac-2A thermocouple gauge measures the roughing pressure between the diffusion pump and the roughing pump. Unionized beam molecules continue their straight-line path through an easily changed ionization gauge aperture (17) mounted in a slide valve assembly (18) into an ionization gauge tube (19), Varian type 563 with Varian Model 842 controller. The molecular beam intensity can be monitored by this pressure as well as by the mass spectrometer. The 25 mm Pyrex tubulation of the gauge tube was sealed by a standard 25 mm stainless steel to borosilicate glass graded seal (Kontes), the other end of which was TIG welded to a commercial stainless steel copper-gasket seal flange. The double-sided slide valve (part 18, similar to part 14, Figure 6) permits removal of the ion gauge tube to change the entrance aperature without breaking vacuum in the rest of the system. The compact slide valve assembly, 13 mm clear opening, is designed to bolt directly between two standard copper-gasket type flanges. A roughing port on the gauge tube side is used to evacuate that tube before the valve is reopened to the mass spectrometer vacuum. The beam width at the aperture can be determined by ion gauge readings for various aperture diameters. The distance from the upstream side of the collimator flange to the plane of the aperture is 26.6 cm and the distance from the aperture plane to the center of the gauge tube is about 16.4 cm.

With the electron beam on but with zero accelerating voltage in the mass spectrometer source, ionized beam molecules should travel straight through the source. A current detecting electrode (part 20, Figure 6) can be turned into the beam path as an optional method of beam detection. When not in use, the electrode is turned completely out of the beam centerline. The electrical lead between the electrode and the amplifier was kept very short by mounting the amplifier circuitry directly on the high vacuum feedthrough for the electrode. A stainless steel and aluminum enclosure shields the amplifier. The amplified signal is then transmitted to a range switch and readout meter contained in the electronics cabinet. The circuitry, with ranges 1 nA to 10 pA full scale, is presented in Figure B2, Appendix B. The current detector and ionization gauge are connected to the ion source block by a stainless steel cross (part 21, Figure 6) which is also connected to a CVC MCF-300 diffusion pump (300 ℓ/sec) with either a Hitachi Model 4 VP-C5 (100 ℓ/min) or a Welch Model 1376 (300 ℓ/min) roughing pump. Another Varian type 801 thermocouple gauge monitors the roughing pressure between the diffusion pump and the roughing pump.

A scale, exploded drawing of the nozzle assembly (part 1, Figure 6) is presented in Figure 9. In this diagram, Part T is the inlet tube (3 mm (1/8") O.D. stainless steel) for the dense gas. Originally this part was fabricated from 0.51 mm (0.020") I.D. tubing; a duplicate from 0.15 mm (0.006") I.D. tubing was made to decrease the volume between the chromatograph column and the tip of this piece. Part P is a circular piece of nickel shim stock which contains a laser drilled pinhole. Various pinhole diameters are available commercially from Optimation, Inc. and The Ealing Corporation (Utility and Precision pinholes). The first several pinholes used were purchased from PBL International, Inc., who no longer supplies them. The pinholes are supplied in different shapes and thicknesses of shim stock depending upon the manufacturer. Both Optimation, Inc. and The Ealing Corporation describe their pinholes as having a variable diameter with the smallest diameter as the nominal diameter. Figure 10 is a cross section of a pinhole according to The Ealing Corporation and shows how it is mounted in this application so that it resembles a converging nozzle. A special punch/centering jig was constructed to center the pinhole to within 0.002" (0.05 mm) in the exit hole of the pinhole holder (part C, Figure 9) and then punch it against surface S of that part. Further details of the jig and the punching procedure, as well as flow rate measurements with various orifice diameters, are given in Appendix C. The pinhole shim is firmly clamped between the tip of part T and surface S of part C by part D. Part D threads into part E and also makes an o-ring seal with part H. The external, non-threaded surface of part E is polished for various o-ring seals in two differentially pumped vacuum locks to be discussed below. The threaded O.D. at the other end of part E and not shown in Figure 9 mates with the separation-control nut which adjusts the nozzle-skimmer distance.

The pinhole is kept in alignment with the skimmer aperture by part H, Figure 9. The large outer diameter, H1, is constrained to move along the six aligning assembly rods while the smaller outer diameter, H2, slides through the o-ring seal separating the nozzle-skimmer chamber from a vacuum lock (part 23, Figure 6). A view of the nozzle assembly within the aligning assembly from the skimmer is given in Figure 11. Here, part 1 is the aligning O.D. of the aligning assembly mounting flange and part 2 is one of the six rods which determine the precisely machined aligning assembly I.D. Six

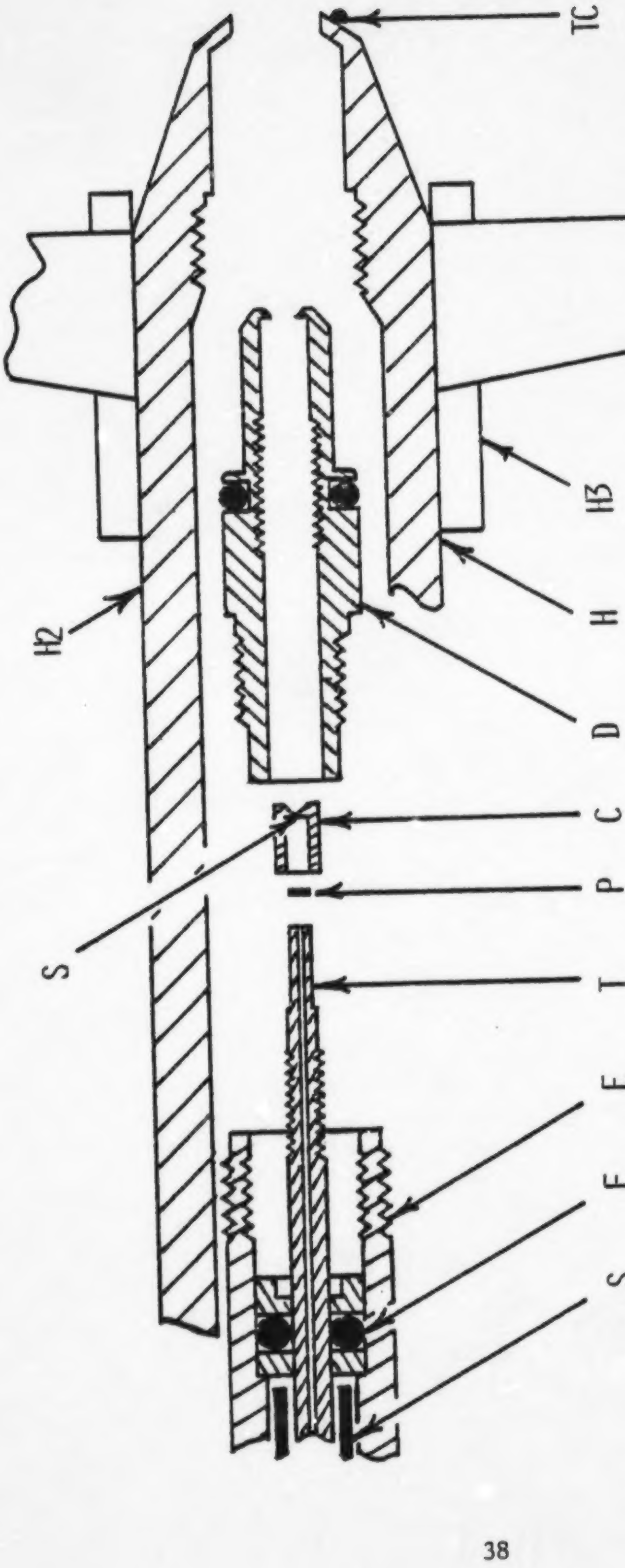
TC
H1
H3
H
D
C
P
T
E
F
S
S
H2

Figure 9. Exploded view of the nozzle assembly.

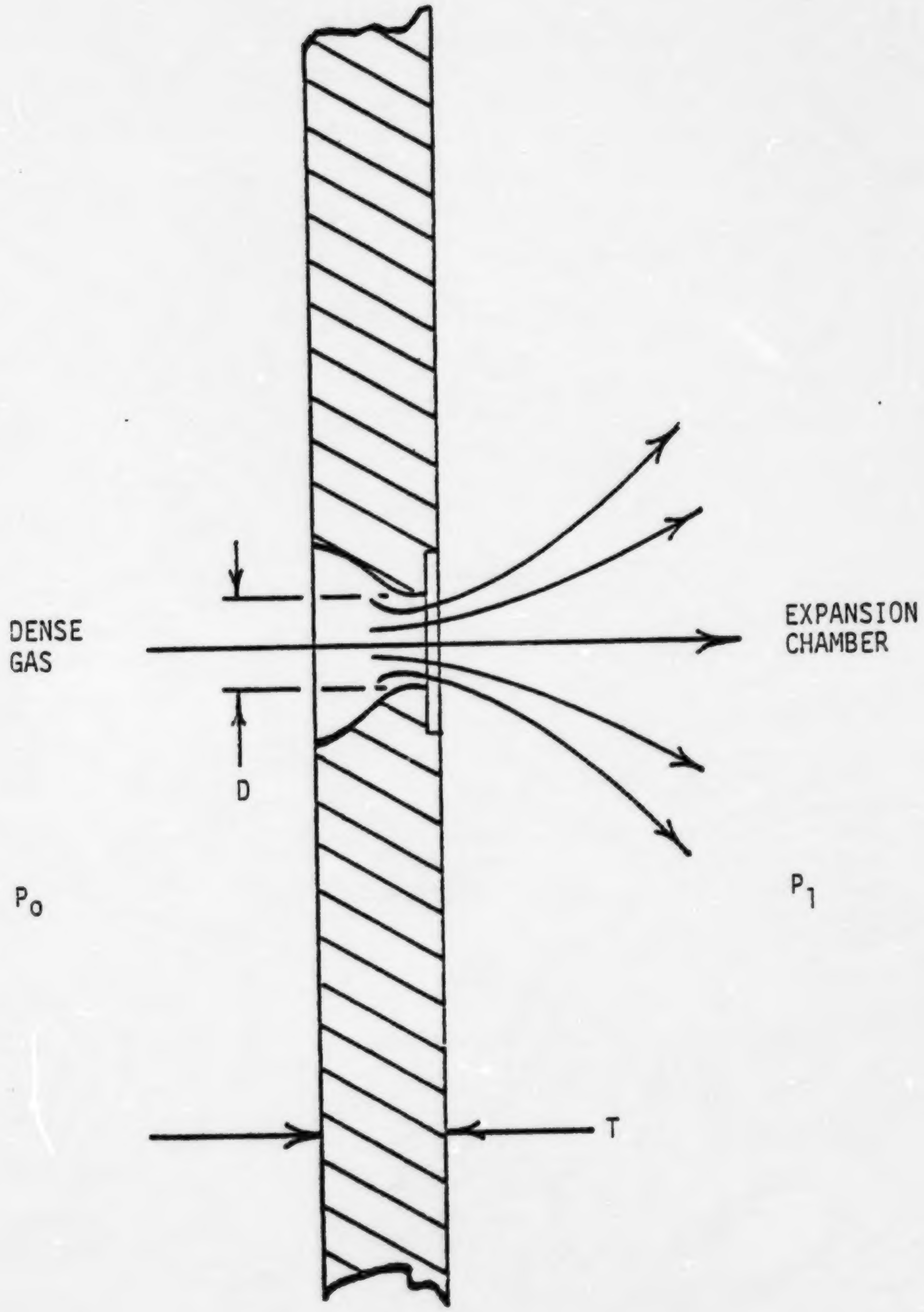

DENSE GAS
EXPANSION CHAMBER
D
P_0
P_1
T

Figure 10. Cross section of a laser-drilled pinhole, according to supplier. (Reproduced with permission from the Ealing Corporation)

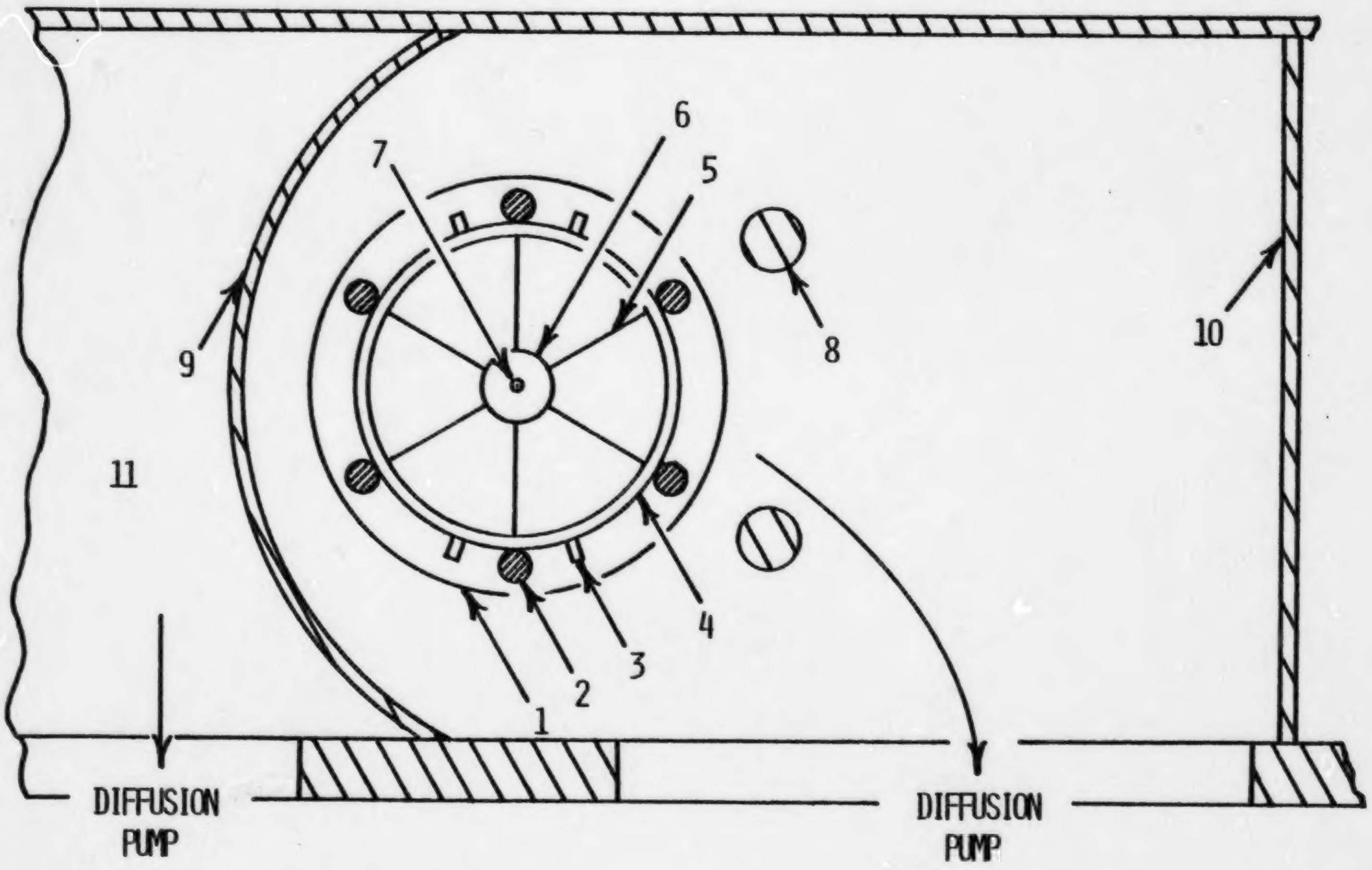
1
2
3
4
5
6
7
8
9
10
11
DIFFUSION PUMP
DIFFUSION PUMP

Figure 11. Nozzle assembly as seen from skimmer.

thin fins (5) connect the ring (4, part H1 in Figure 9) which slides within the I.D. defined by the rods to the cylindrical surface (6, part H2 in Figure 9) which slides in the o-ring seal. This "wagon wheel" construction of the nozzle assembly is very open and allows fast unobstructed pumping of the region about the nozzle orifice (7). Four pins (3) screw into the ring after placement of the brazed assembly (part H in Figure 9) of parts 4, 5, and 6 in the aligning assembly. The curved plate (9) and two posts (8) locate the center plate which, along with (9) and another oppositely curved plate, separate the two chambers of the vacuum housing. Part 10 refers to the outer shell of the vacuum housing. The region labeled 11 is part of the skimmer-collimator chamber and is separate from the nozzle-skimmer chamber except for the connection through the skimmer orifice.

Primary temperature control of the nozzle assembly, particularly of its inlet tubing (part T, Figure 9), is provided by circulating thermostatted water from the DGC water bath along the entire length of part T from the o-ring (part F, Figure 9) to its connection to the DGC components within the water bath. Part S in Figure 9 is one of four lengths of stainless steel tubing (0.058" O.D. X 0.042" I.D.) that are part of the nozzle assembly water manifold (part 22, Figure 6) by which the water is supplied to the nozzle assembly. Figure 12 shows a cross-section of the water manifold screwed onto the threaded end of the nozzle assembly (part E, Figures 9 and 12). An annular volume (A) connects the bath water at high pressure (HP) to the four lengths of tubing, S, which carry the water close to the nozzle orifice (about 5 cm away). The water returns around the outside of tubes S in the annular space R between tubes T and E. Two chromel/alumel thermocouple junctions (0.010" wire with fiberglass insulation) have been attached to the tubes, S, using heat-shrink tubing and household epoxy: one is at the end very close to the o-ring seal and the other is at the mid-point in length. Additional bath water at low pressure (LP) is circulated around the nozzle assembly inlet tubing, T, back to the DGC bath through the flexible bellows coupling, B. High pressure water streaming through regions R mixes with the low pressure water in the manifold and also returns to the bath via the flexible bellows. Clamping surfaces (CS) on both the water manifold and the water bath allow easy attachment of the bellows (plastic corrugated hose) to its mating parts with simple tubing clamps. The electrical feedthroughs (FD) for the thermocouples are indicated.

For clarity the nozzle assembly with all parts clamped together is shown in Figure 13. In addition to those already discussed, some other features are indicated. The o-ring labeled simply "Vacuum Seal" isolates the internal volumes of the nozzle assembly from the nozzle-skimmer chamber. Those internal volumes, formed from the threaded sections and small gaps between mating pieces (and isolated from the water bath by the o-ring, "Water/Vacuum Seal"), are connected by the path formed by the "Pump-Out Holes" and the annular channel, "Vacuum Pumping Region", to the vacuum region labeled 23 in Figure 6. Pumping of this region, referred to as Vacuum Lock II in the discussion below, not only evacuates the volumes within the nozzle assembly but also provides differential pumping across the sliding o-ring seal about surface H2 (Figure 9). The "Clamp Screws" in Figure 13 keep all internal nozzle assembly parts tightly clamped together so that they may be assembled to or removed as a unit from the outer aligning wheel assembly, H, Figure 9.

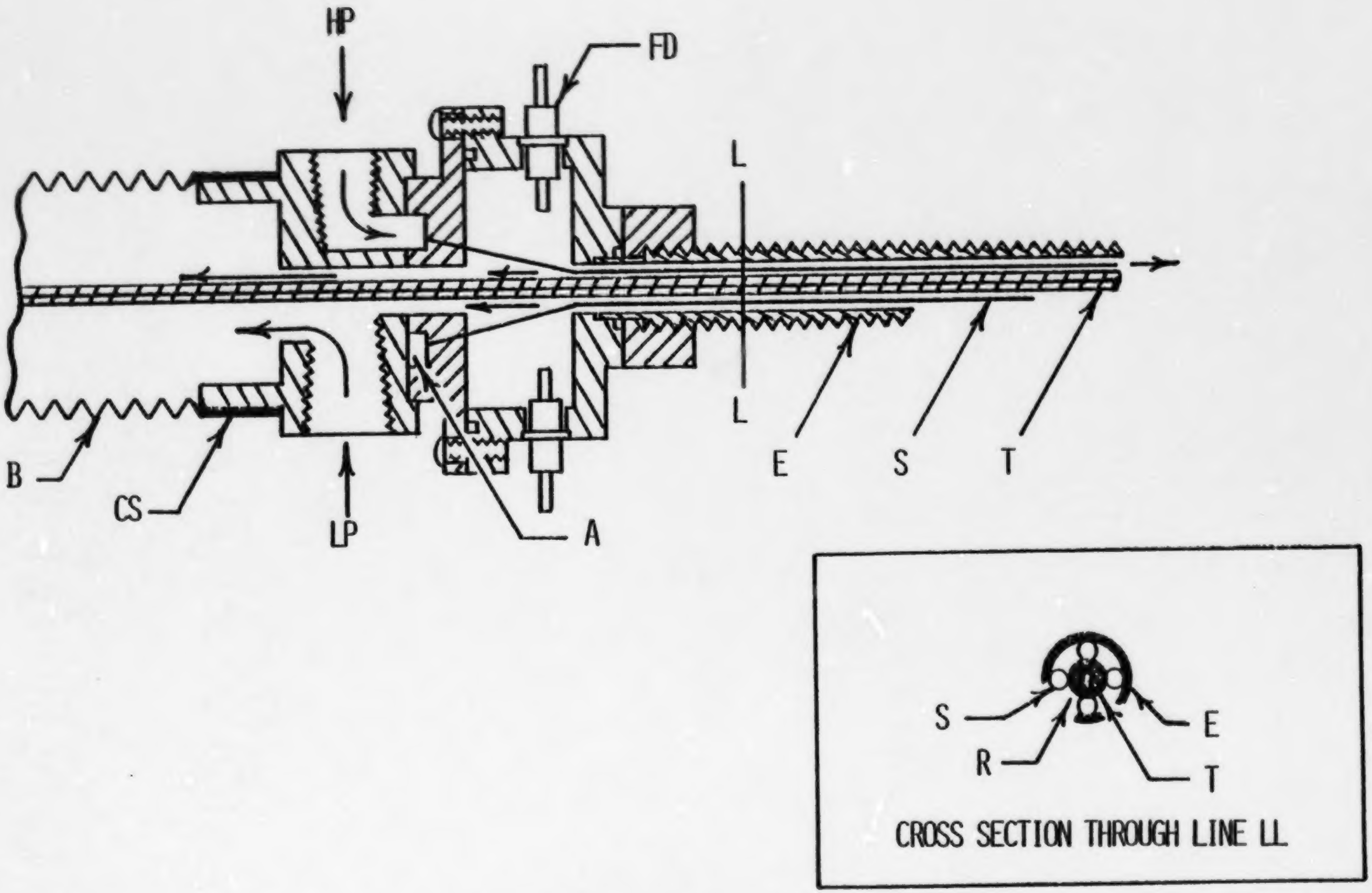
HP
FD
L
L
B
CS
LP
A
E
S
T
S
R
E
T
CROSS SECTION THROUGH LINE LL

Figure 12. Nozzle assembly water manifold cross section.

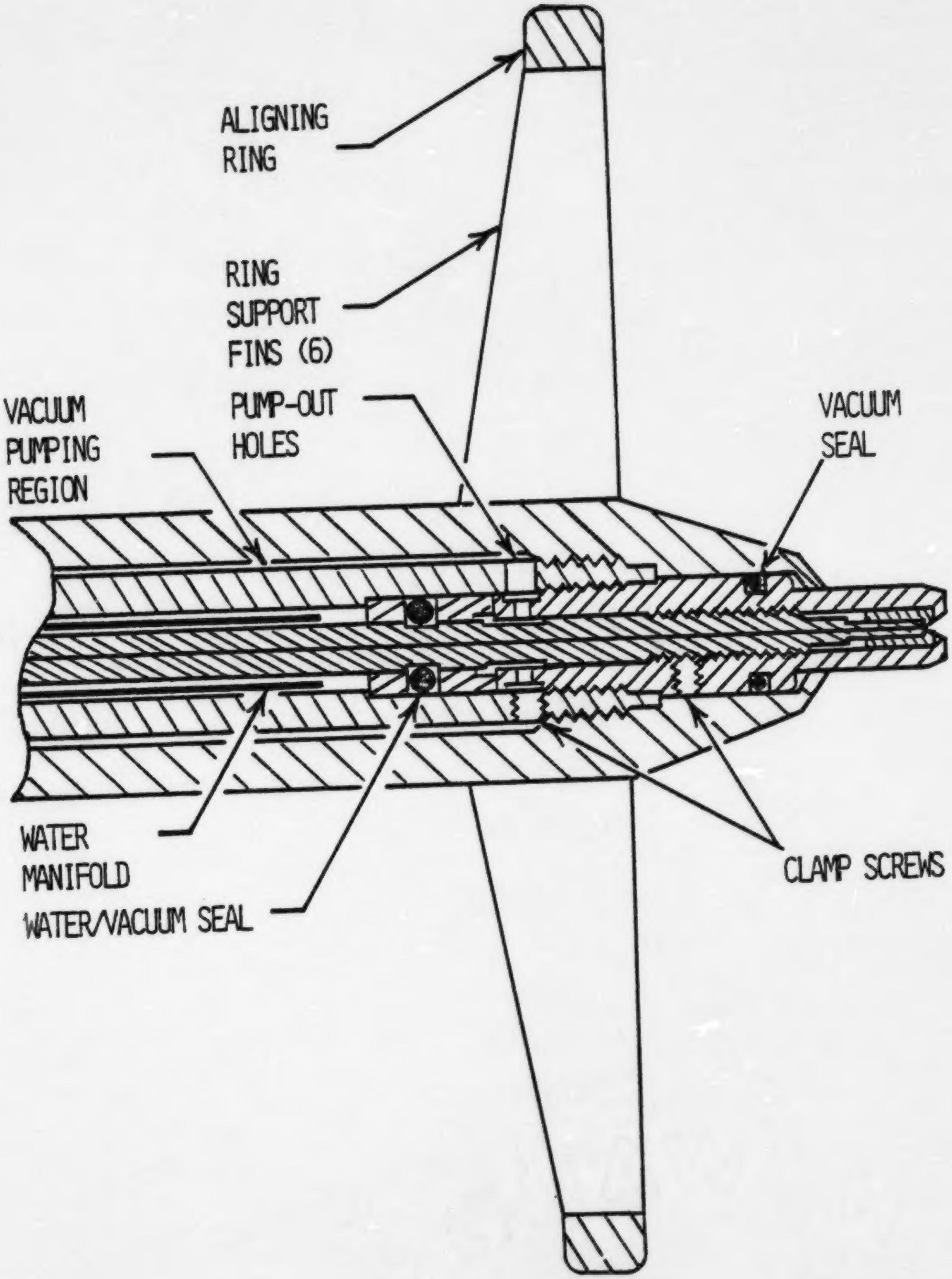
ALIGNING RING
RING SUPPORT FINS (6)
VACUUM PUMPING REGION
PUMP-OUT HOLES
VACUUM SEAL
WATER MANIFOLD
WATER/VACUUM SEAL
CLAMP SCREWS

Figure 13. Nozzle assembly.

Therefore, pinhole replacement without disassembling other interface parts is possible simply by unscrewing part E (Figure 9) assembled with parts T, P, C, D, F, and S from part H which remains in the aligning assembly. Removal and reinsertion of this subassembly with the nozzle-skimmer chamber still at high vacuum is made possible by movement of the subassembly through the two vacuum locks and a double-sided slide valve--parts 23, 24 and 25 in Figure 6 --with the necessary seals provided to part E by an o-ring at the end of each vacuum lock more distant from the interface. Vacuum lock I (25) is pumped by a Welch duoseal mechanical pump (1402, 160 ℓ/min). The pressure is measured by a Varian 801 thermocouple gauge. Vacuum lock II (23) was pumped by an old CVC VMF-80 (60 ℓ/sec) diffusion pump backed by either a Welch 1402 or a Welch 1405 (60 ℓ/min) with the pressure measured by a Varian 860 cold cathode gauge and another Varian 801 thermocouple gauge between the diffusion and roughing pump. In recent experiments, the diffusion pump and the cold cathode gauge on Vacuum Lock II have not been used since standard procedure now is to close both the VHS-6 and VHS-4 diffusion pump slide valves and open the vacuum housing to atmospheric pressure for subassembly removal. The Welch 1405 pump was found to be adequate for a differential vacuum across the sliding o-ring seal about diameter H2 (Figure 9) of the nozzle assembly; however, it is not adequate for the original subassembly removal design.

Originally, the nozzle assembly (including the tip) was heated solely by a ceramic insulated nichrome heater (24 gauge, 7.4 watts) surrounding the assembly as indicated by H3, Figure 9. A chromel/alumel thermocouple junction, TC, (0.010" wire, Omega Engineering, Inc.) was placed close to the exit tip on Part H as indicated. After preliminary experimentation, it was evident that a separate heater for the nozzle tip was required. Figure 14 shows this heater, assembled from carefully machined ceramic (Aremcolox 502-1100, Aremco Products, Inc.), beryllium copper, and nichrome wire (26 gauge, 6 watt). Two thermocouples, description as above, are now located as follows: TCA on the nozzle assembly and TCB cemented on the beryllium copper piece (Ceramacoat 512, Aremco Products, Inc.) very close to the nozzle exit plane. Placement of all of the heaters and thermocouples for the vacuum section of the molecular beam system is shown in Figure 15; however, details of electrical feedthroughs and wiring are omitted. Labeled parts designate the nozzle assembly heater (1) and thermocouple (A), the nozzle tip heater (2) and thermocouple (B), the skimmer thermocouple (C), the skimmer flange heater (3) and thermocouple (D) and the collimator heater (4) and thermocouple (E).

Finally, the 3 mm O.D. tubing, 26 in Figure 6 (T, Figures 9 and 12), connects the molecular beam system to the high pressure supply via the thermostatted DGC with an optional chromatograph column; the high pressure supply system, to be described later, has a pressure range capability from atmospheric pressure to 273 atm (4000 psig) at this time. It should be noted that since part 26 is part of the moving nozzle assembly, the gas supply lead must be capable of the 70 mm movement required of the nozzle.

While the Perkin-Elmer 270 mass spectrometer was equipped with thermocouples specifically for that part of the system, it was found to be highly desirable to monitor other temperatures in the DGC/MS interface. Provisions were made for 15 thermocouples of which any three can be read at one time. A typical thermocouple circuit diagram is given in Figure B3 in Appendix B.

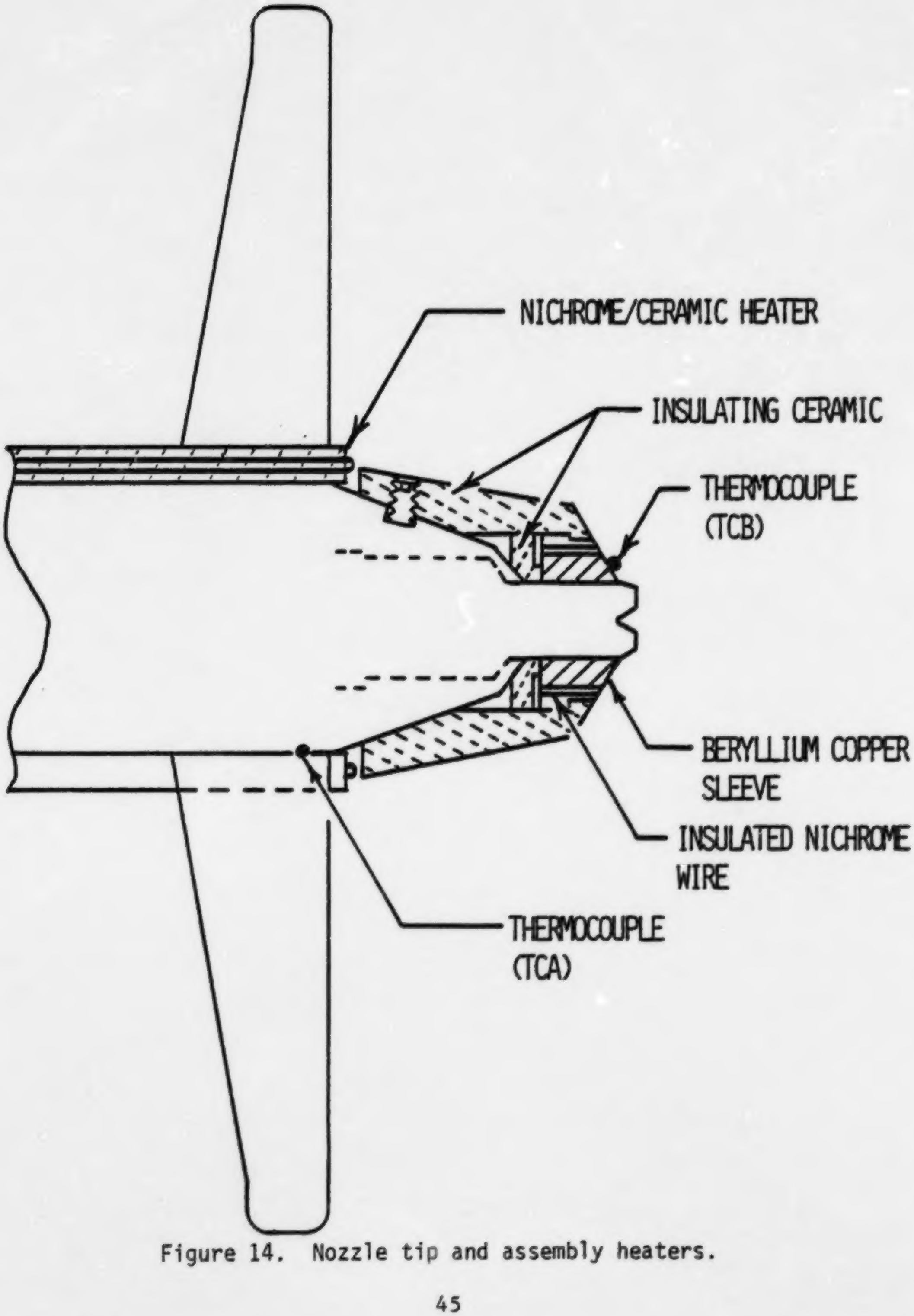
NICHROME/CERAMIC HEATER
INSULATING CERAMIC
THERMOCOUPLE (TCB)
BERYLLIUM COPPER SLEEVE
INSULATED NICHROME WIRE
THERMOCOUPLE (TCA)

Figure 14. Nozzle tip and assembly heaters.

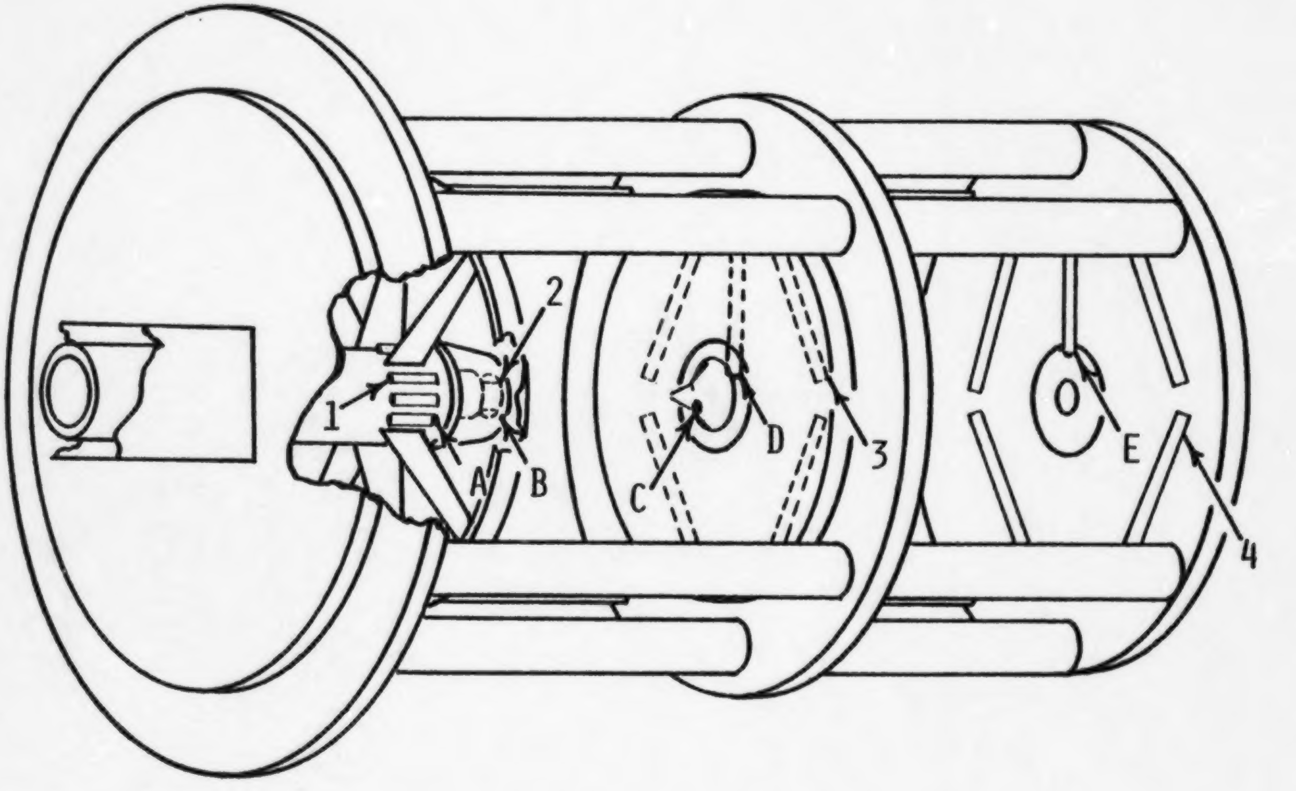

Figure 15. Thermocouples and heaters of the molecular beam system. The nozzle assembly, skimmer, and collimator are shown mounted in the aligning assembly.

Several temperature ranges with different degrees of precision are possible: ∓9.9 to ±99.9°C and ∓99 to ±999°C. Chromel/alumel thermocouples were chosen because the thermoelectric voltage is more nearly linear with temperature over the temperature range -50°C to +150°C and the wires are more oxidation-resistant than the other commonly used base metal thermocouples. Several precautions were taken in installing the wiring for the thermocouples: correct extension wire was used and was shielded for its length by enclosing it in electrical conduit separate from other interface circuitry; appropriate chromel and alumel hardware was used at every junction except vacuum and water bath feedthroughs; and the reference junctions were enclosed in an asbestos-lined box to prevent temperature fluctuations around them.

Temperature control and monitoring of the molecular beam system alone required four heaters and 5 thermocouples in the vacuum chambers as indicated in Figure 15 as well as those in the water bath and non-vacuum regions. With so many necessary thermocouple and heater feedthroughs, the cost of the feedthroughs could have been prohibitive. It was found that ceramic feedthrough capacitors from Centralab (100 pf value arbitrarily chosen, with the value markings mostly removed by mechanical grinding followed by refluxing in benzene) when soldered in place are adequate both for vacuum at least to 5 x 10^{-7} torr and for immersion in the water bath at a fraction of the cost (~$0.20 each) of more standard feedthroughs (e.g., ~$10.00 each for a comparable size from Ceramaseal, Inc.). Easy, positive slip connections on both sides of the feedthroughs were made with Molex female connectors--again at a cost significantly less than the typical two-tapped-hole connectors.

The switches, heater controls, meters and electronics for interface pumps, pressure gauges, heaters, thermocouples, and solenoid valves were all contained in a second electronics cabinet separate from the mass spectrometer controls in the original cabinet.

3.4.4. Mass Spectrometer

A Perkin-Elmer Model 270 mass spectrometer--a double focusing Nier-Johnson type with a 90°/12.7 cm radius electrostatic sector and 60°/15 cm radius magnetic sector--was modified to use in this experiment. The gas chromatograph oven and the solids inlet probe were removed. The gas inlet system that had previously been added to the machine was re-designed as were the diffusion pump leads and cold cathode gauge placements.

The analyser region, i.e., both sectors and the electron multiplier, like the ionization source is pumped by a two inch Veeco (Type EP2W, 90 ℓ/sec) diffusion pump with a Hitachi Model 3VP-C3 (50 ℓ/min) mechanical pump. A Televac-7A cold cathode gauge just above the water-cooled baffles bolted to the diffusion pump measures the pressure of the analyser region; a Televac-2A thermocouple gauge measures the roughing pressure between the diffusion and mechanical pumps. The vacuum system components for both the molecular beam system and mass spectrometer were listed in Table 1 in the previous subsection, 3.4.3.

The resolution of the machine is stated to be 1 in 850 by the 10% valley definition. Since this much-used instrument has been in this laboratory, the resolution has never approached that value. Extensive alignment procedures have resulted in the resolution improved from about 1 in 100 to 1 in 200 by the 10% valley definition. The theoretical sensitivity was defined by the manufacturer in terms of gas chromatography performance: 3 ng/sec of methyl stearate should give a significant parent peak relative to noise using a 1 sec/decade scan rate. During recent experiments approximately 15-20 ng/sec was seen with difficulty using a longer scan rate (by a factor of 5 to 10) with compounds which produce mainly the parent ion (vs. methyl stearate with parent m/e intensity < 1/10 m/e 74, the most abundant fragment ion). Hence, the sensitivity does appear to be lower than optimum. The instrument was initially purchased by the Department of Chemistry for routine use. It had many, often inexperienced operators and so received some abuse including the warping of the magnet sector. Therefore, some of the lack of sensitivity and resolution can be attributed to the poor condition of the machine while some has been attributed to the nature of the electron beam collimating magnetic field in the ion source.

Figure 16 is a diagram showing (a) the original ionization chamber design, (b) a modified design, and (c) the new chamber design. The directions of the molecular beam (MB) and the ion beam (IB) are indicated. In all three designs the dimensions of the chamber exit slit (H) and the molecular beam entrance and exit holes were the same. Similarly, the internal dimensions of the ion chamber (CH) and the placement of ion focusing lenses beyond the source exit slit (and not shown here) also were unchanged. In configuration b, the ion source back plate (B) has been separated and insulated from the rest of the chamber and another wedge-shaped electrode (W), added. The electrodes were added to increase the ionized molecular beam species flux into the electrostatic sector. Configuration c is similar to b in that it has two additional electrodes--this time as a split back plate (B,W); however, configuration c also included a new electron beam collimating magnet. Diagrams a', b', and c' show cross sections of the three designs in the plane of the molecular beam and electron beam (EB) and perpendicular to the ion beam. In Figure 16, a' and b' show the original collimating magnet and indicate its probable inhomogenous field lines (dashed lines) as determined from the pattern of iron filings placed in the field. The field appears very weak in the section between the entrance and exit molecular beam holes, and the magnetic field lines are not uniform across the chamber but appear as a slender group clustered in the center with gaps at either side. This field pattern was predicted upon analyzing the construction of the magnet: four bar magnets (MT) aligned in soft steel (FE) pieces at both ends and in the middle. A crude approximation made by constructing field lines perpendicular to magnetic "equipotential lines" (derived from a computer electrostatic field program) also indicates this field. As it appeared that this non-homogeneous field might be responsible for some of the problems discussed in subsection 3.5 of this report, a new collimatimg magnet giving a more homogeneous field was constructed. An approximation to the field is shown in c'; in actuality, the field lines are probably more distorted than shown here. In this design the C-shaped magnet is not part of the ion source chamber. In fact, only the soft steel pole pieces can be seen in the cross section; the Alnico magnets are located at some distance behind the chamber. The chamber, the filament, and the electron trap are all immersed in the field and no magnetically susceptible materials are present in their assembly to distort the field.

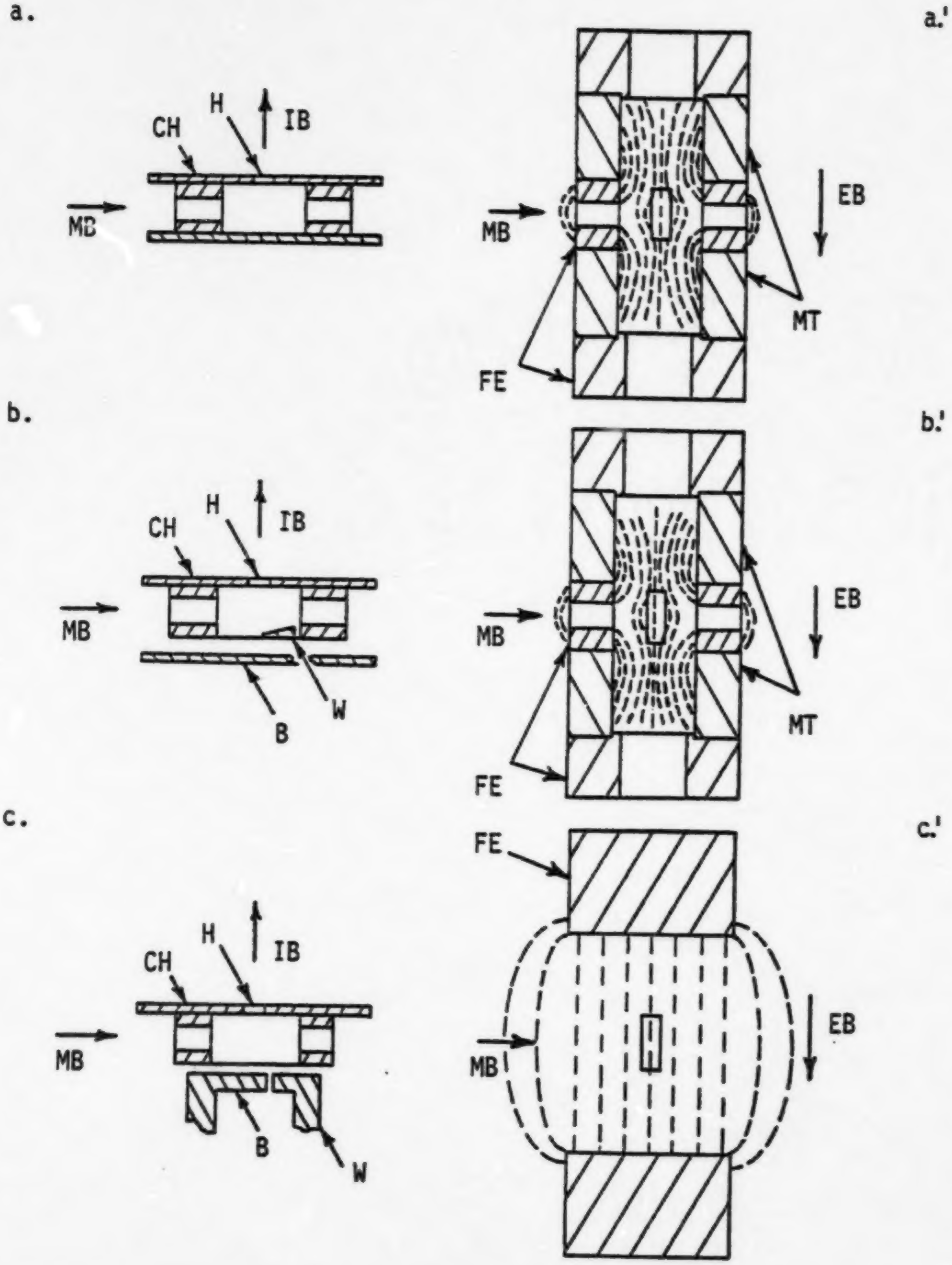
a.
a.'
CH
H
IB
MB
EB
MT
FE
b.
b.'
CH
H
IB
MB
B
W
EB
MT
FE
c.
c.'
CH
H
IB
MB
B
W
FE
EB
MB

Figure 16. Cross sections of ionization chamber designs (a, b, c) and corresponding electron beam collimating magnet designs (a', b', c').

Figure 17 shows more explicitly the electrodes constituting the ion optics that may be adjusted in potential for maximum signal. While the ion chamber (CH) may assume nominal values of 750, 1000, 1500 and 2000 V, the highest value was normally used. The possible potential range applied to the added electrodes (B,W in Figures 16 and 17) has depended upon the experimental stage of development--i.e., at first -16 to +30 V on B and 0 to +50 V on W, later 0 to +66 V on both, and finally 0 to +240 V on both. However, during all experiments the electrodes could assume chamber potential and any voltage supplied to them was referenced to chamber voltage. The voltage drop from chamber to the focus plates (L1 and L2) is determined by coarse and fine adjustments (coarse focus, CF, and fine focus, FF). The potential difference referred to as "Focus" in Figure 17 is adjustable from about 40 to 300 volts with an additional variation of each of the focus plates of ±15 V when the total accelerating voltage is 2000 V. The exit slits are at ground potential. Further focusing involves the electrostatic sector plate potentials, E1 and E2. The sector offset, SO, adjustment varies the values of E1 and E2 with respect to ground but does not affect the potential difference (E2-E1) between the plates. The analyzer adjustment (AN) does vary the potential difference between the plates. Typically E1 can vary from -60 to -125 volts and E2 from +70 to +120 volts. The potential difference can be varied from about 140 to 230 volts. The sector offset adjustment is not usually included in the electronics tuning procedure which involves maximizing the total ion current signal or that of a particular mass by adjusting in a definite order CF, FF, L1, L2, AN, W and B to give a maximum signal and then repeating the procedure. Often the electron energy (~30 to 120 eV) is added to the list of adjustments.

After passing through the electric and the magnetic sectors, ions are detected by a 16 stage electron multiplier with copper beryllium dynodes. The output of the multiplier is amplified by the original mass spectrometer circuit, then fed into a new galvonometer-driver circuit (designed in this laboratory) which drives the four galvonometers of an oscillographic recorder, Model 460 by Century Electronics and Instruments, Inc. The fast repetitive scanning for long periods of time required to detect chromatograph peaks cannot be satisfactorily accommodated by continuous oscillograph recording for two reasons: 1. the enormous number of useless paper scans to be analyzed just to find the eluted compounds, and 2. the large expense of the photosensitive paper. Hence, the typical chromatographic detection used for these experiments is to display the continuous scanning on an oscilloscope and "hard copy" only during elution periods. Figure 18 is a simple diagram of this detection set-up. The ion current signal for the scope vertical input is tapped after the first amplifier stage of the galvo driver amplifier (AMP-1). A voltage proportional to magnet current is amplified by a second amplifier, AMP-2, and used to drive the horizontal sweep of a long persistence oscilloscope, the Memo-Scope 104 by Hughes Products. The amplifier, AMP-2, was also designed in this laboratory (circuit diagram given in Figure B4 in Appendix B); amplifier controls permit the m/e range displayed on the screen to be shifted and expanded or compressed depending upon the number of masses to be monitored. A magnet sweep relay in the mass spectrometer enables the recorder only during actual scanning and not during field return after the switch, SW, is manually closed on observing a new peak on the oscilloscope screen. Hence, this system allows full-time monitoring with a minimum of wasted permanent recording.

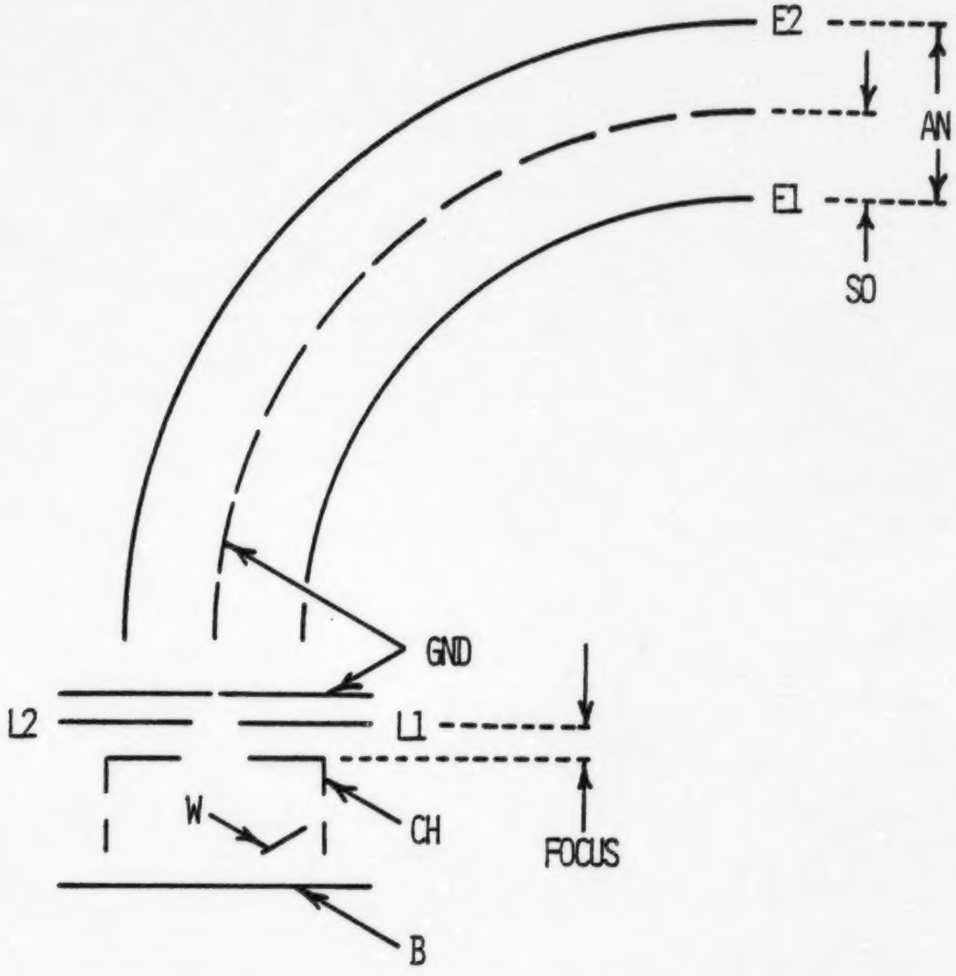
E2
AN
E1
SO
GND
L2
L1
W
CH
FOCUS
B

Figure 17. Ion source and electric sector electrodes (not to scale).

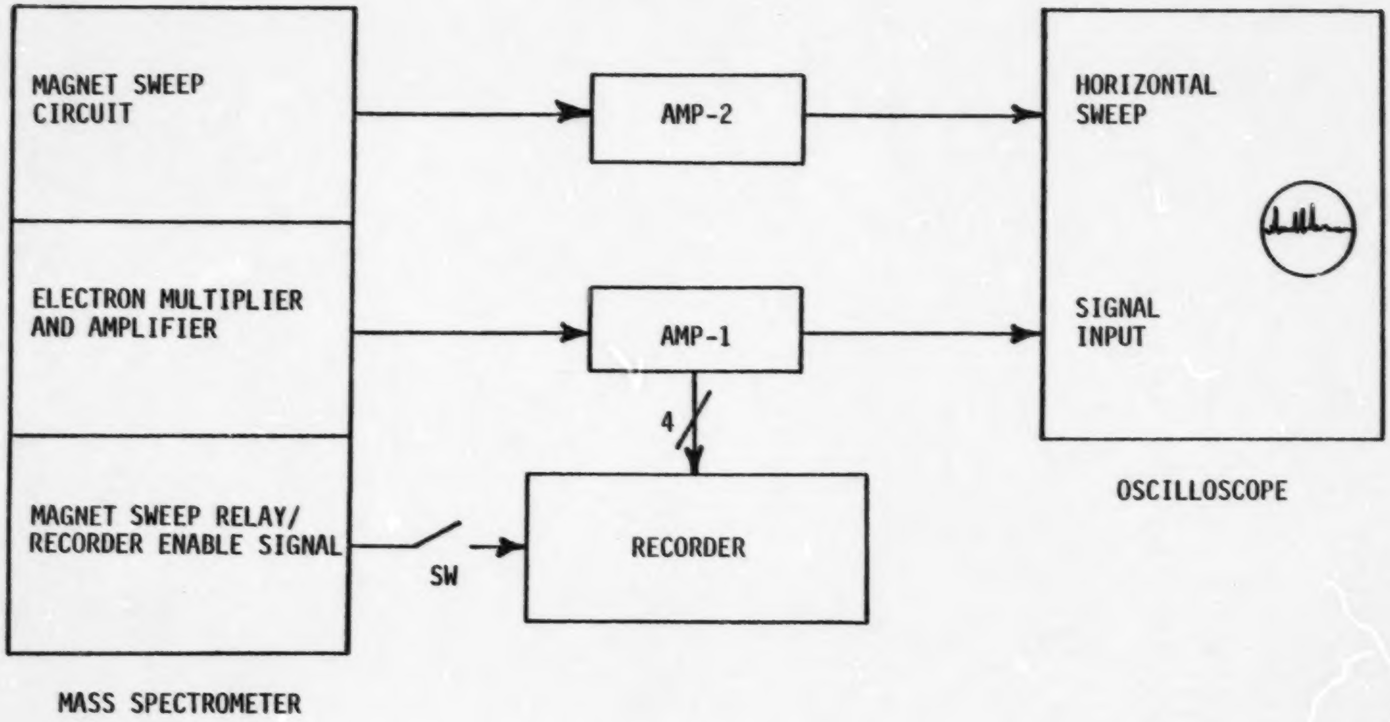
MAGNET SWEEP CIRCUIT
ELECTRON MULTIPLIER AND AMPLIFIER
MAGNET SWEEP RELAY/ RECORDER ENABLE SIGNAL
MASS SPECTROMETER
AMP-2
AMP-1
4
SW
RECORDER
HORIZONTAL SWEEP
SIGNAL INPUT
OSCILLOSCOPE

Figure 18. Block diagram of system for full-time monitoring/part-time recording of mass spectra.

3.4.5. Dense Gas Supply

Most of the high pressure equipment used in the DGC/MS experiments was borrowed from Dr. J. C. Giddings, Department of Chemistry, University of Utah and had been used in earlier DGC experiments. Figure 19 shows the configuration and equipment used thus far. The maximum supply pressure possible at present is 4000 psig (273 atm). Briefly, the various parts are

Compressor--Aminco 2-stage, air-operated diaphragm type, 5000 psi first stage and 30,000 psi second stage.

Reservoir--Aminco reaction vessel, 35,000 psi at 100° F, 1150 ml internal volume.

R1--Victor high pressure/low flow piston regulator, 0-1500 psig delivery range with 4000 psi maximum input.

R2--Consolidated Controls Corporation (formerly APCO design) high pressure adjustable regulator, 0-4000 psig outlet delivery range with 6000 psig maximum inlet pressure.

G1--pressure gauge from Jas. P. Marsh Corp. (Mastergauge), 0-5000 psig.
G2--pressure gauge from ACME Gauge and Instrum. Co., 0-4000 psig.
F--Aminco filters, 30,000 psig, 4 sintered stainless steel elements with the smallest 5 μm.
W1, W2, W3--Whitey valves, stainless steel, 3000 psi maximum pressure 1/4" Swagelok® fittings.
S1, S2--Swagelok crosses, 1/4" stainless steel.
V1--Aminco high pressure valve, 1/4", 30,000 psi.
V2, V3, V4--High Pressure Equipment Company, Inc. high pressure valves, 1/8", 30,000 psi.
H1, H2, H3--High Pressure Equipment Company, Inc. high pressure couplings, 1/4", 1/8", 1/8", 30,000 psi.
RD--High Pressure Equipment Company, Inc. safety head with Baker rupture disk, 5250-5500 psi burst.
RV--Nupro adjustable relief valve, 3-50 psi cracking pressure range.

Stainless steel tubing was chosen for each connection depending upon gas flow, flexibility, and maximum pressure: 3/16" O.D. x 0.118" I.D. (Type 304, seamless) between the tank regulator (R1) and the input tee (S1); 1/4" O.D. x 0.120" I.D. (Type 304, welded) between S1 and W1, W2, and V1 and between W2 and S2; 1/4" O.D. x 0.083" I.D. (Type 304, cold drawn seamless) for the rest of the input lines to the compressor and the reservoir; 1/8" O.D. x 0.020" I.D. (Type 316, cold drawn seamless) for all other lines except for the one to the vacuum pump which is 1/4" O.D. copper refrigeration tubing.

Dashed lines on Figure 19 indicate actual physical separation of the components. Both the compressor and the reservoir are surrounded by a sectioned, protective housing (3/8" aluminum plate) with a blow-out door and a baffled exit for a blowout disk in line with the reservoir. The inside of

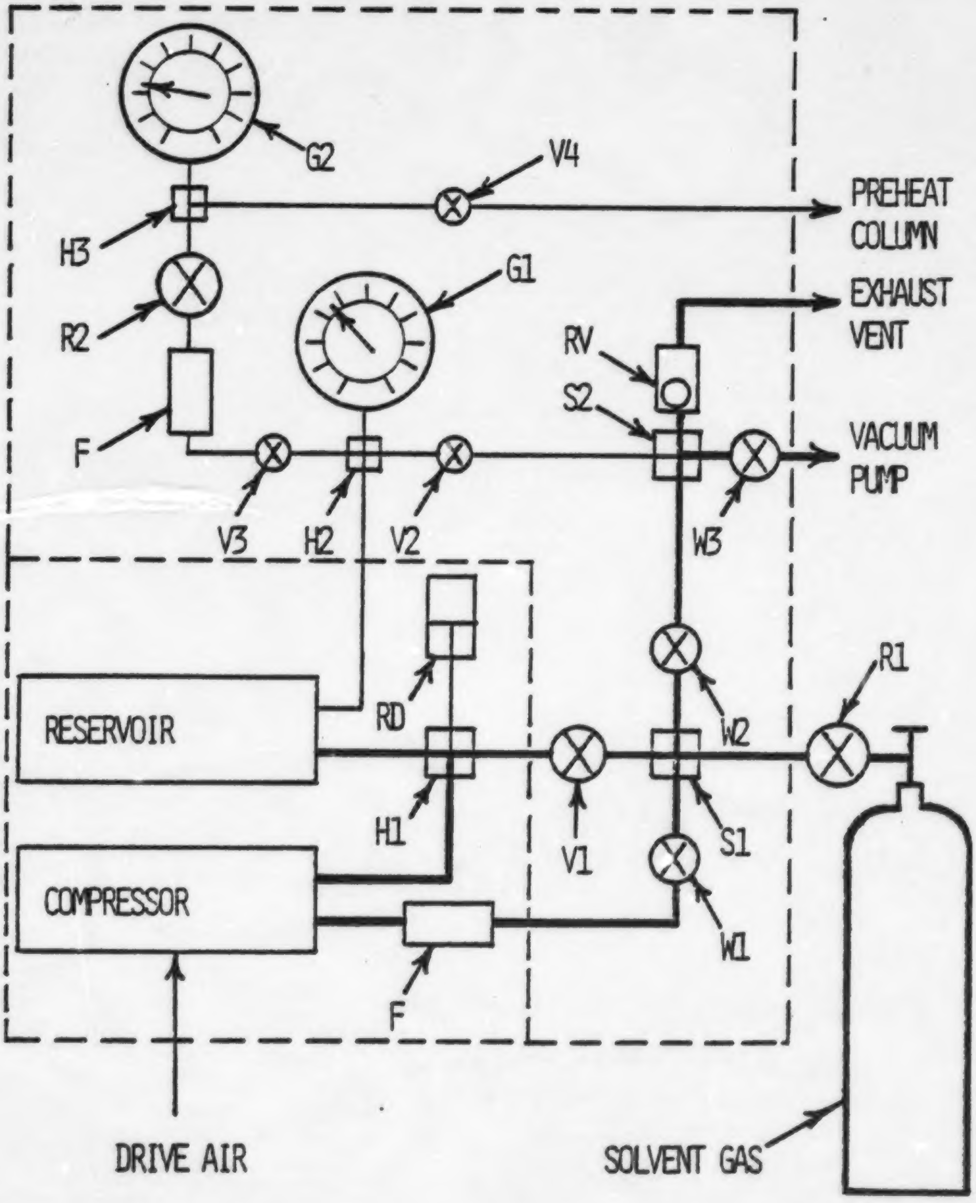
G2
V4
H3
PREHEAT COLUMN
G1
R2
EXHAUST VENT
RV
S2
F
VACUUM PUMP
V3
H2
V2
W3
RD
R1
RESERVOIR
W2
H1
V1
S1
COMPRESSOR
W1
F
DRIVE AIR
SOLVENT GAS

Figure 19. Dense gas supply.

the housing is fully lined with plywood and cardboard (8 cm deep about the reservoir and 1 cm deep about the compressor) to absorb explosion shocks and to help capture flying metal in case of component failure. Such failure is extremely unlikely since both of the two components are rated for operation to at least 2000 atm pressure--over seven times the pressure presently used and three times as high as any pressure planned in future operation. As just indicated, the high pressure tubing after the reservoir is mostly 3 mm O.D. and 0.51 mm I.D., of type 316 stainless steel; it also is rated for operation at 2000 atm. Some 3 mm O.D., 1.5 mm I.D. tubing has been used as a packed column; it is safe for pressures up to at least 1000 atm. In addition to the large safety factor in working pressure, such tubing has a very small internal volume so that the amount of stored energy in the dense gas outside the protective enclosure is too small to be a significant hazard. The remaining components are surrounded by a 3/4" plywood (styrofoam and felt insulated) compartment on top of the protective housing. The different sections of the protective housing and the regulator enclosure are each equipped with heaters, fans and thermoswitches with all electric leads protected to avoid electrical sparks; see Figure B5 in Appendix B for circuit control. The thermoswitches have been set to maintain 40°C in the supply system. A flexible, fiberglass heating tape (384 watt) is wrapped about the length of the reservoir for fast heat-up of this large piece of metal (about 45 kg); power to the heater is always turned off before admitting flammable gas to the reservoir. Chromel/alumel thermocouples monitor the reservoir and regulator chambers while thermomenters (±1°C) are occasionally used in the reservoir and compressor chambers.

About three meters of the 3 mm O.D. x 0.51 mm I.D. stainless steel tubing is used to connect the preheat column of the DGC to the regulator shut-off valve (V4, Figure 19). This gas supply line and the two parallel lines of a heating loop (1/4" copper refrigeration tubing) are enclosed in Insultube® (Hallstead and Mitchell) insulation for the whole distance with water from the DGC bath circulated through the loop.

3.4.6. Dense Gas Chromatograph

After experiments indicated that less volatile compounds dissolved by dense gases could be transported to the mass spectrometer detector via the molecular beam and that this process was highly sensitive to gas and nozzle tip temperatures, the thermostatting system and the chromatograph were designed.

A circulating water bath was chosen as the temperature control system because of the high heat capacity of water and the greater ease of circulating a liquid into almost inaccessible sections of the nozzle assembly. The design of the thermostatted dense gas chromatograph was made more difficult by the fact that in the molecular beam system, the skimmer remains stationary while the nozzle assembly is moved in and out by the separation-control nut. As described in the section on the molecular beam system, the bath manifold for the nozzle assembly is part of that assembly, so a flexible coupling between the bath and the nozzle assembly water manifold is necessary. Also the dense gas chromatograph is attached to the nozzle assembly by the 3 mm O.D. stainless steel inlet tubing; hence, nozzle movement requires dense gas chromatograph movement. This has been accomplished by mounting the dense gas chromatograph components on a movable frame suspended in the water bath.

The insulated bath (53 ℓ) was made from 1/8" thick aluminum plate with glued-on layers of 1" styrofoam and 1/8" masonite. Heat loss from the top surface is efficiently decreased by floating styrofoam packing noodles on the surface. This type of cover does not interfere with movement of the dense gas chromatograph panel and allows easy access to various components. The bath is equipped with two permanently installed 450 watt heaters and a third temporary heater for fast heating. A cooling coil of approximately 18 m of 1/4" copper refrigeration tubing mounted on a separate removable frame covers most of the bottom surface area and approximately 5 cm of the lower bath perimeter. Gaps between the loops allow easy water circulation. Cold tap water (approximately 13° C) with flow manually controlled by a Nupro valve (Series J, 1/4" Swagelok® fittings) has been used for cooling. The cooling coil can be used for rapid bath cooling or balanced against the heat input from circulating components as well as the heaters for constant temperature control. An adjustable mercury thermoregulator (Cole-Parmer Instruments Company) with a sensitivity of 0.005°C controls one of the permanent heaters in a part-time mode while the other heater is used in a full-time mode. Power output from each heater is controlled by a triac circuit presented in Figure B6, Appendix B. Since the scale of the thermoregulator is only calibrated in 1°C intervals, a precision thermometer from Brooklyn Thermometers (-10 to 55° C, in 0.1°C intervals) is used to adjust the set-point of the thermoregulator and to calibrate the bath chromel/alumel thermocouple (0.010" wire, silver brazed junction). The stirrer was assembled from a 1/8 HP Dayton motor and a heavy-duty stainless steel propeller from VWR Scientific. Thermostatted bath water is filtered through two layers of fine brass screen and then circulated as indicated in Figure 20. All circulating lines were insulated by Insultube® (Hallstead and Mitchell) or open cell packing foam. The components are as follows:

Rotary gear pump - Teel, close coupled to Dayton 1/3 HP motor, 2.2 gal/min free flow and 1.3 gal/min at 100 psi.
Centrifugal pump - Eastern Industries, Model number D-11, 1/8 HP motor, 8 gal/min free flow and 18 psi at shut-off.
C1 - Dense gas supply heating loop, 1/4" copper refrigeration tubing, about 6 m long.
C2 - Vacuum lock heating coil, 3/16" copper refrigeration tubing, about 1.5 m long.
F - filter - Two layers of fine brass screen (approximately 100 mesh) soldered over a brass shim stock (0.3 mm thick) box, 20 cm x 10 cm x 1 cm, having a 5/8" I.D. copper sweat fitting exit to the water pump intakes.
PG - water pressure gauge, U.S. Gauge, 0-100 psi.
RV - Adjustable pressure relief valve, Delavan, 5-300 psi, set at about 90 psi.
CV - Nupro valve, Series J, brass, 1/4" Swagelok® Fittings.
B - Flexible bellows, made from 1 3/8" I.D. x 1 19/32" O.D. x 4 1/2" long plastic corrugated vacuum cleaner hose. Approximately 5 turns of inner support wire was cut out on each end to permit the soft plastic to be clamped over the sealing gaskets made from rubber tubing on the bath flange (CS1) and nozzle manifold (CS2). The tubing

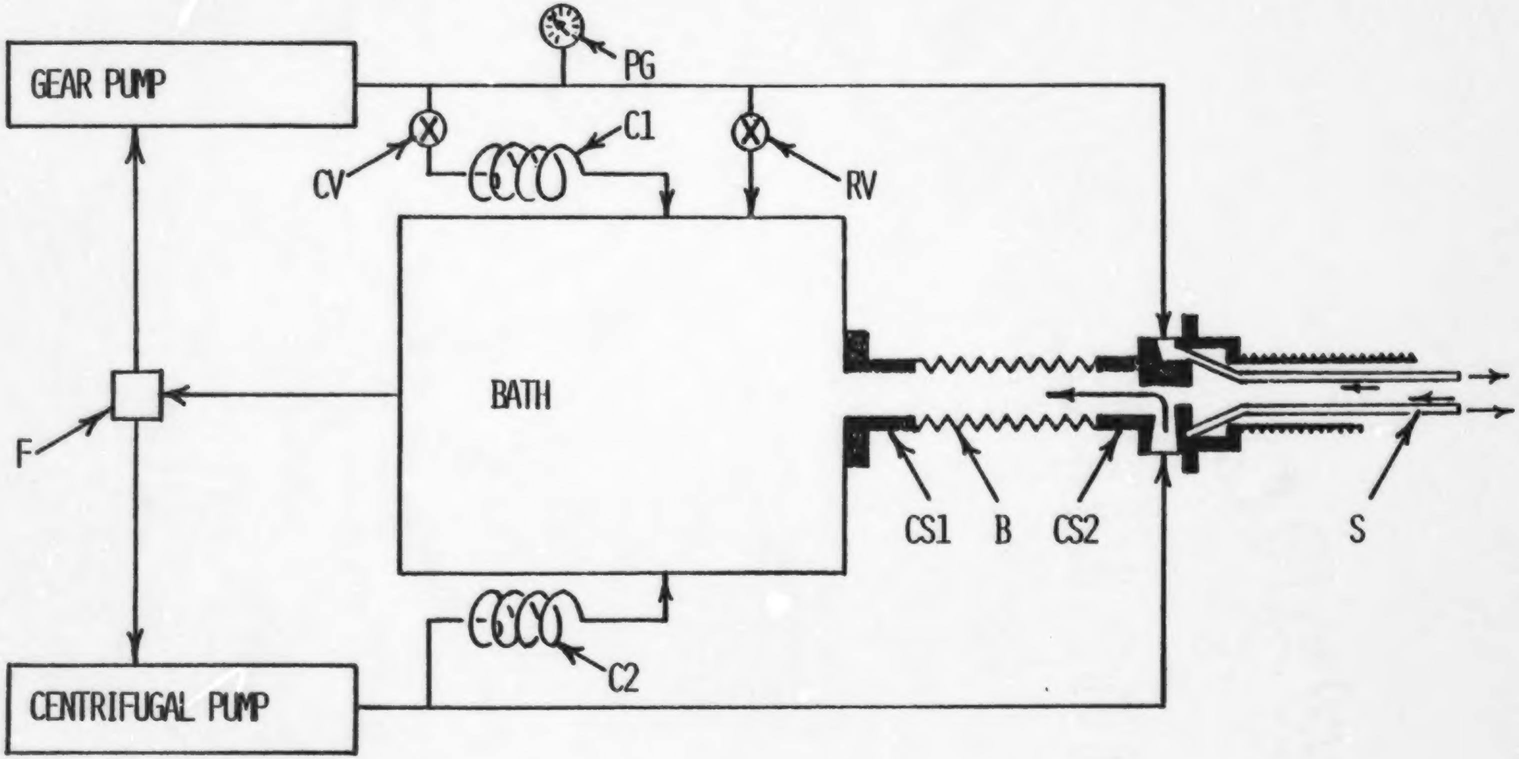
GEAR PUMP
PG
C1
CV
RV
BATH
F
CS1
B
CS2
S
C2
CENTRIFUGAL PUMP

Figure 20. Circulation of water from the DGC thermostatted bath.

can be stretched to about twice its normal compressed length.

S - 4 parallel lengths of stainless steel (syringe) tubing, 0.058" O.D. x 0.042" I.D. from Hamilton. The tubing extends almost to the water bath/vacuum o-ring seal (about 5 cm from the nozzle orifice) in the nozzle assembly (Figures 9 and 13) and surrounds the 3 mm O.D. nozzle assembly inlet tubing. High pressure water is pumped through these lengths and returns through the unoccupied volume in the 6.4 mm I.D. nozzle assembly barrel piece (Part E, Figure 9). The measured flow rate through the four parallel lengths with the Teel gear pump was 1.3 ℓ/min at 42 psig and 2.2 ℓ/min at 100 psig.

Figure 21 is the top view of the suspended mounting panel for the DGC. It is an open structure constructed of 1/8" thick aluminum plate. Two cross members with teflon pads (P) at each end to prevent aluminum-on-aluminum galling fit closely within the bath width to steady the panel during valve actuation. Three 3/8" aluminum rods, CS, extend from 15 cm above to 3 cm below the plane of the panel to support 23 cm I.D. columns, CO. Standard stainless steel flat washers can be used to separate the loops of the column for good water circulation. The stirrer shaft, ST, and the mercury thermoregulator, HG, are suspended from the top of the bath through the open center of the movable panel. The whole panel is suspended by three lengths of stainless steel wire rope, WR* (1/16" diameter, with 400 pound break strength), from a pulley/crank framework about 50 cm above the top of the bath. This system allows the depth of the panel in the bath to be adjusted for different configurations and also permits easy removal of the panel from the bath for servicing to it or other parts of the system. Several other bath components are indicated in Figure 21: the permanent heaters (H); the cooling coil support frame which was constructed from flat 1/8" aluminum plate (FR) and four vertical, threaded studs (FS); valves (V) for sample introduction and manipulation; the flexible bellows coupling (B); and again the nozzle assembly inlet tubing (T) which connects the DGC to the nozzle assembly of which it is a part.

The initial sample introduction system for solubility studies is shown in Figure 22. Dense gas was supplied to a stainless steel preheat column (PC), 3 m long x 3mm O.D. x 0.51 mm I.D. The sample chamber, SC, was a modified high pressure ball check valve from High Pressure Equipment Company, Inc. which contained a glass wool plug with deposited solute. The two high pressure needle valves, HP1 and HP2, and the high pressure tee, HPT, were all from High Pressure Equipment Company, Inc. and are the same type as those used in the dense gas supply assembly. The Aminco high pressure filter, HPF, is also like those used in the dense gas supply assembly. The valves and the tee accommodated 1/8" O.D. tubing while reducing couplings adapted the filter from the usual 1/4" fittings to 1/8" fittings. All connecting tubing was the same as that used in the preheat column. All components were mounted on the suspended panel immersed in the water bath. Obviously, the dead volume was quite large with this configuration; also, there was no way to bypass the sample chamber. Soon after positive solubility results were obtained, this configuration was replaced with an improved one. With the preheat column

---

*Donated by Mr. Bill Wall, Wire Corporation of America.

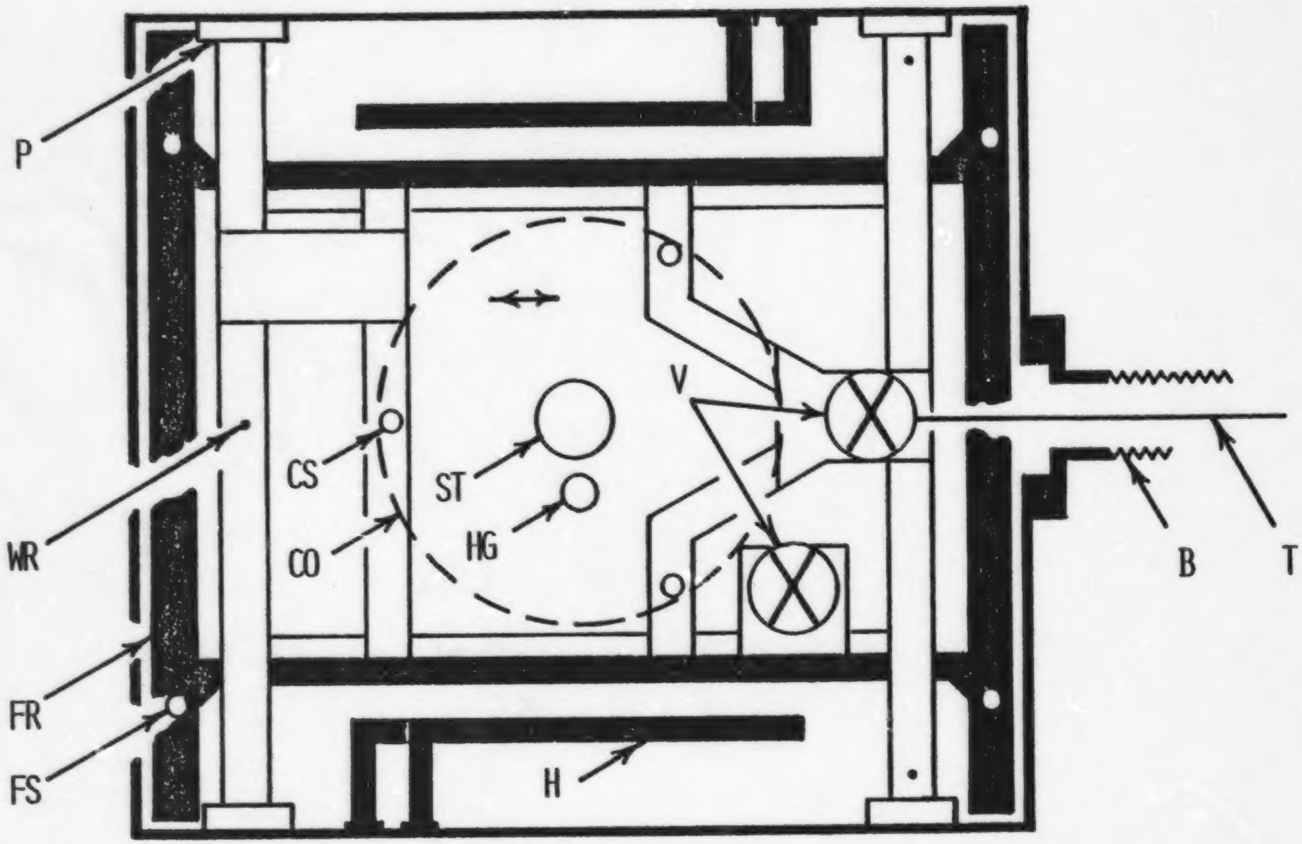
P
WR
FR
FS
CS
CO
ST
HG
V
H
B
T

Figure 21. Top view of the DGC suspended panel.

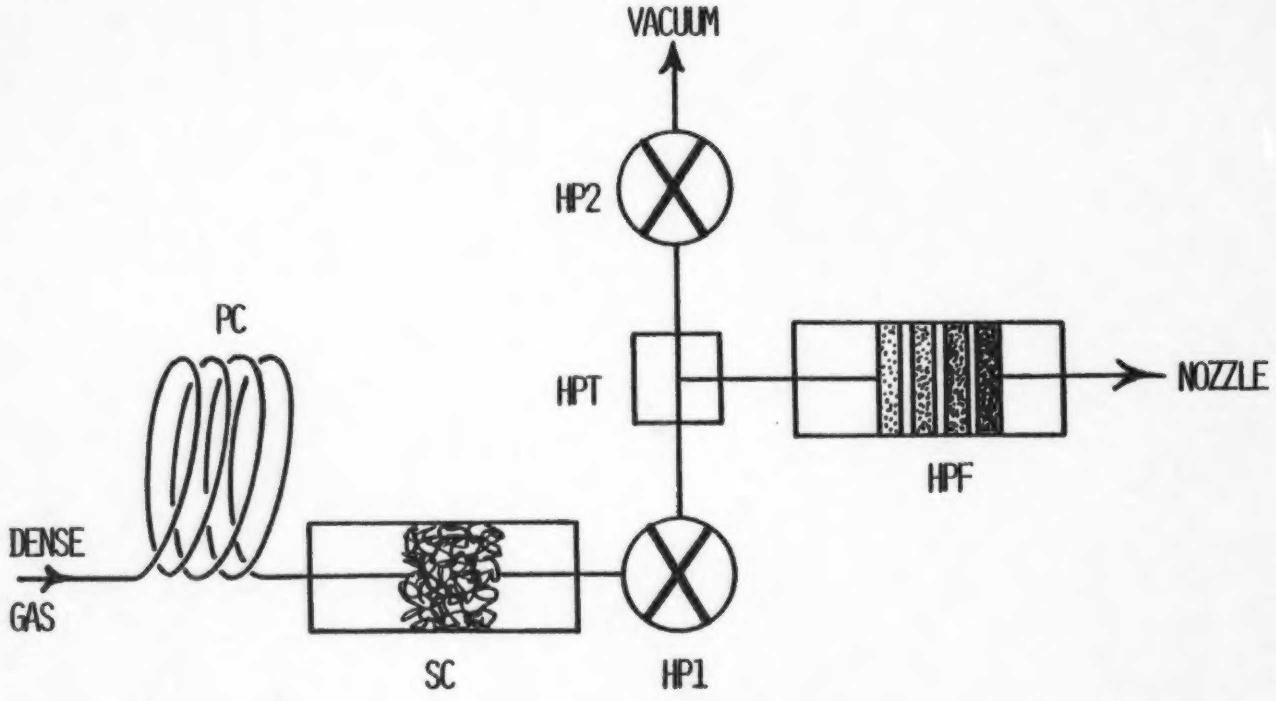
VACUUM
HP2
PC
HPT
NOZZLE
HPF
DENSE
GAS
SC
HP1

Figure 22. Initial sample introduction system.

omitted, this configuration is the same as that used before installation of the water bath at which time the supply gas from either gas cylinders or the dense gas supply was connected directly to an additional high pressure needle valve just upstream of the sample chamber.

Figure 23 from reference 140 is a schematic of the general design of the dense gas chromatograph used in most experiments. The zero dead volume filters, F, were supplied by Valco Instruments Company. The filter elements, press-fit in the coupling bodies, are 1/8" O.D. x 1/16" thick sintered stainless steel. The standard pore size supplied by the company is 5 µm. Figure 24a emphasizes the loss of filtering area that occurs when small bore tubing is used. A partial solution to the problem is shown in Figure 24b which illustrates the design used in most of the experiments. A drill (e.g., #42, 0.0935" D) or a centering drill was touched to the end of the machined tubing to make a conical depression. This conical volume which adds 1-2 µl dead volume significantly increases the exposed filter disk area. However, there is still loss of filtering area on the downstream side of the filter element where it is pushed firmly against the retaining inner diameter of the filter body. Hence, the original 0.038" I.D. of the filter body was drilled out to 0.082" I.D. as shown in Figure 24c. Since the dead volume as well as the area is increased by a factor of about 4.7 by enlarging the orifice, a better approach would have been to machine a conical depression in the retaining inner diameter as indicated by the dashed lines in Figure 24c. However, the larger straight-through hole facilitates removal of the press-fit filter elements for replacement. Filter elements in a variety of pore sizes, particularly 10, 5, 2, and 0.5 µm, are manufactured by Mott Metallurgical and can be easily press-fit in place. For each Valco fitting, the tubing end was carefully machined to have an end square to the centerline axis and burr-free. Often the machining, particularly the coning, smears a small diameter hole shut--especially the 0.15 mm (0.006") I.D. stainless steel tubing. Grinding with 600 grit carborundum opens a square end. Treatment with aqua regia deburrs the square end and opens and deburrs the conical end.

In Figure 23 the filter used on the dense gas inlet was 5 µm and the filter between the column, A, and three-way shut-off valve (E) varied in pore size and number of elements depending upon the column used. Between the three-way valve and the nozzle assembly where the requirements were the strictest, a 2 µm filter followed by another filter containing two sandwiched 0.5 µm elements was used.

Valves B and E (Figure 23) are HPLC valves (Valco Instruments Company). Both were ordered with the high pressure option and are rated to 7000 psig (liquid) up to 100 °C. Valve E is a three-port, three-position switching valve that was specially machined by the manufacturer for this work so that it would connect any two of the three ports (vs. the typical two-position, two-pair selection). Valve B is a zero-dead-volume sampling valve which introduces a sample without interruption of the solvent flow. For clarity the valve in the load and inject positions is shown in Figure 25, a diagram similar to the manufacturer's. With this configuration the sample is pushed out of the same sample loop port into which it is loaded and is not pushed through the entire sample loop.

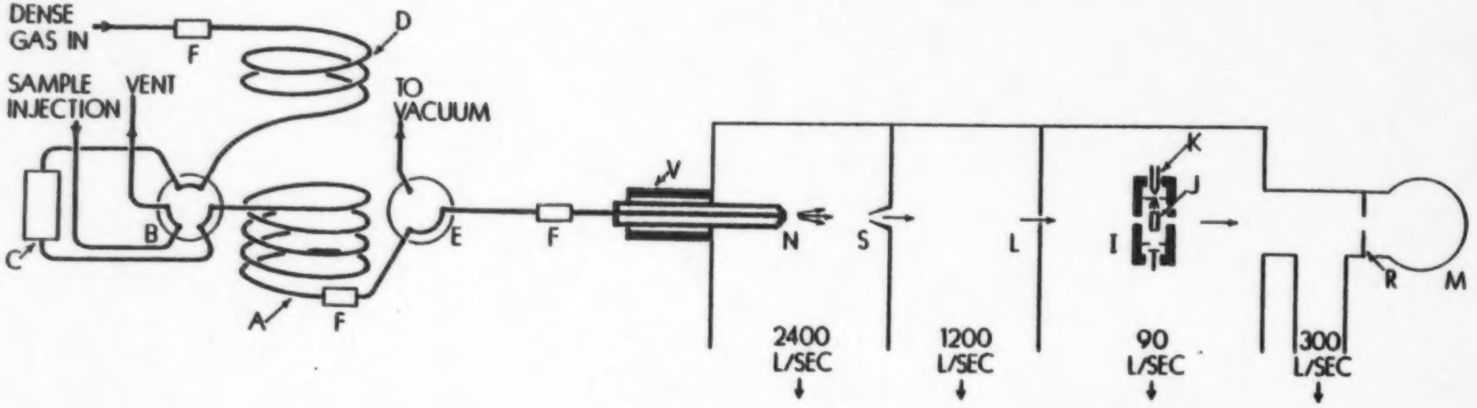
DENSE
GAS IN
F
D
SAMPLE
INJECTION
VENT
TO
VACUUM
C
B
A
F
E
F
V
N
S
L
K
J
I
R
M
2400
L/SEC
1200
L/SEC
90
L/SEC
300
L/SEC

Figure 23. General design of the DGC/MS (Reprinted with permission from Analytical Chemistry 50, 1703 (1978). Copyright by the American Chemical Society.)

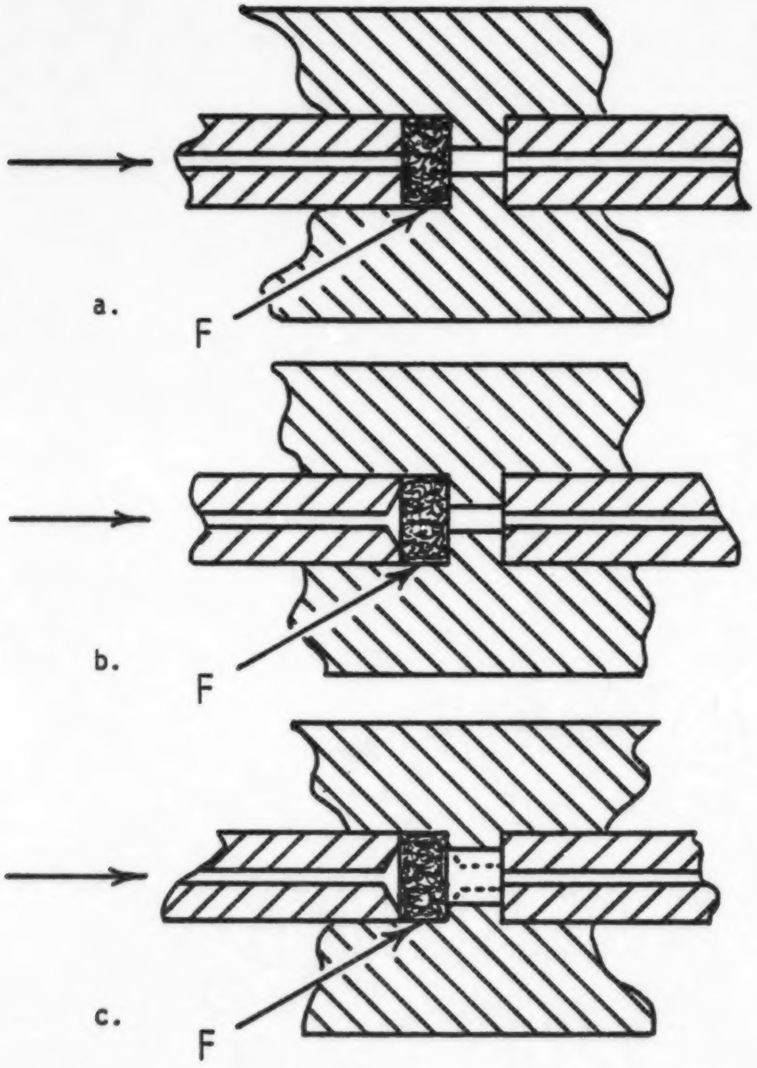

Figure 24. Comparison of useful filter areas, 3 mm O.D. X 0.5 mm I.D. tubing.

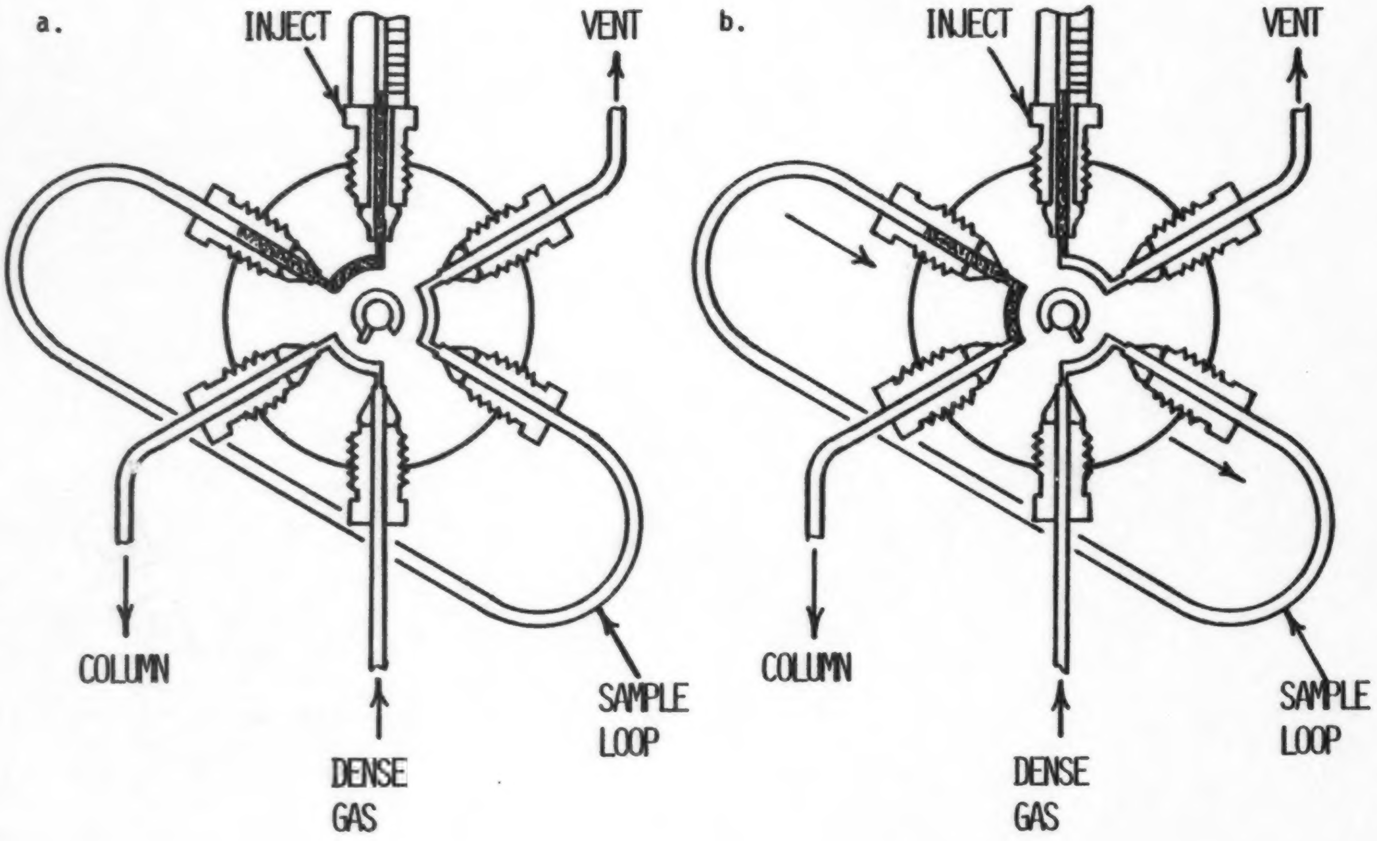
a.
INJECT
VENT
COLUMN
DENSE GAS
SAMPLE LOOP
b.
INJECT
VENT
COLUMN
DENSE GAS
SAMPLE LOOP

Figure 25. Operation of the HPLC sampling valve.
a. Load sample into sample loop with uninterrupted column flow.
b. Inject sample into fluid moving phase.

The sample loop can be easily changed to permit experimentation with different internal volume loops and various configurations. Three different sample loop/chambers, shown in Figure 26, have been tried thus far. Design "a" is simply a modified ball check valve (CV) from High Pressure Equipment Company, Inc., such as that used in part of the dense gas Ph.D. thesis work of Bowman.[97] In his work and earlier stages of this work, sample solutions were deposited on a plug of glass wool, the solvent was evaporated, and the glass wool plug was placed in the chamber. When this chamber was incorporated as part of the sampling loop of the HPLC valve, a 2 μm sintered stainless steel Nupro filter element (SF) was placed as shown in the figure so that the sample solution would be deposited on the large surface area of the filter element. The internal volume of this sample chamber was estimated to be close to 1 ml. The connecting tubing, T1, was 3 mm O.D. x 0.51 mm I.D. Sample chamber "b" was designed to decrease dead volume while providing a large surface area. A 10 cm length, T2 of 3 mm O.D. x 1.5 mm I.D. stainless steel tubing (Type 316, cold drawn seamless) was packed with 140/170 mesh regular glass beads (GB) from Analabs, Inc. The beads were not silanized before use. Two Valco zero-dead volume filter couplings with 5 μm sintered stainless steel filter elements (VF) contained the beads. The two lengths of connecting tubing, T1, were the same as in chamber design "a". Sample chamber "c" was devised to eliminate the glass beads. It is simply a 23 cm long loop, T3, of 3 mm O.D. x 1.0 mm I.D. stainless steel tubing (Type 321, cold drawn seamless). Aqua regia was used to etch the inside surface (RF) of the tubing to provide a larger surface area for sample deposition; the etched surface was passivated with concentrated nitric acid.

Since the sampling valve is immersed about 13 cm from the water surface, it was necessary to make an extension for the injection port. At first a 15 cm length of 0.51 mm I.D. stainless steel tubing was used; later, it was changed to 0.15 mm I.D. tubing of the same length. The upper end is swaged into a Valco reducing coupling, the other end of which accepts the fill-port fitting assembly that usually threads directly into the valve body.

This extension to the reducing coupling is shown in Figure 27 where ET is the 0.15 mm I.D. x 3 mm O.D. extension tubing to the sampling valve (SV) and FP designates that part of the reducing coupling which accepts the fill-port fitting assembly. Figure 27 also shows the modified inject/vent/sample-loop system used in later experiments to permit pressurization of the sample loop to the dense gas pressure before turning the loop in-line. Valves HP1 and HP2 are 1/8" high pressure needle valves from High Pressure Equipment Company, Inc., as described previously. Stainless steel Swagelok® tees were used at the indicated junctions. The dense gas from the preheat column is filtered through a 5 μm filter (Valco Instruments Company) before entering the valve system. Pressurization is accomplished by substituting a plug for the fill-port fitting assembly after injection of the sample solution into the sample loop (SL) and then admitting the dense gas to the sample loop via the high pressure valve, HP1, with HP2 closed.

Figure 28 is a view of the latest DGC configuration mounted on the suspended panel in the thermostatting bath with the following parts: 1-the insulated dense gas supply line which is coiled to absorb nozzle motion, 2-preheat column, 3-typical chromatograph column, 4 and 5-HPLC valves, 6-high

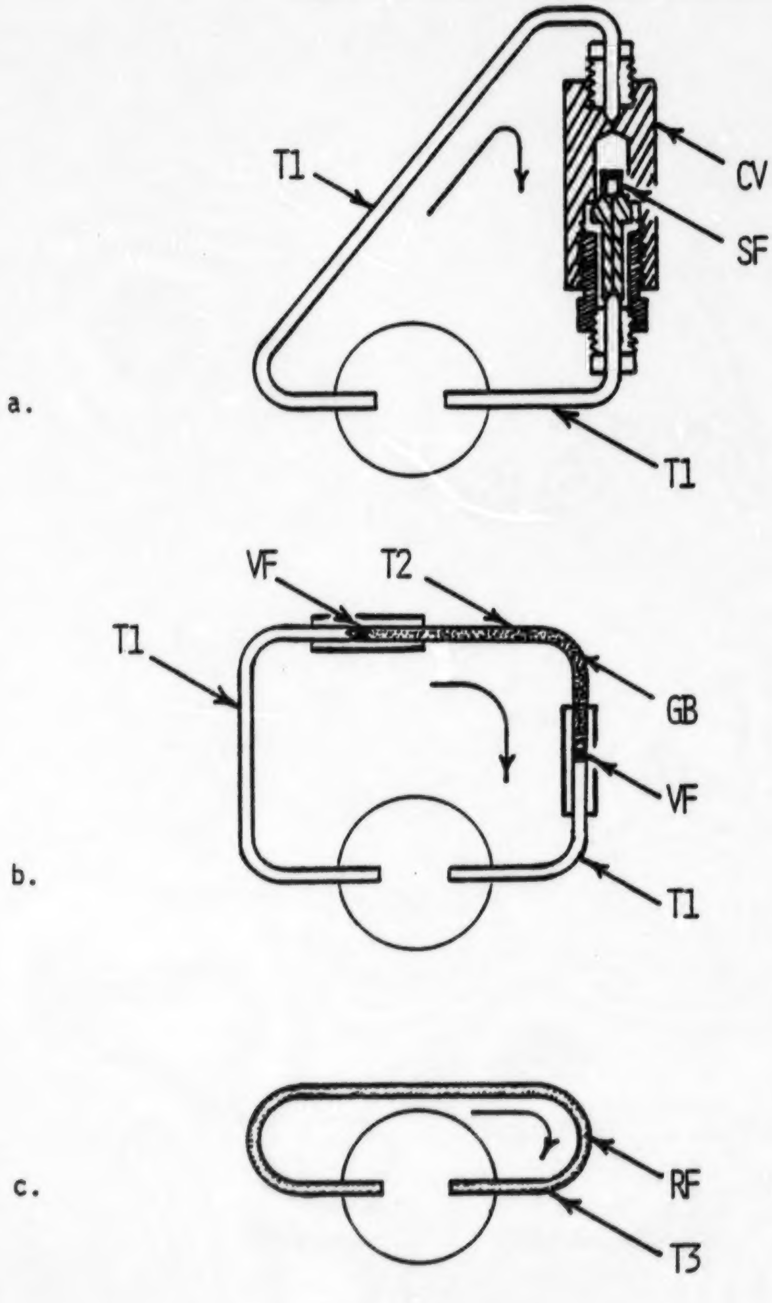
T1
CV
SF
a.
T1
VF
T2
T1
GB
VF
b.
T1
c.
RF
T3

Figure 26. Sample loop configurations studied in this work.

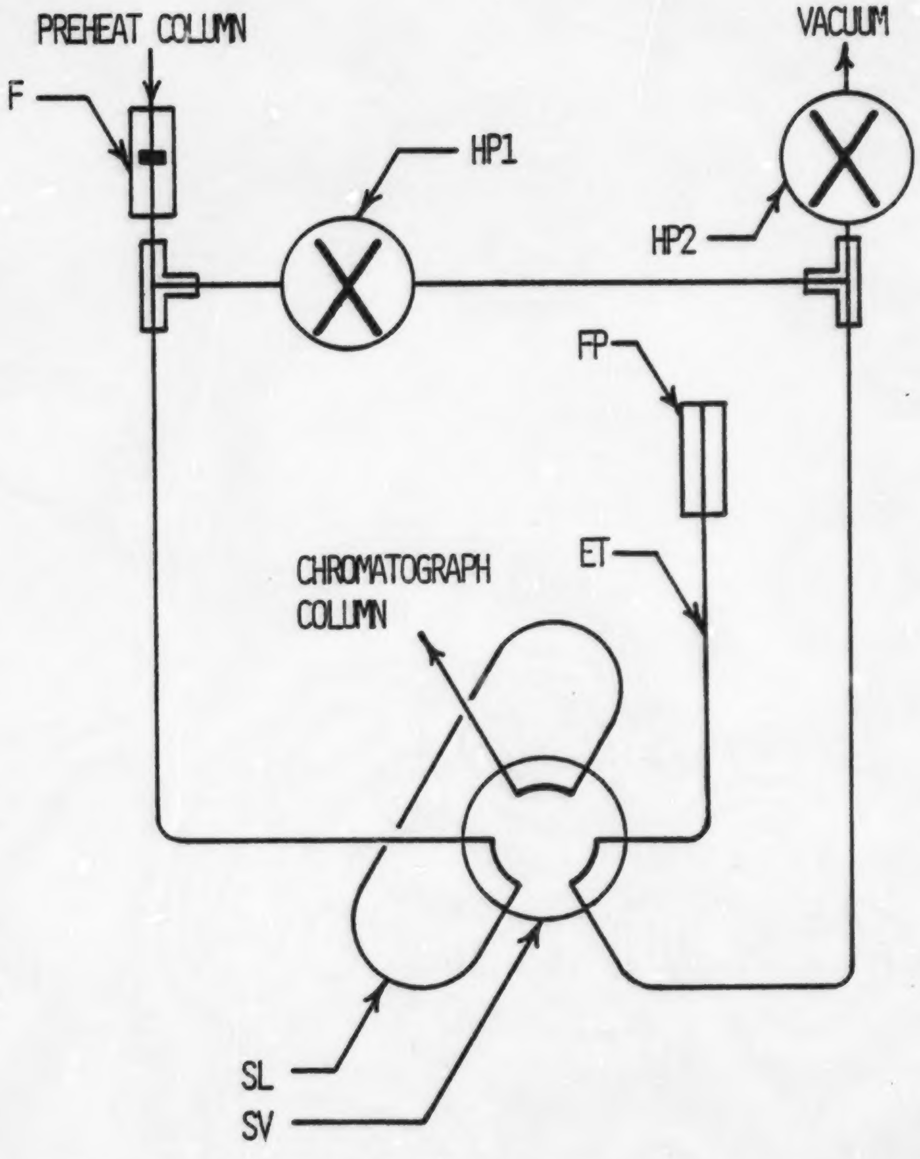
PREHEAT COLUMN
VACUUM
F
HP1
HP2
FP
ET
CHROMATOGRAPH COLUMN
SL
SV

Figure 27. Assembly for sample loop pressurization.

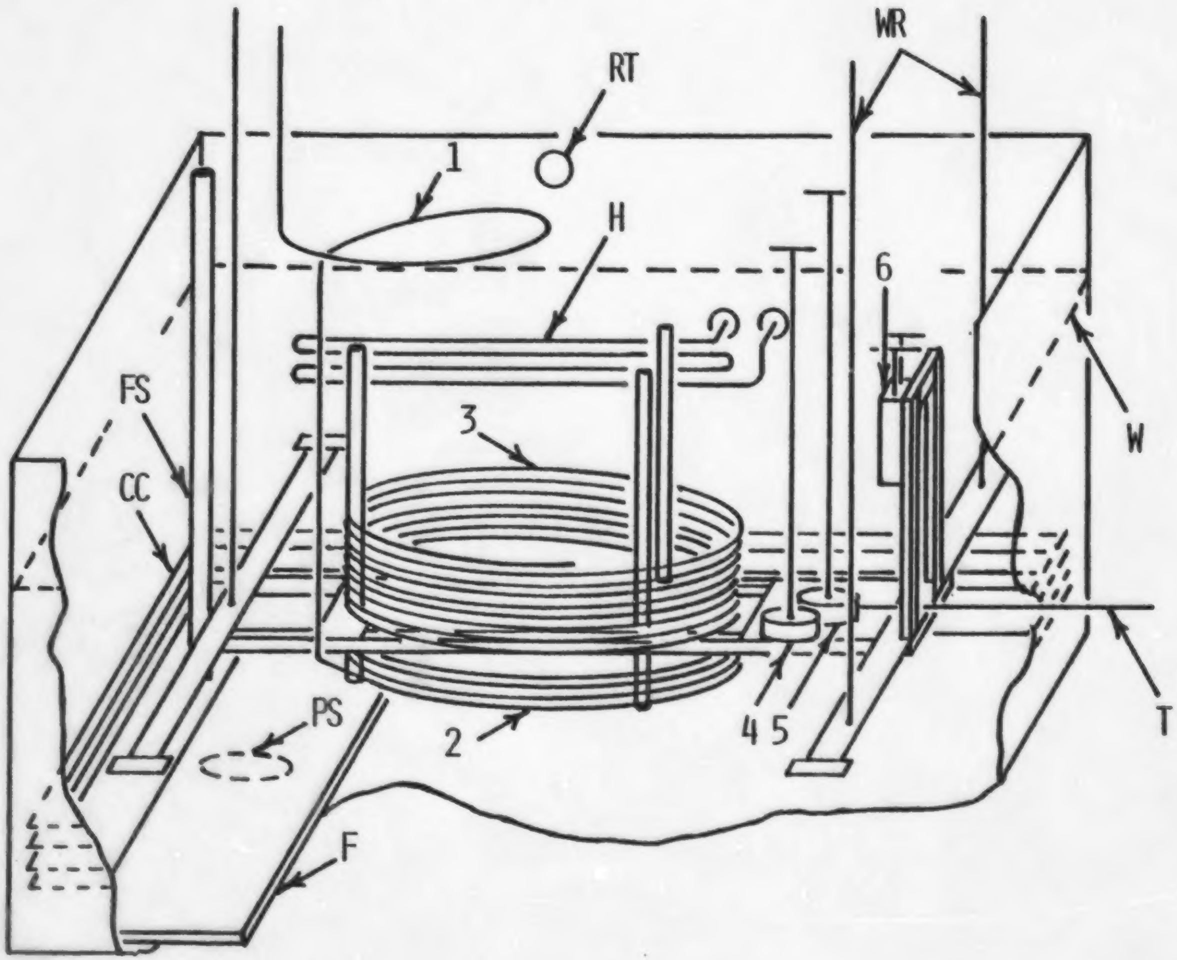
WR
RT
1
H
6
FS
W
3
CC
PS
2
4
5
T
F

Figure 28. Typical placement of DGC components within the water bath.

pressure needle valve assembly, and T, the nozzle assembly inlet tubing (the HPLC filters between parts 5 and T are not shown). Several components previously discussed are also shown in this diagram: the large area brass screen filter (F) with its "hidden" exit (PS) which supplies both the centrifugal and gear pumps, part of the copper cooling coil (CC) wrapped around the vertical stud (FS) of its support frame, a permanent heater (H), the return orifice (RT) for the two external heating coils and the gear pump pressure relief valve, the three lengths of stainless steel wire rope (WR) by which the panel is suspended, and finally the typical water level (W) when the bath is in operation.

In addition to the various sample loops and injection procedures studied, four different chromatograph columns were made and tested.

1. Capillary - the 6 m long capillary column was made from 3 mm O.D. x 0.51 mm I.D. stainless steel tubing (Type 316, cold drawn seamless). For later experiments it was modified by etching the inner surface with aqua regia and passivating with nitric acid. Between the column exit end and the three-way shut-off valve was one filter coupling containing sandwiched 5 μm/2 μm filter elements.

2. Packed column - the stainless steel (Type 321, cold drawn seamless) column, 1.5 m long x 3 mm O.D. x 1 mm I.D. was packed with Permaphase ODS® (DuPont, octadecyl bonded groups, 20-37 μm particles). Each end was capped with Valco 5 μm filters such that the packing touched each filter element. Coupling lengths made from 3 mm O.D. x 0.5 mm I.D. tubing connected the filter capped ends to the sampling valve (11 cm long) and the three-way shut-off valve (7 cm long).

3. Packed column - This column (stainless steel, Type 316, cold drawn seamless) was also packed with Permaphase ODS; however, the column dimensions were changed to 50 cm long x 3 mm O.D. x 1.5 mm I.D. The same size capping filters and coupling lengths were used for this column as for column 2.

4. Packed column - Column 3 was repacked with fresh Permaphase ODS and a 5.5 cm long precolumn, also packed with Permaphase ODS, was added. A 5 μm Valco filter was placed between the precolumn and column to contain the precolumn packing for easy precolumn interchange and conditioning. For this modified column the coupling lengths were made from 3 mm O.D. x 0.15 mm I.D. stainless steel tubing (Type 316) and were of comparable lengths to those used with columns 2 and 3.

The design of the DGC/MS instrument has been presented in detail in this subsection. The next subsection describes the experimental results which contributed to the development of the instrument.

3.5 EXPERIMENTAL PROCEDURES AND RESULTS

Since the development of the DGC/MS instrument was a stepwise procedure requiring experimentation at each step to substantiate its feasibility and to indicate the direction of further work, the experimental procedures and results will be presented together in chronological order. The development can be divided into five areas: 1) formation and detection of the supersonic molecular beam, 2) major improvements and additions to the initial design, 3) initial solute and solvent gas cluster experiments, 4) DGC construction, and 5) chromatographic survey. A brief summary of the important observations and conclusions of these five parts is given in subsection 3.5.6 and future improvements to and experiments with the DGC/MS instrument are outlined in subsection 3.5.7.

3.5.1. Formation and Detection of the Supersonic Molecular Beam

In the experiments with the first trial design, 5 and 10 μm diameter nozzle pinholes had been routinely used. At that time no filtering and assembling precautions were used. The pinholes were punched out of shim stock or foil disks into the cylindrical pinhole holders (identical to Part C, Figure 9) using a simple jig designed upon the assumption that the laser drilled pinholes were very accurately centered in the disk. The same procedure was used in the first experiments with the present design.

However, the success in handling and mounting the pinholes in this manner was short-lived and not unexpectedly so. Problems with pinhole alignment and plugging arose early in the experiments with the present instrument. Measurements made with a moving stage microscope and a dial indicator showed that while some pinholes were well-centered, others were off-center by as much as 0.010" (0.3 mm). In one case the off-center error plus the punching error led to the pinhole being covered by the edge of the pinhole holder inner diameter, so that the nozzle orifice was blocked. Frequent plugging of the pinhole with dust particles during assembly or operation emphasized the need for much care in handling the pinholes. Later experiments showed that precise finish-machining and cleaning of the pinhole holder and the nozzle inlet tubing (Parts C and T, Figure 9) were necessary. An aligning punch jig that can be used for different supplied geometries of the shim stock containing the pinhole was designed. A diagram of it, the punching and assembly procedures, and comments about the machining of the pinhole holder and the nozzle assembly inlet tubing are given in Appendix C which also contains a subsection detailing the experimental volumetric flow rates through pinholes of different diameters.

The first experiments, conducted to establish the formation of a molecular beam by the presence of the characteristic beam-intensity vs. nozzle-skimmer separation profile, were very disappointing. When helium (10 to 48 atm, room temperature) was expanded through a 5 μm nozzle diameter, it was not detected at all by the mass spectrometer. Subsequent troubleshooting led to the discovery that after the mass spectrometer electronics warmed up, the minimum current through the magnet coil was too high to allow scanning through m/e 4. Experiments with carbon dioxide (55 atm, room temperature) and nitrogen (11 atm, room temperature) also failed to show the expected beam intensity behavior--both with the mass spectrometer and the molecular beam detector ionization gauge. The problem was traced to broken brazed joints on Part H of the nozzle assembly in Figure 9 causing the expanding jet to be directed away from the nozzle-skimmer centerline. Both the electronics and the mechanical problems were easily remedied without lengthy delay.

Because of the difficulties with detecting jet gases and problems with plugging nozzle orifices (5 μm), it was decided to approach the experiments from the other extreme--i.e., large, not small, nozzle diameters. A 100 μm (0.004") diameter pinhole was made in stainless shim stock (0.001 to 0.002" thick) with a sharp sewing needle point. The results for 2 atm CO_2 expanding through the 100 μm nozzle diameter are shown in Figure 29 which compares region pressure vs. nozzle-skimmer separation relations for four regions: nozzle-skimmer, skimmer-collimator, ion source, and molecular beam detector/trap. Of all the pressure gauges, only the molecular beam detector ionization gauge is on the molecular beam centerline. The ionization gauge pressure does show the "correct" beam intensity--nozzle skimmer separation profile.

Further data from this experiment is shown in Figure 30 in which graph c compares the ion gauge intensity to the mass spectrometer signal for m/e 44. Here the mass spectrometer appears to be as sensitive a detector for the CO_2 beam as the ion gauge. Increasing the CO_2 pressure to 3 atm (graph d) results in a noisy ionization gauge signal and a less well-defined maximum of the m/e 44 intensity. Still, for these two pressures of CO_2, one can say that the mass spectrometer is slightly more sensitive than the ionization gauge. However, for 2 and 3 atm of N_2 (a and b, Figure 30), the ion gauge is a better detector.

An argument to explain these inconsistent results can be made in terms of attenuation from high expansion chamber background pressure, much larger cluster formation for CO_2 than N_2, and scattering and ionization cross sections in the mass spectrometer ion source; however, such an argument is lengthy and of doubtful validity. The important information in Figure 30 is that a molecular beam was being formed and that the mass spectrometer response was less than it should have been according to the molecular beam detector (ionization gauge).

While it seemed unlikely that the small amount of directed translational energy possessed by the beam (1.5 RT to 3.5 RT, or 0.04 to 0.09 eV for N_2 at 300°K, depending upon the extent of rotational and vibrational relaxation in the expansion) would affect ion collection, we could not exclude the possibility that the molecules might be too energetic to be turned orthogonal to their direction of motion and properly focused on the ion source exit slit for collection. Hence, the two electrodes discussed in subsection 3.4.4 were added to the source at the same time other changes were made in the beam system.

3.5.2. Improvements

While the earlier data indicated that a molecular beam could be generated with this nozzle-skimmer-collimator system, it was often difficult to understand the behavior during operation. Therefore, several design additions were made: two focusing electrodes to the ion source, a variable entrance aperture to the molecular beam detector ionization gauge, a current detector, and heaters and thermocouples in the beam generating system.

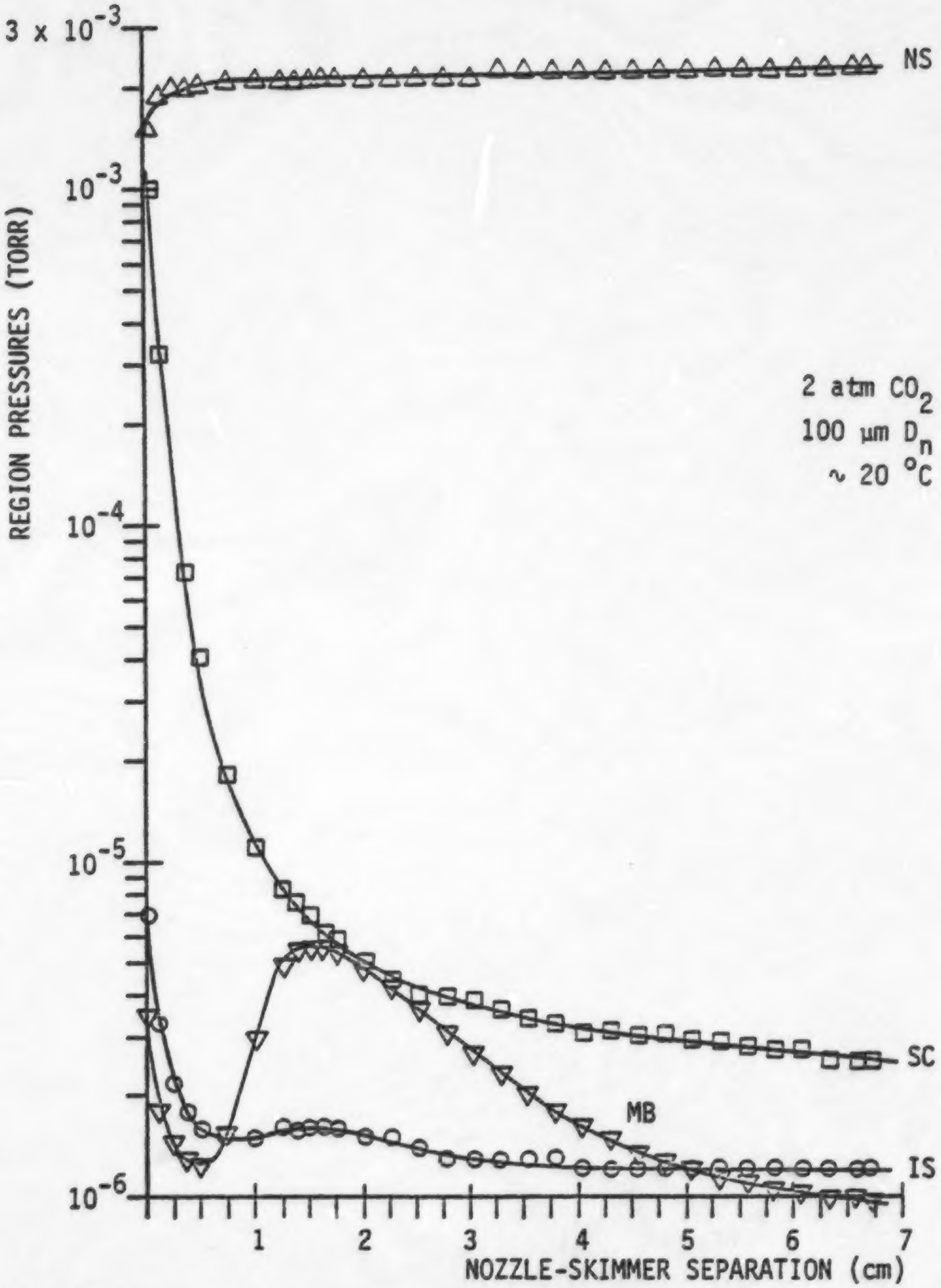

Figure 29. Region pressure vs. nozzle-skimmer separation for four regions of the molecular beam-mass spectrometer system: NS--nozzle-skimmer, SC--skimmer-collimator, IS--mass spectrometer ion source, and MB--molecular beam detector ion gauge.

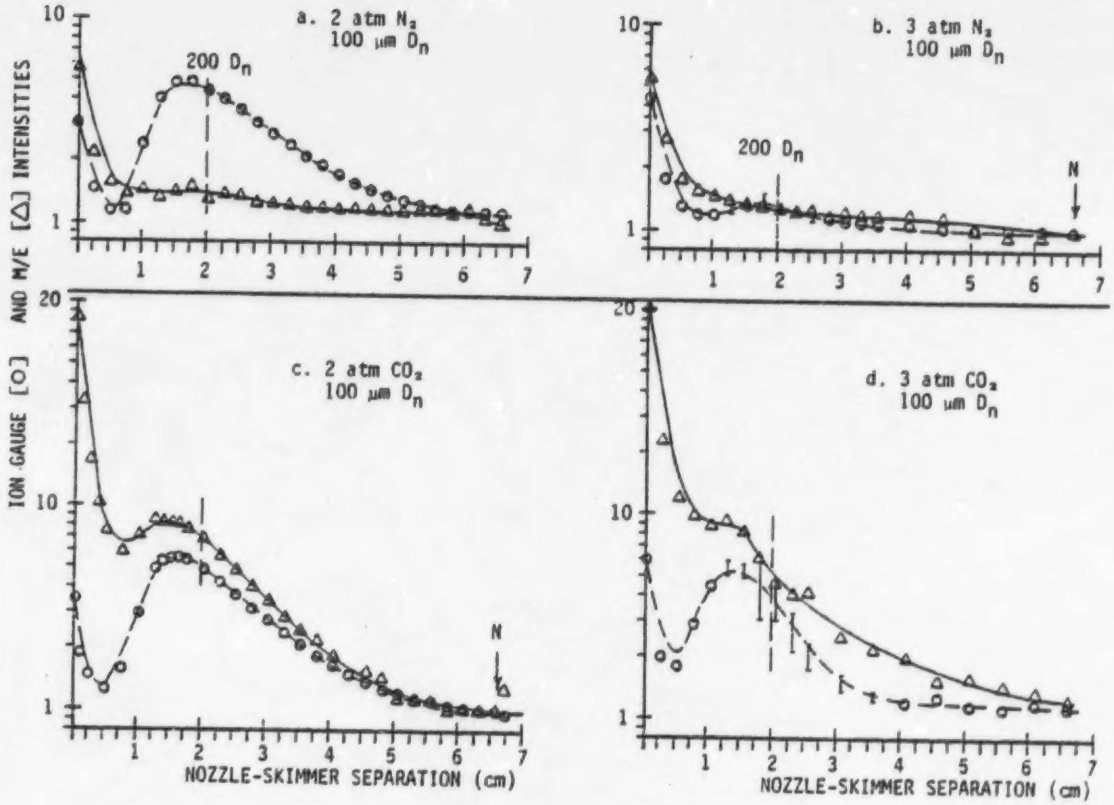

Figure 30. Molecular beam intensity vs. nozzle-skimmer separation for N_2 and CO_2 at 2 atm and 3 atm with the original ion source configuration using a 100 μm nozzle diameter.

△ M/E 28 for N_2 and M/E 44 for CO_2

○ Ionization gauge pressure

All curves in a and b normalized to point N in b and all curves in c and d normalized to point N in c.

Electrode addition. The original ion source of the Perkin-Elmer Model 270 mass spectrometer relied solely on field penetration to focus and accelerate ions into the electrostatic sector. As previously discussed, it was thought that perhaps molecular beam ions had too much translational energy along the molecular beam axis to be properly focused on the source exit slit; therefore, the two electrodes described in detail in subsection 3.3.4 were added.

The tuning procedure was also described in that subsection. As indicated, one method of measuring the ion current is by the Total Ion Current (TIC) electrode (16, Figure 6), placed between the electric and magnetic sectors. It was found that it was better to set the magnet voltage to focus the desired mass on the electron multiplier entrance slit and measure the multiplier amplifier output voltage with either a voltmeter or with an oscilloscope. Tuning for the maximum TIC should correspond very closely to tuning for the maximum multiplier output for all masses. Experimentally, this is true for background molecules but not for molecular beam molecules. Maximizing response to beam molecules can reduce the TIC and the response to background molecules by a factor of 10. Appreciable potentials always were required on the added electrodes to maximize response to beam species. Study of burn marks in the ion source and the entrance slit to the electrostatic sector indicated that the molecular beam is so well collimated (~0.3mm wide x 2.84 mm tall) that ions from it should pass cleanly through the square aperture (4.72 mm x 4.72 mm) in the TIC electrode.*

Tuning operations have often produced two sets of potential values for which there is a maximum in the monitored m/e, but one of the maxima is larger. In those experiments for which there were two maxima for a particular m/e, the larger maximum for the beam species corresponded to a greater degree of discrimination against background species.

Generally, larger potentials on the wedge than on the back plate were required for beam species maximization. The tuning procedure was strictly empirical; maximizing electrode potentials varied with the gas used and often the particular fragment ion focused upon even when stagnation conditions and nozzle orifices were identical. The tuning procedure is made easier if the ion has a low background intensity--e.g., one should maximize m/e 26 or 27 for ethylene instead of the parent m/e 28 because of the high m/e 28 background. The potentials required on the added electrodes were much larger than would be expected if they were merely compensating for beam kinetic energy. We have not been able to interpret the values in any reasonable way.

The brief inquiry into the dependence of the beam species signal upon ion source potential settings included experiments with CO_2, Ar, He, C_2H_4 and C_3H_8 with 100 and 25 μm nozzle diameters at pressures up to 18 atm, all at room temperature. Typical results are presented in Figure 31. Here, W refers to the wedge electrode and B to the separated back plate electrode.

---

*The beam dimensions given are estimated from burn marks on the source exit slit. Burn marks in the electrostatic sector entrance slit after both normal operation and beam operation in a variety of experiments give dimensions of 1.6 mm wide x 3.63 mm tall. Since the molecular beam entrance hole diameter to the ion source is 2.5 mm, the beam height of 2.84 mm is reasonable.

There are differences between the mass peak intensity curves and the ion gauge intensity curves and these differences were present to some extent in all of the studies made at the ion source potential settings maximizing the molecular beam intensity. The minimum at small nozzle-skimmer separations is much lower for the pressure measurement than for the mass measurement. Also, the increase in beam intensity for even smaller separations (re-expansion through the skimmer) is more rapid for the mass detection and often exceeds the intensity at the profile maximum. Finally, the ion gauge intensity at larger separations falls off less rapidly from the maximum than the m/e intensity.

The results as the separation is decreased from the value at the profile maximum can be interpreted in terms of first, beam attenuation; then, beam destruction; and finally, formation of less directed secondary flux as the pressure builds up at the skimmer opening. The mass spectrometer will be far more sensitive than the ion gauge to this secondary flux. At larger nozzle-skimmer separations, the less rapid fall-off from maximum intensity shown by the ion gauge readings might be due to increased beam entrainment of nozzle-skimmer region background molecules (i.e., N_2, pump oil) to which the mass spectrometer is not sensitive when monitoring a selected m/e.

Current detector. At the same time the new electrodes were being designed and installed, it was decided to add an electrode (Part 20, Figure 6) beyond the molecular beam exit from the ion source. The reasoning was as follows: if beam molecules are ionized but have too much momentum to be accelerated into the electrostatic sector and leave the ion source with unionized beam molecules, a current sensing electrode placed directly in their path should detect them. The current ranges are 10^{-11}, 10^{-10}, and 10^{-9} amp full scale. The electrode senses a large electron current from the ionization gauge, so that gauge is not operated when the current detector is inline. Since the installation of the electrode and its circuitry, very little work has been done with it other than to note that (1) with zero ion source and accelerating potentials, the ion current varied with nozzle-skimmer distance in similar fashion to the ionization gauge pressure; (2) with zero accelerating potential, the wedge and back plate potentials had major effects upon the ion current; and (3) no ions were detectable with the ion accelerating voltage on.

Since the two added electrodes were so effective in extracting the ionized molecular beam species and since the study of ion optics was not the main concern of this project, studies with the current detector were not pursued. However, it would be desirable in future work to characterize beam flux more completely using this available parameter.

Computer calculations for ion source configurations. Because so much effort had been expended to focus ionized beam species and increase the mass spectrometer sensitivity, a short theoretical diversion was made with the hope of gaining even more control and understanding of the beam ionization. When the electrodes were designed, hand calculations for the electric field poten-

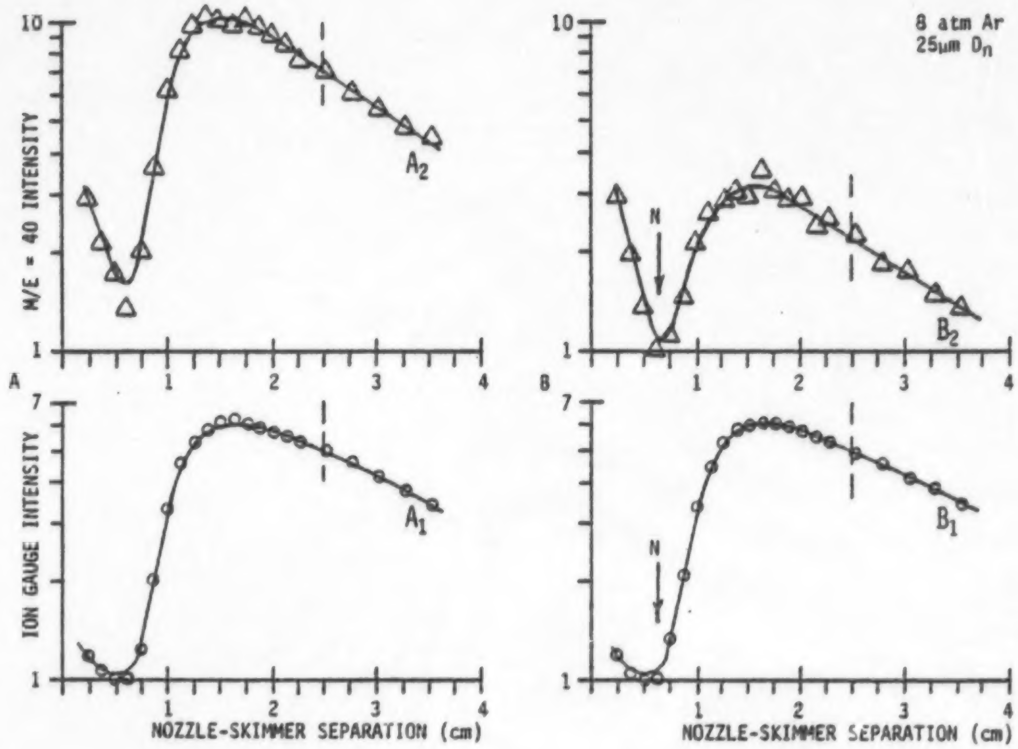

Figure 31. Molecular beam intensity vs. nozzle-skimmer separation for two potential settings of the ion source:

A. W = chamber + 63 V and B = chamber + 29 V to maximize m/e 40

B. W and B both at chamber potential.

Vertical dashed lines are at 1000 nozzle diameters. Curves A_2 and B_2 are normalized to point N on B_2 and curves A_1 and B_1 are normalized to point N on B_1.

Conditions: 8 atm argon, 25 μm nozzle diameter, room temperature.

tials had been made. These were necessarily crude. After the electrodes had been installed and experiments were underway, a computer program to construct field potentials and diagram ion trajectories in the field was given to us.* (The original purpose of the program was to aid in the design of ion optics and it has been successfully applied to such a problem.[141])

Figure 32 shows equipotentials in the original ion source and the trajectories of ions (molecular weight 40) with an initial energy in the molecular beam direction of 0.03 eV ionized at various points in the source. Figure 33 depicts the added electrodes with the wedge 63 V more positive than chamber and the back plate 29 V more positive than chamber. Molecules (molecular weight 40) of 0.03 eV energy in the molecular beam direction are again ionized at various points. The original source design was found to be excellent in collecting ions formed over a wide band in the source. Quite unexpectedly (and contrary to experiment) the original source design also appeared to be superior for focusing beam molecules. The conflict between the computer calculated predictions and the experimental results indicated that there was some discrepancy between the idealized modeling of the source and its actual construction, and apparently ion collection from background molecules was not so susceptible to the discrepancy as ion collection from molecular beam molecules. It has since been decided that the added electrodes in part compensated for poor electron beam collimation and misalignment of the ion source components. In later experiments as alignment problems in the source were discovered and corrected, the electrode potentials required for maximum intensity progressively decreased, but never to zero.

Variable entrance aperture of the ionization gauge. The ionization gauge tube, first mounted directly on the pumping cross (Part 21, Figure 6), was constructed with a removable disk containing a centered 3.2 mm hole between the gauge tube and the rest of the system. The purpose of the small entrance aperture was to restrict the pumping speed on the tube and thereby increase the sensitivity of the gauge to the collimated molecular beam. Since it is convenient to set the nozzle-skimmer distance for maximum beam intensity by observing the ion gauge pressure, the net flux (between beam flux into and pumping flux out of the gauge tube) giving the maximum gauge pressure is desired. Therefore, the size of the entrance aperture to the gauge tube should be quite close to the beam width of the aperture and will depend primarily upon the diameters of the skimmer opening and the other collimating orifices.

Hence, the in-line slide valve (Part 18, Figure 6) which permits rapid interchange of aperture disks while maintaining vacuum in the mass spectrometer was designed and installed.

Heaters and thermocouples. The first attempts to generate a molecular beam often resulted in wild pressure fluctuations in the nozzle-skimmer chamber. It was postulated that the expanding gas "iced" over the skimmer orifice and then the plug dropped away and quickly vaporized. Initially, no heaters

---

*Provided by Professor J.D. Morrison and written by Dr. L.P. Johnson, La Trobe University, Melbourne, Australia.

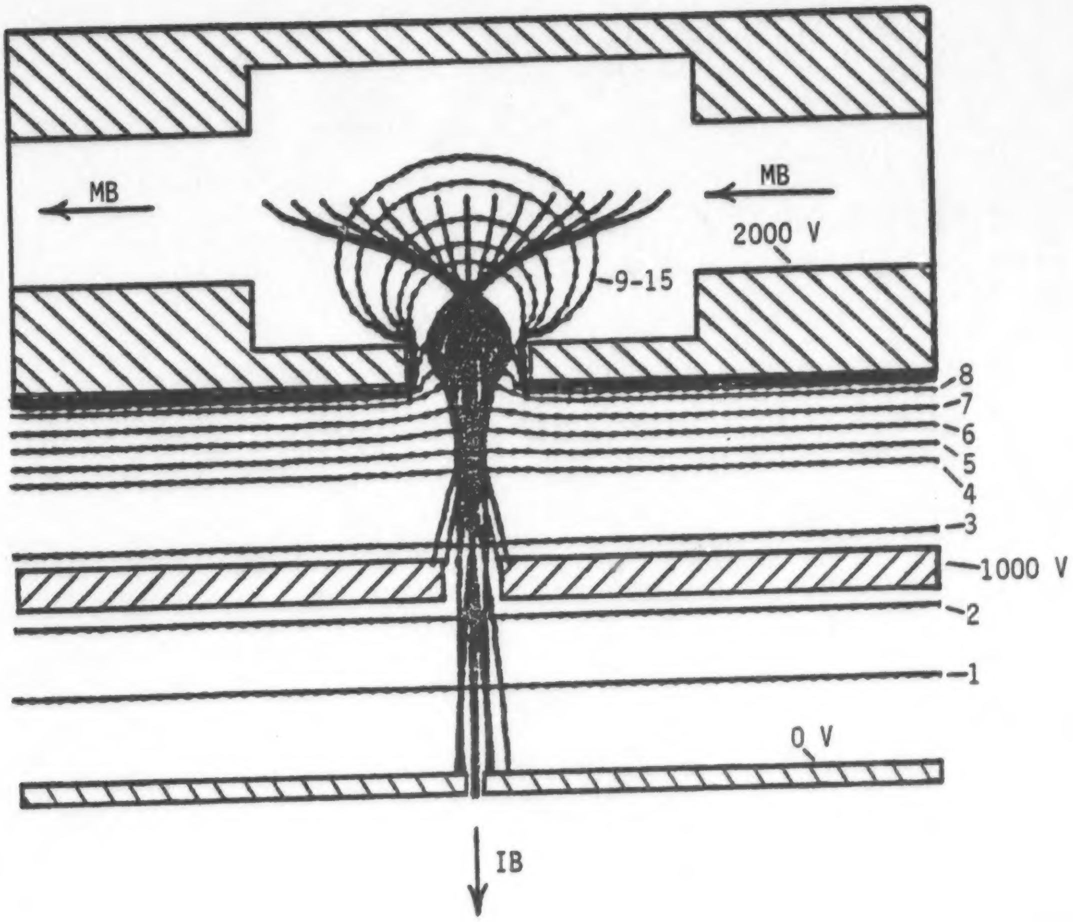

1 - 500 V
2 - 900 V
3 - 1100 V
4 - 1500 V
5 - 1600 V
6 - 1700 V
7 - 1800 V
8 - 1900 V
9 - 1950 V
10 - 1980 V
11 - 1990 V
12 - 1992 V
13 - 1994 V
14 - 1996 V
15 - 1997 V

Figure 32. Calculated equipotentials and ion trajectories of ions for the original ion source configuration. Ions with molecular weight 40 and 0.03 eV energy along the molecular beam (MB) axis are ionized at various points along the molecular beam axis. Equipotential lines are numbered and the values are given below the figure. The ion beam direction (IB) is indicated.

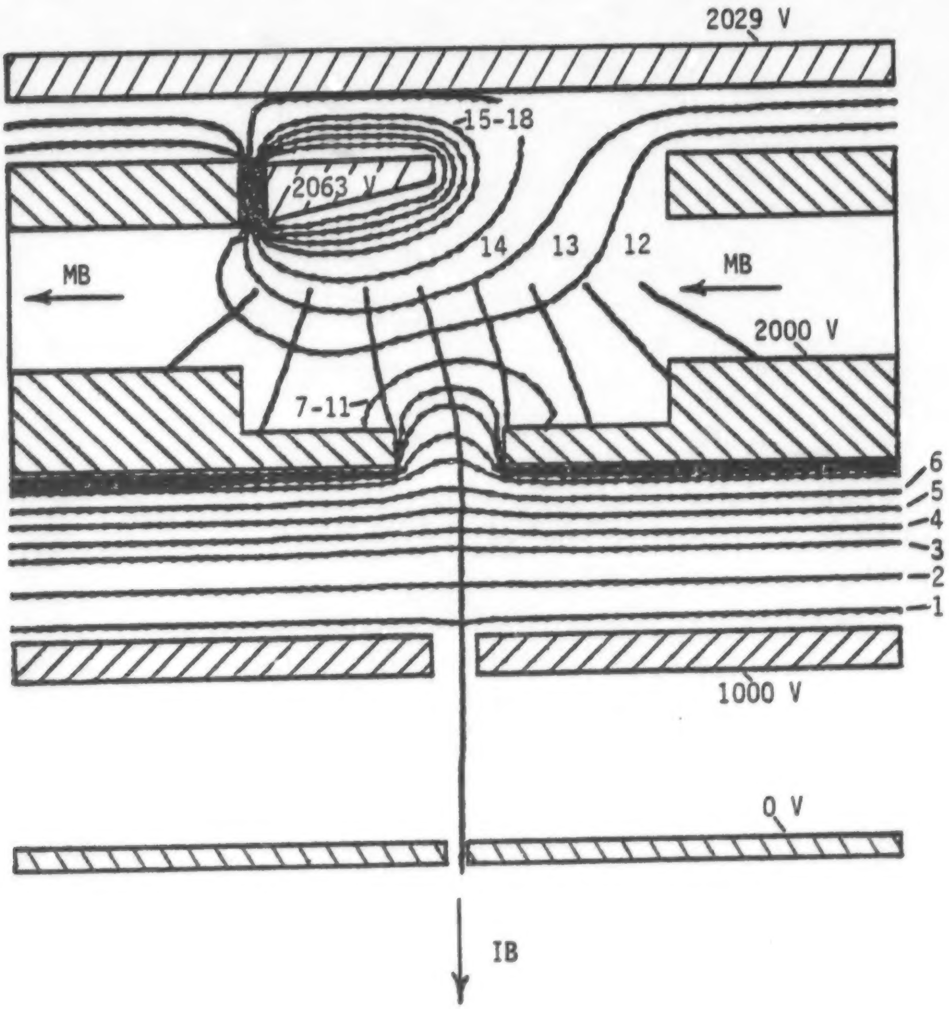
2029 V
15-18
2063 V
14
13
12
MB
MB
2000 V
7-11
6
5
4
3
2
1
1000 V
0 V
IB

1 - 1100 V
2 - 1300 V
3 - 1500 V
4 - 1600 V
5 - 1700 V
6 - 1800 V

7 - 1900 V
8 - 1950 V
9 - 1980 V
10 - 1990 V
11 - 2000 V
12 - 2010 V

13 - 2020 V
14 - 2030 V
15 - 2040 V
16 - 2045 V
17 - 2050 V
18 - 2055 V

Figure 33. Calculated equipotentials and ion trajectories of ions for the two electrode configuration. Ions with molecular weight 40 and 0.03 eV energy along the molecular beam (MB) axis are ionized at various points along the molecular beam axis. Equipotential lines are numbered and the values are given below the figure. The ion beam direction (IB) is indicated.

or thermocouples were included in the molecular beam generating system. The placement of the heaters and thermocouples added to the skimmer and collimator is shown in Figure 15. Heater 1 and thermocouple A on the nozzle assembly also were added at this time; heater 2 and thermocouple B were added later when the thermostatting water bath was constructed. Until that more elaborate temperature control system was added, some temperature control of the nozzle assembly inlet tubing (Part T, Figure 9) was provided by resistive heating of that tubing. Two thermocouples attached to T with TORR SEAL® epoxy (one about 5 cm back from the nozzle assembly and the other at the midpoint) monitored the temperature along that part. The major drawbacks of this system were that it did not compensate for varying heat loss along the inlet tube and it allowed only heating above ambient temperature in the important region between sampling and expansion at the nozzle. Hence, this system was totally unsatisfactory with dense ethylene whose critical temperature is below room temperature and inadequate for CO_2, etc.

Perhaps the most interesting and valuable components of this initial temperature control system were the two skimmer thermocouples. With a pure gas beam, the skimmer thermocouple mounted at the junction of the two conical surfaces gave a temperature reading some 10 to 30°C lower than the one on the downstream side of the skimmer mounting flange. Cessation of that temperature difference is an immediate indication of nozzle orifice plugging or beam deflection from the nozzle-skimmer centerline. The large temperature difference of about 30° C between the two thermocouples was observed in earlier experiments while in later experiments the difference was not so great. The smaller nozzle orifices used in the later experiments could be partly responsible for the difference. It is also thought that the nozzle inlet tubing (T, Figure 9) was possibly not seated properly in the pinhole holder (C, Figure 9) in the early experiments, thereby allowing some small leakage about the pinhole shim. Solute elution has always caused a large temperature difference between the two thermocouples. Upon solute elution the skimmer mid-point temperature at times has dropped erratically to as low as -35°C with the skimmer base temperature close to 30°C.

While the addition of the current detector and variable ionization orifice did not prove to be so necessary as originally conceived, the primary goal of the first set of modifications was met: implementation of this mass spectrometer as a molecular beam detector. The rudimentary temperature control/monitoring system was necessary for further experimentation and proved to be indispensable for beam monitoring.

3.5.3. Initial Solute and Cluster Experiments

In the intial experiments, tank gases were used without additional compression, so the maximum pressure possible was severely limited; also at this time there was no temperature control of the supply gas so all experiments were at room temperature.

Sample introduction. At first solutes were introduced to the high pressure gas in a manner similar to that of Bowman[97] in his initial DGC work: a concentrated solution of solute in benzene was deposited on a plug of glass wool, the benzene was evaporated, and the glass wool plug was placed in the chamber formed from a high pressure ball check valve as discussed in subsection 3.4.6 and shown in Figure 22. The sampling assembly shown in Figure 22 had a large dead volume. However, that did not interfere with solubility studies and it was deemed necessary to prove that solute could be introduced to the ion source by the molecular beam system before constructing a more elaborate dense gas chromatograph.

Molecular beam/mass spectrometer alignment check. Two of the first solutes tried were naphthalene and phenylstearate with up to 550 psig (38 atm) ethylene. According to the work of Bowman,[97] these solutes had threshold pressures of 46 atm and 7 atm with CO_2. It was felt that these compounds would elute even more easily with ethylene but they were *not* detected with the mass spectrometer. First, the possibility that the molecular beam system was not properly aligned with the mass spectrometer ion source was checked by assembling the nozzle without the inlet tubing and without a pinhole orifice and then illuminating the 0.013" exit hole of the pinhole holder from the high pressure side while sighting the pinpoint of light through the ionization chamber and the ionization gauge orifice after removing the ion gauge tube. The light was well-centered in the orifice. The alignment was checked for vacuum-caused distortion by clamping glass plates over both the high pressure end of the nozzle assembly and the ion gauge aperture and rough-pumping to about 10 torr. There was no detectable distortion.

Evidence for solute transport. Upon removal of the molecular beam cage, clumps of white crystals "shotgunned" over the skimmer were noted. Therefore, solutes had been eluted and carried with the expansion at least as far as the skimmer. The situation became even more puzzling when background mass scans were run prior to opening the interface slide valve to continue the solute experiments: extremely large parent ion intensities for both naphthalene and phenylstearate (m/e 128 and 360) were recorded. Apparently, the solutes had reached the ion source but had not been detected until they were distilled from ion source surfaces upon heating and detected as background.

Cluster detection. The fact that solvent gas clusters as well as the above solutes had not been detected led to further confusion. Meticulous alignment of ion source ionizing components followed by completely de-focusing and then re-focusing (at potentials greatly different than those typically used) ion source optics resulted in the detection of CO_2 cluster ions. The ion source potentials were first adjusted to maximize mass 44, then 88, and finally 132. Figure 34 shows the relation of the relative intensities of CO_2^+, CO^+, $(CO_2)_2^+$, $(CO_2)_3^+$ and $(CO_2)_4^+$ with nozzle-skimmer separation. There are no clusters detected until the nozzle-skimmer separation is about 1/2 cm while there is a substantial monomer CO_2 intensity at all separations. The background m/e values for CO_2 and its clusters are <1/2 unit on the normalized intensity scale. Background of CO^+ is 14 units--a large contribution from N_2^+.

Condensation clusters were also observed for nitrogen (76 atm) and ethylene (82 atm) at room temperature with a 12.5 μm nozzle diameter. Evenly spaced cluster peaks out to $(N_2)_9^+$ were obtained for the above conditions. Later, after installation of the thermostatting bath, clusters for ethane, ethylene and carbon dioxide--all at temperatures within 5°C of their

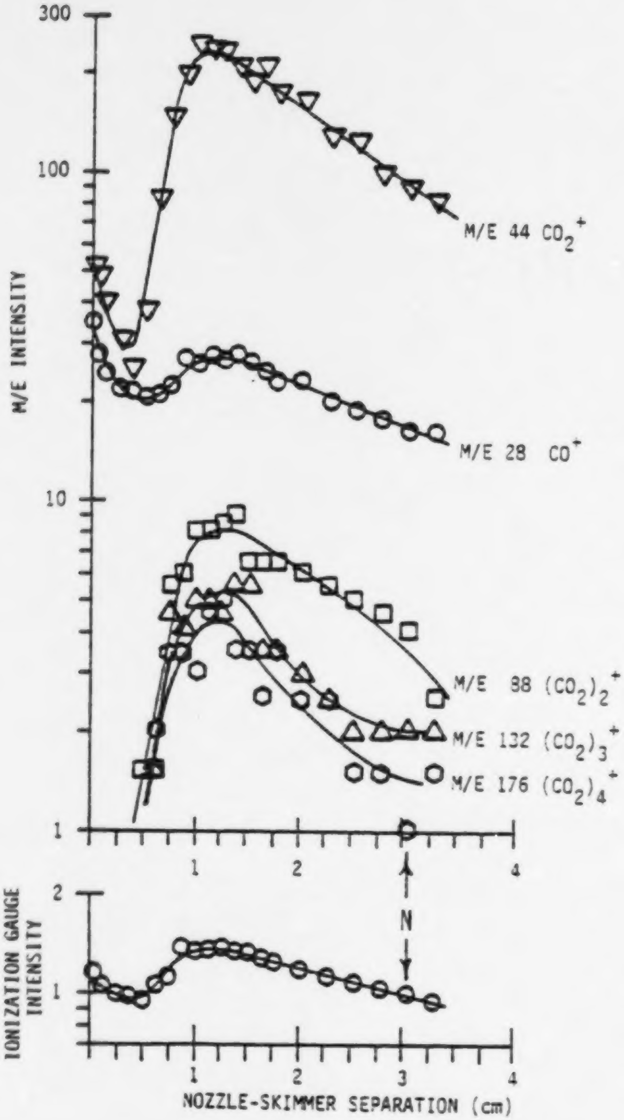

Figure 34. CO_2 cluster intensities as a function of nozzle-skimmer separation. All m/e intensities and the molecular beam detector ionization gauge pressures are normalized to those points labeled N, i.e., the m/e 176 intensity and the ion gauge pressure at ∿ 3 cm separation. The intensity of m/e 132 was maximized by adjusting ion source electrode potentials so that W = chamber + 52 V and B = chamber + 10 V.

Conditions: 69 atm carbon dioxide, 12.5 μm nozzle diameter, room temperature.

respective critical temperatures--were seen out to $(C_2H_6)_{17}^+$, $(C_2H_4)_{20}^+$ and $(CO_2)_{13}^+$. Clustering comparable to CO_2 clustering but not recorded out to the larger masses was observed for N_2O. As ionization by the electron beam occurs in a low pressure region and the ions are immediately drawn out of the molecular beam by a drawout field, it seems certain that these were true condensation clusters and not the result of ion-molecule reactions. Molecular beams of argon, helium, and hydrogen at room temperature produced no clusters. For reasons unknown, the ion source potentials in the ion source had to be adjusted differently for each gas for optimum detection of the clusters: the ion focusing voltage (Focus in Figure 17) varied by 60 V, the voltage difference between the two halves of the focusing lens (L1 and L2 in Figure 17) varied from 2 to 18 V (0-30 V possible range), the wedge electrode potential varied from 11 to 24 V above the chamber voltage, the back plate electrode potential varied from 1 to 21 V above the chamber voltage and the electron energy varied from 30 to 70 V.

An illuminated viewing port was installed for observation of the nozzle-skimmer region indicated in Figure 6 by "11". Since small clusters were finally observed and the skimmer mid-point thermocouple indicated low temperatures, it was of interest to look for solid particles. No cluster particles of observable size have been seen--either with pure solvent gas or later with solute/solvent mixtures.

Solute detection. The first solute detected was naphthalene in dense CO_2 with a threshold pressure of less than 25 atm at room temperature. Solvent gas clusters were observed, particularly m/e 88, 132, 176, and in addition a few low-intensity solute-solute and solute-solvent clusters were observed: $(C_6H_6)_2^+$, $(C_6H_6 \cdot CO_2)^+$, and $[C_6H_6(CO_2)_2]^+$--benzene was the solvent for naphthalene introduction into the sample chamber.

Naphthalene was also detected using dense ethylene at room temperature as the solvent gas; again, the detectable threshold pressure was about 25 atm.

Further ion source alignment. During these intial solute studies, the ion source was again disassembled. At this time it was discovered that two aligning circular edges which should have been concentric had been originally machined non-concentric by about 0.4 mm, causing misalignment of the source exit slit. Readjustment of the source exit slit (0.08 mm width) greatly reduced the potential required on the wedge electrode for maximum intensity.

Further solute experiments at room temperature. Experiments with anthracene in ethylene (up to 65 atm) demonstrated the need for a higher pressure gas supply. The maximum cylinder pressure was not high enough to dissolve anthracene to an appreciable extent and the cylinder pressure varied with room temperature. Therefore, the dense gas supply was constructed with the protective housing and the compressor, reservoir, valves, regulators and gauges as discussed in subsection 3.4.5 and shown in Figure 19.

Anthracene was easily dissolved in 110 atm ethylene at room temperature. However, the experiments with higher pressure ethylene with anthracene and 1,3,5-triphenylbenzene were plagued by oscillating pressures in the nozzle-skimmer expansion chamber and in the molecular beam detector; erratic skimmer temperatures, cluster intensities and solute intensities; and often a loss of the beam intensity altogether. The most probable cause appeared to be lack of adequate temperature control. Since it had been shown that two solutes, naphthalene and anthracene, could be transported by the molecular beam and detected by the mass spectrometer,* it seemed appropriate to construct the DGC system with temperature control both on the DGC and on the nozzle assembly.

3.5.4. DGC Construction with Temperature Control

The DGC bath, water circulating systems, nozzle assembly water manifold, nozzle tip heater, and reservoir housing temperature control system were constructed as described in subsection 3.4.6. Preliminary temperature controlled experiments were conducted with a simple system assembled from the same modified check valve sample chamber and high pressure needle valves described earlier and pre-heat column (Figure 22); a chromatograph column was not included.

Preliminary Studies. A number of experiments were performed using dense ethylene without solute in order to study the effect of temperature change using the new temperature controls. As expected, cluster formation was now more reproducible. It was again verified that the ion source electrode potentials for maximum ion current depended not only upon whether one looked at background or beam molecules, but also on the mass of the beam molecule. Two mass scans, identical except for source potential adjustments, are shown in Figure 35 (see legend for details). The general decrease in intensity of background peaks and of dimer and trimer peaks and the substantial increase of the higher polymer peaks is obvious.**

---

*So much 1,3,5-triphenylbenzene had been eluted that it was deposited on the expansion side of the nozzle orifice in a big lump, causing deflection of the jet away from the nozzle-skimmer centerline so that the expanding mixture completely missed the ion source.

**Also of interest are the substantial (28n + 1) peaks clearly observable and much too large to be isotope peaks of m/e = 28n. Since the pressure in the ionization region is so low, ion-molecule reactions such as

$$(C_2H_4)_n^+ + C_2H_4 \rightarrow (C_2H_4)_nH^+ + C_2H_3,$$
$$C_2H_4^+ + (C_2H_4)_n \rightarrow (C_2H_4)_nH^+ + C_2H_3$$

are not probable. A more likely explanation is that ionization causes not only simple fragmentation of polymers, but also reactions involving proton transfer

$$(C_2H_4)_p + e \rightarrow [(C_2H_4)_p^+]^* + 2e$$
$$\hookrightarrow (C_2H_4)_n^+ + (C_2H_4)_{p-n}$$
$$\hookrightarrow (C_2H_4)_nH^+ + \text{or} \begin{array}{l} (C_2H_4)_{p-n-1} \cdot C_2H_3 \\ (C_2H_4)_{p-n-1} + C_2H_3 \end{array}$$

At this time we have no way of predicting how directly the peak heights of clusters as shown in Figure 35 represent the actual relative abundances of the clusters entering the ion source.

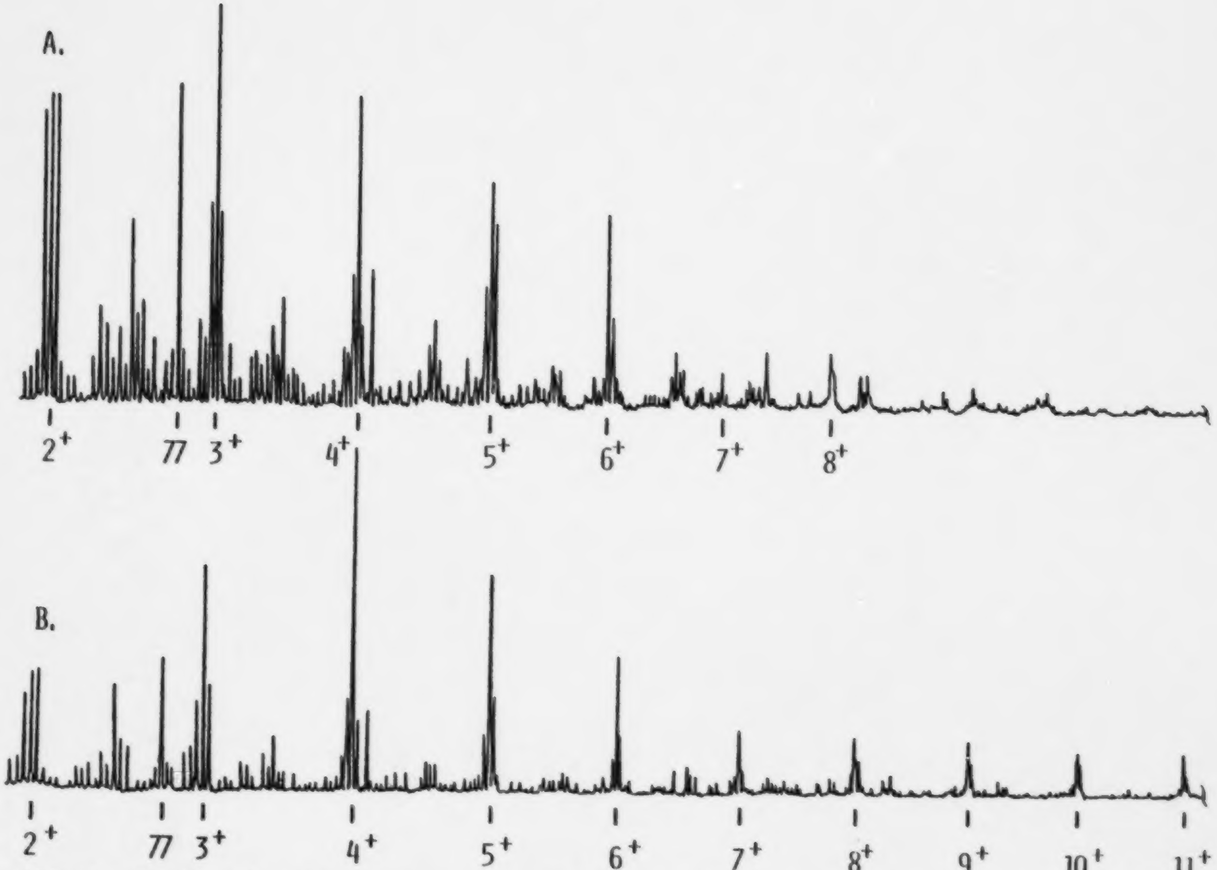

Figure 35. Effect of adjusting ion source potentials to maximize an ethylene cluster ion intensity.
A. Scan taken at MS settings previously found to maximize m/e 56 for 82 atm C_2H_4, room temperature, 12.5 μm nozzle diameter. (This scan was taken long after maximization procedure.)
B. Scan taken after maximizing m/e 112, $(C_2H_4)_4^+$.
Conditions for A and B: DGC bath, 17°C; nozzle tip, 19°C; 103 atm C_2H_4; 12.5 μm nozzle diameter
A, B are at identical MS sensitivity settings. Peaks labeled n^+ are $(C_2H_4)_n^+$.

Experiments on changing the nozzle tip temperature only indicated, as expected, that a temperature increase decreased the relative intensity of aggregates and also decreased the nozzle-skimmer chamber pressure due to the lower gas density, hence lower mass flow, at higher nozzle tip temperatures.

Clustering as a function of stagnation and expansion chamber pressures. The important effect of both stagnation pressure and expansion chamber pressure on clustering is shown in Figure 36 where cluster intensity vs. expansion chamber pressure is plotted for four stagnation pressures of ethane at 35-36°C bath temperature and a constant, comparable nozzle-tip temperature. The expansion chamber pressure was increased by partially closing the slide valve separating the chamber from the diffusion pump while all other parameters remained unchanged. Clusters out to $(C_2H_6)_{15}^+$ were seen for the 1.1 x 10^{-4} torr expansion chamber pressure for 18 atm ethane. For 35 atm, ethane clusters out to $(C_2H_6)_{17}^+$ were seen for all expansion chamber pressures except 5 to 6 x 10^{-3} torr where all cluster intensities were zero. For 52 atm, clusters out to $(C_2H_6)_{15}^+$ were sighted for the range 3 to 5 x 10^{-4} torr expansion chamber. For 69 atm clusters only up to $(C_2H_6)_5^+$ were observed. The curves were drawn to connect points for the same value of n for the cluster formula, $(C_2H_6)_n^+$; their shapes are not significant. The drop to zero for all curves as expansion chamber pressure increases is definitely real. An increase by a factor of two in either the stagnation or expansion chamber pressure can dramatically alter the cluster pattern.

Anthracene in dense ethylene. Anthracene was readily dissolved and eluted by 55 atm ethylene (16-17°C bath and 22°C nozzle tip) in such quantities that it plugged the nozzle orifice (probably because of the hotter nozzle tip temperature). Increasing the ethylene pressure to ~103 atm and the nozzle tip temperature to 25°C cleared the plug for only a few minutes. The nozzle plugging in this experiment emphasized the importance of maintaining an appropriate temperature gradient in the instrument.

Temperature effects of various apparatus sections upon solubility. The maximum in the capacity ratio-temperature relationship not far above the solvent gas critical temperature for DGC discussed in subsection 3.2 indicates that near critical it is necessary to have all sections of the DGC cooler than or at the same temperature as the sample chamber. Otherwise, the great temperature sensitivity of the mixture may cause sample deposition at any point where the temperature is *higher* than at sample injection/solvation because of the lower density (solvent power) of the solvent gas. With our apparatus, it was not possible to keep the nozzle assembly and vacuum locks cooler than a subambient bath. Typically components beyond the bath were 1 to 5°C higher than a sub-ambient bath temperature even though those components were themselves somewhat lower than room temperature. With bath temperatures higher than room temperature, components beyond the bath can be maintained 1 to 5°C *lower* than the bath temperature. This thermostatting problem is the reason that ethylene/anthracene solutions plugged the nozzle orifice so often. Therefore, we directed our attention to gases with critical temperatures slightly above room temperature: C_2H_6, CO_2 and N_2O.

Installation of special zero-dead-volume HPLC valves. In one experiment the nozzle orifice remained open for an entire afternoon with a saturated

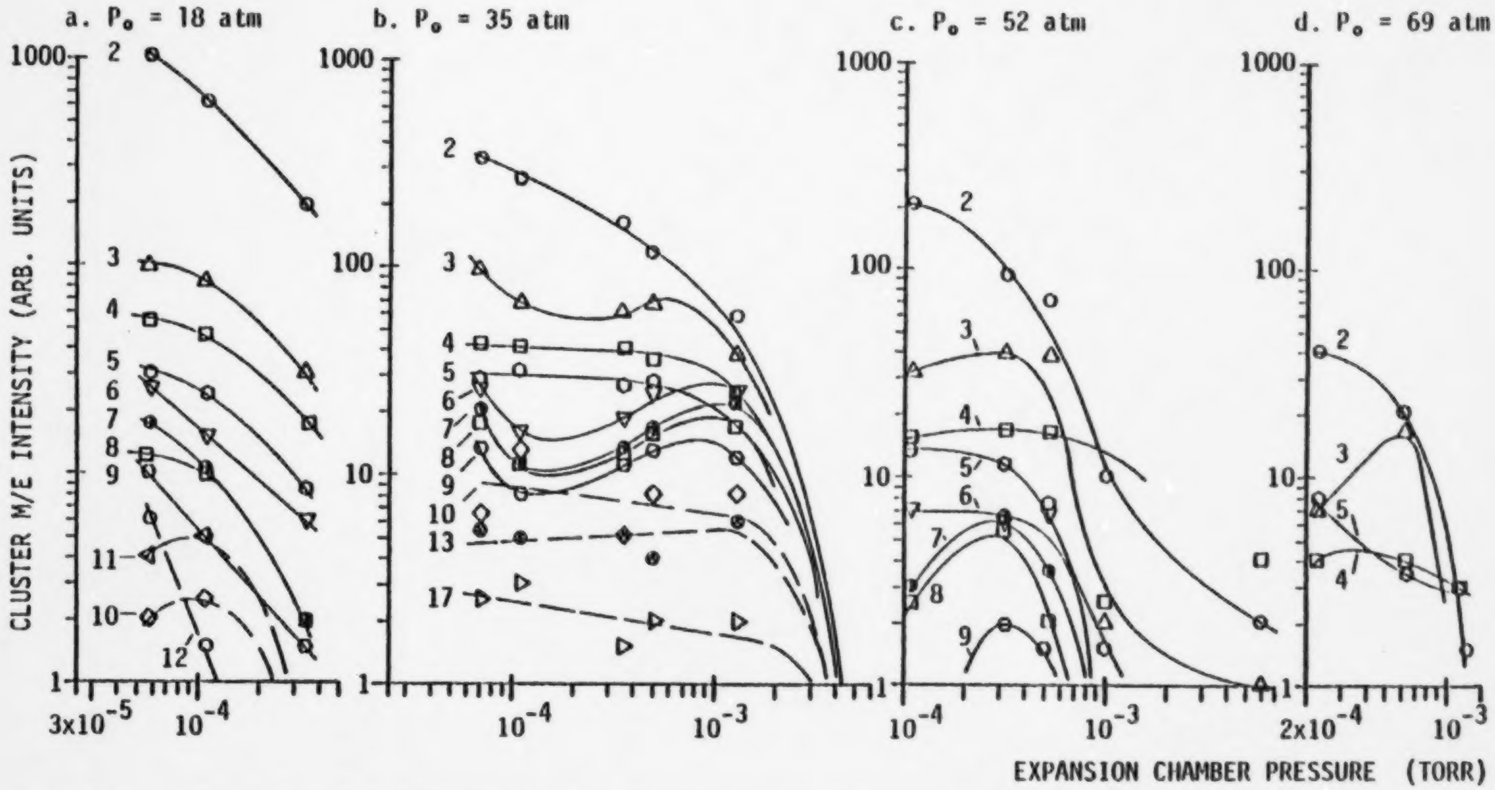

Figure 36. Solvent gas cluster intensities as a function of expansion chamber pressures (P_1) for four stagnation pressures (P_o) of ethane. The number, n, on each curve specifies the ethane cluster, $(C_2H_6)_n^+$.

Conditions: 35-36 °C, 12.5 µm nozzle diameter.

anthracene/ethane mixture flowing the whole time with the result that all the anthracene (several mg) was removed from the glass wool plug. This sample depletion emphasized the need for an improved sampling system at this time because of the inconvenience of draining the bath to remove the sample chamber, disassembling and reassembling it, and the bath re-equilibration. Hence the HPLC sampling and shut-off valves were installed as shown in Figure 23 (excluding the chromatograph column). The sample chamber was the one shown in Figure 26a, where a sintered stainless steel filter element was used instead of a glass wool plug for a sample deposition surface.

After installation of the valves we encountered a series of plugged nozzles. The cause was finally traced to the graphite impregnated fluorocarbon (VALCON H) valve seats of the HPLC valves.*

Even with a zero-dead-volume filter unit containing sandwiched 5 μm/2 μm filter elements between the shut-off valve and the nozzle orifice, some particles worked through the filter elements. The most spectacular case was the one where microscopic examination revealed a long, thin particle (carbon filament) with an estimated size of 2-3 μm x 15 μm located as an orifice diameter and accompanied by black deposits around the entire orifice circumference. Often the plugging of the orifice was gradual and could be observed during running time as the expansion chamber pressure slowly fell. This slow, partial plugging sometimes allowed the use of 12.5 μm nozzle diameters with much higher stagnation pressures (up to 205 atm) than possible with an open 12.5 μm diameter orifice. Supposedly, as the valve seats became worn, fewer particles would be produced. Nevertheless, adequate and long-lived protection of the nozzle orifice is achieved only with the severe combination of a 2 μm filter followed by a two sandwiched 0.5 μm elements in a filter body.

Removal of nozzle orifice plugs. When a particulate plug of the nozzle orifice occurs, the only way to open the orifice is to remove the nozzle assembly. Often the particulate plug could be removed with a solvent-dampened twisted corner of a Kim-Wipe® tissue. Otherwise, the pinhole foil must be pushed out and another orifice punched into place.

With the polycyclic aromatic solutes utilized in most of the experiments it was often possible to dissolve solute plugs by alternately applying high pressure gas and vacuum to the nozzle tubing often simultaneously varying its tip temperature. In some cases a simple increase in dense gas pressure was enough to clear the nozzle. Another procedure which has had some success is to evacuate the column (if any) and the nozzle assembly inlet tubing, inject liquid solvent appropriate for the solute via the sampling valve, and admit the high pressure gas from the dense gas supply to push the liquid slug right up against the nozzle orifice while heating the nozzle tip.

---

*The problem encountered with the Valco Instruments Company HPLC valves is similar to one discussed in a "Technical Note" by Rheodyne, Incorporated.[142] Wear particles from their HPLC Sample Injection Valves with rotor seals of carbon fiber reinforced Tefzel caused clogging of column inlet frits. Their data shows that "worn-in" rotor seals produce fewer wear particles. Furthermore, they recommend the same conical geometry of the tubing ends against a filter element that had already been incorporated in the DGC filter assemblies (Figure 24) to use a much greater area of the filter element.

3.5.5. Chromatographic Survey

The various solutes, solvent gases, columns, sample chambers and chromatographic conditions studied in this work are summarized in Table 2.

Solubility of anthracene and 1,3,5-triphenylbenzene compared to prior DGC work. Before adding a chromatographic column to the system, some solubility studies were conducted with CO_2. The first system studied was anthracene/CO_2 at 35-38°C. Approximately 300 μg anthracene was placed in the sample chamber (via an anthracene/$CHCl_3$ solution with the $CHCl_3$ pumped off). The sample chamber was exposed to various pressures of CO_2 while m/e 178 was recorded after which the mass spectrometer multiplier voltage was decreased to measure m/e 44 intensity. At 500, 750, and 1000 psig (35, 52, and 69 atm) no anthracene was detected. A slight amount was detected at 1250 psig CO_2 (86 atm). The same procedure was followed for 1,3,5-triphenylbenzene (introduced to the sample chamber as an ether solution) with the DGC bath held at ~32°C. The parent ion, m/e 306, was monitored. The following maximum intensity ratios (I_{solute}/I_{CO_2}) were noted for higher CO_2 pressures;

CO_2 Pressure	Anthracene I_{178}/I_{44}	Triphenylbenzene I_{306}/I_{44}
1500 psig (103 atm)	2.1×10^{-3}	2.4×10^{-4}
2000 " (137 ")	2.7×10^{-3}	2.7×10^{-4}
2500 " (171 ")	3.4×10^{-3}	2.6×10^{-4}
3000 " (205 ")	2.4×10^{-3}	--

Comparing this data to the solubility data of Bowman,[97] one sees that

	Max. Ion Current Ratio--this work	Correction to Mole Ratio--this work	Max. Mole Ratio Bowman[97]
Anthracene/CO_2	3.4×10^{-3} (35-38°C)	0.53×10^{-3}	0.91×10^{-3} (~40°C)
Triphenylbenzene/CO_2	2.7×10^{-4} (~32°C)	0.25×10^{-4}	0.67×10^{-4} (~40°C)

Since the solute molecules have larger ionization cross sections than CO_2, the current ratios should be corrected to obtain mole ratios; calculated cross sections from the data of Otvos and Stevenson[143] give factors of 6.4 and 11 relative to CO_2 for $C_{14}H_{10}$ and $C_{24}H_{18}$, respectively.

At the time of these experiments, a mass intensity was not monitored continuously with an oscilloscope; permanent scans were made only periodically. Hence, the maximum solute/CO_2 mole ratio could have been higher during elution than actually recorded on one particular scan; also, it is not known that

TABLE 2. SUMMARY OF STUDIES BY DGC/MS LISTING SOLUTES AND DENSE SOLVENT GASES*

Solvent Gas / Solute	C_2H_4 P_c = 50.5 atm T_c = 9.9°C	C_2H_6 P_c = 48.5 atm T_c = 32.3°C	CO_2 P_c = 72.9 atm T_c = 31.0°C	0.1 mole % 1-bromonaphthalene in CO_2	N_2O P_c = 71.6 atm T_c = 36.4°C
Naphthalene MW 128	32 atm, RT a,1,LVG		71 atm, RT b,1,LVG		
Azobenzene MW 182		170 atm, 33-34°C b,2,LVF			
1,3,5-Triphenyl benzene MW 306		88-170 atm, 33-34°C b,2,LVF 88-123 atm, 33-55°C b,2,P	102-170 atm, 32°C b,1,LVF		
Phenanthrene MW 178		102-171 atm, 34°C b,1,LVF			99-109 atm, 50-55°C b,3,P
Anthracene MW 178	136 atm, RT b,1,LVG 54 atm, 16°C b,1,LVG	102 atm, 34°C b,1,LVG 68-170 atm, 33-34°C b,2,LVF 88-123 atm, 35-55°C b,2,P	85-204 atm, 35-38°C b,1,LVF 102-143 atm, 34-55°C b,3,P	116 atm, 34°C b,3,P	99-109 atm, 40-55°C b,3,P 119-238 atm, 40-60°C c,3,E
Fluoranthene MW 202					102 atm, 40-52°C b,3,P 119-238 atm, 40-60°C c,3,E

(continued)

TABLE 2 (continued)

Solvent Gas / Solute	C_2H_4 P_c = 50.5 atm T_c = 9.9°C	C_2H_6 P_c = 48.5 atm T_c = 32.3°C	CO_2 P_c = 72.9 atm T_c = 31.0°C	0.1 mole % 1-bromonaphthalene in CO_2	N_2O P_c = 71.6 atm T_c = 36.4°C
Pyrene MW 202			95-157 atm, 34-55°C b,3,P	116 atm, 34°C b,3,P	102 atm, 40-52°C b,3,P 119-238 atm, 40-60°C c,3,E
Anthraquinone MW 208		88-170 atm, 33-34°C b,2,LVF SMALL			
Caffeine MW 194					238 atm, 42°C c,3,E 184 atm, 39°C d,4,E
ℓ- Histidine ? MW 155					238-259 atm, 42°C c,3,E 184 atm, 39°C d,4,E
Inosine ? MW 268		170 atm, 33°C b,2,LVF			

(continued)

TABLE 2 (continued)

Solvent Gas / Solute	C_2H_4 P_c = 50.5 atm T_c = 9.9°C	C_2H_6 P_c = 48.5 atm T_c = 32.3°C	CO_2 P_c = 72.9 atm T_c = 31.0°C	0.1 mole % 1-bromonaphthalene in CO_2	N_2O P_c = 71.6 atm T_c = 36.4°C
L-(+)-Arginine MW 174					238 atm 42°C b,3,E no visible elution

*For each combination studied, pressure and temperature are given, followed by code symbols defined as follows:

Nozzle diameter: a-25μm, b-12.5μm, c-5μm and d-enlarged 5μm, ~8μm

Column: 1-none, solubility studies; 2-capillary, 6m x 0.5mm I.D.; 3-Permaphase ODS, 50 cm x 1.5 mm I.D.; 4-capillary, 6m x 0.5 mm I.D., etched inner surface

Sample loop: LVG--~1ml internal volume, sample deposited on glass wool; LVF--~1ml internal volume, sample deposited on 2μm sintered stainless steel filter element; P-140/170 mesh glass beads packed in tubing 10cm long x 1.5mm I.D., estimated 74μl free space; E-open tube, 22.9cm long x 1mm I.D., inner surface etched, 180μl internal volume

?: Possible elution and detection of small amounts; confirmation needed

RT: Room temperature

saturation of solvent occurred. Another source of error is the questionable reproducibility of multiplier sensitivity ratios when the electron multiplier voltage is changed several steps to permit comparison of very different intensities. The total calibration error may be as high as, perhaps higher than, a factor of two. The mole ratios from Bowman's work may be in error by as much as a factor of 1.5. Thus, the two methods agree within their error limits. However, the correction for the difference in temperature would lessen the agreement.

These experiments were conducted with a nominal 12.5 μm pinhole. The very high stagnation pressures were tolerated because of partial closure by valve wear particles as discussed previously. Complete plugging of the orifice terminated the triphenylbenzene/CO_2 measurements before the desired pressure range was covered.

Initial capillary column study. The first column used was a 6 m x 0.51 mm I.D. capillary column. Several compounds and mixtures of these compounds were eluted with ethane and detected: anthracene, 1,3,5-triphenylbenzene, anthraquinone and azobenzene. The sample size of each one was on the order of 30-300 μg. Of those four compounds, anthraquinone gave a very small and sometimes questionable signal. Further experiments with anthraquinone either with higher pressure ethane or with CO_2 and N_2O are necessary. Another involatile compound, inosine, was injected. While no large signal was seen for it, a pattern in the mass spectra indicated that a trace amount may have been dissolved. Very small peaks just barely larger than baseline noise corresponding to the parent mass and plausible fragments ($C_{10}H_{11}O_4N_4^+$, m/e 251; $C_{10}H_{10}O_3N_4^+$, m/e 234; $C_9H_9O_4N_4^+$, m/e 237; $C_9H_8O_3N_4^+$, m/e 220) would appear for several scans. Suddenly, ethane cluster masses appeared and the suspected inosine fragments disappeared. Then the above mass peaks reappeared with the loss of ethane clusters. The behavior fit the nozzle plugging pattern and seemed too ordered for random noise spikes. However, the above fragments are not those reported for inosine (e.g., EPA/NIH Mass Spectral Data Base[144]) and further solubility studies with this compound must be pursued before a claim of positive elution and detection can be made.

There was no distinct retention and separation of any of the compounds on this column. The linear flow rate was about 8 cm/sec, reasonably close to the 20 cm/sec considered appropriate for capillary columns;[145] however, the length of 6 m is short for an open capillary column.

It is informative to compare fragmentation patterns of compounds introduced via the molecular beam interface to those normally obtained. Standard electron ionization mass spectra for several of the solutes and solvents used here, with parent ion masses underlined, are presented in Table 3. Because of short scanning ranges and interference with a particular solute pattern from the solvent dense gas, dense gas clusters, other solutes, and other background, experimental data as extensive as those in Table 3 were not obtained.

A typical anthracene mass spectrum shows the following relative intensities in the fragmentation pattern:

TABLE 3. THE RELATIVE ABUNDANCE OF THE TEN MOST INTENSE FRAGMENT IONS OF SELECTED COMPOUNDS

COMPOUND			DATA										REF.
Anthracene		m/e	178	176	179	89	76	88	151	152	75	63	146
		Abund.	1000	170	160	142	110	88	64	59	49	47	
1,3,5-Triphenyl-benzene		m/e	306	307	289	302	228	303	153	290	226	308	147
		Abund.	1000	260	78	46	43	42	40	40	39	35	
Anthraquinone		m/e	208	180	152	76	151	209	207	75	150	50	147,148
		Abund.	1000	766	507	421	250	154	142	117	116	105	
Azobenzene	#1	m/e	77	182	51	78	152	153	183	27	39	64	147
		Abund.	1000	273	208	63	48	41	34	27	25	21	
	#2	m/e	77	182	51	78	152	153	105	183	50	39	147
		Abund.	1000	229	173	75	37	34	32	32	29	20	
	#3	m/e	77	51	182	105	50	152	78	39	38	63	147
		Abund.	1000	580	380	240	160	130	120	100	60	60	
Chloroform	#1	m/e	83	85	47	35	48	49	87	37	50	82	147,148
$[CH^{35}Cl_3]^+$		Abund.	1000	640	371	201	163	119	102	62	50	36	
MW 118	#2	m/e	83	85	47	87	48	49	35	82	50	84	148
		Abund.	1000	657	215	105	98	72	51	36	32	34	
	#3	m/e	83	85	35	48	49	87	37	51	82	84	148
		Abund.	1000	636	186	160	122	95	58	50	38	37	

TABLE 3 (continued)

COMPOUND			DATA										REF•
Ethanol	#1	m/e	31	45	27	29	46	26	43	28	30	42	147
		Abund.	1000	344	239	234	165	83	76	69	60	29	
	#2	m/e	31	45	29	27	43	28	44	46	26	30	148
		Abund.	1000	522	239	179	139	89	85	73	59	54	
Diethyl Ether	#1	m/e	31	59	29	45	27	43	41	28	73	15	147
		Abund.	1000	530	410	390	170	70	60	50	40	30	
	#2	m/e	31	59	29	45	74	27	43	28	41	44	147
		Abund.	1000	469	395	375	304	177	69	61	52	35	
	#3	m/e	31	59	29	45	74	27	43	41	28	73	148
		Abund.	1000	510	405	390	348	157	65	55	42	37	
Caffeine		m/e	194	67	109	55	82	42	40	41	56	195	147,148
		Abund.	1000	665	661	442	386	283	181	156	113	107	

m/e	178	177	176	152	151	179
Abund.	1000	130	170	80	60	110

The anthracene pattern is not very different from what is expected. The same is true for 1,3,5-triphenylbenzene. In its spectra several small peaks before m/e 306 are present. The m/e 289 peak has a higher mass shoulder that is about half its intensity. Generally, with the given resolution of the mass spectrometer it is difficult to assign mass numbers over about 200. However, two consecutive scans taken during the elution of triphenylbenzene shows the following pattern:

	m/e	306	289	228-229	226-227
Abund.	#1	1000	65	75	40
	#2	1000	60	50	35

where the agreement with the data in Table 3 is fairly close.

For anthraquinone just as for anthracene and 1,3,5-triphenylbenzene, the parent ion is expected to be the most intense and a very small signal was seen for it. The intensity of m/e 180 should be almost comparable to the anthraquinone parent ion and it does appear in the mass spectrum. However, the origin of m/e 180 is not clear-cut: $(C_2H_6)_6^+$ along with other ethane clusters appears sporadically. Additionally, the amount of anthraquinone dissolved and eluted was very small so it was difficult to distinguish other major fragments of anthraquinone from background intensities. Hence, no experimental fragmentation pattern was obtained.

A variable relative abundance pattern was observed during the elution of azobenzene in dense ethane. At the start of the detected elution zone the parent ion (m/e 182) was significantly larger than the expected m/e 77 ion intensity. Of the four following scans (recorded consecutively at intervals of about 15 seconds), only the last two show any agreement with each other and with the fragmentation pattern in Table 3.

	m/e	182	152	105	77	51
Abund.	#1	1000	130	180	355	40
	#2	1000	50	260	990	90
	#3	480	80	160	1000	210
	#4	390	95	210	1000	230

A second elution of azobenzene in a mixture of azobenzene, anthracene, and triphenylbenzene showed the same preliminary predominance of parent followed by m/e 77 predominance. One explanation may be impurities in the sample. Another is that perhaps the solute concentration during the jet expansion affects the energy distribution within the solute molecules thereby affecting fragmentation patterns. While more careful studies which duplicate this behavior are necessary, these data indicate that an unusual abundance of parent ion may be possible with the supersonic molecular beam introduction.

The following patterns were obtained for chloroform at different conditions:

m/e	83	84	85	87	118	119	120	35
Abund.	1000	40	640	95	30	13	30	110
	1000	30	600	100	25	15	25	--

The parent ion (m/e) is not among the ten most intense fragments but all three fragmentation patterns in Table 3 indicate that the relative abundances of m/e 118 and m/e 120 range from 17 to 20. One might say that there is a slightly higher parent ion abundance in the above data, but it is not significant.

Slightly high parent ion intensities can be seen in the following ethanol data acquired from two consecutive but widely separated (by 40 seconds) scans during elution:

	m/e	31	45	46
Abund.	#1	1000	630	320
	#2	1000	580	220

The ethane and background contributions were subtracted from the total m/e 31 intensity.

Diethyl ether, like ethanol, is expected to have as its most abundant ion m/e 31. The following data were obtained from two different attempted mixture separations:

	m/e	31	59	45	74	60
Abund.	#1	1000	580	410	370	20
	#3	1000	790	400	330	70
	#1	1000	730	530	440	30
	#3	1000	330	240	230	13
	#4	1000	310	190	150	10

Because of the age of the light-sensitive recorder paper, and the interference to m/e 31 from ethane, the intensities of m/e 31 were estimated with much difficulty and then corrected for the ethane and background contributions. In two cases, a value of m/e 31 simply could not be determined--hence, the non-sequential numbering of the scans taken during the two elutions. Therefore, the m/e 74 to m/e 45 ratio appeared to be a more reasonable indication of parent ion intensity and was found to range from a low of 0.78 to a high of 0.96 with an average of 0.87 compared to Table 3 values of 0.81 to 0.89.

Finally, although caffeine was not studied until much later in the chromatography work, the following data is presented here:

m/e	194	109	82
Abund.	1000	360	440

No scans were recorded that included m/e 67 and all the other lower masses. As expected from Table 3, m/e 194 is the most intense ion.

Typically in the chromatography experiments only parent ions were monitored in order to keep scan ranges and scan times as short as possible. While there are indications that parent ion intensities may be somewhat higher than in typical MS spectra, that fact will have to be verified by experiments with compounds giving very low parent ion intensities.

Improvements - continuous scope monitoring, glass bead packed sample loop, and Baratron pressure gauge. Three changes were made before proceeding with further chromatography studies. The special oscilloscope sweep amplifier described in subsection 3.4.4 was added, making it possible to display repetitive fast scans (~2 sec/scan) on a storage oscilloscope during the chromatographic elution so that an elution could be studied in detail before making a permanent recording.

A second sample loop was installed (Figure 26b). The sample loop was designed to have a much smaller internal volume but with a large surface area for sample deposition. The first sample chamber fabricated from the high pressure check valve and the filter element for sample deposition (denoted by LVF in Table 2) had an internal volume of almost 1 ml. The new chamber/loop, 1.5 mm tubing packed with glass beads and denoted by P in Table 2, had an internal volume of about 75 μl in the packed section and another 15 μl in the connecting tubing. Sample injection was followed by a 15 to 30 μl rinse volume of pure solvent to rinse the 15 cm (0.15 mm I.D.) injection port assembly and the connecting tubing between the valve and the sample loop to place the sample slug on the glass beads. The solvent then was gently evacuated from the loop with a roughing pump on the HPLC vent port.

One source of confusion in operating the DGC/MS was the nozzle-skimmer chamber pressure indicated by the cold cathode ionization gauge. Since the pressure reading is dependent upon the gas ionization cross-section, similar stagnation pressures for different gases could give very different expansion chamber pressure readings. Since it was necessary to monitor that pressure carefully to avoid overloading the diffusion pump and because the pressure was of interest for its effect upon beam intensity, an absolute pressure gauge --a capacitance manometer--was added to the vacuum system of the nozzle-skimmer chamber.

Temperature study for separation of 1,3,5-triphenylbenzene and anthracene on a capillary column. A study was conducted using bath temperatures from 35 to 55°C, dense ethane pressures from 88 to 123 atm, and a 12.5 μm nozzle diameter in order to attempt a separation of 1,3,5-triphenylbenzene from anthracene on the capillary column. No significant separation was achieved. Separate injections of the two compounds at 45°C and 89 atm ethane had indicated there would be 30 seconds difference in elution times. During the elutions of mixtures, however, each compound eluted sporadically, sometimes in several narrow peaks 10-13 seconds wide. Sample sizes of each compound ranged from 25 to 100 μg, large enough to give intermittent plugging of the nozzle.. However, spectrometer sensitivity was too low and the noise level was too high to permit detection of much smaller samples.

Installation of the new ion source. As discussed in subsection 3.4.4, the magnetic field of the electron beam collimating magnet was thought to be very non-uniform in the region of the intersection of the molecular and electron beams and was possibly one source of the low sensitivity of the mass spectrometer when using the molecular beam sampling system. In the separation experiments described in the preceeding paragraph (anthracene and 1,3, 5-triphenylbenzene), the 25 μg sample sizes were seen with difficulty. For that reason a new ion source with a more uniform electron beam collimating magnetic field was designed and installed. In subsequent experiments 0.5 to 1 μg samples have been detected, so the sensitivity was improved. Some of that improvement is also due to the re-wiring of the output signal amplifier, AMP-1 in Figure 18, to reduce noise.

Permaphase ODS packed columns - initial problems and capacity ratios. It was then decided to attempt separations using a packed column. Permaphase ODS® (Dupont) was the packing chosen since it is recommended for polynuclear aromatic compound separations.[149] Dense CO_2 was chosen as the solvent gas since it had been studied by Bowman[97] and has often been used with polynuclear aromatic compounds (Table A1). Experiments with the first Permaphase ODS® column (1.5 m long x 1 mm I.D.) and 1,3,5-triphenylbenzene and anthracene were as disappointing as those with the capillary columm. There appeared to be some separation but the retention time was very long, often a minimum of 13 minutes, with the compounds eluting erratically over several minutes. Volumetric flow measurements at the exit end of the column indicated the pressure drop was unacceptably high, about 20 atm. During the experiments the nozzle orifice became completely plugged. Inspection of the nozzle orifice showed white crystals filling the conical exit volume of the combined pinhole holder and the clamping piece (parts C and D, Figure 9). The crystals were also on the upstream side of the orifice.

It was decided to make a second Permaphase ODS column, 50 cm long and 1.5 mm I.D., to reduce the pressure drop across the column. The pressure drop across this column was found to be negligible, as shown in Figure 37.

Pure solvent retention times with acetone, chloroform and ethanol were about one minute and 10 μl aliquots eluted as narrow peaks that were only 10-20 seconds broad. Only a few sample solution injections of first anthracene and then triphenylbenzene were made before the nozzle orifice again plugged with white crystals.

One idea about the plugging substance was that it was triphenylbenzene since it often was the compound last injected before a plug. It was thought that perhaps the triphenylbenzene/CO_2 solution was too unstable to be successfully expanded through the orifice. Therefore, it was decided not to use it again as a sample.

Another suggestion made to us was that the substance may have been the bonded phase from the Permaphase ODS--either there was some non-bonded amount with the bonded portion or perhaps the chemical bonds were actually being broken. The column was removed from the system and "conditioned" on a HPLC.*

---

*250 ml toluene, 400 ml chloroform and 250 ml acetone at a flow rate of 2 ml/minute.

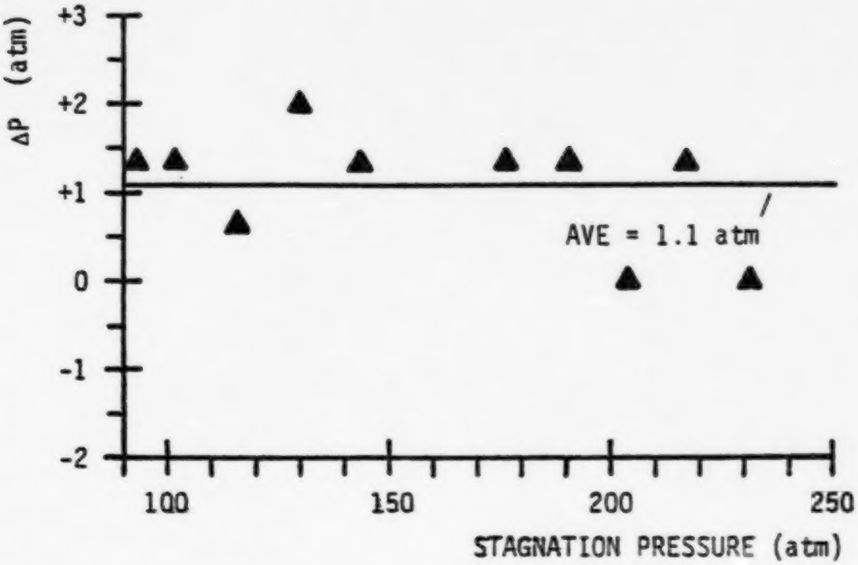

Figure 37. Pressure drop (ΔP) across a packed chromatograph column as a function of stagnation pressure. A pressure gauge identical to and calibrated by the dense gas supply regulator gauge was inserted between the HPLC shut-off valve and the filters before the nozzle orifice (12.5 μm). Nitrogen at room temperature was used to measure the pressure drop.

Column: Permaphase ODS packed in 1.5 mm I.D. X 50 cm long stainless steel tubing.

The results of the column conditioning are inconclusive. It appeared that the running time between plugging and nozzle orifice replacement was increased. However, when the column described above was repacked and a precolumn added, those components were conditioned before use and yet plugging was exceedingly rapid. The impression after-the-fact is that the longer times between plugging were due to some type of continuing conditioning by the two dense gases, CO_2 and N_2O, used with the Permaphase ODS packing.

The next set of experiments run was the estimation of the capacity ratios of anthracene and pyrene on this Permaphase ODS column with dense CO_2. Capacity ratios (k') are usually defined in chromatography as $k'=t_R/t_G - 1$, where t_G is the travel time of a non-retained substance and t_R is the retention time of a partitioning substance. Usually these times, t_G and t_R, are measured from the injection time to the centroid of the chromatogram peak. Here, we measure the time from injection to the first appearance of the appropriate m/e peak. Figure 38 shows the k' values for the Permaphase ODS/CO_2 system as a function of temperature and pressure. The capacity ratio does exhibit the same behavior as discussed by Sie and Rijnders[104] and Nieman and Rogers[103] in the temperature range just above critical: k' increases with increasing temperature rather than decreases as in typical GC work. (Sample sizes for both compounds ranged from 5 to 30 μg for these measurements.)

Although the data are rather scanty, they do show the large effect of conditions upon retention. They especially indicate those conditions that are suitable for separation of anthracene and pyrene.

Capacity ratios for anthracene, fluoranthene and pyrene for a Permaphase ODS/N_2O system, as determined in later experiments, are presented in Figure 39. Here, the temperature range studied is slightly higher than for the dense CO_2. While the plots for k' vs. temperature appear to have maxima, the number of points and their precision are both inadequate to determine curve shape. In both Figures 38 and 39 the solid lines are drawn only to connect data points. However, we believe the trends are correct. The data in Figures 38 and 39 indicate a more marked temperature dependence of k' for the Permaphase ODS/CO_2 system (34-55°C region) than for the Permaphase ODS/N_2O system (50-60°C).

Dense gas mixture - 1-bromonaphthalene/CO_2. Ion source potentials were regularly adjusted to obtain the maximum beam species signal, usually by tuning on solvent dense gas clusters with molecular weights of 150 to 200 (approximately the range for test solutes). Cluster formation and/or detection was often nonexistent at higher stagnation temperatures and expansion chamber pressures (Figure 36) with the result that spectrometer tuning using clusters was not possible at those (operating) conditions. A better approach was thought to be beam seeding at the operating conditions for more appropriate and dependable electronics tuning. Therefore, a 0.1 mole-% bromonaphthalene in CO_2 mixture was made by injecting the 1-bromonaphthalene directly into the large dense gas reservoir and then pressurizing it.

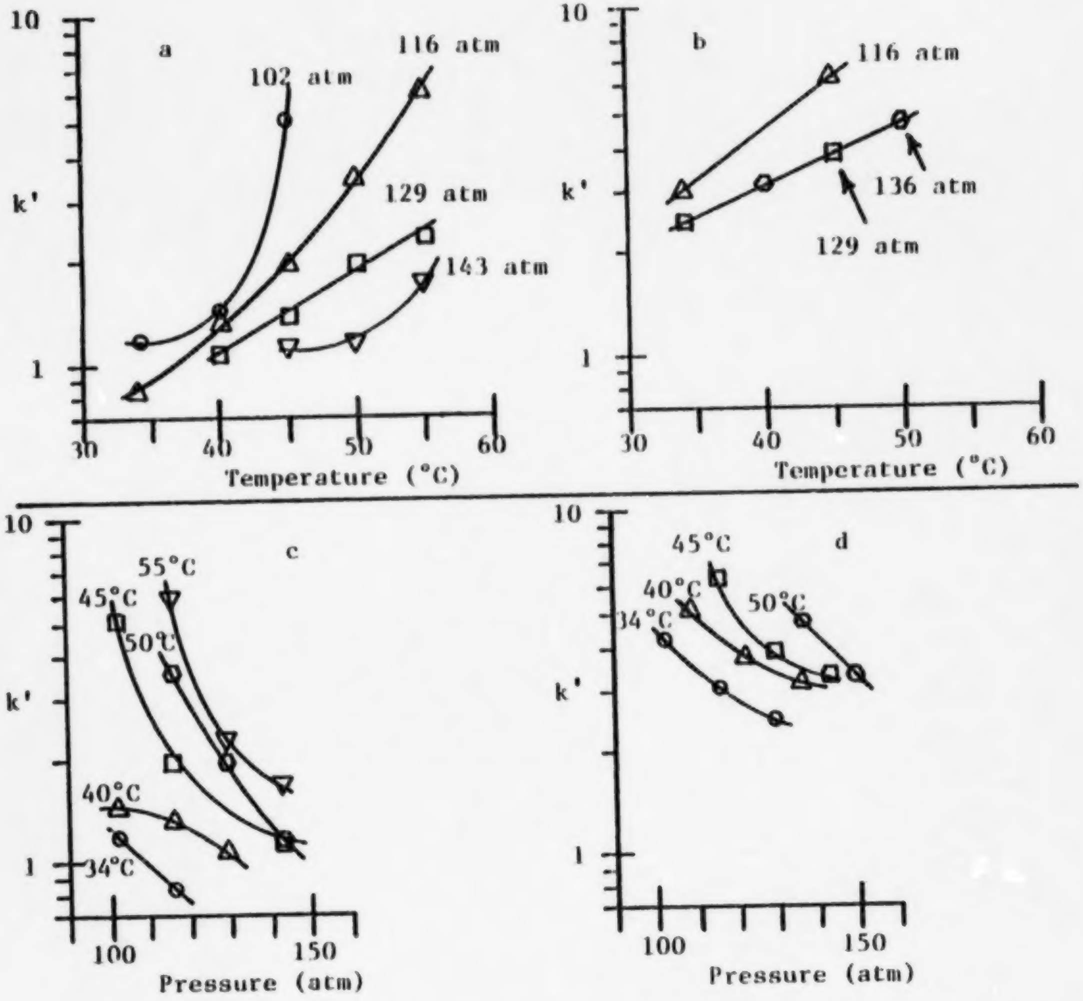

Figure 38. k' as a function of temperature or pressure for anthracene (a,c) and pyrene (b,d) in dense CO_2 on a Permaphase ODS column (50 cm long X 1.5 mm I.D.) using a 12.5 µm nozzle diameter.

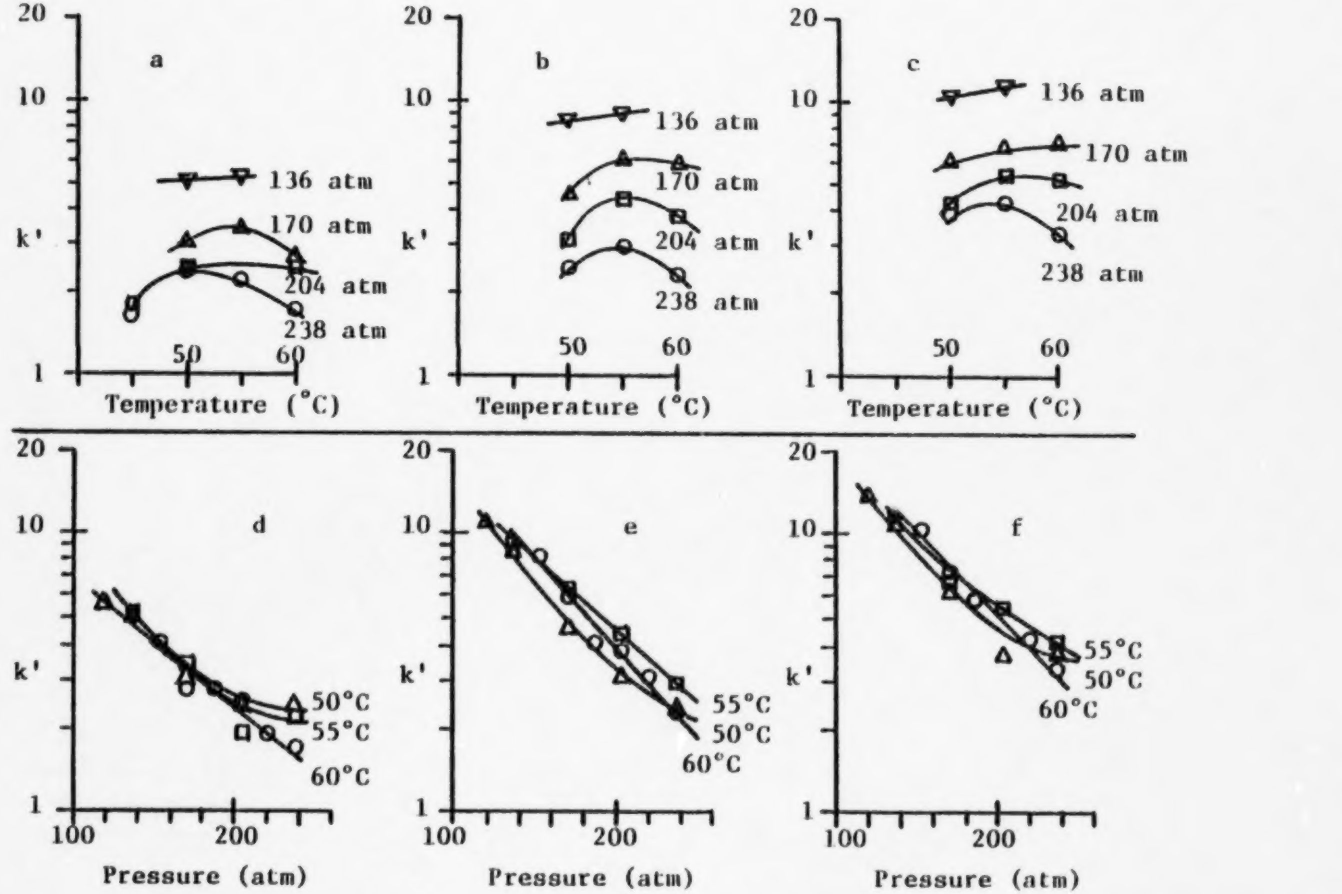

Figure 39. k' as a function of temperature or pressure for anthracene (a,d), fluoranthene (b,e), and pyrene (c,f) in dense N_2O on a Permaphase ODS column (50 cm long X 1.5 mm I.D.) using a 5 µm nozzle diameter.

anthracene 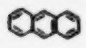

fluoranthene 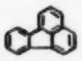

pyrene

After the tuning experiments,* some elution experiments were conducted even though the 1-bromonaphthalene remained in the dense CO_2. With the dense 1-bromonaphthalene/CO_2 mixture the retention times of anthracene and pyrene were reduced to 70% and 90%, respectively, of their values with pure dense CO_2. These rather large and selective changes relative to the small amount of the second component in the carrier indicated the advantages that may exist with dense gas mixtures.

Studies with dense gas mixtures will be imperative in future DGC/MS work for another reason. A common value that is quoted in chromatograph/mass spectrometer interface studies is the enrichment factor. While no detailed study to determine this factor was undertaken during the preliminary experimentation described in this report, the experiments with the 1-bromonaphthalene/CO_2 mixture did provide a means for an order-of-magnitude approximation. The mass spectrum intensities of the mixture components indicated a mole ratio of $1\text{-}3 \times 10^{-3}$ (bromonaphthalene to CO_2)--reasonable agreement with the theoretical 0.1 mole percent. Because of the approximations in the calculations and the manner in which the mixture was prepared, neither number is precise. However, their comparison does show that there is not dramatic concentration of either component in the molecular beam. Further testing of the DGC/MS will require more work in this area to obtain the necessary characterization of this technique.

Successful separation on a Permaphase ODS column. Attempts were made to separate four compounds: phenanthrene, anthracene, fluoranthene and pyrene. With an N_2O pressure and temperature (103 atm, 50° C) suitable for fast elution of fluoranthene and pyrene, anthracene and phenanthrene eluted practically at the same time. Conditions (100 atm, 55°C) which led to some separation between phenanthrene and anthracene led to retention times three times as long for fluoranthene and pyrene with the chromatograph "peaks" smeared over such a long time that it was difficult to distinguish an increase in m/e 202 intensity over background and also to distinguish between those two compounds which both have a molecular weight of 202. However, the four compounds do elute in the same order[149] as in HPLC with a Permaphase ODS stationary phase and gradient elution.

Finally a rudimentary separation was achieved with anthracene, fluoranthene, and pyrene at three different temperatures. These separations are shown in Figure 40. Particularly interesting is the effect of temperature upon retention time: as shown in B and C, only 3°C can change the retention time of fluoranthene and pyrene by a minute.

---

*In other tuning experiments, the signal maximizing potential difference to the focus plates for $(N_2O)_5^+$ (m/e 220) was significantly different from that for seeded 1-bromonaphthalene (m/e 206) or seeded anthracene (m/e 178) even though all masses are similar. This difference may be important when maximizing solute detection, and its origin should be determined for that reason.

Figure 40. Separation of anthracene (1), fluoranthene (2), and pyrene (3) with □ - m/e 178 intensity and △ - m/e 202 intensity.

Nozzle diameter - 12.5 μm

Column - Permaphase ODS, 50 cm long X 1.5 mm I.D.

Sample loop - Regular glass beads (Analabs) packed in stainless steel tubing 1.5 mm I.D. X 10.2 cm long.

A - N_2O at 102 atm and 50 °C
(quantities of 1, 2, and 3--4.3 μg, 4.3 μg, 6.5 μg)

B - N_2O at 102 atm and 52 °C
(quantities of 1, 2, and 3--4.3 μg, 6.4 μg, 8.5 μg)

C - N_2O at 102 atm and 49 °C
(quantities of 1, 2, and 3--2.3 μg, 3.4 μg, 4.5 μg)

• - Data points smoothed by $X_i' = (X_{i-1} + 2X_i + X_{i+1})/4$

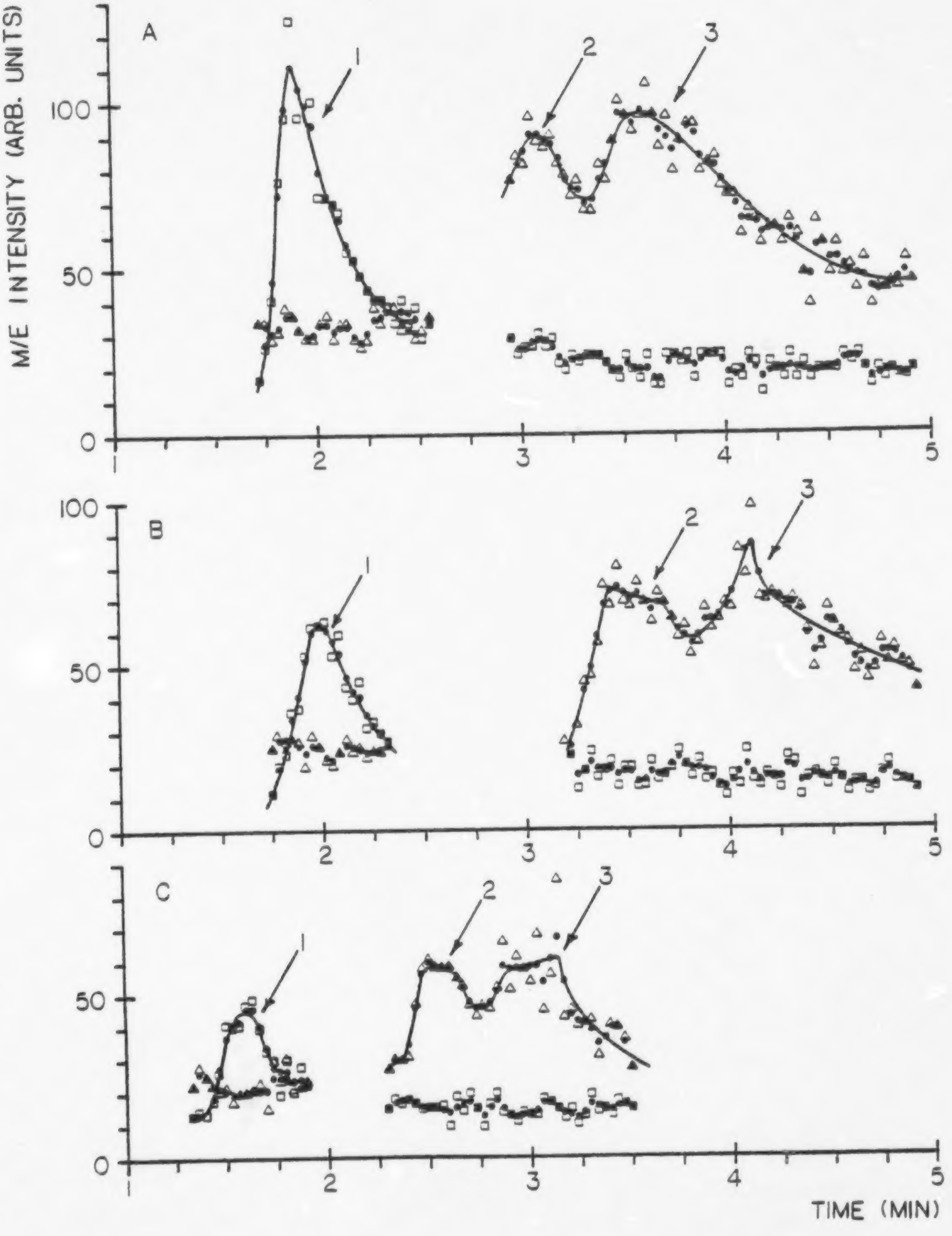
M/E INTENSITY (ARB. UNITS)
A
B
C
1
2
3
0
50
100
1
2
3
4
5
TIME (MIN)

Final sample loop configuration. The broad chromatogram peaks in Figure 40 were thought to be caused in part by the sample loop with the unsilanized glass beads. A new sample loop was constructed as described in Section 3.4.6. (Figure 26c). It has a 194 µl internal volume and 7.5 cm^2 internal surface (smooth) area. The small sample and rinsing aliquots used, 1 to 10 µl, should have deposited the sample in a narrow band right next to the valve port.

During the first capacity ratio studies, the stagnation pressure was limited by the 12.5 µm nozzle orifice. Because of the marginal pumping speed of the VHS-6 diffusion pump, higher CO_2 pressures (137-151 atm) could be used only with higher bath temperatures above 45°C. Therefore, a 5 µm nozzle orifice was substituted. The capacity ratios for the Permaphase ODS/N_2O system in Figure 39 were obtained with the new sample loop and a 5 µm nozzle diameter.

Injection procedures and modifications. It had become common practice by this time to allow the sample to equilibrate* with the dense gas before sweeping it on column. For large liquid solvent samples (1-10 µl), such equilibration reduced the travel time (again, the time from injection to the first m/e detection) to 63% of that of the non-equilibrated sample. With small solute samples where most of the liquid solvent had been pumped off before equilibration and the solute size was ~10 µg, the retention time was reduced from 87 to 95% of non-equilibrated values for anthracene, fluoranthene and pyrene. The equilibration procedure necessarily stopped flow through the nozzle for some length of time, required extra shut-off valve actuation (with extra wear particles generated), and had large initial pressure drops along the system when flow was reestablished. The large pressure drop created by the equilibration procedure probably caused the described reduction in travel/retention time from the non-equilibrated values. (Another factor for this effect may be the elimination of a mixing time.) Of course, with the flow stopped, the nozzle-skimmer expansion chamber pressure would drop and often was never reestablished at the pre-equilibration value but at a lower pressure. It was feared that this was an indication of partial plugging.

A new method of sample introduction was hastily devised; very little time has been available for its testing and refinements. The additional valving required for this method is shown in Figure 30; during the complete loading process, flow through the nozzle is never interrupted.**

---

*The procedure for equilibration was the following: turn the HPLC shut-off valve roter 60° so that no ports are connected, turn the HPLC sampling valve loop in-line, equilibrate for 1/2-10 minutes, and reestablish flow through the system by turning the shut-off valve back to the column-nozzle configuration.

**The procedure is as follows: the sample is injected into the fill-port assembly, followed by a small amount of pure solvent to rinse the sample into the sample loop; the solvent is gently pumped off through a 0.15 mm I.D. restrictor on the vent side of the high pressure valve, HP2; another small portion of solvent is placed in the fill-port assembly extension; the teflon-lined injection nut on the assembly is replaced with a solid plug; and the high pressure valve, HP2, is closed while the second high pressure valve, Decreasing volume in the nozzle assembly. At the same time the extra valves for injection were added, the nozzle assembly inlet tubing (part T, Figure 9) was replaced with 0.15 mm I.D. tubing. Hence, the volume of the tubing after the shut-off valve should have been decreased from about 150 μl to 15 μl. Approximate calculations indicate that the pressure drop along this tubing might be too large, thereby causing solute precipitation. While this result was not encountered in the very limited work with this tubing, a larger size would be preferable (e.g., 0.25 mm I.D.).

Repacking the Permaphase ODS column and adding a precolumn. The flow through the Permaphase ODS column had seemed slow; measurements with it removed from the system showed that the volumetric flow rate had decreased by about a factor of 5 from when it was originally packed. The entrance packing was dark brown and appeared wet. The column was repacked with new Permaphase ODS and a 5.5 cm precolumn also packed with Permaphase ODS was added. This assembly was then conditioned.*

Nozzle orifice plugging possibly associated with column packing. After just five injections of a chloroform/anthracene solution, the nozzle plugged, halting further experimentation with the new injection valves, the decreased volume nozzle assembly tubing, the newly packed and conditioned column and a newly mounted 5 μm pinhole. Since this was the last 5 μm pinhole in the laboratory stock, much effort was devoted to unplugging it. Microscopic examination of the pinhole mounted in its holder showed that the plugging resulted from a white, apparently crystalline, deposit. None of the following solvents would dissolve the white crystals--even when immersed in an ultrasonic bath of the solvent: chloroform, ethanol, acetone, methanol, toluene, distilled water, cyclohexane, benzene, n-pentane, or various combinations of these. Swiping the surface with a wet Kim Wipe® tissue did not budge the crystals down in the concave part of the hole (see Figure 10). Finally the pinhole foil (shim stock), which had fallen out of the pinhole holder, was placed on a Petri dish on a hot plate at its highest setting (~300°C). The foil was dropped into an ultrasonic bath of ethanol and acetone and the hole cleared. The foil was remounted; flow measurements with N_2 on the bench top indicated it had enlarged to over 8 μm by comparison with 5 μm orifices under the same conditions.

It was decided that the pinhole plugging was caused by the column packing, since all solutes used throughout experiments with the Permaphase ODS packing should have dissolved in one of the solvents tested. Even with prior HPLC conditioning, exposure to a dense gas (at lease CO_2 and N_2O) resulted in very fast plugging. We thought the bonded octadecyl groups were being stripped

---

HP1, is opened to admit dense gas to the isolated sample loop. After some time for equilibration the high pressure valve, HP1, is closed and the sample loop is turned in-line.

*The first part of conditioning was on a HPLC with approximately 200 ml aliquots of distilled water, methanol, distilled water, acetone, chloroform, toluene and acetone. The packed assembly was dried in an 80°C oven with N_2 flowing through it for ~12 hours.

off the glass beads. Communication with Mr. Hank Clemente of Waters Associates indicated that low pH solutions can dissolve the glass beads. In our experiments no care had been taken to dry or to obtain specially dried gases. It is possible that H_2CO_3 and $H_2N_2O_2$ were formed under the dense conditions—especially when some samples were dissolved in water. These acids may have eroded the glass beads with the result that SiO_2 was deposited on the pinhole. Only trace amounts would be required to plug the pinhole. This identity would account for the inability to dissolve the white crystals with common organic solvents.*

For the final solute experiments, the capillary column (with its inner surface etched) and the original 0.51 mm I.D. nozzle assembly inlet tubing were re-installed.

Solubility studies of caffeine, L-(+)-arginine, and ℓ-histidine. Before the last improvements to the system were made (i.e., the injection valving, the decreased volume inlet tubing, and the freshly packed Permaphase ODS column just described), some further solute experimentation was done. Figure 41 shows the elution of a large sample of caffeine, ~62 μg, by dense N_2O at 238 atm and 38°C on the Permaphase ODS column. Injection procedure greatly affected the retention time of caffeine on the column. When the caffeine/chloroform solution is introduced directly to the packed column with no chloroform evacuated, the retention time of caffeine is shown to be about 5 minutes while the travel time of pure chloroform is 3 minutes and the chloroform chromatograph peak width is about 1 minute. Simply evacuating the chloroform increases the caffeine retention time to greater than 7 minutes. When the chloroform is not removed, the caffeine apparently remains in the solvent slug for a significant part of the column length. Earlier experiments with anthracene showed essentially no retention of the solute on the column when it was introduced as a solution slug, although in the earlier experiments more solvent was present because of the large "rinsing" solvent aliquots used in injection.

The success with caffeine prompted experiments with L-(+)-arginine and ℓ-histidine. Both compounds were somewhat soluble in a 2:1 methanol/water mixture (~100 mg compound in 10 ml solution). No evidence was seen for the dissolving and the elution of arginine. However, almost 9 minutes after introducing the histidine to the column as a solution slug, the nozzle orifice plugged. The N_2O was at 238 atm and 38°C. Increasing the N_2O pressure to 259 atm did not clear the pinhole. For both the arginine and the histidine, water had been introduced to the column, thereby possibly causing column decomposition as discussed above. However, after the arginine injection, flow continued undisturbed through the nozzle orifice for about an hour. By comparison, the histidine injection caused plugging in a suspicious length of time: after the methanol/water mixture had been eluted and not much longer than the similar caffeine elution time (Figure 41).

---

*Support for this view was obtained when it was recently learned (personal communication at the 27th Annual Conference on Mass Spectrometry and Allied Topics; that experimenters with HPLC/MS instruments have observed an increase in the m/e 60 (SiO_2) intensity when using similar packings.

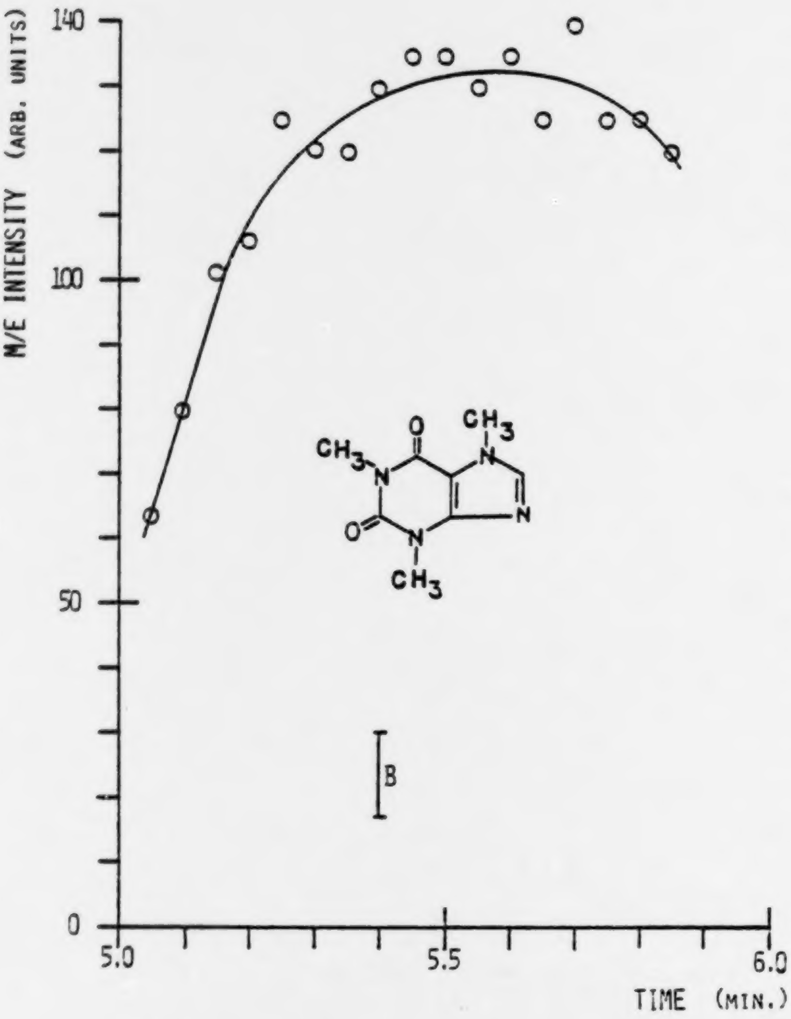

Figure 41. Elution of caffeine (∼62 μg) by dense N_2O.
Conditions - 238 atm and 38.0 °C.
Column - Permaphase ODS, 50 cm long X 1.5 mm I.D.
Sample loop - stainless steel, 1 mm I.D. X 22.9 cm long with etched inner surface.
Nozzle diameter - 5 μm.

A solution (100 mg/10 ml) of caffeine in $CHCl_3$ was injected directly onto the column with no evacuation of $CHCl_3$ and no equilibration with N_2O. Pure $CHCl_3$ (∼2 μl) has a 3-minute travel time and an elution width no longer than 1 minute. An identical solution sample with the $CHCl_3$ pumped off and no equilibration with dense N_2O is first detected after 7 minutes. B--background intensity of m/e 194, parent ion.

When the system was finally operating again with the enlarged 5 μm orifice and the 6 m capillary column, experiments with caffeine and ℓ-histidine were again attempted. Figure 42 shows the elution of caffeine with dense N_2O at 184 atm and 39°C. A very small difference between the center of the chloroform travel time and the caffeine chromatograph peak centroid can be seen. The caffeine sample was introduced with the dense gas equilibration/continuous dense gas flow method. The chromatograph peak is still broader than desired, especially for a capillary column. The linear flow rate here, about 5 cm/sec, is lower than the 20 cm/sec often considered to be optimum in typical GC capillary studies.[143] However, it was not possible to increase the flow rate here by increasing the stagnation pressure because the 184 atm pressure was the maximum pressure possible with the enlarged nozzle diameter, due to the marginal expansion chamber pumping speed.

Almost 10 mg of ℓ-histidine was dissolved in 10 ml of a 50/50 methanol/water solution. A 10 μl aliquot of this solution was introduced to the sample loop, the solvent was evacuated, and the sample loop was pressurized with dense N_2O at 184 atm and 39°C. Almost four minutes after injection the nozzle orifice plugged. Mass scans taken before and during the plugging indicate there may have been some ℓ-histidine eluted. At 3.77 minutes after injection, the m/e 155 (MW 155 for ℓ-histidine) intensity increased 50% over the average of three background scans and stayed up for the next two scans. However, by 3.87 minutes the m/e 155 intensity had fallen to background values and the expansion chamber pressure had decreased sharply. While m/e 155 is not a reported ion for histidine (EPA/NIH Mass Spectral Data Base[144]) and a much larger increase in that ion or in the expected most abundant ion, m/e 82 (not monitored here), is required for positive identification, the sequence of small intensity increase followed by plugging does imply that the increase in m/e 155 was more than random noise. This plug was dislodged after some 20 minutes; however, in all experiments thereafter, the stagnation pressure had to be lowered to maintain the expansion chamber pressure at some reasonable value since the diffusion pump for that region was erratically turning off due to overloading. After a few more temporary plugs, which also occurred almost four minutes after injection of other histidine samples, a final sample resulted in an unmovable plug.

Since 5 μm pinholes which would have permitted work at higher solvent gas pressures were not immediately available and since the final date for experimental work on the project supported by the Environmental Protection Agency had past, experiments were terminated.

3.5.6. Brief Summary of Experimental Observations, Results and Conclusions

Molecular beam generation and detection. The molecular beam system design described in this report has successfully resulted in molecular beam formation. Moreover, that beam and the various species within it (i.e., monomer gas, condensation clusters, and seeded species) can be monitored by the detecting mass spectrometer.

Detecting mass spectrometer. The Perkin-Elmer Model 270 mass spectrometer used in these experiments was furnished by the Department of Chemistry. It had been used as a routine instrument by inexperienced operators and was

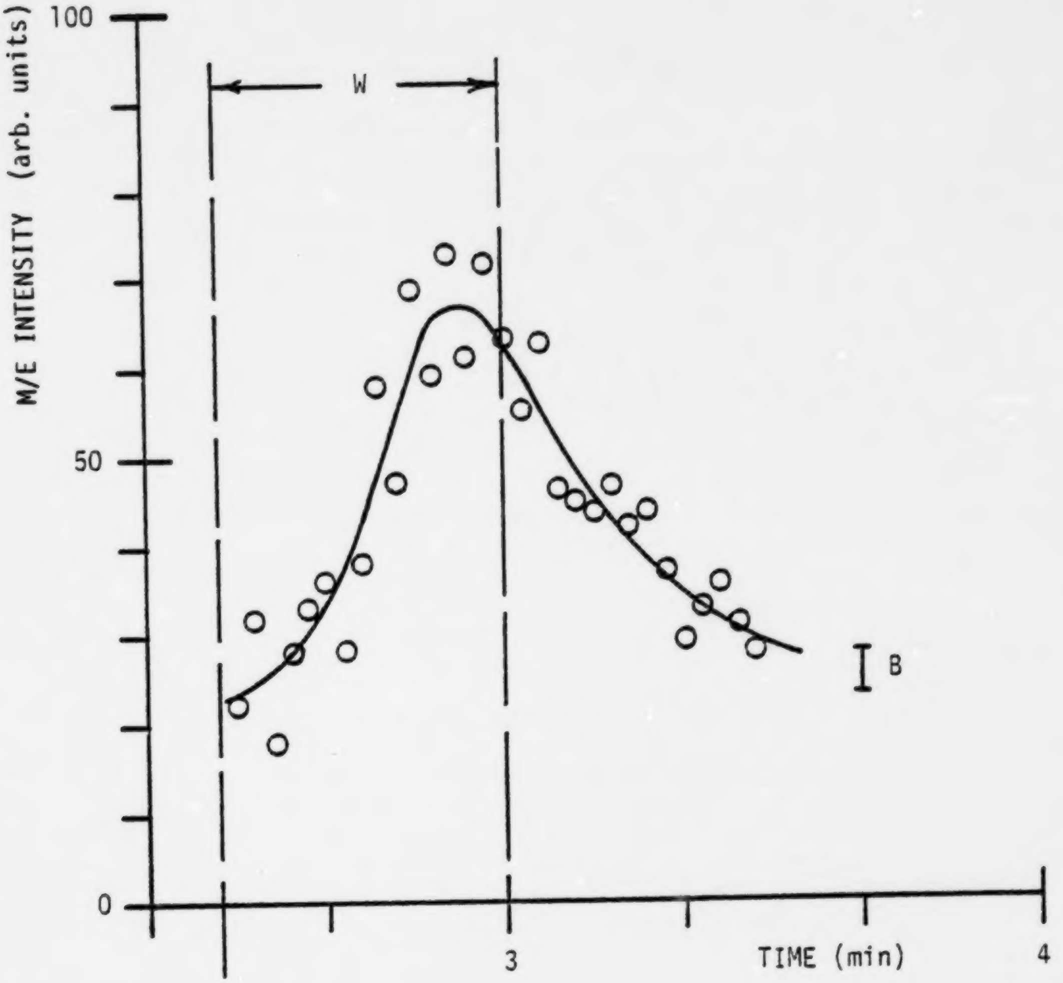

Figure 42. Elution of caffeine (∿11 μg) by dense N_2O.
Conditions - 184 atm and 39.0 °C.
Column - 6 m long X 0.51 mm I.D. with etched inner surface.
Sample loop - stainless steel, 1 mm I.D. X 22.9 cm long with etched inner surface.
Nozzle diameter - enlarged 5 μm (estimated to be approximately 8 μm).

A solution (10 mg/10 ml) of caffeine in $CHCl_3$ was loaded into the sample loop. The solvent $CHCl_3$ was pumped off, the sample loop was filled with dense N_2O and equilibrated several minutes before valving to the column, and then the parent caffeine peak (m/e 194) was monitored. W--time interval for elution (time above background) of a 2 μl $CHCl_3$ slug in another run under same conditions. B--background intensity of m/e 194, parent mass of caffeine.

abused. Additionally, design and machining flaws were found in it--e.g., electron beam collimating magnet and aligning surfaces--that were unimportant for common applications but became very important for this application. For these reasons the performance of this mass spectrometer has been far from ideal and has required an unexpected and disproportionate amount of effort and funds to adapt it for this research.

The unusual behavior of the ion optics, while pursued only enough to gain the desired results in this work, certainly indicates a fertile area for more theoretical studies and for experimental modification leading to higher sensitivity.

Cluster formation. As was discussed in subsection 3.3, condensation in the beam to form solvent-solvent, solvent-solute, and solute-solute clusters is possible. Thus far we have seen limited clustering of the solvent gases from dimers up to $(N_2)_9^+$, $(C_2H_6)_{17}^+$, $(C_2H_4)_{20}^+$, $(CO_2)_{13}^+$ and N_2O comparable to CO_2 but not recorded. Cluster formation and detection is a sensitive function of nozzle tip temperature, stagnation pressure and temperature, and, most particularly, expansion chamber background pressure. We have seen no large cluster masses (i.e., out to m/e = 1000) in the mass spectra. Also, we have not visually observed any particles between the nozzle and skimmer when viewing that region through a lighted port. However, if the particle size is on the order of 8 nm as calculated in subsection 3.3, one would not expect to see such clusters with the present illumination and it is possible that these large clusters (e.g., calculated average number of molecules in a cluster, $\bar{N}$, is 10^4) are being formed. Such clusters are far too energetic to be extracted into the mass spectrometer orthogonal to their direction of motion. As pointed out by Hagena[133] and others, clusters are quite stable when ionized by electron beams having about the same energy as typically used in this work (~50 eV) so one would not see fragmentation in the ion source. The large clusters, if present, would travel straight into the ionization gauge. The important question is how much solute is lost in clustering. Hagena states that condensation of the solute is enhanced by the solvent gas below a carrier gas mole fraction of about 0.95; above this fraction solute cluster growth is controlled by solute collisions. In subsection 3.5.5 maximum solubilities in terms of mole ratios of $\sim 0.5 \times 10^{-3}$ anthracene/CO_2 and $\sim 0.3 \times 10^{-4}$ 1,3,5-triphenylbenzene/CO_2 were presented and shown to agree fairly well with the work of Bowman.[97] If most solutes are dissolved to this small an extent, the review by Hagena indicates there will be negligible solute-solute clustering. Some solute molecules would be incorporated into the large solvent clusters ($\sim 10^4$ molecules) if they are formed, but our negative finding of clusters $\bar{N} > \sim 20$ and our agreement with the solubility data of Bowman indicate that the amount of solute lost in this way is insignificant. The lack of solvated solute species $[Su(Sv)_n]^+$ in the mass spectra shows not only that condensation is not a problem but also that the solutes studied thus far do not remain solvated (even partially) in the expansions. The net result is that the mass spectra are sometimes complicated by the presence of solvent clusters but rarely by solute-solute or solute-solvent clusters in DGC/MS analysis with stagnation pressures up to 238 atm, temperatures as low as $T_c + 5°$ for T_c = 283 to 310°K, and nozzle diameters of 5 and 12.5 μm.

Versatile beam generating and sampling system. The easily variable temperature and pressure stagnation conditions as well as nozzle orifice should make our design particularly attractive to those interested in condensation kinetics and cluster beam formation where often there has been little versatility in experimental conditions.[133] Without the chromatograph column, our system can be used as a convenient seeded beam source operating at atypical pressure extremes.

Our situation is unlike that of Levy *et al.*[132,150,151] who also use the high pressure/small nozzle diameters that we do. They conduct spectroscopy within the space between the nozzle orifice and the Mach disk. Therefore, their experiment can tolerate higher background pressures such as 0.06 torr. Our purpose is to transmit the jet molecules about 20 cm into the ion source without their passing through a Mach disk or any other shock wave. The beam system most closely resembling ours is one designed for obtaining maximum beam velocity.[152] These studies, using stagnation pressures up to 200 atm and nozzles as small as 29.5 μm, show that a proper skimmer does permit beam extraction with an expansion chamber pressure between 10^{-2} and 1 torr from Roots pumps. The advantages claimed for such a system over one using a diffusion pump are not applicable to our problem, where initial pressure and flow rate are separately determined by chromatographic considerations. Also, the discussion did not consider the relative cost of Roots pumps and diffusion pumps. It is interesting to note that "high pressure" in the literature on molecular beam sampling systems for mass spectrometers generally refers to pressures less than 7 atm[153,154] (compared to the sampling of the 250 atm stagnation pressure achieved in this work).

Parent ion abundance. Slightly increased parent ion abundances (chloroform, azobenzene, ethanol) indicate that there might be an additional advantage of the molecular beam introduction method: decreased fragmentation due to the low internal energy of solute molecules. Hence, molecular mass determination may be simplified as with chemical ionization, but without the complications of proton or hydride transfer and with some fragmentation remaining for compound discrimination. Since most of the work presented in this report was with compounds that are expected to yield high parent ion intensities, further work is necessary before claims of greatly simplified spectra can be made.

Nevertheless, supersonic expansion does result in cooling of translational and internal degrees of freedom so the DGC/MS instrument--again, without the chromatograph column--may be a feasible source of " cold" species for low temperature mass spectroscopy. A molecular beam system as presented here may be easier to implement than a specially cooled ion source especially with substances which have low vapor pressures at low temperatures. Of course, the latter source would produce an equilibrated, Boltzmann distribution while the former results in a non-equilibrium distribution.

Chromatographic studies. The solute, solvents, sample chamber/loops, chromatographic columns and chromatograph conditions studied in this work are summarized in Table 2. The following compounds have been eluted and detected: naphthalene, anthracene, 1,3,4-triphenylbenzene, azobenzene, phenanthrene, fluoranthene, pyrene, and caffeine. Anthraquinone was detected in small amounts. There is some evidence that inosine and ℓ-histidine were eluted and transported to the ion source; however, the observed mass peaks were not those usually reported and the experiments need further verification. The results with the compound L-(+)-arginine were negative. Solvent dense gases studied were ethylene, ethane, carbon dioxide, and nitrous oxide.

Capacity ratio studies for Permaphase ODS/CO_2 and Permaphase ODS/N_2O were presented in subsection 3.5.5. The capacity ratio temperature dependence is in accord with previous DGC studies.

Moreover, the more general characteristic of a highly temperature-dependent solubility near the critical temperature requires the use of an appropriate temperature gradient to avoid solute deposition--particularly at the nozzle orifice.

The separation of anthracene, fluoranthene and pyrene at three temperatures was presented. The separation of anthracene from phenanthrene at different conditions is possible but separation of all four compounds under isobaric and isothermal conditions with Permaphase ODS/dense N_2O was not achieved.

A 0.1 mole-% 1-bromonaphthalene/CO_2 mixture preferentially altered retention times for anthracene and pyrene on Permaphase ODS. This experiment shows the great versatility dense dilute mixtures may have.

Flow rates. The nozzle orifice limits the flow rate. The orifice size must be selected to limit the flow to within the gas-handling capacity of the pumps at the highest pressure to be used and yet give an adequate flow rate for effective chromatographic compound separation at as low a pressure as possible. This imposes conditions on the column and the entire system not found in DGC, HPLC, GC, and GC/MS instruments and limited the use of the present instrument with any one pinhole to a relatively narrow pressure range (about a factor of two).

Nozzle orifice plugging. The problem of nozzle plugging was far harder to eliminate than expected. Plugging by foreign material seems to have been solved by the present system of filters. Plugging by sample has been greatly reduced by the present temperature control system and should be eliminated by a more complete system. Plugging caused by possible column packing decomposition has not been solved and will require further experimentation.

Chromatographic equipment/supplies problems. Because of the great development of HPLC, much technology from that field can possibly be applied to DGC. However, two such applications have caused much difficulty in this work. The HPLC valves purchased from Valco Instruments, Inc. are of high quality. However, normal usage produces wear particles that require extra precautions in the DGC/MS apparatus. While the HPLC valves have been successfully employed in the experiments so far, it has been impossible to use the bonded phase packing routinely without problems. This packing, Permaphase ODS from DuPont, appeared to be ideal for DGC. Its use in the DGC system (by experimenters somewhat inexperienced in this area of chromatography) appears to have resulted in decomposition of the packing but additional experiments with dry gases and other HPLC packings are needed. The nozzle orifice plugging problem tentatively attributed to Permaphase ODS may not have been caused by that packing; the cause remains to be unequivocally ascertained.

Conclusions. All of the results show that DGC/MS is a feasible analytical method. Puzzling and time-consuming problems have been present at many points of development but none of them has been insurmountable. The DGC/MS is a complicated instrument that may not develop into a common laboratory tool; however, it will most certainly be usable in better equipped analytical laboratories with competent technicians. This method should be applicable to high pressure reactions and extractions for kinetics studies as well as identification/monitoring purposes. Not only is the instrument applicable in these types of experiments, but also it appears to be a unique and versatile molecular beam sampling system for mass spectrometers. The variable stagnation conditions of the beam gas, the easily changed nozzle orifice, the wide range of the nozzle-skimmer separation, and the other design features of the molecular beam system make it usable in molecular beam applications.

We believe the principle goal of this work has been reached: the development of a new analytical instrument, the DGC/MS. While the system is clearly in need of further improvement, separation of similar compounds with MS detection has been obtained. The next step, unquestionable evidence that MS analysis is possible for involatile substances, will require only minor improvements to the present instrument.

3.5.7. Suggested Improvements and Experimentation

Several improvements that should make operation of this DGC/MS instrument easier, more reproducible, and more useful are 1) improved temperature control, 2) improved sample introduction, 3) density or pressure programming, 4) addition of mixture-making capabilities to the dense gas supply system, 5) increased dense gas supply pressure range, 6) improved mass spectrometer and molecular beam trap pumping, 7) addition of a molecular beam chopper, and 8) addition of a data handling system.

Temperature control. With the present temperature control system, the injection system including the sample loop is held at the same temperature as the chromatograph column and the nozzle supply tubing between the column and the nozzle tip. The experiments described in this report have shown that a temperature gradient from sample loop to nozzle tip is desirable. Hence, independent control of four regions is indicated: sample loop, chromatograph column, nozzle assembly supply tubing, and the nozzle tip.

Sample introduction. The sampling procedure influences chromatograph peak width and shape strongly. A high pressure sampling system with minimum dead volume which permits equilibration of the sample with the dense gas without disturbing flow through the column and the nozzle orifice must be devised. It must accept solid samples as well as solutions, since many substances of interest are not soluble in a convenient volatile solvent. Additionally, the injection time must be minimized to yield an acceptable plug injection.

Density programming. The experimental difficulties with separating a mixture of phenanthrene, anthracene, fluoranthene, and pyrene at any one pressure, in addition to the number of references cited in subsection 3.2 and Appendix A which use density (pressure) programming, emphasize the need to add programming capabilities to the present dense solvent gas supply. Density (pressure) programming is a unique and powerful advantage of DGC.

Dense gas mixture. As the experiments with 1-bromonaphthalene in carbon dioxide indicated, it would be desirable to study dense solvent gas mixtures. The present system has no provision for the use of dense gas mixtures. Further meaningful experimentation, for both chromatographic application and molecular beam interface characterization, will require precise control of the mixture composition.

Dense gas supply pressure. At this time the maximum outlet pressure from the dense gas supply is 273 atm (4000 psig). The experiments to date have been limited to a maximum pressure of 250 atm (with 5 μm nozzle orifice). Examination of the studies listed in Table A1 in Appendix A shows that a pressure capability of at least 600 atm would be desirable. By using an even smaller laser drilled pinhole (1 μm and 2.5 μm available), it would be possible to increase the dense gas supply pressure and still maintain low expansion chamber pressures.

Improved mass spectrometer and molecular beam pumping. The low-speed diffusion pumps with water-cooled baffles on the mass spectrometer should be replaced by modern pumps with refrigerated baffles to reduce background interference. Also, the pump on the molecular beam detector/trap is very old and of doubtful quality and also should be replaced. The data in Table 1 do indicate that the pumps give background pressures of about 10^{-7} torr in their respective sections. However, mass peaks at most masses up to about m/e 200 are observed.

Molecular beam chopper. The addition of a molecular beam chopper between skimmer and collimator and phase sensitive detection of the resultant A.C. ion beam component would largely eliminate the peaks due to background molecules and also improve the signal/noise ratio for the system.

Data handling. As noted, the present oscillographic system for obtaining data is unsatisfactory because it lacks sensitivity, is likely to lead to nonrecording of data, is time-consuming to reduce, and is wasteful of expensive photographic recorder paper. Thus, a mini- or micro-computer based data collection system is essential.

Other improvements are necessary but cannot be implemented without the construction of a completely new instrument: improved expansion chamber pumping, increased temperature range, and improved mass spectrometer. The first is a direct consequence of the nozzle-orifice controlled flow rate. In order to avoid frequent orifice changes during pressure studies and in order to use larger orifice diameters to give good chromatographic resolution at low pressures and yet operate at pressures high enough to volatilize involatile samples while using density programming, a pumping speed several times higher than that presently used (2400 ℓ/sec) is required. The present system is limited to a maximum temperature of approximately 70°C; temperatures as high as 250°C have been used in other DGC work. An increased temperature range would allow the use of interesting gases and gas mixtures with higher critical temperatures. Implementation of a system with a higher temperature limit would require thermal isolation of the nozzle assembly and modifications to the chromatograph. Finally, a mass spectrometer with high ionization efficiency, faster scanning, easily selected scan ranges, selected peak monitoring capability, more stable electronics, a higher resolution and a higher sensitivity is needed.

Future studies. Obviously, a new instrument with all the indicated improvements would be desirable. However, the instrument described in this report can be used for further experimentation after incorporating the first eight additions. The future studies that should be conducted with this instrument are:

A. Solvent gas studies. Additional gases that have critical temperatures within the present equipment temperature range, 15° to 70°C, such as CHF_3 (T_c = 25.9°C), $CClF_3$ (T_c = 28.8°C), and $CH_2{:}CF_2$ (T_c = 29.7°C) should be tried.

B. Mixed solvent gas studies. Mixtures with $T_c < \sim 60$°C should also be studied, including programmed variable composition if it appears to be of sufficient importance.

C. Column studies. There are several HPLC packings to be studied for this application. The matching of column length and I.D. to nozzle diameter must be further explored.

D. Compound survey. The basic purpose of the development of this DGC/MS instrument is to determine ultimately the range of compounds and mixtures for which the DGC/MS is superior to other chromatographies. The initial studies begun by this work should be continued.

SECTION 4

THE DIRECT COUPLING OF A HIGH PRESSURE LIQUID CHROMATOGRAPH TO A MASS SPECTROMETER BY A SUPERSONIC MOLECULAR BEAM INTERFACE UTILIZING ULTRASONIC ATOMIZATION

Jean H. Futrell

4.1. PRIOR HPLC/MS INTERFACES

The most serious limitation to widespread application of high speed liquid chromatography--a rapidly growing, exceedingly powerful new separation technique which is especially important for the analysis of polar, involatile and thermally unstable compounds[149]--is the lack of a versatile, highly sensitive, and compound-selective detector. Since involatile samples comprise such an overwhelming majority of the compounds of analytical interest, HPLC research has been very much emphasized in recent years, greatly intensifying the search for a universal detector. The mass spectrometer is an obvious choice, by analogy with GC/MS, to complete the provision of an extremely powerful tool for the analysis of complex mixtures of volatile substances. However, the formidable problems associated with the molecular flux required by HPLC and the vacuum requirements of the mass spectrometer are very difficult to satisfy simultaneously--much more so than in GC/MS. This is readily appreciated by noting the roughly thousandfold difference in densities of liquids and atmospheric pressure gases. Moreover, the solvents used in HPLC are much more difficult to handle as vapors than the usual GC carrier gas, helium. Despite these formidable obstacles, the incentives for achieving a continuous interface are so great that a substantial research effort to achieve this objective is easily justified.

The simplest approach, developed by Tal'rose and colleagues in the USSR[155] has been in use for more than a decade.[156] It consists of a splitter device which allows 0.01-0.1% of the liquid effluent to enter the ion source through a capillary tube. The LC solvent must be readily vaporized, without clogging the tube or depositing a residue inside the source. This approach is moderately successful, despite these limitations, and has been developed into a practical device in several laboratories.[71,72,74,75,157-162]

Other approaches directly related to GC methodologies have included depositing the LC eluent on a moving wire,[69] belt,[68] or probe[70] which flash vaporize the solvent in a heated vacuum lock device, transport the sample mechanically into the ion source, and vaporize the high boiling substance in a subsequent heating cycle. A membrane separator enrichment device directly modeled from a GC/MS interface[163] has also been applied successfully as an LC/MS interface.[76] Since they depend so strongly upon volatization behavior of individual compounds, however, these approaches are intrinsically incapable of dealing with those thermally labile or truly involatile substances of greatest interest for HPLC as a fractionation method.

A method potentially applicable as an LC/MS interface is the "electrospray" technique to atomize and ionize the LC effluent.[164,165] This method yields extremely fine droplets as small as 0.1 μm in diameter; many are charged as a result of the high potential applied in the electrospray process. The feasibility of this approach for some macromolecules has been demonstrated; molecules studied include lysozyme and zein[164] and polystyrene of molecular weights 51,000 and 411,000.[165] However, there are several disadvantages to the method, including the particular limitations imposed by the dielectric requirements of the electrospray process upon the solvents that may be used, the need to use a very high potential, approximately 10KV, in the spray chamber, and the need to use exceedingly dilute solutions which yield a very low ion current.

Intimately related to the "electrospray" method is the electrodynamic ion source developed by Evans and co-workers,[166] which also relates to field ion microscopy[167] for its basic operating principles in the same manner as field ionization.[168] It differs in that a capillary placed in a strong electric field supplies the liquid at a controlled rate to a zone in which evaporation and field ionization take place. The electric field is increased to the point ($E \sim 10^8$ v/cm across a cone defined by a capillary tip and the field plate) that ionization occurs. Because the emitter is a liquid, it is continuously renewed rather than eroded away. It has been applied to liquid metals[166] and to organic molecules dissolved in salt solutions.[169] Potentially applicable as an LC/MS interface for conductive (salt solution) solvents, this intriguing method is also not applicable as a general interface.

It is clear from the foregoing remarks that a number of novel techniques have been devised for interfacing HPLC to a mass spectrometer. However, a general purpose, continuous interface which permits the efficient transmission of resolved molecules into the ion source of a mass spectrometer has not been achieved. Further, since most of these approaches have been variations of previously successful GC/MS interface techniques, it appears that a markedly different approach should be investigated.

Accordingly we proposed the exploration of molecular beam techniques as the basis of an LC/MS interface. The fundamental rationale is that molecular beam techniques are now relatively well established for the study of unstable species (free radicals or excited states) in the gas phase. Since an involatile molecule is, in a sense, also an unstable species which is intolerant to collision with solid surfaces, the same strategy is, in principle, applicable to involatile molecules. This approach also requires that the involatile molecule be stable with respect to dissociation; this should also be true for the LC interface problem, provided the internal energy in the species is less than the activation energy for dissociation of its weakest bond. Consequently, solute molecules can be vaporized from solutions intact, without fragmentation, provided precise control of energy input to the solution is achieved and provided the sampled beam portion of the solute molecules does not collide with any surface. Some support for the plausibility of these hypotheses is provided by the work of Buehler, Flanigan, Green and Friedman[170] and of MacFarlane and Torgerson,[171] who have shown that both labile and extremely involatile molecules may be desorbed intact into the vapor phase in high vacuum by very rapid heating.

As discussed in the Introduction, three approaches to involatile sample analysis, all using closely related molecular beam methods, have now been investigated. The dense gas chromatography/mass spectrometry technique was discussed in Section 3. The laser vaporization approach explored by Professor Marvin Vestal at the University of Houston and described in detail elsewhere is discussed briefly in the next section. The third concept, using ultrasonic energy to increase the surface area and enhance heat transfer to the solvent as the molecular jet is formed, will now be discussed.

4.2 MOLECULAR BEAM LC/MS STUDIES

4.2.1. Apparatus

Figure 43 summarizes the essential components for a general purpose LC/MS interface utilizing the molecular beam approach. An apparatus embodying these features was constructed at the University of Utah during the time period November, 1976 - June, 1978 and is diagrammed in Figure 44. A complete set of mechanical drawings was supplied to Dr. John McGuire of the Athens Environmental Research Laboratory. Dr. John McGuire, technical monitor for this project, may be contacted for details.

Of key significance in this design is the incorporation of a high degree of differential pumping which makes this apparatus a general purpose test bed for the evaluation of alternative approaches as an LC/MS interface. Six separate pumping systems are shown in Figure 44. The first stage is shown in the chamber in which an exponential horn of an ultrasonic generator is mounted. This section vaporizes the solvent and handles the major gas load. It is pumped by a 16 ℓ/sec two stage forepump (Welch Model 1375) and drops the pressure to less than 1 torr for a solvent flow rate of 1 ml/min.

The second stage of differential pumping consists of a 4200 ℓ/sec diffusion pump (NRC Model VHR-10) backed by a matching high speed forepump (Welch Model 1375). This drops the pressure of the expanding jet to 10^{-3} - 10^{-4} torr stagnation pressure. A third stage diffusion pump (1250 ℓ/sec, NRC Model VHR-6) drops the pressure to 10^{-6} torr in the ion lens and mass analyzer section. A smaller pump (175 ℓ/sec, Varian Model VHR-4) provides the highest vacuum of the assembly in the electron multiplier section of this four stage differential pumping sequence. Additional pumping stations maintain low pressures in the electron gun (285 ℓ/sec, Varian Model VHR-4) and beam trap (175 ℓ/sec, Varian Model VHR-4) regions, respectively.

Not shown in the figure are two liquid nitrogen traps which condense solvent in the beam trap at the rear of the apparatus (RH side) and which protect the forepump in the first stage of beam expansion (LH side).

A cross sectional scale drawing of the apparatus is shown in Figure 45. Figure 46 is an enlarged view of the critical beam-forming region. The

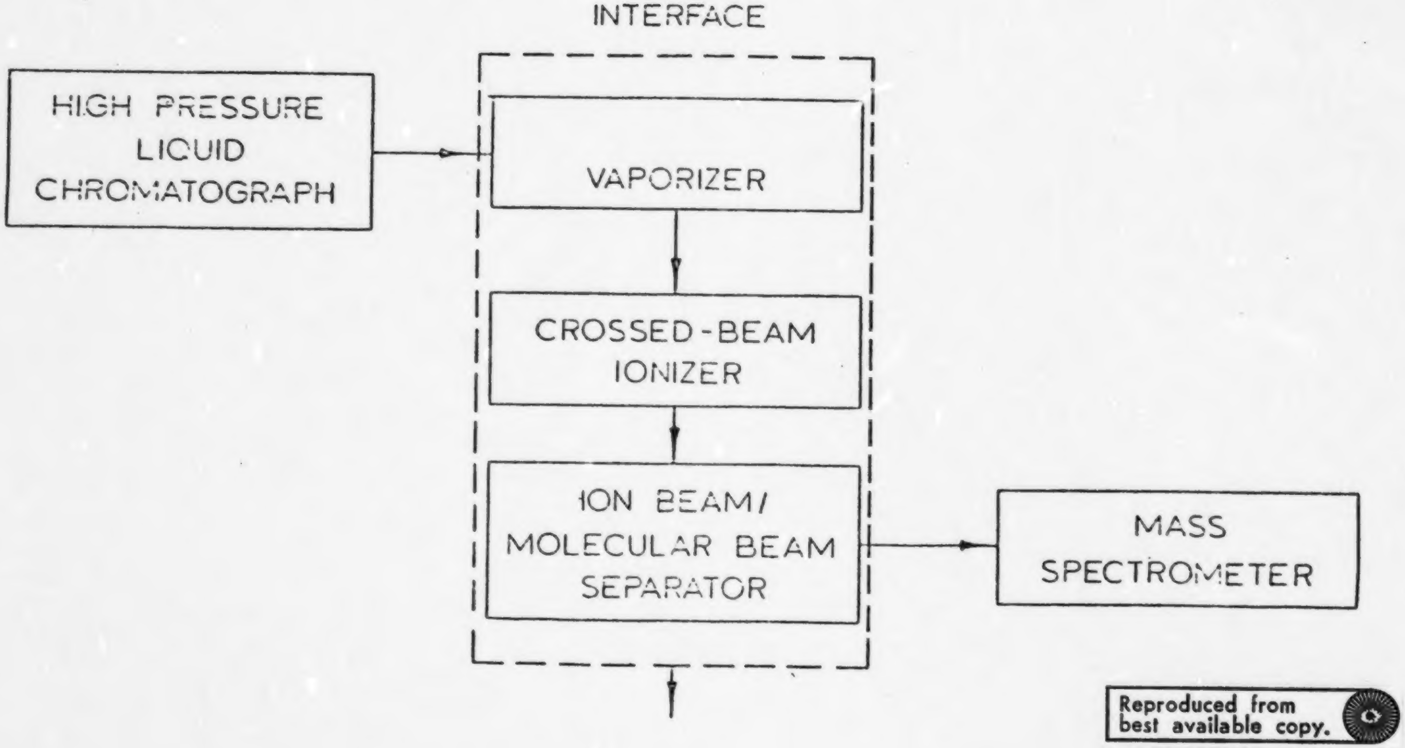
INTERFACE
HIGH PRESSURE LIQUID CHROMATOGRAPH
VAPORIZER
CROSSED-BEAM IONIZER
ION BEAM/ MOLECULAR BEAM SEPARATOR
MASS SPECTROMETER

Reproduced from best available copy.

Figure 43. Functional illustration of liquid chromatograph-mass spectrometer interface. Key components and the required sequence of operations are indicated within the dashed lines headed "Interface".

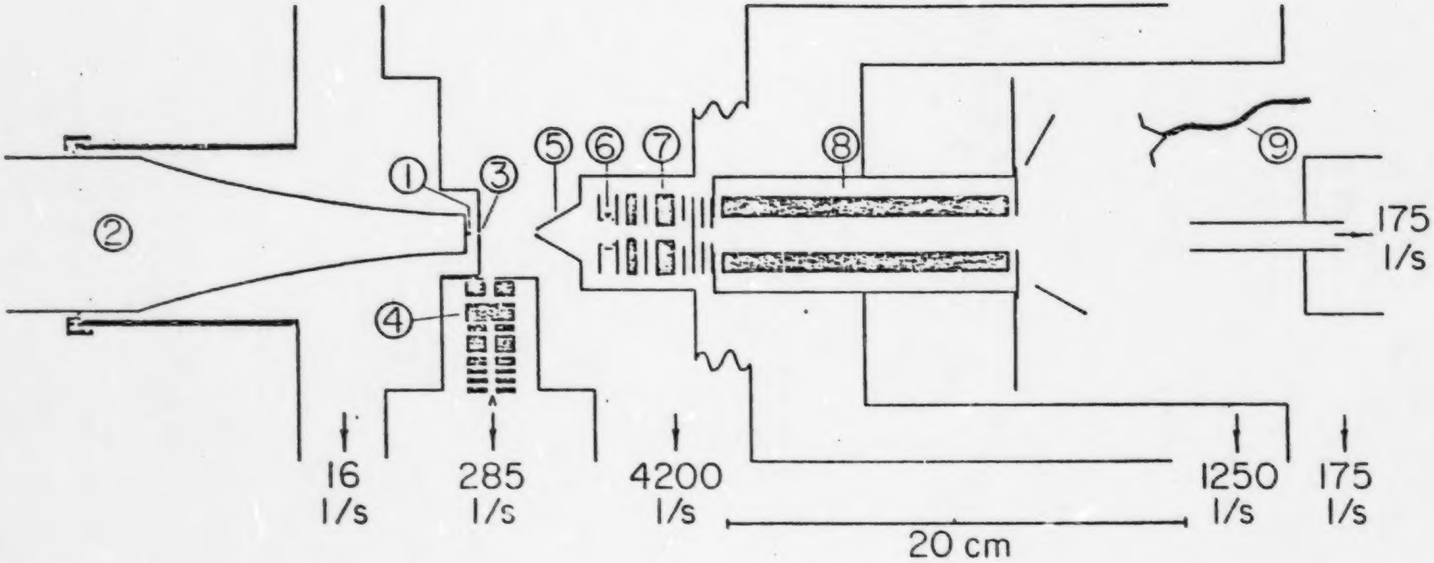
②
①
③
④
⑤
⑥
⑦
⑧
⑨
175
l/s
16
l/s
285
l/s
4200
l/s
1250
l/s
175
l/s
20 cm

Figure 44. Schematic of the LCMS. 1) Capillary tube, 2) Ultrasonic horn, 3) Pinhole, 4) CI electron gun, 5) Skimmer, 6) EI ion source, 7) Ion lens, 8) Quadrupole mass filter, 9) Multiplier.

Figure 45. Scale sectional drawing of the LC-MS interface of Figures 1 and 2. Section A is the first-stage vaporizer unit in which the majority of solvent is stripped and beam formation is initiated. Section D is the high vacuum region containing the mass spectrometer, detector and beam dump elements. Between these two sections are the ionization and supersonic jet nozzle-skimmer regions. Full scale blueprints are available from Dr. John McGuire of the Athens Environmental Laboratory of the Environmental Protection Agency.

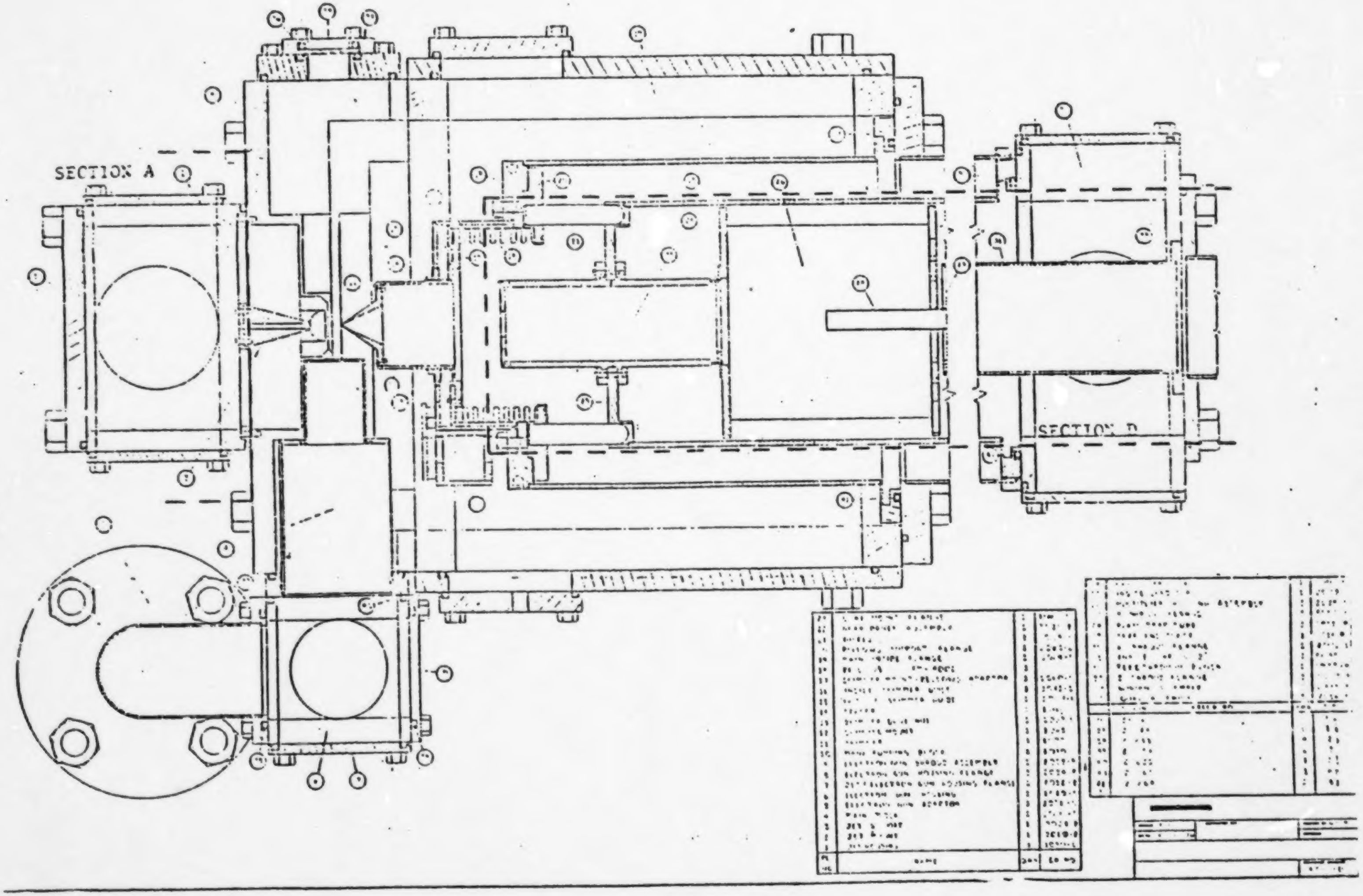
SECTION A
SECTION D

SECTION A and SECTION D

Reproduced from best available copy.

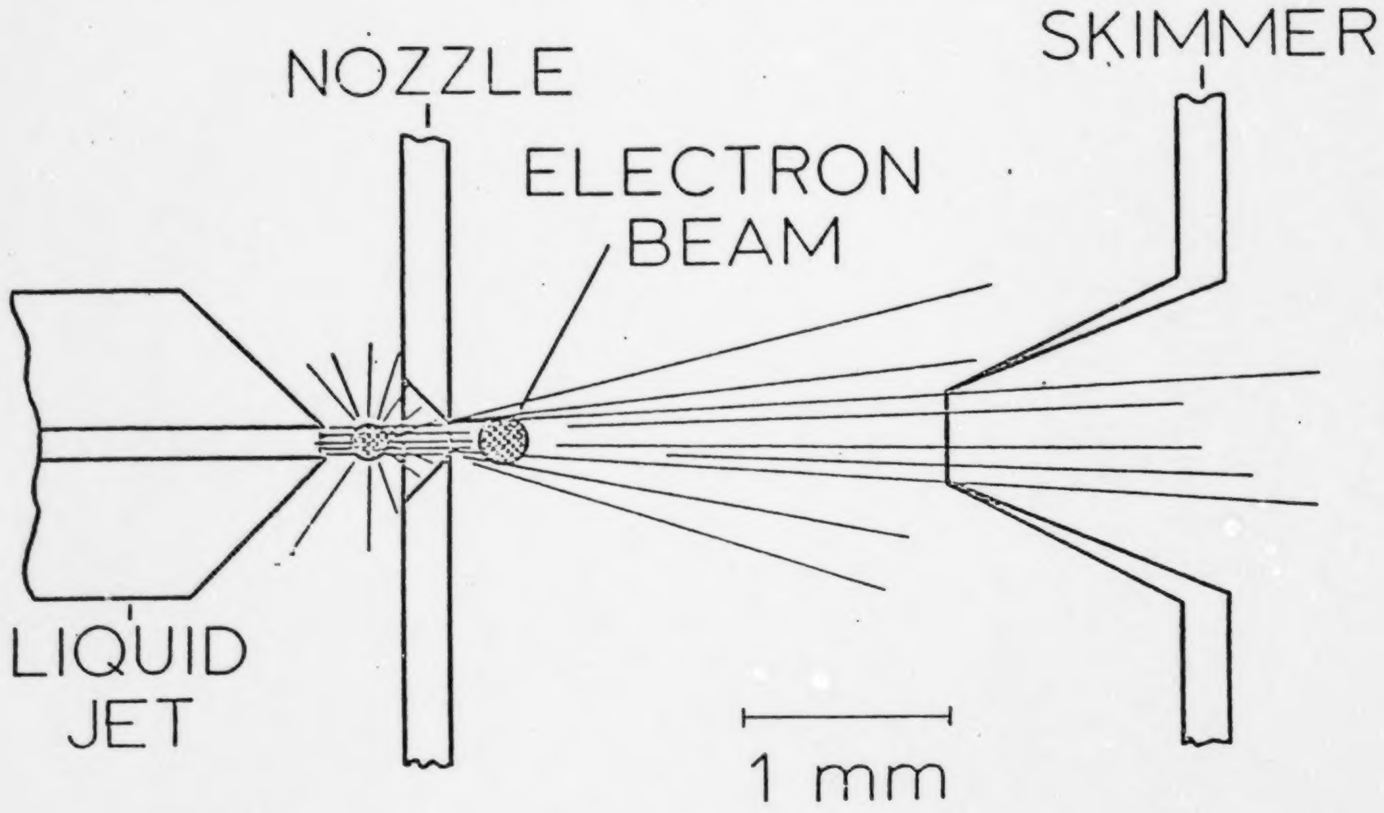
NOZZLE
SKIMMER
ELECTRON BEAM
LIQUID JET
1 mm

Figure 46. Approximately-to-scale drawing of the critical liquid jet, supersonic expansion and crossed-beam ionizer section of the LC-MS interface. The capillary tip of the ultrasonic horn is shown at the left. Three regions of differential pumping--liquid vaporization (forepump and liquid nitrogen traps), supersonic expansion (diffusion pumped) and stagnation region (diffusion pumped)--are shown.

combination of Figures 44-46 provides a convenient reference frame for describing the successive operations required for converting a portion of the liquid effluent from the LC into a set of characteristic ions which can be used to identify the resolved components of a mixture. Section A of Figure 45 is the section in Figure 44 in which the ultrasonic horn is mounted. Section D is the high vacuum, collision-free region. The nozzle-skimmer assembly and electron guns are mounted in the transition region in which the supersonic beam is formed. This process is shown schematically in Figure 46, with the appropriate configurations of the critical elements and spacings shown approximately to scale.

The essential mechanical and vacuum requirements for forming a supersonic molecular beam are relatively well established.[93,114,117,118,154,172] Provided the enthalpy of vaporization required to strip all solvent molecules can be provided in Section A, the physics of the process of supersonic expansion is relatively well understood.[114] From this point forward the device operates in the same manner described for the DGC/MS interface in Section 3 of this report. In the region between the nozzle and skimmer (see Figure 46) the vapor will undergo isentropic expansion. At the proper nozzle-skimmer distance, and for matched nozzle and skimmer diameters, the transition (Mach disk) from viscous flow to molecular flow can be made to occur at or near the skimmer orifice.

In the present apparatus an axial worm-gear drive allows adjustment of the nozzle-skimmer distance to a precision of about 0.001 cm via a rotary feedthrough connected to an indicator external to the vacuum chamber. As is usual in supersonic jets, final adjustment is made empirically to ensure the proper nozzle-skimmer distance. Figure 47 illustrates the procedure and demonstrates the formation of a supersonic molecular beam with carbon dioxide gas as a simulated driver for vaporized LC solvent. (Since the average molecular weight and heat capacity of the mixture are the characteristic parameters in hydrodynamic expansion, the solvent is, to a high approximation, the only species which need be considered.)*

The intensity of CO_2^+ is plotted in the figure as a function of the nozzle-skimmer distance. Starting at zero distance the total gas flow from the nozzle is transmitted and no differential pumping occurs. Moreover, the flow mechanics is properly described as non-directional, effusive expansion into a vacuum. As the distance is increased, the gas flow (and ion intensity) drops sharply as a result of the development of shock waves which reflect from the throat of the skimmer and disrupt gas flow. At a greater distance--at 1.5 cm for the present example--the shock wave is an attached, bow shock wave[117] and the skimmer orifice samples the transition region properly for the transmitted beam. At still greater distances the intensity drops off in an approximately exponential fashion because the transition to molecular flow has already occurred. Thus, Figure 47 defines the optimum spacing and also demonstrates that a supersonic beam is formed.

---

*One must add the caveat that very little is known about complex molecules, in particular, about the coupling of internal energy with collision processes in adiabatic expansion. Therefore the proper heat capacity ratios, C_p/C_v, for calculating stagnation temperatures, and the time scale for freezing

Figure 47. Intensity of CO_2^+ as a function of nozzle-skimmer distance. The characteristic shape of this curve demonstrates the formation of a supersonic beam and establishes 1.5 cm as the optimum spacing for a driver gas (simulated solvent) of molecular weight 44. See discussion in text.

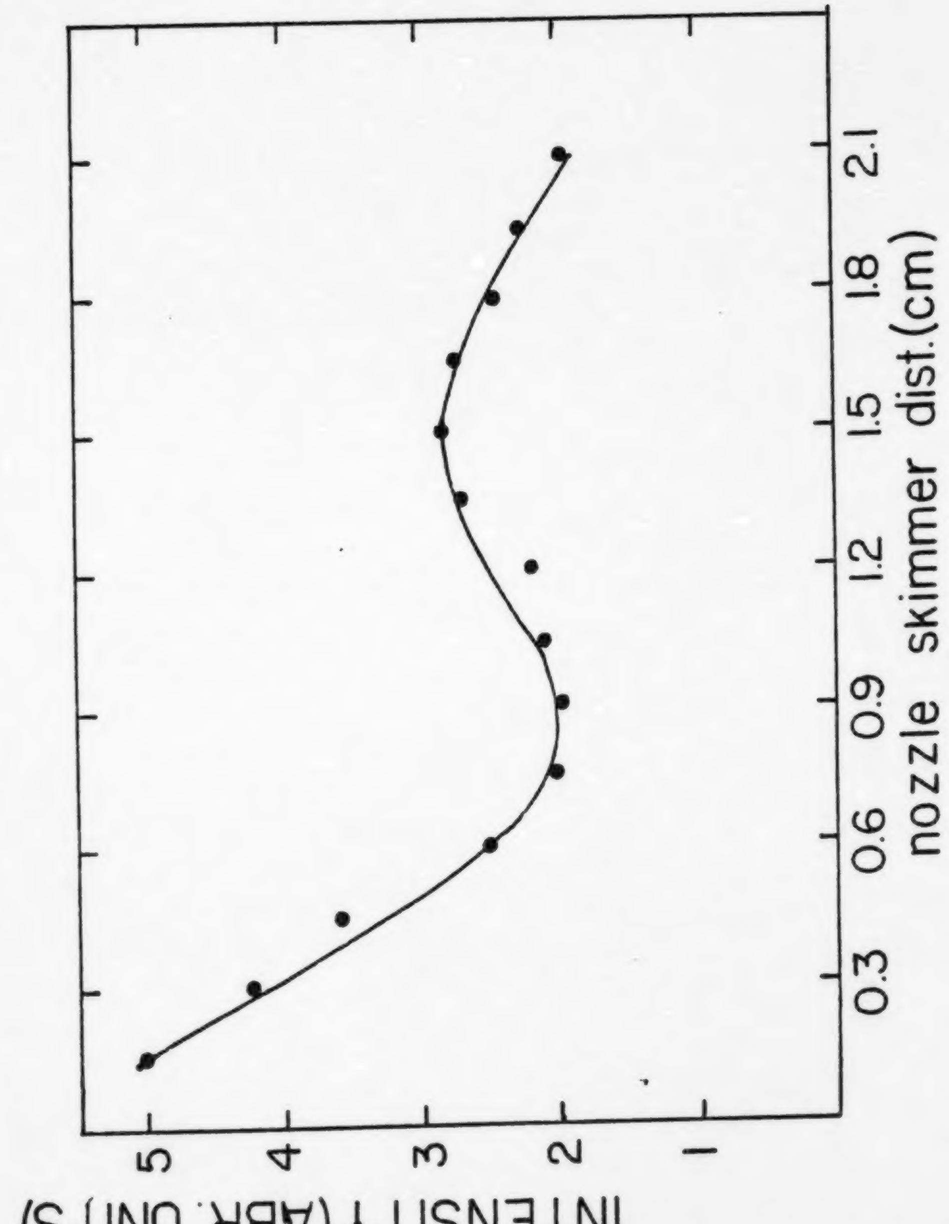
INTENSITY (ABR. UNITS)
5
4
3
2
1
0.3
0.6
0.9
1.2
1.5
1.8
2.1
nozzle skimmer dist.(cm)

In Figures 44 and 45 are shown the differentially pumped chamber of an electron gun which intersects the expanding beam and ionizes primarily the solvent molecules. This occurs in the viscous flow regime and was provided as a chemical ionization source with the solvent serving as the reagent gas. Downstream, in the collision-free regime, a simpler electron gun in the low pressure chamber generates normal electron impact spectra for both solvent and solute molecules.

In practice the CI electron gun has not worked satisfactorily. No electric fields are present in the jet expansion region and it was assumed that hydrodynamic flow would transmit ions into the low pressure chamber where a series of lenses focus the ions on the entrance aperture of the quadrupole mass filter. In fact, only very low and fluctuating intensities of ions are observed. We attribute this to space charge blow-up of the ion beam and to flow fluctuations which may reflect condensation from the adiabatic cooling effect associated with the beam-forming process. In any case, this feature of the apparatus did not generate useful ion beams, and a capability for generating EI and CI spectra simultaneously or in rapid succession was not realized with this apparatus. Moreover, there is no simple way to modify the apparatus to minimize this problem; an electric field between the nozzle and skimmer would provide some focusing effect but would also enhance collision-induced dissociation. Lenses could be added downstream of the skimmer, of course, to focus ions in the collision-free region. However, it would be preferable, in our opinion, to design a separate CI system. This will be discussed later.

The electron impact ionizer is an open structure consisting of a simple shield, filament, grid and collector assembly which crosses the molecular beam and ionizes several tenths of a percent of the solvent and solute molecules. A lens system consisting of a pair of unipotential lenses and deflection plates of similar design to those incorporated in other mass spectrometer systems in this laboratory[173,174] provides both focusing and directional correction. The ion beam is focused by this lens system on the entrance aperture of an Extranuclear Model 4-162-5 quadrupole with a mass range of 0-1000 amu. The large central aperture (and large rod diameter) of this mass filter permits the collimated neutral beam to pass through the entire apparatus without striking any surfaces. A "beam tube" shown in Figure 46 extends the vacuum chamber constructed as a beam trap for the neutral beam up to the point immediately behind the multiplier detector. A readily removable liquid nitrogen trap condenses the solvent molecules of the beam; an isolation valve facilitates its removal for periodic cleaning.

The electron multiplier is a bakeable ceramic continuous dynode multiplier (MuRata Corporation Ceratron-E Model 1081B) mounted off-axis to prevent electrical noise from ion source photons and contamination by the neutral beam. Deflection plates are utilized to separate the mass-selected ions from the neutral beam and impact them on the entrance cone of the multiplier. Ion intensities are monitored either by conventional current amplification or are pulse-counted. The output is connected (using either an ADC or PAD module, as

---

out of T_{11} and T_1 for vibration, rotation, and translation are unknown. Consequently, the Mach numbers estimated from necessarily simplified assumptions may be somewhat in error.

appropriate) to a 1024 channel Tracor Model 1700 multichannel analyzer as a storage and integrator device. After data smoothing the resulting mass spectra are transferred to a strip chart recorder. Of course, the data may also be transmitted through similar signal conditioners directly to a computer.

The overall transmission efficiency of the apparatus may be estimated from the expression

$$E_T = E_{\ell-v} \cdot E_i \cdot E_{ma} \tag{1}$$

where $E_{\ell-v}$ is the efficiency of transfer of solute molecules from the liquids to the vapor phase, E_i is the ionization efficiency and E_{ma} is the transmission and detection efficiency of the mass analyzer.

The vaporization efficiency is least well known. It depends critically on alignment of the capillary tube and the nozzle. Geometric considerations and pumping speeds lead to an estimate that approximately 10^{-5} of the solvent molecules will be transmitted by a 1 mm diameter skimmer. Pressure profiles support this estimate when optical alignment of the capillary orifice with the nozzle and empirical adjustment of the axial alignment have been used to optimize throughput. Further, Mach focusing[117] of heavier molecules present in the beam enhances their transmission by the ratio of their molecular weight to that of the driver gas. Consequently, we conclude that

$$E_{\ell-v} \leq 10^{-5} \frac{M_{solute}}{M_{solvent}} \tag{2}$$

The ionization efficiency is readily deduced from the definition for ionization efficiency.

$$E_i = F_i/F_n \tag{3}$$

where F_i is the ion flux and F_n the neutral molecule flux. Further, the ion flux for the low density case is given by

$$F_i = I_e Q_i \, D \, F_n/v \tag{4}$$

where I_e is the electron current, Q_i is the ionization cross section, D the width of the larger (defining) beam, F_n the neutral flux, and v the velocity of the neutral beam. For a 1 ma electron beam (6×10^{15} electrons/sec) a cross section of 5 Å^2, D (molecular beam) = 4 mm, and $v = 10^4$ cm/sec , the overall ionization efficiency may be estimated from the combined equation [(3) x (4)]

$$E_i = \frac{I_e Q_i D}{v} \tag{5}$$

to be $E_i \leq 1.2 \times 10^{-4}$.

For constant velocity ions the transmission of the quadrupole at constant resolution falls off with increasing mass and may be approximated by the equation

$$E_{ma} \simeq C \frac{M_{solvent}}{M_i} \tag{6}$$

where C is a constant representing the transmission efficiency for solvent molecular ions. With ideal optics it may approach unity; for approximation purposes we may use C = 0.1.

For those cases where the molecular ion is the major ion species, the mass ratios in equations (2) and (6) cancel and the overall efficiency should be of the order of the product of equations (2), (4) and (6), or $E_t \leq 1.2 \times 10^{-10}$. For molecular weight 200 this corresponds to 1.1×10^{-14} coulombs/μg of sample. Assuming an LC peak width (uniform) of 30 sec and that 100 ions/sec are required to identify a substance in scanning mode, we can estimate a detection limit of 1 nanogram. In actual practice readily identifiable spectra have been obtained from about five times this amount using the ultrasonic method. This is slightly lower than, but comparable to GC/MS detection limits.

4.2.2. Ultrasonic Vaporization Studies

As is well known, the phase transition from the liquid to the vapor phase is rate-limited by transport across the phase boundary. The rate of this process is increased by increasing the surface area. At equilibrium the rates of evaporation and condensation are equal. By decreasing the concentration of vapor species--i.e., in an expansion process--equilibrium is displaced such that rapid evaporation occurs. Rapid cooling accompanies this process unless the latent heat of vaporization is supplied to the system. Thus the conversion of liquid to vapor is facilitated by (1) increasing the surface area, (2) decreasing the number density of vapor phase molecules and (3) heating the sample.

It is well established that ultrasonic energy quite effectively nebulizes liquids, drastically increasing their surface area.[175] An approximate theory[176] leads to the following relationship for the dependence of the mean droplet diameter, D, on liquid parameters and oscillator frequency;

$$D = 1/2 \left(\frac{8\Pi\gamma}{\rho f^2}\right)^{\frac{1}{3}} \qquad (7)$$

where γ is surface tension, ρ is density, and f the oscillator frequency.

Further, one can argue that ultrasonication effectively promotes heat transfer. In fluid flow the major barrier to heat tranfer from a tube to a moving fluid is the stagnant film at the surface. Ultrasound generates tremendous shearing forces along this film, dramatically increasing heat transfer. In addition, for gas-liquid heat transfer, the rate is directly proportional to the area of the phase boundary. Consequently, for two potentially important heat transfer mechanism --solid-liquid and gas-liquid--the technique of ultrasonication greatly facilitates energy transport.

From equation (7) above it is apparent that the highest frequency oscillator obtainable would generate the smallest drops. However, with increasing frequency, one rapidly encounters strength of materials limitations. Consequently, for reasonable power levels one is restricted to less than 100 KHz frequency. Our experiments with an ultrasonic nebulizer have utilized a 400 W commercial system operating at 20 KHz (Heat Systems-Ultrasonics, Inc., Model W350S).

Three configurations for connecting an LC capillary to an ultrasonic horn were investigated in this research and are illustrated in Figure 48. The problem of coupling these two elements together proved formidable, and an apparently completely satisfactory solution was achieved only after the project had officially ended. The problem is basically that of impedance matching of divergent elements. Amplitudes of oscillation at moderate power levels are such that standing waves set up in the capillary are of sufficient amplitude to shear thick wall stainless steel capillaries in less than a minute. In order for the horn to withstand these shear forces, a relatively massive piece of metal fabricated from a material (e.g., Titanium) with a high Young's modulus must be used. Attaching the horn to the apparatus via a vacuum seal and welding, flanging, or bolting the capillary tube in place both loaded and unbalanced the oscillator, making it difficult, if not impossible, to retune to resonance.

A partially satisfactory solution is illustrated in configuration (A) of Figure 48. This was a modification of the standard flow-through horn furnished by Heat Systems-Ultrasonic, Inc. The "O"-ring seal indicated schematically in the figure was located empirically by sliding the horn back and forth in the vacuum seal until a point of minimum loading of the oscillator was located. This empirical procedure apparently located a node for the normal mode oscillation of the horn. A "press fit" was used to attach the tip of the capillary to the tip of the horn using a length of stainless steel milled to size and welded to a length of capillary of smaller diameter which could be pushed through the special horn. The "press fit" section was forced into position by a hydraulic press and sawed off to a sufficiently short length that the assembly oscillated satisfactorily.

Using this assembly a number of important features of this approach to ultrasonic evaporation were demonstrated.[177] It was shown that coaxial alignment of the LC capillary with the apparatus is extremely important. Placement of the capillary orifice and tilt of the horn are both important; very slight displacement changed ion intensities and ion gauge pressures by more than two orders of magnitude. It is apparent, therefore, that the shape and location of the capillary strongly influence the beam-forming properties of the system.

By using a volatile solvent, hexane, it was possible to evaluate the effect of turning the ultrasonic oscillator on and off without experiencing immediate freezing and plugging of the capillary. It was found that solvent ion intensities (and gas pressure in the MS and beam trap chambers) were increased by more than an order of magnitude by having the ultrasonic generator turned on. The maximum increase was by a factor of 50, and the rate of increase depended upon the power setting of the oscillator. It was also noted that there was a time lag in reaching maximum throughput after turning on the oscillator and also a time lag in fall-off of ion intensity. Further, a detuning of the oscillator accompanied both buildup and fall-off.

A series of bench top experiments with the ultrasonic horn helped to clarify the phenomena just described. With the LC pumps turned on, drops of solvent slowly oozed from the capillary tip. When the oscillator was turned on a very fine mist was observed which disappeared in of the order of a minute. At the same time a pronounced temperature rise of the tip of the horn was noted, and the oscillator required retuning for continued operation. Upon

Figure 48. Schematic illustrations for three configurations of the ultrasonic nebulizer tested. Configuration A (top) is an adaptation of a standard flow-through horn in which a stainless steel capillary was installed. Configuration B (middle) the capillary, contacts the tip of the horn at the point where maximum energy (amplitude) oscillations occur. In Configuration C (bottom) a capillary is drilled in the horn to avoid sound wave discontinuities produced by using two materials of construction in (A) above. In all cases the horn must be attached into the vacuum system at a stationary point (node) shown for (A) and (B). In (C) a half-wave extender unit locates the node to the left of the portion of the horn illustrated.

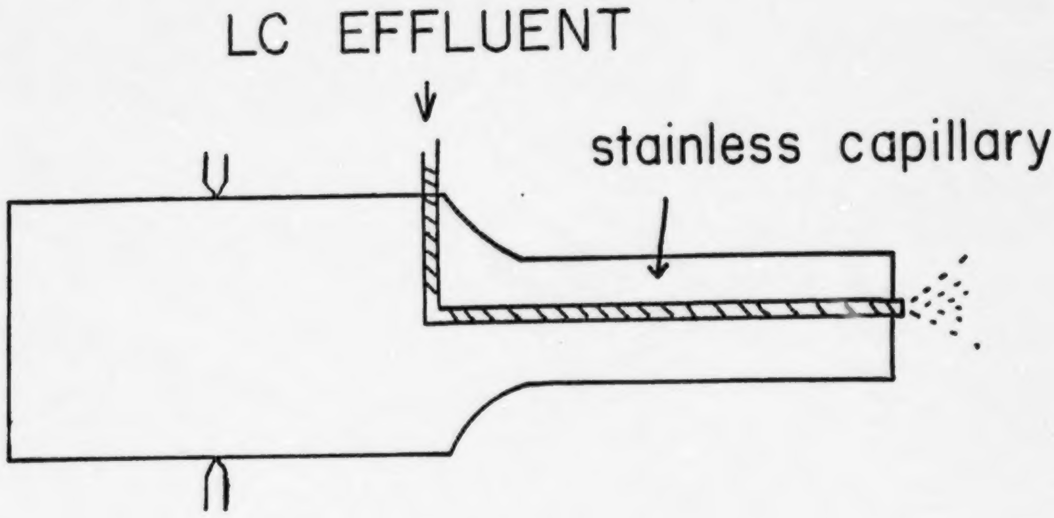
LC EFFLUENT
stainless capillary

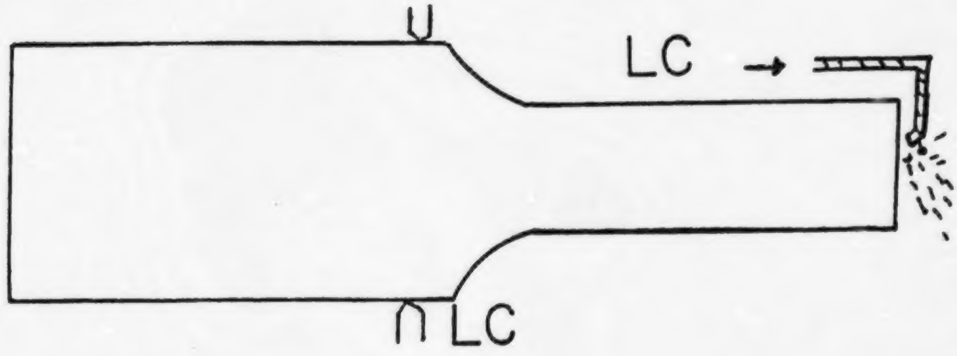

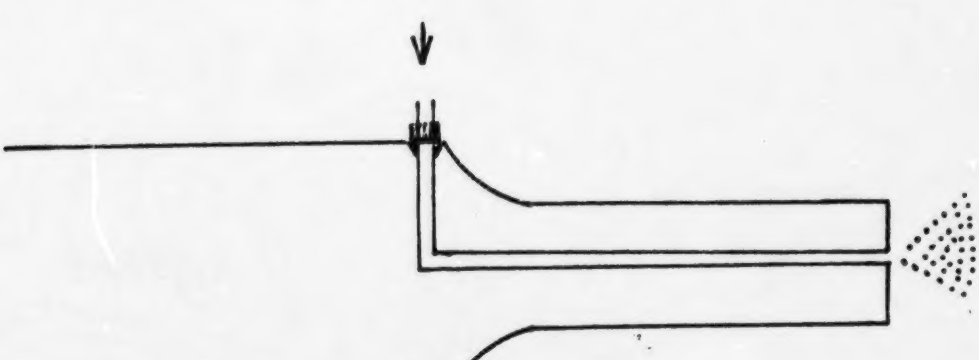

flow through horn

shut down of the oscillator, the horn cooled, tuning shifted, and drops of solvent were once again visible. At intermediate stages of temperature, turning the oscillator on and off would cause the droplet mist to disappear and reappear. Clearly, therefore, part of the effect of ultrasonic excitation is heating of the capillary, accompanied by an undetermined amount of heat transfer to the liquid and only part of the effect is ultrasonic nebulization.

With this configuration of the horn-capillary system quite good sensitivity was demonstrated. Figure 49 compares the spectrum of naphthalene with a library spectrum. This spectrum represents ca. 5000 counts of the molecular ion from an injected sample of 250 ng of naphthalene. Assuming 100 ion counts are required to clearly identify an ion, this corresponds to a detection limit of 5 ng. Similar results were obtained for benzene, naphthalene and anthracene, as reported elsewhere[177] and summarized in Table 4.

Installation of thermocouples in the capillary plus examination of the horn for erosion demonstrated that frictional heating of the press fit junction produced a pronounced temperature rise in the horn and capillary, no doubt responsible for the detuning phenomenon noted above. Visual observation through a viewport revealed a dull red glow after 10-15 minutes of operation. Attempts to optimize the coupling between the horn and the capillary proved futile. Further erosion of the press fit led to a situation in which ultrasonic energy was not coupled to the capillary at all, while welding the two units so loaded the oscillator that it would not function. Accordingly this general design concept was abandoned.

Transverse coupling of the capillary and horn was then attempted, as shown schematically in Figure 48B. Tight coupling, by welding or mechanical attachment, quickly sheared the capillary. Accordingly, spring tension was used to contact the effluent with the tip of the ultrasonic horn, with a modest degree of success. Figure 50 shows the time dependence of the mass spectrum of naphthalene along with the UV trace of the LC. Obviously, peak spreading is introduced by this indirect coupling of the capillary with the horn. Low sensitivity was also an intrinsic property of this design.

Accordingly, it was concluded that a redesign of the horn to eliminate any coupling of dissimilar metals was required. The solution arrived at is shown as part (C) of Figure 48. As illustrated in the figure, a one piece horn has been fabricated and a capillary core has been drilled out. Because of its high Young's modulus and relative ease of machining, aluminum was used to test the concept. The horn was machined somewhat longer than calculated for half wave sections[174] and was attached to the ultrasonic oscillator crystal driver for empirical location of its nodes. Small sand particles were dribbled on the horn to locate nodes and maxima of the standing waves. The horn was then cut to an empirically determined size to locate the Swagelok® seal at a node so that no motion is transmitted to the LC capillary. A second length of horn (not shown) serves as a coupling extension to provide another node at a convenient location for establishing a vacuum seal. Finally the length was chosen to provide maximum amplitude oscillations at the tip. This design therefore meets all the criteria for ultrasonic coupling to the LC eluent and effectively separates the ultrasonic activation and heating steps phenomenologically. This design has been demonstrated to nebulize solvent molecules efficiently and appears to be a satisfactory solution to the problems described

Figure 49. Comparison of electron impact spectrum of naphthalene obtained with the LC-MS interface (top figure) with a library reference spectrum (NIH-EPA compilation of reference spectra). Only the molecular ion region is shown.

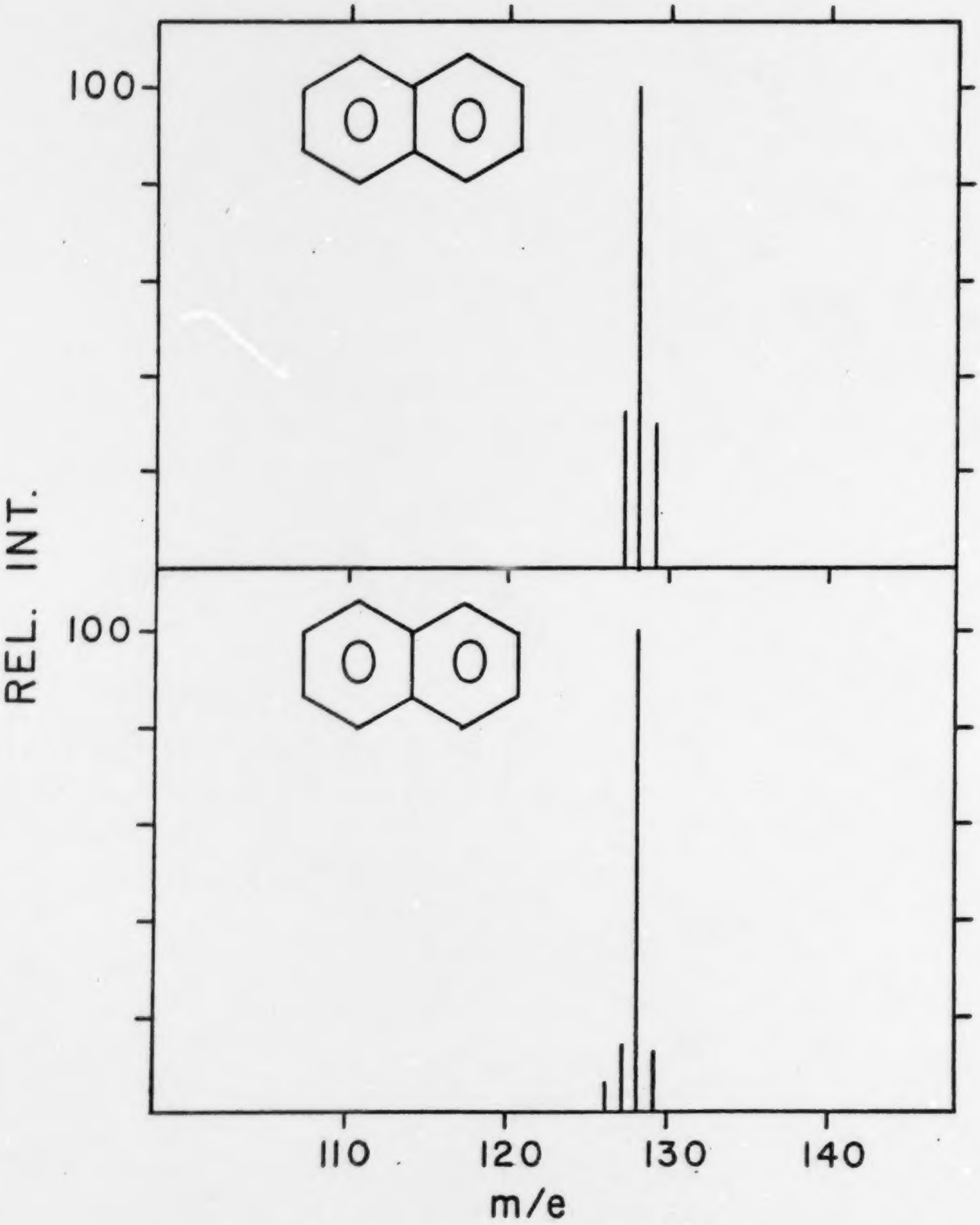
100
100
REL. INT.
110
120
130
140
m/e

TABLE 4

Sensitivity Estimates for Ultrasonic Vaporization by LC/MS Interface Using Hexane Solvent

A. Scanning Mode Detection for Horn Configuration A of Figure 48.

Sample	Accumulated Counts of Molecular Ion	Counts/ng.
100 ng. Naphthalene	1830 ± 60	18
250 ng. Naphthalene	5000 ± 80	20
500 ng. Naphthalene	11210 ± 110	22
1.0 μg. Naphthalene	21090 ± 150	21

B. Single Ion Monitoring Mode Detection for Horn Configuration A of Figure 48.

Sample	Accumulated Counts of Molecular Ion	Counts/ng.
50 ng. Naphthalene	53186[a]	1063

C. Scanning Mode Detection for Horn Configuration B of Figure 48.

Sample	Accumulated Counts of Molecular Ion	Counts/ng.
250 ng. Naphthalene	4260 ± 80	17
250 ng. Benzene	3610 ± 70	14

---

[a] Only one experiment.

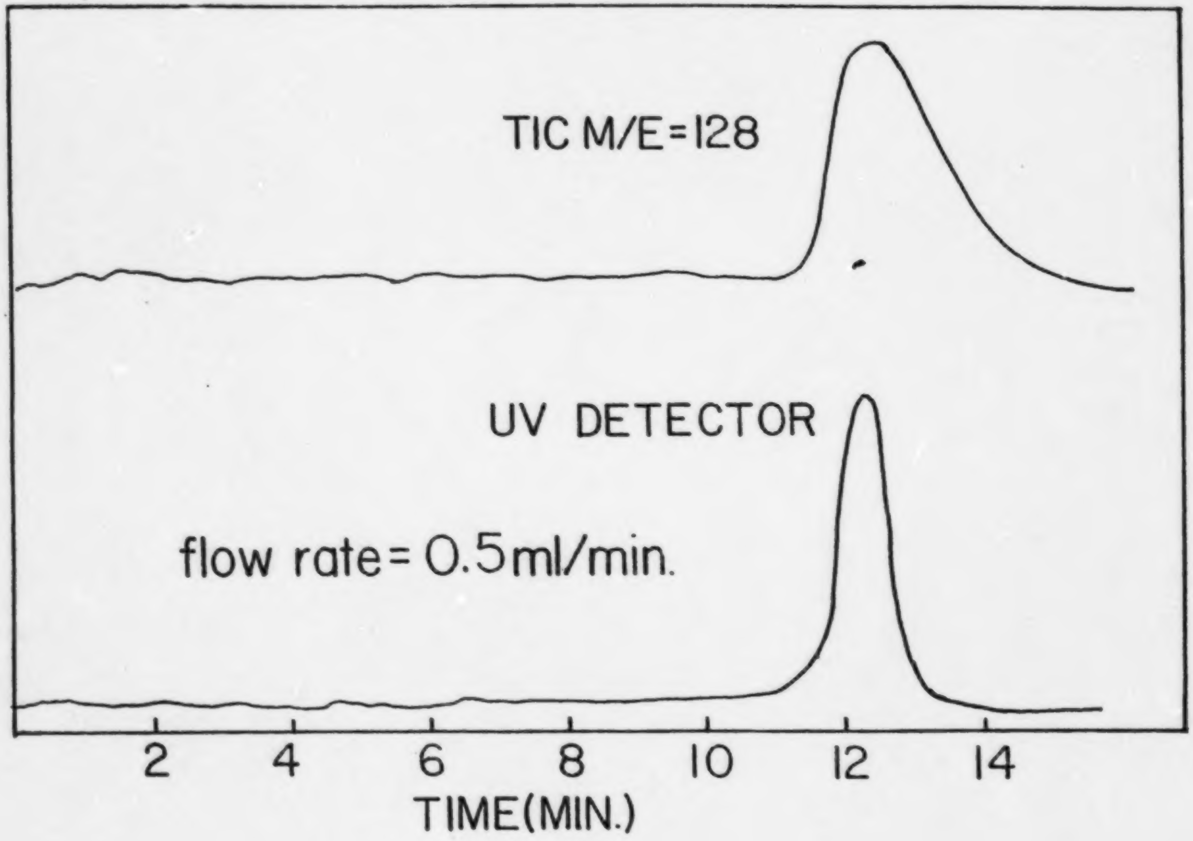

Figure 50. Comparison of molecular ion (m/z 128) trace with the UV detector trace for naphthalene injected into the liquid chromatograph. Configuration (B) of Figure 48 was utilized in this study, and some peak broadening is evident.

above. However, aluminum erodes very rapidly and it was not feasible to evaluate this design in the complete LC/MS assembly. It will be necessary to construct a similar model from titanium prior to further testing of the ultrasonic nebulizer/molecular beam concept.

Independent studies of ultrasonic nebulizers as component parts of LC/MS interfaces have recently been reported. Japanese patent SHO53-3290 dated January 12, 1978, claims that the nebulizing effect concentrates the solute in microdroplets, vaporizing only solvent molecules by heating in an intermediate stage.[178] The fog of solute molecules with attached solvent is transmitted to the ion source for final evaporation, ionization and mass analysis.

Tsuge, Hirata and Takeuchi have recently described a vacuum nebulizing interface for coupling a micro-LC to a mass spectrometer which incorporates many of the conceptual ideas we have described.[162] A helium driver gas generates (presumably) ultrasonic energy to transport molecules efficiently into the ion source of a spectrometer. Mixtures of aromatic amines, drugs, amino acids, glycols to MW 500, oligopeptides and steroids dissolved in alcohols, hydrocarbons, ketones, esters, water, and nitriles were efficiently transported into the spectrometer. Chemical ionization was used to generate characteristic $(M + 1)^+$ ions for the compounds and solvents reported.

It appears, therefore, that a judicious combination of ultrasonic nebulization with heating is very promising as an LC/MS interface. An ultrasonic horn patterned after Figure 48C is a much more efficient nebulizer than the gas driven version. Combination of the nebulizer with a ceramic discharge source described in the last section is the recommended next step for achieving a continuous, general purpose LC/MS interface.

4.2.3. Laser Vaporization

The work of the Houston group is summarized in a recent paper by Blakley, McAdams and Vestal.[179] This impressive report shows that compounds as diverse as aromatic hydrocarbons, nucleic acid components, and phosphoric acid are vaporized and transmitted into the mass spectrometer. Although some problems remain, notably rather low sensitivity, it was suggested that the laser method could be developed into a completely general LC/MS interface.

Subsequent work has challenged some of these conclusions, however. In a visit to Houston by the Principal Investigator in July, 1978, it was noted that the laser vaporization method is only effective when the laser beam impinges at grazing incidence on the capillary tip such that it heats the tip to a red glow. Very few ions are detected when the laser is not heating the capillary quite strongly. Moreover, the ion yield is further increased by inserting a heated surface in the path of the molecular beam inside the ion source of the transversely mounted spectrometer described as an improved version of the device.[180]

From these and related observations it is concluded that the laser beam is ineffective at removing the last traces of solvent molecules. Just as we observed with the ultrasonic horn of Figure 48(A), heating of the capillary tip is important in the beam-forming process and for much of the solvent evaporation. The explosive vaporization of solvent apparently expels the microcroplets of solute plus solvent into the apparatus. Final evaporation of adhering solvent is accomplished by bouncing the microdroplets off a hot surface. Condensation of vapor molecules in the process of expansion may play a role in the observed phenomena. In any case, the major role of the laser beam appears to be that of providing a means for localized heating of the beam-forming capillary rather than stripping solvent from solute molecules.

4.2.4. Surface Desorption

In contrast with these rather discouraging results, a recent report by Meuzelaar et al. describes the use of a pulsed CO_2 laser as an effective means for desorbing polar non-volatile molecules from surfaces.[180] Cation attachment to the intact molecule is observed for oligosaccharides--glucose, sucrose, gentiobiose, raffiniose and stachyose--glycosides, nucleotides, amino acids, oligopeptides, steroid conjugates, antibiotics, chlorophyll and sodium acetate. Clearly this method is extremely promising as a means for volatizing complex, labile molecules. Exploratory studies with a Nd-glass laser, emitting at 1.06 μ where organic molecules are essentially transparent, also generated cationated molecular ions for oligosaccharides. Essentially identical spectra were generated, supporting the hypothesis that rapid heating of the substrate was the dominant desorption mechanism. This result is consistent with earlier reports of the effect of heating rate on vaporization of involatile molecules[170,171] and suggests that the failure to evaporate microdroplets in the beam experiments results from inadequate absorption of laser energy at low solvation numbers--e.g., the absence of dielectric absorption of laser power under these conditions.

4.2.5. Discharge Ion Source Studies

The failure to generate CI spectra using an electron gun crossing the molecular beam under viscous flow conditions of the freely expanding jet prompted an investigation of glow discharges as an ion source for the LC/MS interface. Interposing a gas source at moderate pressure in the beam path will interrupt the molecular beam and solvent and other molecules destined for the beam trap in Figure 45 would be injected into the source. Buildup of insulating deposits and creation of strange electric fields would cause the operation of a conventional CI source to deteriorate rapidly. However, the elimination of the filament, electron gun, and extraction electrodes made possible by operating a glow discharge inside the source appears to be an attractive strategy for creating a rugged, dependable ion source.

The use of a glow or Townsend discharge as a means of generating ions for examination by mass spectrometry is of relatively recent interest. The atmospheric pressure discharge has been extensively investigated by Professor E. Horning and colleagues at the Baylor College of Medicine.[181] This discharge source has been investigated as a general purpose detector for gas chromatography and liquid chromatography. Professor D.F. Hunt and his collaborators at the University of Virginia have investigated a discharge ion source which is a modest adaptation of a conventional chemical ionization source and which operates in the range of 1 torr pressure.[182] In the course of our study Kambara and Kanomato reported their investigation of an ion source of similar geometry to the one which we designed for our investigation.[183] To date, no extensive investigation has been carried out of the effects of changing the ion source geometry operating pressure or electrode spacings. Consequently the present investigations addressed these issues plus the question of whether a discharge source constructed from an insulator rather than stainless steel or some other metal, would be sufficiently stable for use as an ion source. This was considered particularly important if the source is to be operated as a liquid chromatographic detector with a high probability that insulating deposits would form from the decomposition of organic compounds injected into the source.

The general physics and chemistry of electric discharges have been a subject for experimental studies for many years and the overall characteristics are well known.[184] Figure 51 presents schematically the voltage-current characteristics of an electric discharge maintained between planar electrodes with a current-regulated circuit. At very low currents there is a residual background level of ionization present in the tube resulting from background cosmic radiation. The sustained voltage across the discharge plates is indicated by V_s in the figure and is a relatively high value. As the current is increased the plateau labeled AB in the figure is generated. This is known as the Townsend discharge region. As the current is increased still further, a drop in gap voltage shown by the line BC is noted. This decrease in gap voltage reflects the increased conductivity of the discharge tube. A faint glow is also detected in the tube, representing primarily the excitation of neutral gas species. With further increases in current the plateau CD is observed, a region in which the discharge voltage remains constant at the value V_g while the discharge current may be varied by about two orders of magnitude. This region is known as the "normal glow discharge" region and the increase in the discharge current is accompanied by an increase in the diameter of the glow discharge passing between the electrode surfaces. The magnitude of increase in the discharge current is limited by the area of the electrodes. The "abnormal glow discharge" is indicated by the line segment DE in the figure and the point E of the plots defines the point at which the discharge becomes unstable and passes over into an arc discharge. In the arc discharge region the voltage across the discharge drops from hundreds or thousands of volts to tens of volts and the current increases to amperes. This phenomenological development results in the excessive dissipation of power by the discharge and heats the gas very strongly.

The source design which was investigated in our laboratory is indicated schematically in Figure 52, and the basic circuit used to measure the discharge parameters is indicated in Figure 53. The source block was constructed of Teflon® for ease of manufacture. Gas inlets and static pressure measuring tubes are indicated in the figure. The second electrode consists of a threaded plunger constructed of Delrin with a needle electrode inserted in the center. A platinum wire sharpened to a point was used as the repeller electrode and, as indicated in the sketch, a stainless steel aperture shielded by the platinum wedge was used as the counter, or extraction electrode. The threaded plunger allows precise adjustment of the relative position of the electrodes. The zero distance is determined by carefully screwing in the plunger to the point where electrical contact between the two electrodes is made. From the pitch of the thread it is a straightforward procedure to calculate the precise

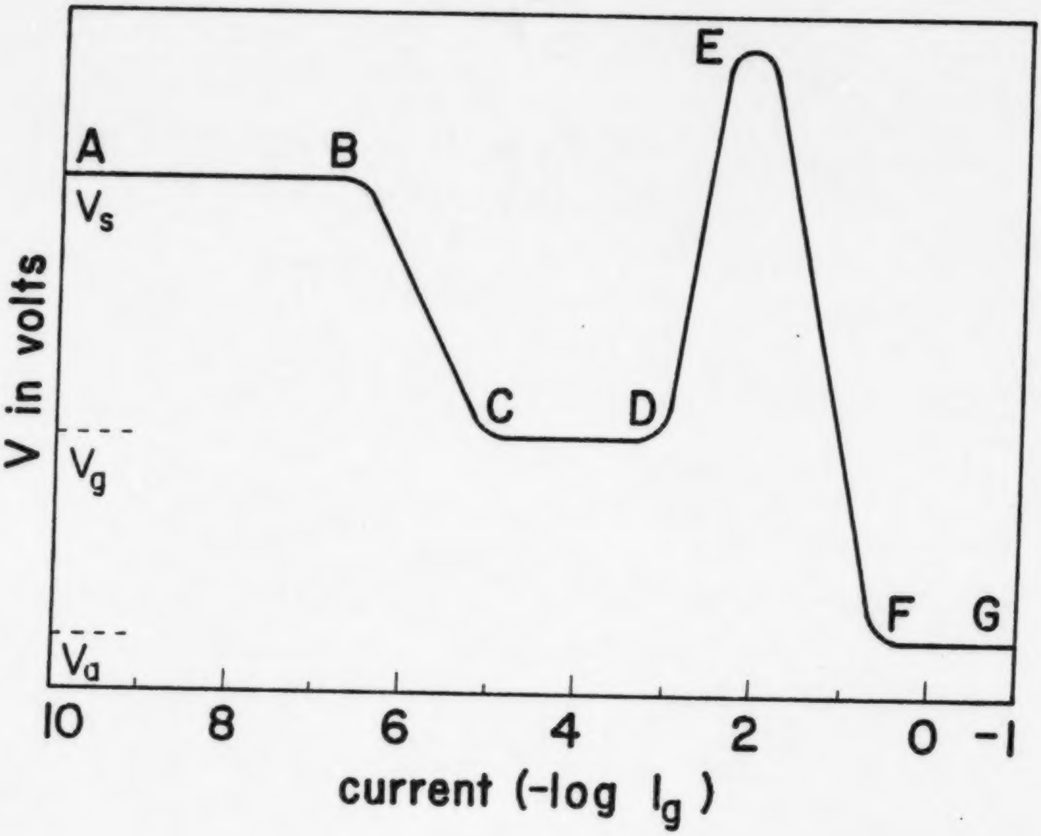

Figure 51. Characteristic curve of a self-limited glow discharge.

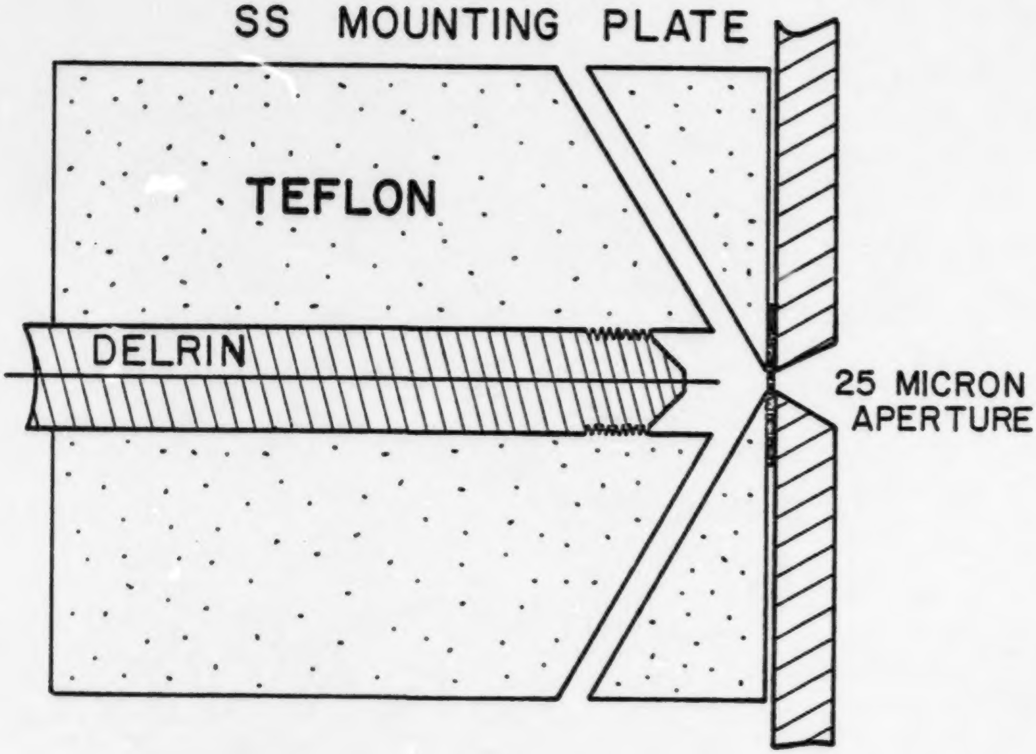
SS MOUNTING PLATE
TEFLON
DELRIN
25 MICRON
APERTURE

Figure 52. Diagram of the glow discharge ion source evaluated in this research.

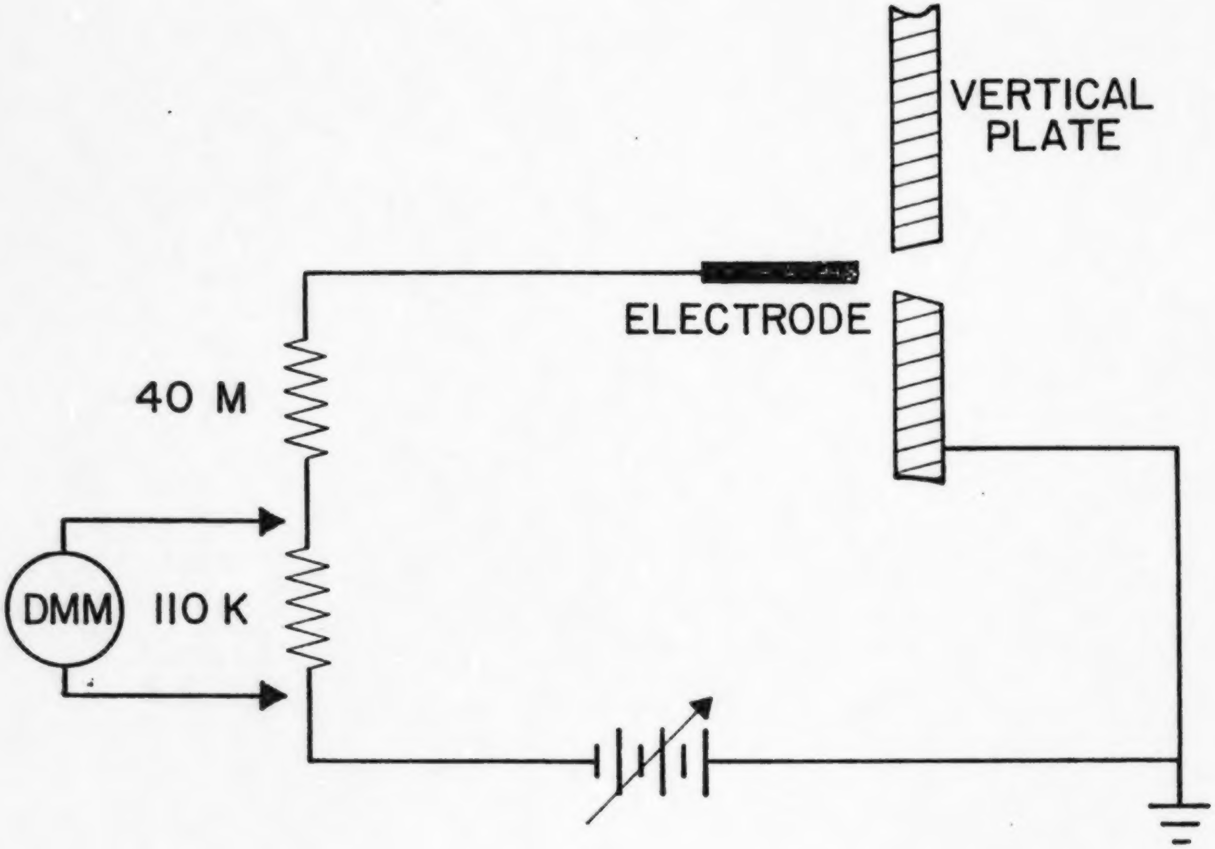
VERTICAL PLATE
ELECTRODE
40 M
DMM
110 K

Figure 53. Circuitry utilized to evaluate performance characteristics of the glow discharge ion source.

spacing from the number of turns by which the plunger is backed away from the zero position. A differential pressure manometer is connected to the source tube by 1/16" stainless tubing in a static line configuration for measurement of ion source pressure. Gas inlet and exit tubes were also 1/16" stainless steel tubing. They were threaded and screwed into the source body using Teflon tape to ensure a gas-tight seal.

External to the source a lens stack was constructed using 1/8" ceramic spacers and stainless steel aperture plates. A three-element Einzel lens configuration was followed by a stainless steel retarding grid assembly for measuring the kinetic energy distribution of the ions exiting the source. A ground-ring shield followed next in the lens stack, followed by a nichrome plate with a 1/16" aperture in the center. The lens assembly is completed by a Faraday cup collector for monitoring ion current. The detector was placed either above or below ground for measurement of negative or positive ions, respectively. The ion current was measured by means of a Keithly Model 600B electrometer.

The region of interest for utilizing a discharge as a mild ionization source is the glow discharge region defined by the plateau CD in Figure 51. This could obviously be explored precisely by tracing the voltage current characteristics of Figure 51 utilizing a current-regulated power supply. However, it was more convenient in our experiments to control the potential across the discharge rather than the current. The circuit shown in Figure 52 illustrates how this was done. The gap current I_g was calculated from the voltage drop across the 110 kilo•ohm resistor, V_r. The gap voltage is the voltage applied across the series of components, V_d, less the voltage drops across the two resistors. Consequently, the discharge current I_g and the discharge voltage V_g may be calculated from the following equations.

$$I_g = V_r/1.10 \times 10^5$$

$$V_g = V_d - 364\ V_r$$

The glow discharge region is easily identified by the voltage-current characteristic indicated in Figure 51. The point at which the current changes by orders of magnitude while the voltages are held constant defines the glow discharge region. With the constant voltage power supply utilized in our circuit, drastic oscillations of voltage drops, across the discharge were observed in the true "glow discharge" region. However, the operation of the source could easily be stabilized by increasing the voltage slightly. At this point the current increased to its maximum value permitted by the stable glow discharge operation of the source. Because the line DE in the discharge characteristic curve (Figure 51) is so steep, there is no difficulty in maintaining the operation of the discharge at point D. Parenthetically we note that this would be the preferred method used to control a practical discharge source as a chemical ionization ion source.

With the indicated experimental configuration measurements were made for electrode gaps from 1 to 10 mm and at pressures ranging from 1 torr to 41 torr. Corresponding gap voltages ranged from tens of volts to 2 kilovolts. From the examination of the discharge characteristics we selected the 4 mm gap spacing as a convenient compromise requiring a moderate gap voltage to drive the discharge and providing a large enough geometric space for collisional relaxation of ions that are generated. A further consideration was the magnitude of the current available from the source. The detected current approaches the space charge limit, as anticipated for discharges operating at point D of Figure 51.

Figures 54 and 55 illustrate the discharge characteristics as a function of pressure for an inter-electrode spacing of 4 mm. Figure 54 is a plot of positive ion current monitored at the collector, while Figure 55 is a plot of negative ions from the discharge source. It is apparent that intense ion currents are generated, ranging from 10^{-5} to 10^{-7} amps at pressures from 5 to 15 torr.

These curves were generated using dry nitrogen as the test gas. The ions formed in nitrogen in a radio-isotope source have been described by McKeown and Siegel[185] and are expected to be very similar under our conditions. Although no mass spectral analysis was carried out with the test source, we did use permanent magnets to distinguish between electrons and negative ions as charge carriers in the negative mode. It was demonstrated that in the pure nitrogen case most of the charge carriers were electrons, while the addition of carbon tetrachloride readily converted them to negative ions, presumably Cl^-.

Since the ion currents observed were orders of magnitude greater than those available in conventional CI sources, it was also of interest to investigate the ion energy distribution to determine what fraction of the actual ion flux represented usable ion currents which could be transmitted by conventional mass analyzers. Energy analysis was accomplished by applying a stopping potential to the retarding grid of the lens stack. As the voltage is incremented upwards, (i.e., made increasingly positive for positive ions and negative for negative ions) the total ion current was measured at the Faraday cup for each voltage. The stopping potential curve represents the integral of the ion energy distribution.

The ion energy distribution may therefore be obtained by differentiating the curve for the total ion current versus retarding grid potential. This was carried out by a computer curve-fitting routine which calculates the best parabola through each successive set of three points and calculates the derivative at the middle data point. Figures 56 and 57 show the ion energy distributions deduced for positive ions and negative ions, respectively.

These figures illustrate that the energy distributions are quite broad for both positive and negative ions but are somewhat broader for positive ions. The distribution at 5 torr, which appears to be a reasonable operating pressure for the discharge source, has a half-width of approximately 120 volts, while the negative ion curve has a half-width of less than 20 volts. In both cases the energy spreads are much larger than those generated by standard ion sources.

A quadrupole mass filter will accept an energy band-width of the order of 10 volts, while a single-focusing magnetic deflection instrument requires an energy spread of two volts or less for moderate mass resolution. However, it

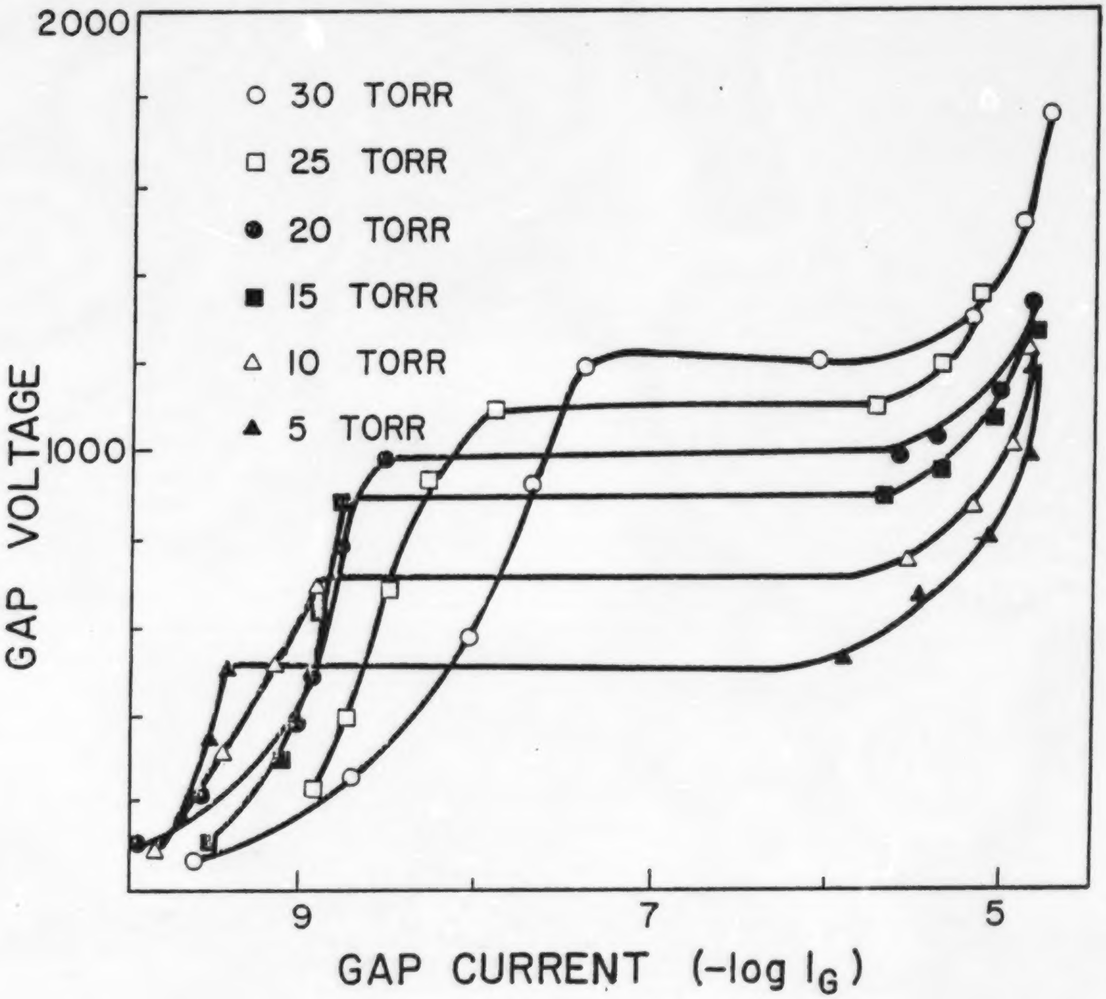

Figure 54. Characteristic curves of established glow discharges for a series of pressures, obtained for a 4.0 mm electrode spacing. Curves shown are for positive ions.

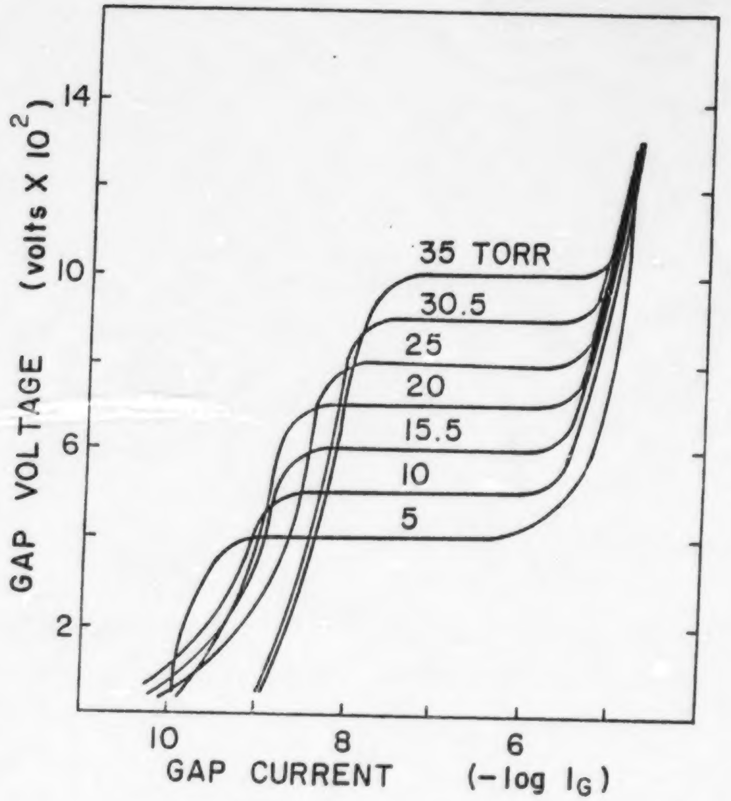

Figure 55. Characteristic curves for established glow discharges for a series of pressures obtained for 4.0 mm electrode spacing. Curves shown are for negative current.

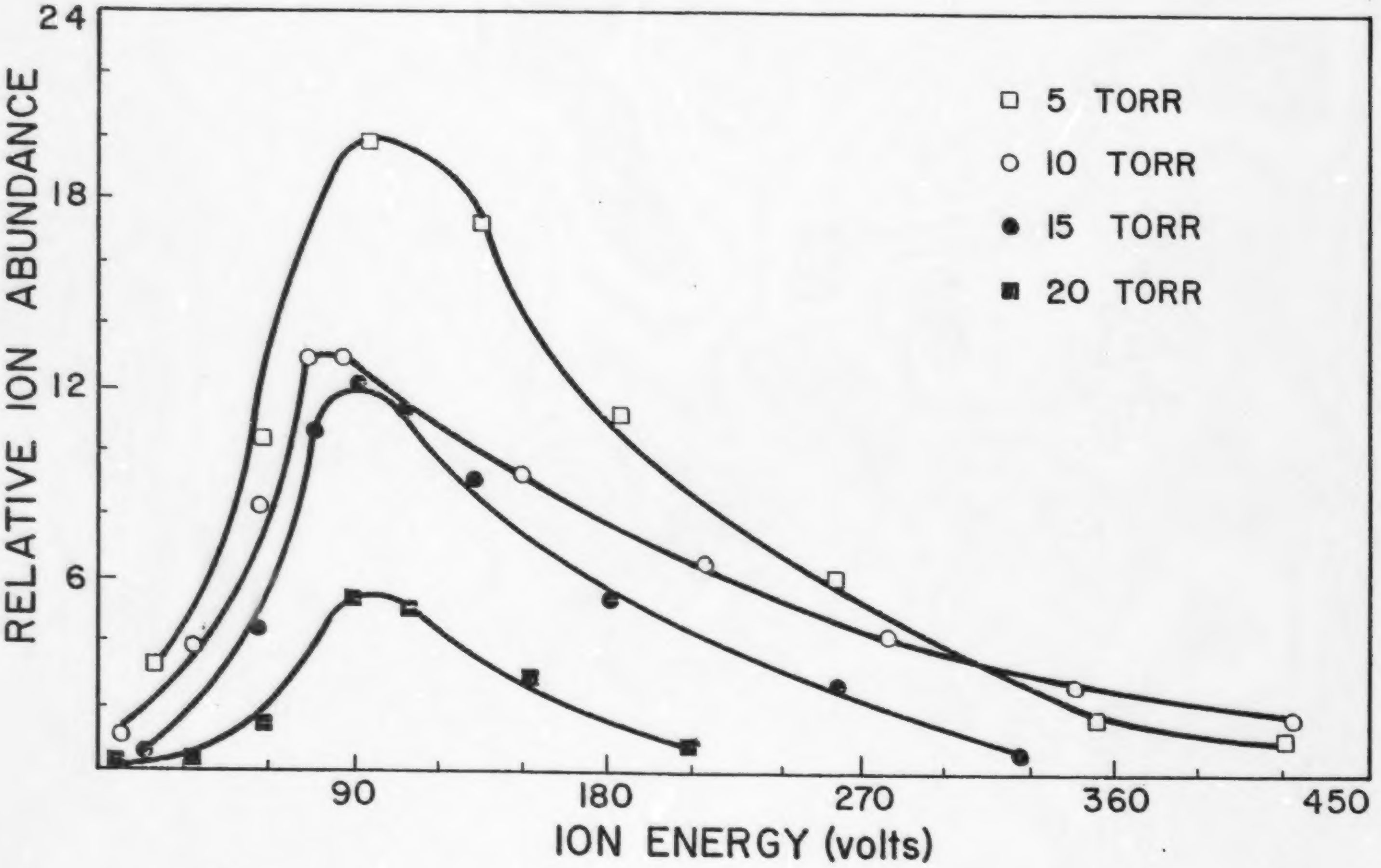

Figure 56. Ion energy distribution for a series of source pressures. The electrode is positive with respect to the vertical plate.

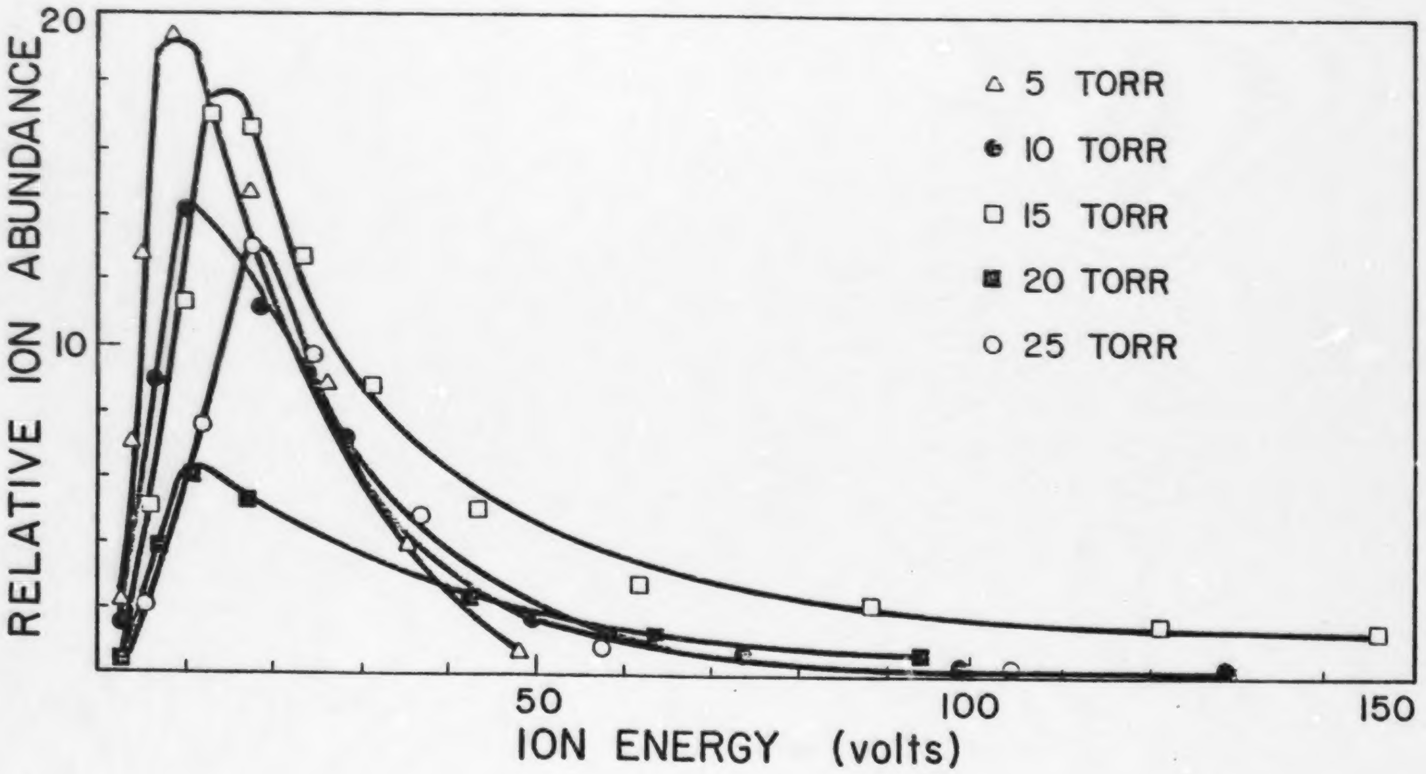

Figure 57. Ion energy distribution for a series of source pressures. The electrode is negative with respect to the vertical plate.

would appear that energy selection using a suitable lensing system will make a discharge source of the type described a quite acceptable ion source for both types of mass spectrometers. With a quadrupole mass filter, of the order of 20% of the ions generated by the source represents usable ion beam, while at least a few percent of the ions would be usable in a magnetic spectrometer. However, because the ion beam intensity extracted from this source exceeds by 1 to 3 orders of magnitude that provided by conventional electron impact ion sources, the usable ion current is at least comparable to conventional CI sources.

It is also noteworthy that no degradation in the source performance was noted over a period of several months of operation. Introduction of organic compounds into the source did not noticeably alter its operating characteristics. Consequently, we conclude that the construction of the source block from an insulator is an acceptable and recommended procedure for constructing a practical discharge source. Teflon is obviously inappropriate, but a machinable and bakeable ceramic body appears to be a practical solution to the problem of fabricating a high efficiency, stable, glow discharge ion source.

REFERENCES

1. Hannay, J.B., and Hogarth, J. Proc. R. Soc. London, 30:178, 1880.
2. Paul, P.F.M., and Wise, W.S. The Principles of Gas Extraction. J. Gordon Cook, ed., Mills and Boon Limited, London, 1971.
3. Pilz, V. Verfahrenstechnik, 9:280, 1975.
4. Thies, Hans. Chemia, 32:79, 1978.
5. Peter, S., Brunner, G., and Riha, R. Chem. Ing. Tech., 46:623, 1974.
6. Stahl, E., and Schilz, W. Chem. Ing. Tech., 48:773, 1976.
7. Alwani, Z., and Schneider, G.M. Ber. Bunsenges. Phys. Chem., 80:1310, 1976.
8. Deiters, U., and Schneider, G.M. Ber. Bunsenges. Phys. Chem., 80:1316, 1976.
9. Prausnitz, J.M. Ber. Bunsenges. Phys. Chem., 81:900, 1977.
10. Patent: Katz, Donald L., and Whaley, Thomas H. Phillips Petroleum Co., U.S. 2,391,576, December 25, 1945. [from Chem. Abst. CA#040/04/1017, 1946]
11. Ellis, S.R.M. Br. Chem. Eng., 16:358, 1971.
12. Zhuze, T.P. Petroleum, 23:298, 1960.
13. Patent: Zhuze, T.P., and Yushkevich, G.N. Institute of Geology and Processing of Mineral Fuels, Ger. Offen., 1,952,233 (Cl. C10g), April 22, 1971. [from Chem. Abst. #CA075/02/8265j, 1971]
14. Patent: Hess, Howard V., and Guptill, F.E., Jr. Texaco Inc., U.S. 3,318,805 (Cl.210-21), May 9, 1967. [from Chem. Abst. #CA067/08/36333h, 1967]
15. Patent: Zosel, Kurt. Studiengesellschaft Kohle m.b.H., U.S. 3,597,464 (Cl. 260-448A; C07f), August 3, 1971. [from Chem. Abst. #CA075/17/110417x, 1971]
16. Patent: Zosel, Kurt. Studiengesellschaft Kohle m.b.H., Ger Offen. 2,332,038 (Cl. C11b), January 24, 1974. [from Chem. Abst. #CA080/19/106983q, 1974]
17. Patent: Zosel, Kurt. Studiengesellschaft Kohle m.b.H., Ger Offen. 2,363,418 (Cl. C11b), July 11, 1974. [from Chem. Abst. #CA081/23/150734d, 1974]
18. Patent: Zosel, Kurt. Studiengesellschaft Kohle m.b.H., Ger. Offen. 2,441,152 (Cl. C11c), March 6, 1975. [from Chem. Abst. #CA083/11/95199x, 1975]

19. Patent: Zosel, Kurt. Studiengesellschaft Kohle m.b.H., Fr. Demande 2,079,261 (Cl. A23f), December 17, 1971. [from Chem. Abst. #CA077/11/73879t, 1972]

20. Patent: Zosel, Kurt. Studiengesellschaft Kohle m.b.H., Ger. Offen. 2,221,560 (Cl. C07d), November 30, 1972. [from Chem. Abst. #CA078/07/41878w, 1973]

21. Patent: Vitzthum, Otto, and Hubert, Peter. Hag A.-G., Ger. Offen. 2,127,596 (Cl. C11b), December 21, 1972. [from Chem. Abst. #CA078/15/95039s, 1973]

22. Patent: Vitzthum, Otto, Hubert, Peter, and Sirtl, Wolfgang. Studiengesellschaft Kohle m.b.H., Can. 987,250 (Cl. 195-14), April 13, 1976. [from Chem. Abst. #CA085/07/44923n, 1976]

23. Patent: Roselius, Wilhelm, Vitzthum, Otto, and Hubert, Peter. Studiengesellschaft Kohle m.b.H., U.S. 3,923,847 (Cl. 260-412.8; C11B), December 2, 1975. [from Chem. Abst. #CA084/13/88294s, 1976]

24. Vitzthum, O.G., Werkhoff, P., and Hubert, P. J. Food Sci., 40:911, 1975.

25. Patent: Vitzthum, Otto, and Hubert, Peter. Studiengesellschaft Kohle m.b.H., Can. 989,662 (Cl. 99-143), May 25, 1976. [from Chem. Abst. #CA085/17/122116t, 1976]

26. Patent: Roselius, Wilhelm, Vitzthum, Otto, and Hubert, Peter. Hag A.-G., Ger. Offen. 2,106,133 (Cl. A23f), August 1972. [from Chem. Abst. #CA077/21/138583p, 1972]

27. Patent: Vitzthum, Otto, and Hubert, Peter. Hag A.-G., Ger. Offen. 2,212,281 (Cl. A23f), September 27, 1973. [from Chem. Abst. #CA080/01/2445z, 1974]

28. Patent: Vitzthum, Otto, Hubert, Peter, and Sirtl, Wolfgang. Hag A.-G., Ger. Offen. 2,357,590 (Cl. A23F), May 28, 1975. [from Chem. Abst. #CA083/07/57015b, 1975]

29. Patent: Roselius, Wilhelm, Vitzthum, Otto, and Hubert, Peter. Hag A.-G., Ger. Offen. 2,043,537 (Cl. A24b), May 31, 1972. [from Chem. Abst. #CA077/13/85883c, 1972]

30. Patent: Roselius, Wilhelm, Vitzthum, Otto, and Hubert, Peter. Hag A.-G., Ger. Offen. 2,142,205 (Cl. A24b), May 15, 1973. [from Chem. Abst. #CA078/23/145393a, 1973]

31. Vitzthum, O.G., Werkhoff, P., and Hubert, P. J. Agric. Food Chem., 23:999, 1975.

32. Whitehead, J.C., and Williams, D.F. J. Inst. Fuel, 48:182, 1975.

33. Maddocks, R.R., and Gibson, J. Chem. Eng. Progress, 73:59, 1977.

34. Bartle, Keith D., Martin, Terence G., and Williams, Derek F. Fuel, 54:226, 1975.

35. Grainger, Leslie. Chem. Ind., 18:737, 1974.

36. Bartle, Keith D. Dtsch. Ges. Mineraloelwiss. Kohlechem. Compend., 77-78:252, 1978.

37. Gangoli, N., and Thodos, G. Ind. Eng. Chem. Prod. Res. Dev., 16:208, 1977.

38. Petersilie, A., and Sörensen, H. Lithos, 3:59, 1970.

39. Reed, W.E. Geochim. Cosmochim. Acta, 41:237,1977.

40. Holloway, J.R., and Reese, R.L. Am. Mineral. 59:587, 1974.

41. Ziegenbein, D., and Johannes, W. Neues Jahrb. Mineral. Abh., 132:145, 1977.

42. Weale, K.E. Chemical Reactions at High Pressures. E. & F.N. Spon Ltd., London, 1967.

43. Manning, W.R.D., and Labrow, S. High Pressure Engineering. I. L. Hepner, ed., The Chemical Rubber Co., Cleveland, 1971.

44. Young, C.L. Chem. Thermodyn.,2:71-104, 1978.

45. Zosel, K. Angew. Chem. Int. Ed. Engl., 17:702, 1978.

46. Wilke, Günther. Angew. Chem. Int. Ed. Engl., 17:701, 1978.

47. Hubert, Peter, and Vitzthum, Otto G. Angew. Chem. Int. Ed. Engl., 17:710, 1978.

48. Schneider, Gerhard M. Angew. Chem. Int. Ed. Engl., 17:716, 1978.

49. Lenz, Harro, and Franck, Ernst Ulrich. Angew. Chem. Int. Ed. Engl., 17:728, 1978.

50. Stahl, Egon, Schilz, Winfried, Schütz, Erwin, and Willing, Eberhard. Angew. Chem. Int. Ed. Engl., 17:731, 1978.

51. Klesper, E. Angew. Chem. Int. Ed. Engl., 17:738, 1978.

52. Peter, Siegfried, and Brunner, Gerd. Angew. Chem. Int. Ed. Engl., 17:746, 1978.

53. Eggers, R. Angew. Chem. Int. Ed. Engl., 17:751, 1978.

54. Schneider, G.M. High-Pressure Science and Technology. Sixth AIRAPT Conference. K.D. Timmerhaus and M.S. Barber, eds., Plenum Press, New York, 1979. Vol. 1, pp. 506-517.

55. Zosel, K. High-Pressure Science and Technology. Sixth AIRAPT Conference. K.D. Timmerhaus and M.S. Barber, eds., Plenum Press, New York, 1979. Vol. 1, pp. 561-564.

56. Brunner, G., Peter, S., Retzlaff, B., and Riha, R. High-Pressure Science and Technology. Sixth AIRAPT Conference. K.D. Timmerhaus and M.S. Barber, eds., Plenum Press, New York, 1979. Vol. 1, pp. 565-572.

57. Hartmann, W., and Klesper, E. High-Pressure Science and Technology. Sixth AIRAPT Conference. K.D. Timmerhaus and M.S. Barber, eds., Plenum Press, New York, 1979. Vol. 1, pp. 573-582.

58. Gouw, T.H., Jentoft, R.E., and Gallegos, E.J. High-Pressure Science and Technology. Sixth AIRAPT Conference. K.D. Timmerhaus and M.S. Barber, eds., Plenum Press, New York, 1979. Vol. 1, pp. 583-592.

59. Irani, C.A., and McHugh, D.J. High-Pressure Science and Technology. Sixth AIRAPT Conference. K.D. Timmerhaus and M.S. Barber, eds., Plenum Press, New York, 1979. Vol. 1, pp. 600-608.

60. Irani, C.A., and Funk, E.W. Recent Developments in Separation Science. Norman N. Li, ed., CRC Press Inc., Cleveland, 1977. Vol. III, Part A, pp. 171-193.

61. Túgrul, Taner, and Olcay, Aral. Fuel, 57:415, 1978.

62. Blessing, James E., and Ross, David S. Organic Chemistry of Coal, ACS Symposium Series 71. John W. Larsen, ed., American Chemical Society, Washington, D.C., 1978. p. 171.

63. Chem. Eng. News, 56:10, 1978.

64. Bartle, K.D., Jones, D.W., Pakdel, H., Snape, C.E., Calimli, A., Olcay, A., and Túgrul, T. Nature (London), 277:5694,284, 1979.

65. Patent: Peter, Siegfried, and Brunner, Gerd. Ger. Offen. 2,737,794 (Cl. A23F/10), March 8, 1979. [from Chem. Abst. #CA090/19/150499s, 1979]

66. Patent: Peter, Siegfried, and Brunner, Gerd. Ger. Offen. 2,737,793 (Cl. A23F1/10), March 8, 1979. [from Chem. Abst. #CA090/19/150500k, 1979]

67. Patent: Stahl, Egon, Schütz, Erwin, and Schilz, Winfried. Deutsche Gold-und-Silber-Scheideanstalt vorm. Roessler. Ger. Offen. 2,709,033 (Cl. B01D11/00), September 7, 1978. [from Chem. Abst. #CA090/04/028998p, 1979]

68. McFadden, W.H., Schwartz, H.L., and Evans, S. J. Chromatogr., 122:389, 1976.

69. Scott, R.P.W., Scott, C.G., Munroe, M., and Hess, J. J. Chromatogr., 99:395, 1974.

70. Lovins, R.E., Ellis, S.R., Tolbert, G.D., and McKinney, C.R. Anal. Chem., 45:1553, 1973.

71. Arpino, P.J., Dawkins, B.G., and McLafferty, F.W. J. Chromatogr. Sci., 12:574, 1974.

72. Horning, E.C., Carroll, D.I., Dzidic, I., Haegele, K.D., Horning, M.G., and Stillwell, R.N. J. Chromatogr. Sci., 12:725, 1974.

73. Baldwin, M.A., and McLafferty, F.W. Org. Mass Spectrom., 7:1111, 1973.

74. Carroll, D.I., Dzidic, I., Stillwell, R.N., Haegele, K.D., and Horning, E.C. Anal. Chem., 47:2369, 1975.

75. Takeuchi, Tsugio, Hirata, Yukio, and Okumura, Yoshio. Anal. Chem., 50:659, 1978.

76. Jones, P.R., and Yang, S.K. Anal. Chem., 47:1000, 1975.

77. Erdahl, W.L., and Privett, O.S. Lipids, 12:797, 1977.

78. Mundy, D.E., and Machin, A.F. J. Chromatogr., 139:321, 1977.

79. Mundy, D.E., Quick, M.P., and Machin, A.F. J. Chromatogr., 121:335, 1976.

80. Vouros, P., Peterson, B.A., Colwell, L., and Karger, B.L. Anal. Chem., 49:1039, 1977.

81. Heck, H., Dyer, R.L., Scott, A.C., and Anbar, M. J. Agric. Food Chem., 25:901, 1977.

82. Hartmann, W., and Klesper, Polym. Sci. Polym. Lett. Ed., 15:707,1977.

83. Jentoft, R.E., and Gouw, T.H. J. Polym. Sci., Part B, 7:811, 1969.

84. Graffeo, A.P., Lin, D.C.K., and Foltz, R.L. J. Chromatogr., 126:717,1976.

85. Giddings, J.C., Myers, M.N., and Wahrhaftig, A.L. Int. J. Mass Spectrom. Ion Phys., 4:9, 1970.

86. Din, F., ed. Thermodynamic Functions of Gases. Butterworths, London, 1962.

87. L'Air Liquide, Division Scientifique. Encyclopedia des Gaz (Gas Encyclopedia). Elsevier, Amsterdam, 1976.

88. Booth, H.S., and Bidwell, R.M. Chem. Rev., 44:477, 1949.

89. Karayannis, N. M. Rev. Anal. Chem., 1:43-83, 1971.

90. Gouw, T.H., and Jentoft, R.E. J. Chromatogr., 68:303-323, 1972.

91. Gouw, T.H., and Jentoft, R.E. Adv. Chromatogr., 13:1-40, 1975.

92. Vigdergauz, M.S., and Semkin, V.I. Russ. Chem. Rev., 40:533-549, 1971.

93. Frank, Lenore Grace Randall. The Direct Coupling of a Dense Gas Chromatograph to a Mass Spectrometer by a Supersonic Molecular Beam. Ph.D. Thesis, University of Utah, Salt Lake City, Utah, 1979.

94. Giddings, J.C., Myers, M. N., McLaren, L., and Keller, R.A. Science, 162: 67, 1968.

95. Czubryt, J.J., Myers, M.N., and Giddings, J.C. J. Phys. Chem., 74:4260, 1970.

96. Klesper, E., Corwin, A.H., and Turner, D.A. J. Org. Chem., 27:700, 1962.

97. Bowman, Lyle Max, Jr. Dense-Gas Chromatographic Studies. Ph.D. Thesis, University of Utah, Salt Lake City, Utah, 1976.

98. Jentoft, R.E., and Gouw, T.H. J. Chromatogr. Sci., 8:138, 1970.

99. Sie, S.T., van Beersum, W., and Rijnders, G.W.A. Sep. Sci., 1:459, 1966.

100. Sie, S.T., and Rijnders, G.W.A. Anal. Chim. Acta, 38:31, 1967.

101. Giddings, J.C. Sep. Sci., 1:73, 1966.

102. Bartmann, D. Ber. Bunsenges. Phys. Chem., 76:336, 1972.

103. Nieman, J.A., and Rogers. L.B. Sep. Sci., 10:517, 1975.

104. Sie, S.T., and Rijnders, G.W.A. Sep. Sci., 2:729, 1967.

105. Sie. S.T., and Rijnders, G.W.A. Sep. Sci., 2:755, 1967.

106. Sie. S.T., and Rijnders, G.W.A. Sep. Sci., 2:699, 1967.

107. Huber, J.F.K., Lauer, H.H., and Poppe, H. J. Chromatogr., 112:377, 1975.

108. Lauer, H.H., Poppe, H., and Huber, J.F.K. J. Chromatogr., 132:1, 1977.

109. Guichon, G., and Pommier, C. Gas Chromatography in Inorganics and Organometallics. Ann Arbor Science Publisher, Inc., Ann Arbor, Michigan, 1973. p. 29.

110. Jentoft, R.E., and Gouw, T.H. Anal. Chem., 44:681, 1972.

111. Sie, S.T., Bleumer, J.P.A., and Rijnders, G.W.A. Gas Chromatography and Its Exploitation. In: Proceedings of the International Gas Chromatography Symposium, C.L. Harbourn, ed., 7:235, 1969.

112. Bocek, J., Novak, J., and Janak, J. J. Chromatogr. Sci., 8:226, 1970.

113. Cashaw, J.L., Segura, R., and Zlatkis, A. J. Chromatogr. Sci., 8:363, 1970.

114. Anderson, James B. Molecular Beams from Nozzle Sources. In: Molecular Beams and Low Density Gasdynamics, Peter P. Wegener, ed., Marcel Dekker, Inc., New York, 1974. pp. 1-91.

115. Ashkenas, H., and Sherman, F.S. Proceedings of the 4th International Symposium on Rarefied Gas Dynamics in 1964, Vol. II, p. 84. J.H. de Leeuv, ed., Academic Press, New York, c. 1966.

116. Hamel, B.B., and Willis, D.R. Phys. Fluids, 9:829, 1966.

117. Anderson, J.B., and Fenn, J.B. Phys. Fluids, 8:780, 1965.

118. LeRoy, Rodney Lash. The Characterization of Supersonic Molecular Beams and Their Application to a Chemical Problem. Ph.D. Thesis, University of Toronto, Toronto, 1968.

119. Bier, K., and Hagena, O. Proceedings of the 3rd International Symposium on Rarefied Gas Dynamics in 1962, Vol. I, p. 478. J.A. Laurmann, ed., Academic Press, New York, c. 1963.

120. Raghuraman, P. Theoretical Study of Molecular Scattering in Supersonic Molecular Beams. Deutsche Luft- und Raumfahrt Forschungsbericht 73-117, Duetsche Forschungs- und Versuchsanstalt für Luft- und Raumfahrt, Institut für Dynamik verdünnter Gas, Göttingen, 1973.

121. Bier, K., and Hagena, O. Proceedings of the 4th International Symposium on Rarefied Gas Dynamics in 1964, Vol.II, p. 260. J.H. de Leeuv, ed., Academic Press, New York, c. 1966.

122. Bird, G.A. Phys. Fluids, 19:1486, 1976.

123. Govers, T.R., LeRoy, R.L., and Deckers, J.M. Proceedings of the 6th International Symposium on Rarefied Gas Dynamics in 1968. Leon Trilling and Harold Y. Wachman, eds., Academic Press, New York, c. 1969. Vol. II, p. 985.

124. Hagene, M., and Pasquerault, D. Entropie, 42:80, 1971.

125. Brown, R.F., and Heald, J.H., Jr., Proceedings of the 5th International Symposium on Rarefied Gas Dynamics in 1966. Vol. II, p. 1407. C.L. Brundin, ed., Academic Press, New York, c. 1967.

126. Campargue, R., and Breton, J.P. Entropie, 42:18, 1971.

127. Campargue, R. J. Chem. Phys., 52:1795, 1970.

128. Anderson, J.B. AIChE J., 13:1188, 1967.

129. Sherman, F.S. Phys. Fluids, 8:773, 1965.

130. Eckelt, W.R., Hose, H., and Schügerl, K. Z. Naturforsch., 24:1365, 1969.

131. Klemperer, W. Ber. Bunsenges. Phys. Chem., 78:128, 1974.

132. Smalley, R.E., Wharton, L., and Levy, D.H. Acc. Chem. Res., 10:139, 1977.

133. Hagena, Otto F. Cluster Beams from Nozzle Sources. In: Molecular Beams and Low Density Gasdynamics. Peter P. Wegener, ed., Marcel Dekker, Inc., New York, 1974. pp. 93-181.

134. Dorfield, William G., and Hudson, John B. J. Chem. Phys., 59:1253, 1973.

135. Dorfield, William G., and Hudson, John B. J. Chem. Phys., 59:1261, 1973.

136. Hagena, O.F., and Obert, W. J. Chem. Phys., 56:1793, 1972.

137. Wegener, Peter P. Gasdynamics of Expansion Flows with Condensation and Homogenous Nucleation of Water Vapor. In: Nonequilibrium Flows, Part I. Peter P. Wegener, ed., Marcel Dekker, Inc., New York, 1969. pp. 163-243.

138. Farges, J., de Feraudy, M.F., Raoult, B., and Torchet, G. Proceedings of the 10th International Symposium on Rarefied Gas Dynamics in 1976. Progress in Astronautics and Aeronautics, Vol. 51, p. 1117. J. Leith Potter, ed., American Institute of Aeronautics and Astronautics, New York, c. 1977.

139. Chang, John. Supersonic Molecular Beam Sampling Systems for Mass Spectrometric Studies of High Pressure Flow Systems. SAMSO-TR-69-113, Research Report 326, Avco Everett Research Laboratory, April 1969. 65 pp.

140. Randall, L.G. and Wahrhaftig, A. L. Anal. Chem., 50:1703, 1978.

141. Johnson, Leslie P., Morrison, James D., and Wahrhaftig, A.L. Int. J. Mass Spectrom. Ion Phys., 26:1, 1978.

142. Rheodyne Incorporated. Clogging of Column Inlet Frits. In: Technical Notes, Bulletin TN 177, Berkeley, California.

143. Otvos, J.W., and Stevenson, D.P. J. Am. Chem. Soc., 78:546, 1956.

144. Heller, S.R., and Milne, G.W.A. (ed's). EPA/NIH Mass Spectral Data Base. United States Department of Commerce, Washington, D.C., 1978.

145. McFadden, William. Techniques of Combined Gas Chromatography/Mass Spectrometry: Applications in Organic Analysis. John Wiley and Sons, New York, 1973. p. 87.

146. Selected Mass Spectral Data. Compiled by Standard Thermodynamics Research Center Data Project, Thermodynamics Research Center, Texas A & M University, College Station, Texas, 1976.

147. Cornu, A., and Massot, R. Compilation of Mass Spectral Data, Second Edition. Heyden, New York, 1975.

148. Stenhagen, E., Abrahamsson, S., McLafferty, F.W. (ed's). Atlas of Mass Spectral Data. Interscience Publishers, New York, 1969.

149. Snyder, L.R., and Kirkland, J.J. Introduction to Modern Liquid Chromatography. Wiley, New York, 1974.

150. Fitch, P.S.H., Wharton, L., and Levy, D.H. Chem. Phys. Lett., 48:132, 1977.

151. Smalley, R.E., Levy, D.H., and Wharton, L. J. Chem. Phys., 64:3266, 1976.

152. Campargue, R., Lebéhot, A., and Lemonnier, J.C. Proceedings of the 10th International Symposium on Rarefied Gas Dynamics. Progress in Astronautics and Aeronautics, Vol. 51, p. 1033. J. Leith Potter, ed., American Institute of Aeronautics and Astronautics, c. 1977.

153. Milne, Thomas A. Mass Spectrometer Study of Metal-Containing Flames. Seventh Quarterly Technical Summary Report. Midwest Research Institute Project Number 2551-P, ARPA Project Code Number 9100, August 1963. 20 pp.

154. Stearns, Carl A., Kohl, Fred J., Fryburg, George C., and Miller, Robert A. A High Pressure Modulated Molecular Beam Mass Spectrometer Sampling System. NASA TM 73720, NASA Technical Memorandum, Lewis Research Center, July 1977. 52 pp.

155. Tal'Rose, V.L., Karpov, G.V., Gasdetskii, I.G., and Skurat, V.E. Russ. J. Phys. Chem., 43:198, 1969.

156. Tal'Rose, V.L. Discussion presentation at panel on LC-MS Seventh Triennial Conference on Mass Spectrometry and Allied Topics, Florence, Italy, September, 1976.

157. Skurat, V.E. Russ. J. Phys. Chem., 46:570, 1972.

158. Arpino, P., Baldwin, M.A., and McLafferty, F.W. Biomed. Mass Spectrom., 1:80, 1974.

159. McLafferty, F.W., Knutti, R., Venkataraghavan, R., Arpino, P.J., and Dawkins, B.G. Anal. Chem., 47:1503, 1975.

160. Henion, J.D. Presented at the 25th Annual Conference on Mass Spectrometry and Allied Topics of the American Society for Mass Spectrometry, Washington, D.C., June, 1977.

161. Horning, E.C., Carroll, D.I., Dzidic, I., Lin, S.N., Stillwell, R.N., and Thenot, J.P. J. Chromatogr. Sci., 142:481, 1977.

162. Tsuge, S., Hirata, Y., and Takeuchi, T. Anal. Chem., 51:166, 1979.

163. Llewllyn, P.M., and Littlejohn, D.P. U.S. Patent #2,429,105, February, 1969.

164. Gieniec, John. Doctor of Philosophy Thesis, University of Wisconsin, 1971.

165. Dole, Malcolm, Mack, L.L., Hines, R.L., Mobley, R.C., Ferguson, L.D., and Alice, M.B. J. Chem. Phys., 49:2240-2249, 1968.

166. Evans, C.A., Jr., and Hendricks, C.D. Rev. Sci. Instr., 44:1527, 1972.

167. Muller, E.W. Phys. Rev., 102:618, 1976.

168. Becky, H.D., Knoppel, H., Metzinger, G., and Schulze, P. Adv. Mass Spectrom., 3:35, 1966.

169. Colby, B.N., and Evans, C.A., Jr. Anal. Chem., 46:1236, 1974.
Simons, D.S., Colby, B.N., and Evans, C.A., Jr. Int. J. Mass Spectrom. Ion Phys., 15:291, 1974.

170. Buehler, R.J., Flanigan, E., Green, L.J., and Friedman, L. J. Am. Chem. Soc., 96:3990, 1974.

171. Macfarlane, R.A., and Torgerson, D.F. Int. J. Mass Spectrom. Ion Phys., 21:81, 1976.

172. Fenn, J.B., and Deckers, J. Proceedings of the Third International Symposium on Rarefied Gas Dynamics in 1962. J.A. Laurmann, ed., Academic Press, New York, c. 1963. Vol. I, p. 497.

173. Vestal, M.L., Blakley, C.R., Ryan, P.W., and Futrell, J.H. Rev. Sci. Instr., 47:15, 1976.

174. Wells, G., Voorhees, K.J., and Futrell, J.H. Rev. Sci. Instr., submitted for publication, 1980.

175. Ensminger, Dale. Ultrasonics. Marcel-Dekker, Inc., New York, 1973. Chapters 3 and 7.

176. Heher, E. Master's Thesis, University of Wisconsin, 1967.

177. Orth, R.G., Udseth, H., and Futrell, J.H. Proceedings of the 26th Annual Conference on Mass Spectrometry and Allied Topics of the American Society for Mass Spectrometry. St. Louis, Missouri, June, 1978. p. 659.

178. Japanese Patent Agency No. SHO53-3290, Hitachi, Inc., January 12, 1978.

179. Blakley, C.R., McAdams, M.J., and Vestal, M.L. J. Chromatogr., 158:261, 1978.

180. Posthumus, M.A., Kistemaker, P.G., Meuzelaar, H.L.C., and de Brauw, M.C.T.N. Anal. Chem., 50:985, 1978.

181. Dzidic, I., Carroll, D.I., Stillwell, R.N., and Horning, E.C. Anal. Chem., 48:1763, 1976.

182. Hunt, D.F., McEwen, C.N., and Harvey, T.M. Anal. Chem., 47:1730, 1975.

183. Kambara, H., and Kanomata, I. Int. J. Mass Spectrom. Ion Phys., 24:453, 1977.

184. Engel, Avon. Ionized Gases. Oxford University Press, London, 1965.

185. Siegel, M.W., and McKeown, M. J. Chromatogr., 122:397, 1976.

186. McLaren, L., Myers, M.N., and Giddings, J.C. Science, 159:197, 1968.

187. Giddings, J.C., Myers, M.N., and King, J.W. J. Chromatogr. Sci., 7:276, 1969.

188. Bartmann, D., and Schneider, G.M. J. Chromatogr., 83:135, 1973.

189. van Wasen, U., and Schneider, G.M. Chromatographia, 8:274, 1975.

190. Jentoft, R.E., and Gouw, T.H. Anal. Chem., 48:2195, 1976.

191. Stahl, Egon, and Schilz, Winfried. Chem. Ing. Tech., 50:535, 1978.

192. Stahl, Egon, and Schilz, Winfried. Z. Anal. Chem., 280:99, 1976.

193. Stahl, Egon. J. Chromatogr., 142:15, 1977.

194. Peter, S., Brunner, G., and Riha, R. DECHEMA Monogr., 73:197, 1974.

195. Panzner, F., Ellis, S.R.M., and Bott, R.R. Inst. Chem. Eng. Symp. Ser., 54:165, 1978.

196. Calimli, Ayla, and Olcay, Aral. Holzforschung, 32:7, 1978.

197. Conaway, J.E., Graham, Jeffrey A., and Rogers, L.B. J. Chromatogr. Sci., 16:102, 1978.

198. Semonian, B.P., and Rogers, L.B. J. Chromatogr. Sci., 16:49, 1978.

199. Klesper, E., and Hartmann, W. Eur. Polym. J., 14:77, 1978.

200. Klesper, E., and Hartmann, W. J. Polym.Sci.Polym.Lett.Ed., 15:9,1977.

201. Fuzita, Kazunori, Shimokobe, Ikuo, and Nakazima, Fnmito, Nippon Kagaku Kaishi, 8:1348, 1975. (from Chem. Abst. #CA083/22/188012, 1975).

202. Karayannis, N.M., Corwin, A.H., Baker, E.W., Klesper, E., and Walter, J.A. Anal. Chem., 40:1736, 1968.

203. Karayannis, Nicholas, and Corwin, Alsoph H. Anal. Biochem., 26:34,1968.

204. Karayannis, N.M., and Corwin, A.H. J. Chromatogr. Sci., 8:251, 1970.

205. Giddings, J.C., Bowman, L.M., and Myers, M.N. Anal. Chem. 49:243, 1977.

206. DeNevers, Noel. Fluid Mechanics. Addison-Wesley Publishing Company, Reading, Massachusetts, 1970.

207. Brown, Eugene F., and Chow, W.L. Supercritical Flow through Convergent Conical Nozzles. In: Flow, Its Measurement and Control in Science and Industry; Part I, Flow Characteristics. ASME Fluids Engineering Conference, H.W. Stoll, ed., Instrument Society of America, Pittsburgh, c. 1974.

APPENDIX A

ABBREVIATED COMPILATION OF PREVIOUS DENSE GAS CHROMATOGRAPHY AND DENSE GAS EXTRACTION WORK

As discussed in Section 3.2, there are two reasons for the inclusion of this compilation in this Report. First, it provides an overview of work in the related fields of dense gas chromatography and dense gas extraction. One can see at a glance the many compound classes for which a DGC/MS instrument will have utility as an analytical tool. The second purpose was to make a working summary which would give a current listing of the dense gas/solute systems that have been studied and also the temperature and pressure ranges used with a particular combination of dense gas and solute. A more extensive compilation that has recently been updated may be found in reference 93.

The table is ordered by solvent gas. Each gas is assigned to one of three groups--inorganic, organic (C,H,O) and halogenated organic. For the inorganic group the order is alphabetic as well as according to number of atoms (e.g., CO_2, N_2O, NH_3, SF_6); for the two other groups the order is based upon the number of carbon, then hydrogen, atoms. The entries for a particular gas are arranged chronologically. Dense gas mixture entries follow the data for the pure major component. Originally the table was to include only studies in dense gas chromatography. However, it has since become apparent that work in dense gas extraction and dense binary and ternary solutions often is readily applicable to DGC. Whenever this appeared to be the case, the information is included in Table A1. In such cases, there is usually no pertinent information to be listed for chromatograph column and detector. One particularly interesting group of entries is that for dense gas extraction combined with thin layer chromatographic detection and identification. The thin layer chromatography is performed under typical atmospheric conditions after the dense gas solution has been decompressed. Hence, this application is not classified as dense gas chromatography in Table A1. Many extraction processes previously described in Section 3.1 are patented; in these cases the information was obtained from "Chemical Abstracts" and the original patent was not consulted. Often the information in the abstracts was not detailed enough to be useful to apply in the laboratory so these extractions are not included in Table A1. In many instances phase studies of dense gas mixtures were with solutes sufficiently volatile to be analyzed easily by gas chromatography, so these studies are usually not entered in Table A1. The discussion about dense gas chromatography in Section 3.2 of this Report was an overview. More references are entered in Table A1 than were cited in that section.

TABLE A1. SOME PREVIOUS WORK IN DENSE GAS CHROMATOGRAPHY AND DENSE GAS EXTRACTION

Dense gas*,+	Compounds Dissolved/Separated	Stationary Phase	Det.‡	Ref.
Carbon dioxide (CO_2)				
40°C 1-81 kg/cm²	Capacity ratio studies with n-alkanes (n = 3 to 13), toluene, n-octane, cumene, sec-butylbenzene, benzene, p-xylene, cis-decalin	25% w squalane on Sil-O-Cel	FI	(1966)
40°C 90-1350 atm	Solubility studies with	--	FI	
	Gum rubber, waxes and oils: Apiezon L, Carbowax 20M, 400, 1000, 4000; squalane; squalene; SE-30 (400,000 MW); dinonyl phthalate; DC-200			(1968)
	Purines: adenine			(1968)
	Terpenes: α,β-carotenes; lycopene			(1969)
	Amino acids; glycine			
	Nucleosides: adenosine, guanosine, uridine (all slightly soluble)			
	Corticol steroids: cortisone, hydrocortisone (both slightly soluble)			
	Sterols: cholesterol, ergosterol, lanosterol			
	Sugars: ribose, arabinose, glucose, maltose, xylose, fructose, mannose, sorbose			
	Alkanes: n-octadecane, n-docosane, n-octacosane			
	Misc.: officinilic acid, polyvinyl chloride			
	Separation of α,β-carotenes	15% Ucon	FI	(1968)

(continued)

TABLE A1 (continued)

Dense Gas$^{*,+}$	Compounds Dissolved/Separated	Stationary Phase	Det.‡	Ref.
CO_2 cont.				
33-40°C 1000-3000 psi (68-204 atm) PP	Separation of thermally unstable (at GC conditions) compounds: ferrocene, cyclopentadienyl $Mn(CO)_3$, dicyclopentadienyl $TiCl_2$ n-alkylbromides (n = 8 to 22)	Carbowax 400/ Porasil F	UV (HP)	(1972)
40°C 51-134 atm PP	Studies of temperature and pressure effects: n-alkanes (n = 5 to 22)	Carbowax 400/ Porasil C Acid alumina	FI (M)	(1972)
	Cyclic hydrocarbons: fluoranthene, phenanthrene, naphthalene, 1,3,5-trimethylbenzene, 1,4-dimethylbenzene, benzene, cyclohexane, cyclopentane,toluene, cumene, fluorene, acenaphthylene, biphenyl, tetralin, indene	Carbowax 400/ Porasil C		(1973)
	Cyclic hydrocarbons: triphenylmethane, diphenylmethane, 1,2,4,5-tetramethylbenzene, phenylacetylene, cyclohexane, cyclopentane, benzene, toluene, camphene, azulene, 1,5,9-cyclododecatriene	Oxidipropionitrile/ Porasil C		
40°C 20-150 bar PP	Capacity ratio studies with n-decane, 1-decine, trans-5-decene, n-decane, fluorene	OPN/Porasil C Carbowax 400/ Porasil C	FI	(1973)
30-70°C 30-170 bar	Capacity ratios as a function of supercritical fluid density using decane, hexadecane, eicosane, squalane	Carbowax 400/ Porasil C	FI	(1975)
33-39°C 1500-3000 psi (102-204 atm) PP	Automobile exhaust: triphenylene, chrysene, benzo(ghi)-fluoranthene, naphthacene, benz(a)anthracene, pyrene, benzo(b)fluorene, 7-methylbenz(a)anthracene, 7,12-dimethylbenz(a)anthracene, benzo(c)phenanthrene, 1-methylpyrene, 3-methylpyrene, 1,3-dimethylpyrene,	Permaphase ETH	UV	(1976)

(continued)

TABLE A1 (continued)

Dense Gas *,+	Compounds Dissolved/Separated	Stationary Phase	Det.‡	Ref.
CO_2 cont.				
	perylene, benzo(e)pyrene, benzo(a)pyrene, benzo(k)-fluoranthene			
35°C 1400-1800 psi (95-123 atm) PP	Automobile exhaust: 6-methylchrysene, naphthacene, chrysene, triphenylene, benz(a)anthracene, benzo(c)-phenanthrene, benzo(b)fluorene, 7,12-dimethylbenz(a)-anthracene, 7-methylbenz(a)anthracene, 1,3-dimethyl-pyrene, benzo(c)phenanthrene, 1-methylpyrene, 3-methylpyrene, pyrene, benzo(a)fluorene	Vydac Reverse Phase	UV	190 (1976)
40°C 0-350 atm DP	Solubility and density programming studies with decane, phenylstearate, pentadecylphenol, eicosanoic acid, hexadecane, 1,3,5-triphenylbenzene, Ethyl 330, pentacene, polystyrene 900 and 2100, diethylstilbestrol dipalmitate, eicosane, di-2-naphthyl sebaccate, 1,1-diphenylethyl-1-adamantanecarboxylate, 1,1,2-triphenyleicosanate	--	UV FI	97 (1976)
	Separation of 9,10-diphenylanthracene, benzene, naphthalene, phenanthrene, anthracene, 2,3-benzanthracene, polystyrene 600 oligomers	Carbowax 400/ Porasil C		
40°C 500-2000 bar	Solubility studies with Amino acids: glycine, phenylalanine, ℓ-tryptophan, leucine Sugars: D-glucose, D-xylose, sucrose Natural products: frangulin A, emodin, 6,7-dihydroxy-coumarin (esculetin)	--	UV	191 (1978)
40°C 70-400 bar PP	Supercritical gas/thin layer chromatography: Fat soluble dye mixture: guajazulene, azobenzene, Ceres Red, Ceres Blue, Sudan Red, indophenol	TLC (thin layer chromatography plate)	TL	192 (1976)

(continued)

TABLE A1 (continued)

Dense Gas*,+	Compounds Dissolved/Separated	Stationary Phase	Det.‡	Ref.
CO$_2$ cont.				
	Pyrone mixture: umbelliferone, flavone, coumarin Raw coffee: fatty oils, caffeine			
40°C 80–300 bar	Vitamin-oil mixture: cholesterol, vitamins D_3, K_3, and A, α-tocopherol, triglyceride, α-tocopherol acetate, steryl ester Alkaloid drug (*Strychnos nux vomica*): brucine, strychnine, fatty oils		TL	193 (1977)
40°C 70–90 bar	Caraway seed: limonene, carvone, fatty oils Sage leaves: eucalyptol, thujone, camphor Peppermint leaves: menthol, menthone Ginger root: gingerone Camomile flowers: herniarin (7-methoxycoumarin), tyrothricin, dicycloether Lemon leaves: eucalyptol, santonin Unrefined coffee: caffeine, fatty oils Pepper: piperine Chillies: capsaicine Hops flowers: humulon, lupulon Marijuana: cannabidiol, cannabinol, tetrahydroxy-cannabinol Sunflower seeds: squalene, cholesterol, fatty oils		TL	6 (1976)
40°C 70–300 bar	Solubility studies with Polyaromatics: naphthalene, phenanthrene, anthracene, pyrene, 1,2-benzanthracene, chrysene, tetracene Phenols: phenol, catechol, resorcinol, hydroquinone, pyrogallol, phloroglucinol Aromatic organic acids: benzoic, cinnamic, salicylic, anisic, veratric, 3-hydroxy-4-methoxyphenylacetic,	--	TL	(1976)

(continued)

TABLE A1 (continued)

Dense Gas *,+	Compounds Dissolved/Separated	Stationary Phase	Det.‡	Ref.
CO_2 cont.	ferulic, vanillic, coumaric, gentisic, syringic, sinapic, caffeic Anthraquinones: anthraquinone, 4-hydroxyanthraquinone, chrysophanic acid, 1,8-and 1,5-dihydroxyanthraquinone, 1,2,4-trihydroxyquinone, emodin, alizarin Pyrones: coumarin, flavone, umbelliferone, fraxetin Lipids: myristyl alcohol, cholesterol, α- and γ-distearin, triolein			
Acetone in carbon dioxide 102°C 155 bar	Variable solvent gas mixture composition for solubility studies of oleic and stearic acids	--	NS	104 (1974)
43-69% (w) Carbon tetrachloride in carbon dioxide 70-135°C 1220-1450 psig (84-100 atm)	Separation of glycerides: mono-, di- and tri-oleate (This dense gas mixture resulted in equipment corrosion.)	Distillation column (1" i.d.) packed with stainless steel KnitMesh	--	195 (1978)
36-47% (w) n-hexane in carbon dioxide 71-134°C 1120-1308 psig (77-90 atm)	Separation of glycerides: mono-, di- and tri-oleate	Distillation column (1" i.d.) packed with KnitMesh	--	195 (1978)

(continued)

TABLE A1 (continued)

Dense Gas*,+	Compounds Dissolved/Separated	Stationary Phase	Det.‡	Ref.
Ammonia (NH_3) 140°C 200 atm	Solubility studies with Gum rubber, waxes, and oils: Carbowax 4000 and 20M, squalane, squalene, OV-17 Nucleosides and nucleotides: adenosine, guanosine, uridine, adenylic acid Corticol steroids: cortisone, hydrocortisone Sterols: cholesterol, ergosterol, lanosterol Sugars: ribose, arabinose, glucose, galactose (slight), maltose, lactose, xylose, fructose, mannose, sorbose Purines: caffeine Amino acids: glycine, leucine, alanine, tryptophane, tyrosine, arginine, lysine, glycylglycine, glycyl-L-leucyl-L-tyrosine Proteins: cytochrome C Misc.: quercitin, α-glucose pentaacetate	--	FI	186 (1968) 94 (1968) 187 (1969)
	Separation of glycine, glycylglycine, glycylleucyl tyrosine	Porasil B		
Sulfur hexafluoride (SF_6) 50°C 39 atm	Threshold solubility of 600 MW polystyrene	--	UV	97 (1976)
Ethylene (C_2H_4) 20–173°C 50–300 bar	Solubility studies of oleic and stearic acids (Other dense gases were studied, but no data presented: propane, CO_2, Freon 13B1 and Freon 13.)	--	NS	194 (1974)

(continued)

TABLE A1 (continued)

Dense Gas *,+	Compounds Dissolved/Separated	Stationary Phase	Det.‡	Ref.
Ethylene mixtures 102°C 155 bar	Variable solvent gas mixture composition with acetone, methylenechloride, benzene or n-heptane in ethylene for solubility studies of oleic and stearic acids	--	NS	194 (1974)
Ethane (C_2H_6) 40°C 63-150 atm	Threshold solubilities of Ethyl 330, diethylstilbestrol dipalmitate, 2030 and 4000 MW polystyrene, hexaphenylbenzene	--	UV	97 (1976)
Acetone (C_3H_6O) 250°C 80 atm	Dense gas extraction of spruce wood followed by silicagel and gel permeation chromatography or NaOH extraction and GC/MS: o- and p-cresol, guaiacol, 4-ethylphenol, 3,4-dimethylphenol, 4-methylguaiacol, p-isopropylphenol, 4-ethylguaiacol, 6-isopropylguaiacol, eugenol, 4-n-propylguaiacol, vanillin, isoeugenol, 6-isopropenylguaiacol, coniferyl alcohol	--	--	196 (1978)
Isopropanol (C_3H_8O) 245°C 40-51 kg/cm^2	di-n-alkylphthalates (n = 2 to 16)	10% (w) polyethylene on Sil-O-Cel	UV	100,104 (1967)
	m-terphenyl, m-quinquephenyl, coronene, decacylene, 2-n-hexylnaphthalene, 2-n-dodecylnaphthalene, 2-phenylnaphthalene, 1,1'-binaphthyl, naphthalene, phenanthrene, 1,2-benzanthracene, picene, biphenyl, o- and p-terphenyl, 2,2'-binaphthyl, anthracene, pyrene, 2-naphthylhexadecyl ether, 2-naphthylpentadecyl ketone	Untreated alumina		105 (1967)

(continued)

TABLE A1(continued)

Dense Gas*,+	Compounds Dissolved/Separated	Stationary Phase	Det.‡	Ref.
Tetrahydrofuran (C_4H_8O) 290°C 80 atm	Dense gas extraction of spruce wood followed by silica-gel and gel permeation chromatography or NaOH extraction and GC/MS: o- and p-cresol, guaiacol, 4-ethylphenol, 3,4-dimethylphenol, 4-methylguaiacol, p-isopropylphenol, 4-ethylguaiacol, 6-isopropylguaiacol, eugenol, 4-n-propylguaiacol, vanillin, isoeugenol, 6-isopropenylguaiacol, coniferyl alcohol	--	--	196 (1978)
Diethyl ether ($C_4H_{10}O$) 200°C 39-50 kg/cm²	Phenols: phenol, hydroquinone, phloroglucinol, pyrogallol Oxidation/polymerization inhibitors: Topanol A, TBC, Ionol, Lubad J Quinones: anthraquinone, 1,2-benzanthraquinone, 6,13-pentacenequinone, phenanthrenequinone Pharmaceuticals and alkaloids: aspirin, phenacetin, caffeine, einchonine, brucine, Epoxy resin out to a 1478 molecular weight	Porapak Q	UV	111 (1969)
n-pentane (C_5H_{12}) 210-213°C 30-50 kg/cm²	2-n-hexylnaphthalene, 2-n-dodecylnaphthalene, di-n-alkylphthalates, dimyricyl phthalate, diphenyl phthalate, benzene, phenanthrene, 9,9'-bifluorenyl, 9-phenylanthracene, 1,2-benzpyrene, biphenyl, m-triphenyl, m-quinquephenyl, 1-dodecyl-4-octadecylbenzene, 2-phenylnaphthalene, 1,1'-and 2,2'-binaphthyl 2-naphthylpentadecylketone, 2-naphthylhexadecylether, 1-phenylhexadecenal, 1-phenyl-1-hexadecenol	23% (w) PEG 6000 on Sil-O-Cel	UV	100,104 (1967)

(continued)

TABLE A1 (continued)

Dense Gas *,+	Compounds Dissolved/Separated	Stationary Phase	Det.‡	Ref.
C_5H_{12} cont. 213°C 36-40 kg/cm²	Naphthalene, phenanthrene, anthracene, pyrene, benz(a)-anthracene, chrysene, naphthacene, perylene, picene, di-n-alkylphthalates 1,3-dimethylnaphthalene	5-10% (w) Alkathene on Sil-O-Cel 23% PEG 1000 on Sil-O-Cel	UV	100,104 cont.
200-300°C 40-50 kg/cm²	Anthracene, 1,1'-binaphthyl, pyrene, 2-phenylnaphthalene, phenanthrene, 9-phenylanthracene, 2-n-hexanaphthalene, 2-n-dodecylnaphthalene, benz(a)anthracene, picene, 1,2-benzpyrene, 3,4-benzpyrene	Untreated alumina	UV	105 (1967)
200-210°C 26-50 kg/cm²	*Alkylbenzenes (up to C_{18} chain)* Fat soluble vitamins: A_1, E_1, K_1 Steroids: benzoate esters of cholesterol and pregnenolene, propionate ester of testosterone, testosterone Organo-metal complexes: ferrocene, 1-acetylferrocene, 1,1'-diacetylferrocene	Porapak Q	UV	111 (1969)
206°C 30-36 atm PP	DC-710 polysiloxane polymer (MW 2600)	Porasil C n-C_8H_{18}/Porasil C Porapak Q Alumina	UV	103 (1975)
220°C 20-80 bar PP	Styrene oligomers (n = 1 to 40)	Porasil A	UV	82 (1977)
208-241°C 375-1700 psi (26-116 atm) PP	Polystyrene oligomers (MW 2200, 4000)	n-C_{18}/Porasil C Phenyl Bondapak CPG-10-170	SP	197 (1978)

(continued)

TABLE A1(continued)

Dense Gas*,+	Compounds Dissolved/Separated	Stationary Phase	Det.‡	Ref.
C_5H_{12} cont. 220°C 125 psi (9 atm)	Column efficiency studies with naphthalene, phenanthrene, pyrene	Porasil A	UV	198 (1978)
5% Methanol in n-pentane 205°C 600-900 psi (41-61 atm) PP	Polystyrene oligomers	n-octyl/Porasil C	UV	83 (1969)
208-214°C 570-1075 psi (39-73 atm)	Cyclic hydrocarbons: phenanthrene, fluoranthene, chrysene, 7,12-dimethylbenz(a)anthracene, benzo(a)pyrene, coronene	Alumina	UV	98 (1970)
	Polystyrene (MW 900, 2100), polyphenyl ethers (MW>522)	n-C_8H_{18}/Porasil C		
192-214°C 540 psi (37 atm)	DC-710 polysiloxane polymer	Porasil C	UV	103 (1975)
180-260°C 20-110 bar PP, TP	Styrene oligomers	Porasil A	UV	82 (1977) 199 (1978)
10% Methanol in n-pentane 220-235°C 20-330 bar PP	Styrene oligomers (MW 900, 2200, 4000)	Porasil A	UV	82,200 (1977) 199 (1978)

(continued)

TABLE A1 (continued)

Dense Gas *,+	Compounds Dissolved/Separated	Stationary Phase	Det.‡	Ref.
0-20% Isopropanol in n-C_5H_{12} 198-216°C 30-36 atm	DC-710 polysiloxane polymers	Porasil C	UV	103 (1975)
5-10% Isopropanol in n-C_5H_{12} 172-260°C 500-1300 psi (34-88 atm) PP, TP	Capacity ratio studies of polystyrene oligomers (MW 2200, 4000)	CPG-10-75 CPG-10-170 CPG-10-240 Porasil C	SP	197 (1978)
0.1-10% Cyclohexane in n-C_5H_{12} 208°C 600-1300 psi (41-88 atm) PP	Capacity ratio studies of polystyrene oligomers (MW 2200)	n-C_{18}/Porasil C	SP	197 (1978)
Hexane (C_6H_{14}) 230-259°C 18-80 kg/cm^2	Polynuclear aromatics: triphenylene, naphthalene, phenanthrene, pyrene, chrysene Coal tar: 8 unidentified compounds	Corasil (II)	NS	201 (1975)
Toluene (C_7H_8) 340°C 80 atm	Dense gas extraction of spruce wood followed by silica-gel and gel permeation chromatography or NaOH extraction and GC/MS: o- and p-cresol, guaiacol, 4-ethylphenol, 3,4-dimethylphenol, 4-methylguaiacol, p-isopropylphenol, 4-ethylguaiacol, 6-isopropylguaiacol, eugenol, 4-n-propylguaiacol, vanillin, isoeugenol, 6-isopropenylguaiacol, coniferyl alcohol	—	—	196 (1978)

(continued)

TABLE A1 (continued)

Dense Gas*,†	Compounds Dissolved/Separated	Stationary Phase	Det.‡	Ref
Fluoroform (CHF_3) 40°C 53-76 atm	Threshold solubilities of Ethyl 330, diethylstilbestrol dipalmitate, di-2-naphthyl sebaccate	--	UV	97 (1976)
Monochlorodifluoromethane ($CHClF_2$) 150-170°C 800-2300 psi (54-157 atm)	Ni etioporphyrin II, Ni mesoporphyrin IX dimethylester	33% Carbowax 20M or Harflex 370 on Chromasorb W	--	96 (1962)
Dichlorodifluoromethane (CCl_2F_2) 150-170°C 800-2300 psi (54-157 atm)	Ni etioporphyrin II, Ni mesoporphyrin IX dimethylester	33% Carbowax 20M or Harflex 370 on Chromasorb W	--	96 (1962)
130°C 925-1000 psi (63-68 atm)	Salicylaldoximates: Ni(II), Cu(II), Zn(II) Thenoyltrifluoroacetonates: Sc(III), Y(III), Eu(III), Al(III), Zr(IV), VO, Fe(III), Co(III), Ni(II), Pd(II), Cu(II), Zn(II), Th(IV), UO_2	2% Kel-F on Chromasorb W HMDS AW	SP	202 (1968)
140-153°C 1000-2700 psig (68-184 atm) PP	Porphyrins and metalloporphyrins: etioporphyrins of Cu, Ni, VO and Mg; etioporphyrin II, mesoporphyrin IX dimethyl ester, mesoporphyrin IX diethyl ester, deuteroporphyrin IX dimethyl ester, desoxophyllery-throetioporphyrin	20% XE-60 or 12% Versamid 900 + 0.2% Mg phthalocyanine or 10% Epon 1001 on Chromasorb W	SP	203 (1968)

(continued)

TABLE A1 (continued)

Dense Gas [*],[+]	Compounds Dissolved/Separated	Stationary Phase	Det.[‡]	Ref.
CCl_2F_2 cont. 115°C 950-1100 psi (65-75 atm)	Acetylacetonates which often decompose at GC temperatures: Li(I), Na(I), K(I), Be(II), Mg(II), Ca(II), Sr(II), Ba(II), Al(III), Ga(III), In(III), Tl(I), Sc(III), Y(III), La(III), Ce(III), Pr(III), Nd(III), Tb(III), TiO, $TiCl_2$, Zr(IV), VO, Cr(III), MoO_2, Mn(II,III), Fe(III), Ru(III), Co(II,III), Rh(III), Ir(III), Ni(II), Pd(II), Pt(II), Cu(II), Zn(II), Cd(II), Pb(II), Th(IV), U(IV), UO_2	10% Epon 1001 on Chromasorb W or 5% Epon 1009 on Chromasorb P AW HMDS	UV	204 (1970)
1,1-Difluoroethane ($C_2H_4F_2$) 118°C 50 atm	Threshold solubility of hexaphenylbenzene	--	UV	97 (1976)
118°C 1088 atm	Exclusion chromatography of toluene, polystyrene 600 and 4000, biphenyl, polyvinylpyrolidine, acetone	Porous silica glass	UV	205 (1977)

---

[*] Conditions: PP-pressure programming, DP-density programming, TP-temperature programming.

[+] Units: 1 atm = 1.0133 bar = 1.0332 kg/cm^2 = 14.696 psi.

[‡] Detectors: FI-flame ionization, UV-ultraviolet, SP-spectrophotometer, TL-thin layer plate, NS-not stated, HP-high pressure, M-modified.

APPENDIX B

ELECTRIC CIRCUITS DESIGNED FOR DGC/MS INSTRUMENT

Page

Figure B1. Baratron output circuit 179

Figure B2. Current detector circuit. 180

Figure B3. Typical circuit used to amplify and display thermocouple voltage as temperature (°C). 181

Figure B4. Oscilloscope drive amplifier 182

Figure B5. Heater and fan control circuits for dense gas reservoir housing 183

Figure B6. Water bath heater control 184

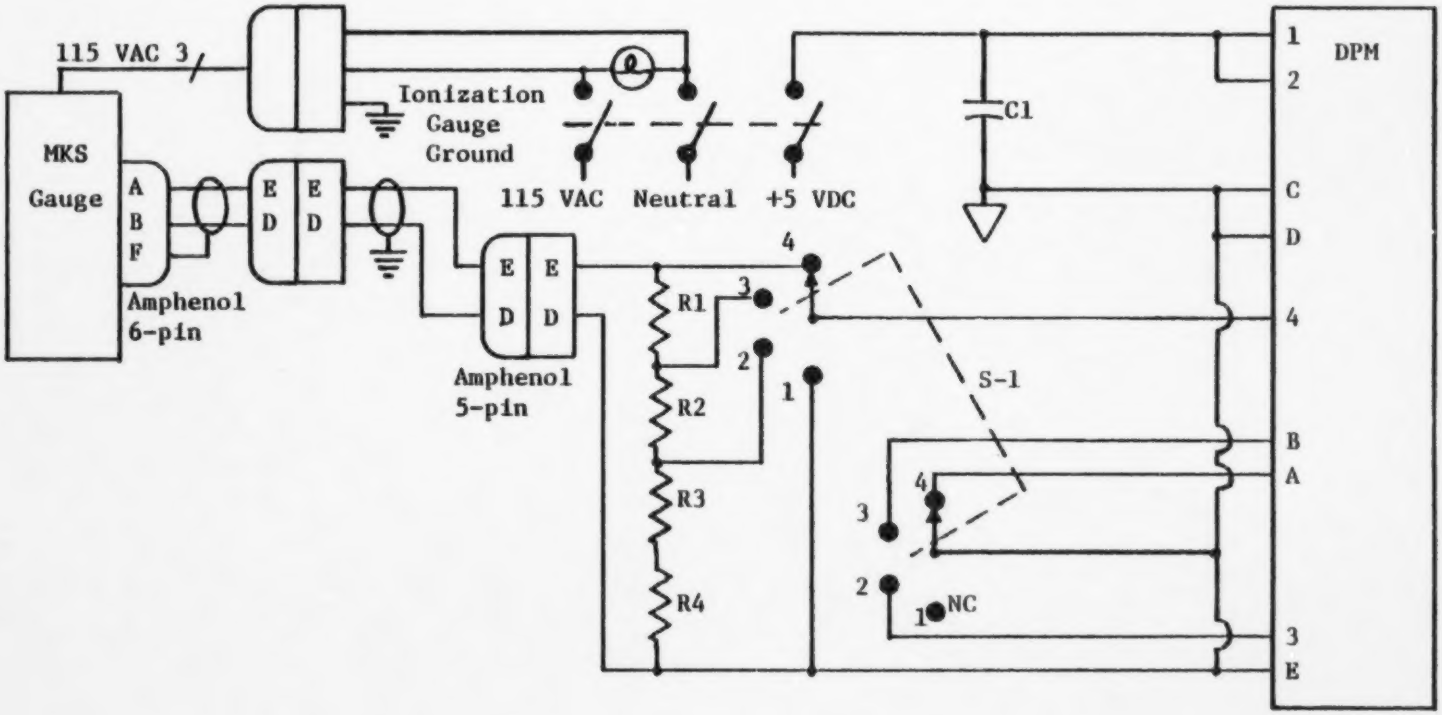
115 VAC 3
MKS
Gauge
A
B
F
Amphenol
6-pin
E
D
E
D
Ionization
Gauge
Ground
115 VAC
Neutral
+5 VDC
C1
E
D
E
D
Amphenol
5-pin
R1
R2
R3
R4
4
3
2
1
S-1
4
3
2
1
NC
DPM
1
2
C
D
4
B
A
3
E

Figure B1. Baratron output circuit.

Pressure gauge: Baratron, Type 220 from MKS Instruments, Inc.; DPM: digital panel meter, AD2026 from Analog Devices; C1: 100μf; R1: 75KΩ; R2: 7.5KΩ; R3: 825Ω; R4: 8.2Ω; S-1: 2 pole, 4 position switch.

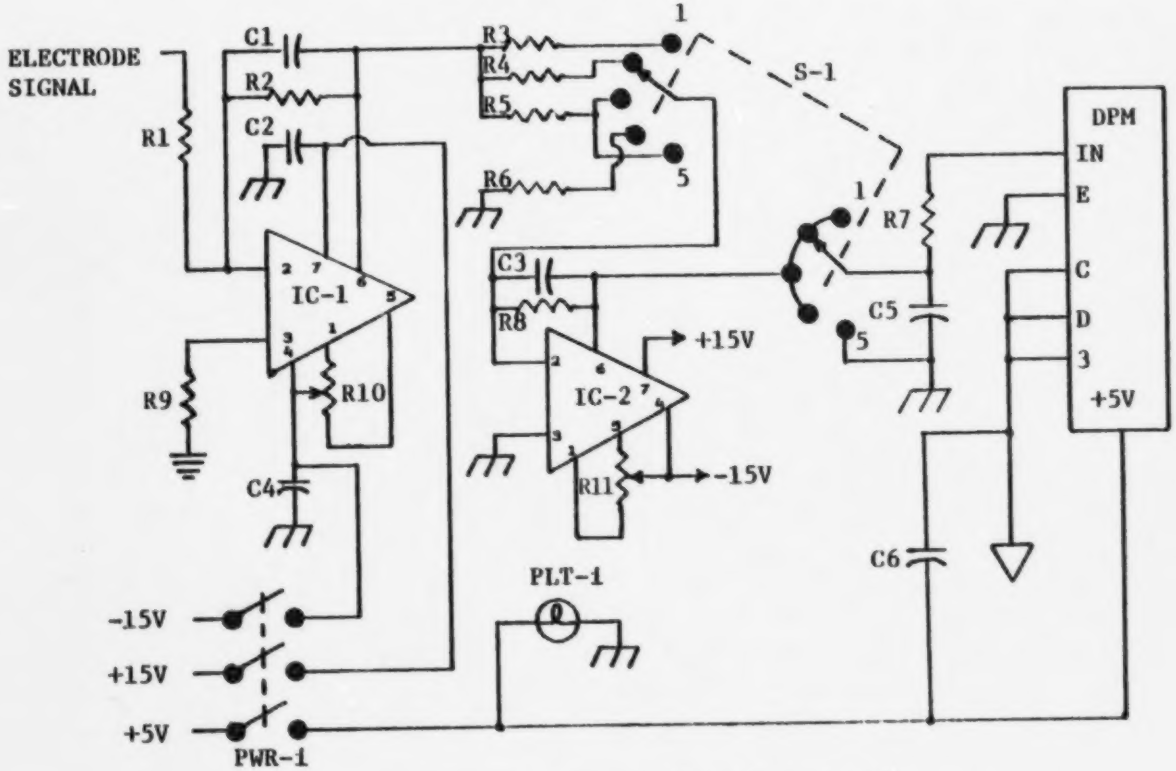
ELECTRODE SIGNAL
R1
C1
R2
C2
IC-1
R9
R10
C4
R3
R4
R5
R6
1
5
S-1
C3
R8
IC-2
+15V
-15V
R11
R7
C5
C6
DPM
IN
E
C
D
3
+5V
PLT-1
-15V
+15V
+5V
PWR-1

Figure B2. Current detector circuit.

C1: 33pf; C2,3,4: 15μf; C5: 7μf, 50V; C6: 100μf, 10V; IC-1: AD540J; IC-2: LM741; PLT-1: LED bulb; PWR-1: TPST; R1,9:1MΩ; R2: 10,000MΩ; R3,6: 1KΩ; R4,8: 10KΩ; R5: 100KΩ; R7: 27KΩ; R10,11: 20KΩ pot.; S-1: 2 pole, 5 position rotary switch; DPM: digital panel meter, AD2026 from Analog Devices.

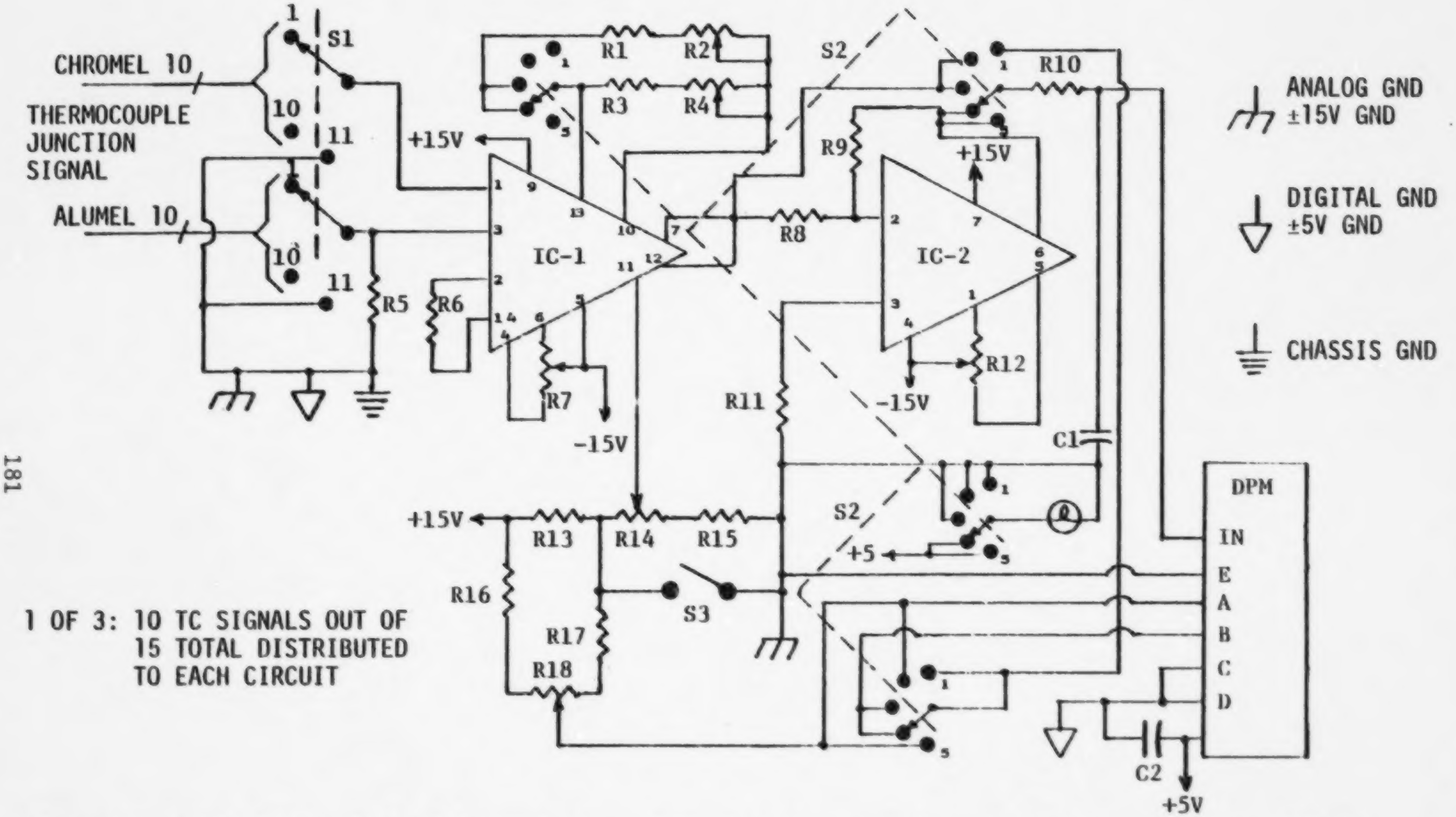
CHROMEL 10
THERMOCOUPLE JUNCTION SIGNAL
ALUMEL 10
S1
1
10
11
1
10
11
+15V
R5
R6
R7
-15V
IC-1
1
9
13
10
11
12
3
2
14
4
6
5
7
R1
R2
R3
R4
1
5
S2
R8
R9
R10
1
5
+15V
IC-2
2
7
3
4
1
6
5
R12
-15V
R11
C1
S2
1
5
+5
+15V
R13
R14
R15
R16
R17
R18
S3
1
5
DPM
IN
E
A
B
C
D
C2
+5V
ANALOG GND
±15V GND
DIGITAL GND
±5V GND
CHASSIS GND

1 OF 3: 10 TC SIGNALS OUT OF
15 TOTAL DISTRIBUTED
TO EACH CIRCUIT

Figure B3. Typical circuit used to evaluate and display thermocouple voltage as temperature (°C).

C1: 7μf, 50V; C2: 100μf, 10V; IC-1: AD521 ; IC-2: LM741; R1: 8.2KΩ; R2: 3KΩ pot; R3: 82KΩ; R4: 30KΩ pot; R5: 10MΩ; R6: 390Ω; R7,12: 10KΩ pot; R8,9,11: 10KΩ; R10: 27KΩ; R13: 68KΩ; R14: 100Ω pot; R15: 82Ω; R16: 4.7KΩ; R17: 2.7KΩ; R18: 1KΩ pot; S1: 11 position, 2 pole rotary switch; S2: 5 position, 4 pole rotary switch; S3: SPST; DPM: digital panel meter, AD2026 from Analog Devices.

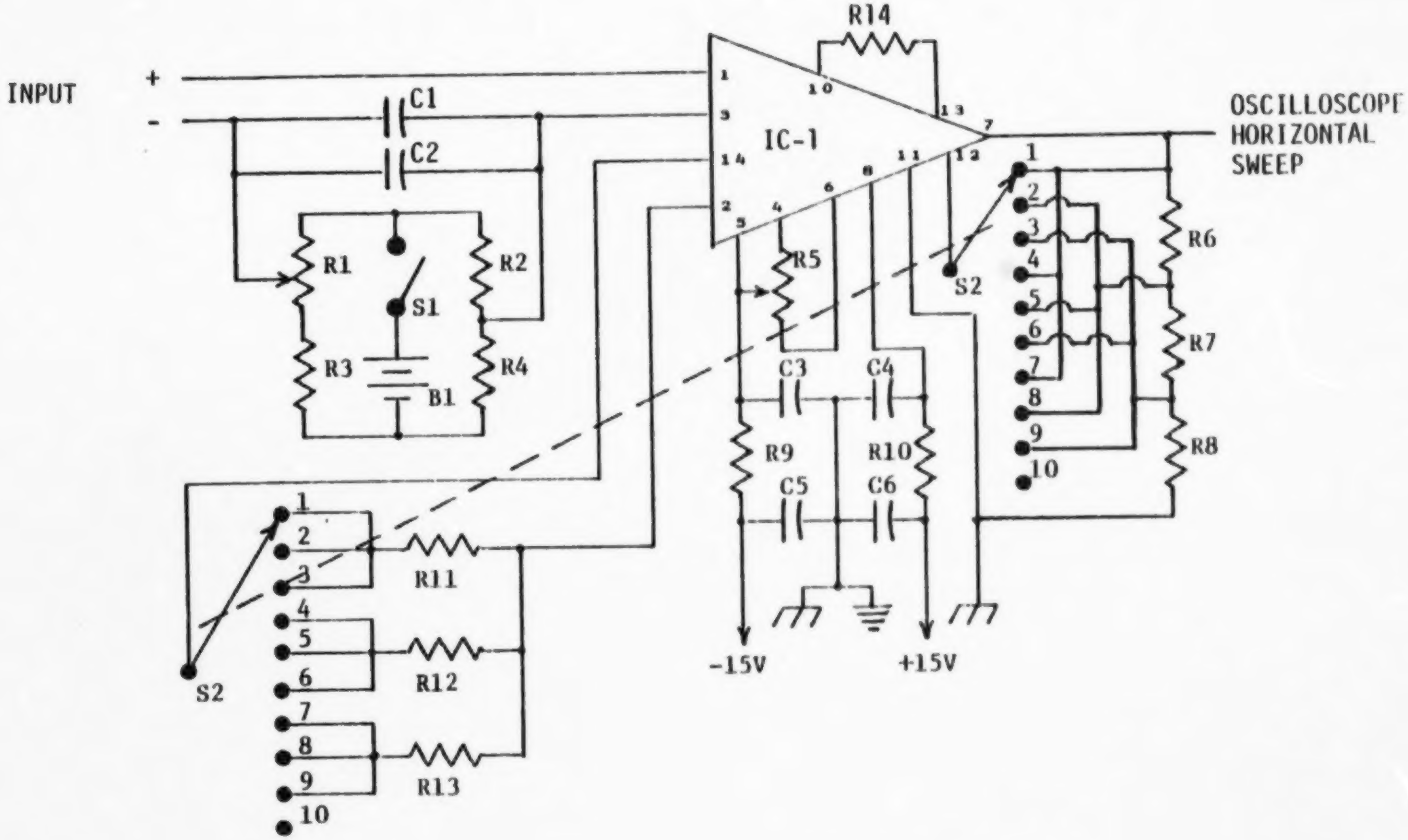
INPUT
+
-
C1
C2
R1
S1
R2
R3
B1
R4
IC-1
1
3
14
2
5
4
6
8
11
12
13
7
10
R14
R5
C3
C4
R9
R10
C5
C6
-15V
+15V
S2
OSCILLOSCOPE
HORIZONTAL
SWEEP
R6
R7
R8
1
2
3
4
5
6
7
8
9
10
R11
R12
R13

Figure B4. Oscilloscope drive amplifier.

B1: 1.5V "D" cell; C1: 0.1μf disc; C2: 20μf tantalum; C3,4: 1000pf; C5,6: 0.1μf; IC-1: AD521 from Analog Devices; R1; 5KΩ pot; R2: 390Ω; R3: 5.11KΩ; R4,12: 10KΩ; R5: 10KΩ pot; R6: 5.1KΩ; R7: 3KΩ; R8: 2KΩ; R9,10: 330Ω; R11,14: 100KΩ; R13: 1KΩ; S1: SPST; S2: 2 pole, 10 position rotary.

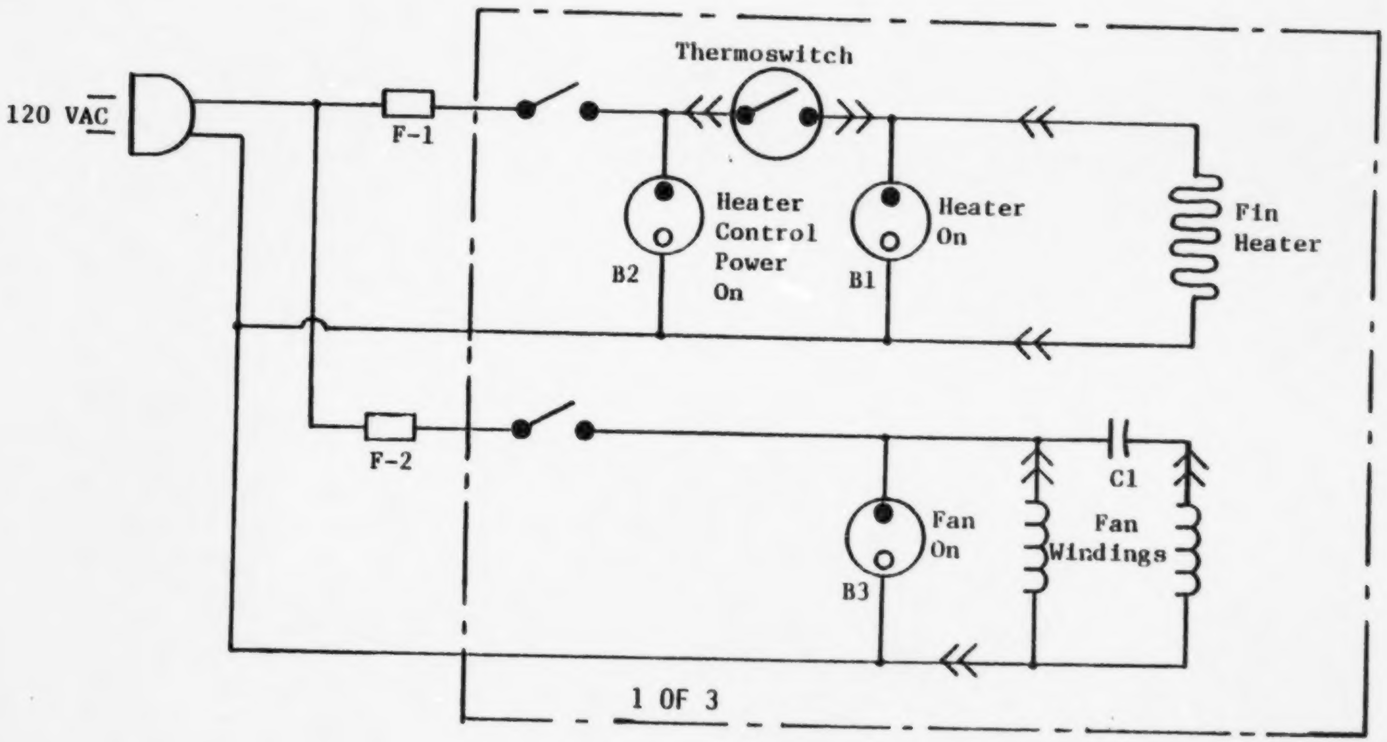
120 VAC
F-1
F-2
Thermoswitch
B2
Heater
Control
Power
On
B1
Heater
On
Fin
Heater
B3
Fan
On
C1
Fan
Windings
1 OF 3

Figure B5. Heater and fan control circuits for dense gas reservoir housing.

B1-3: Neon bulbs; F-1: 8A fuse; F-2: 5AS fuse; C1: 1μf; fin heater: 240V, 1000W (surplus item marked SEF19); fan motors: 1 phase, 115V, 3200rpm from Diehl Mfg. Co. (part # 230 0188 00); thermoswitch: Thermoswitch®- Thermostat from Fenwal, Inc., -100 to 300°F, open on temperature rise.

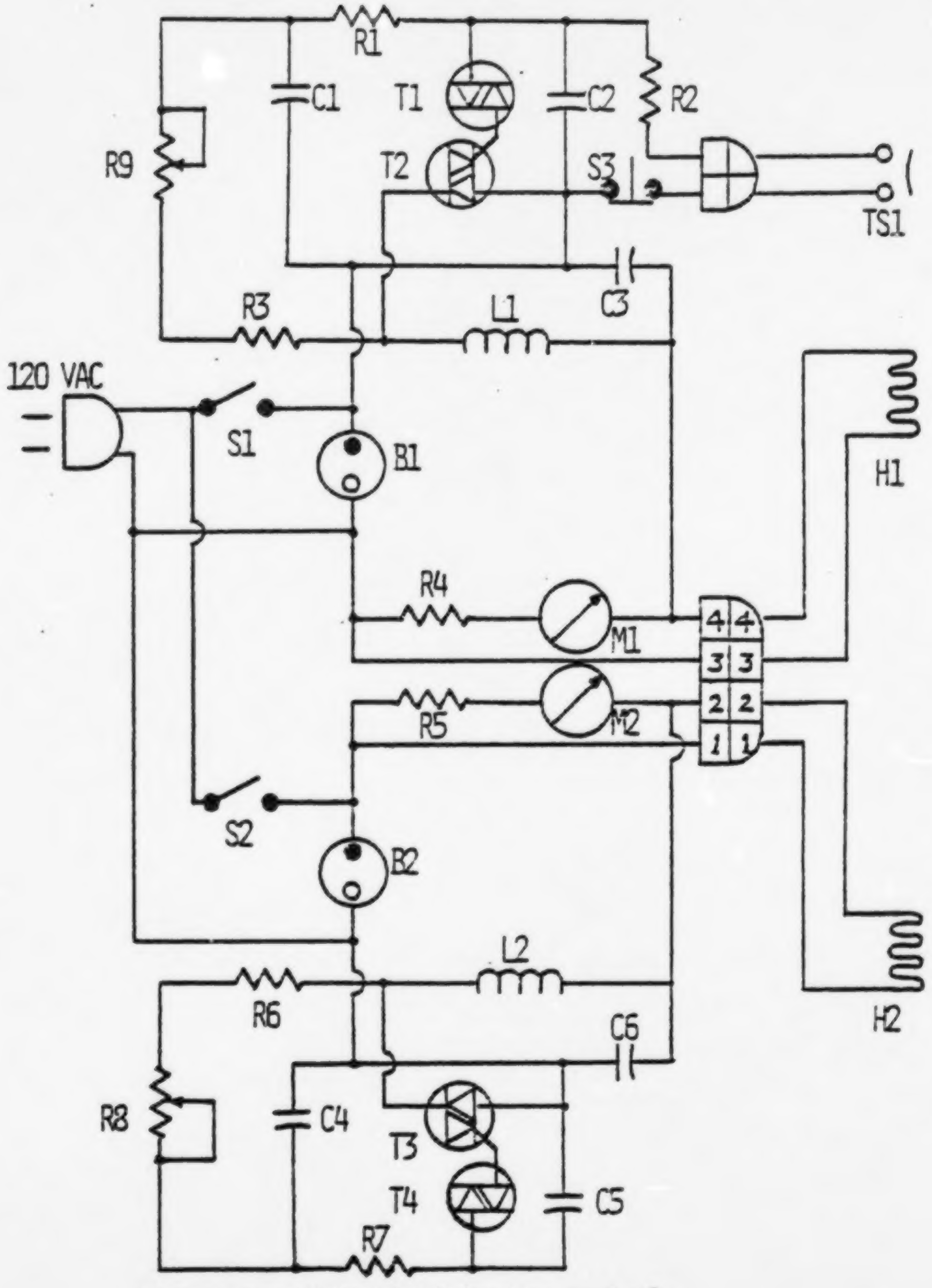
R1
C1
T1
C2
R2
R9
T2
S3
TS1
C3
R3
L1
120 VAC
S1
B1
H1
R4
M1
4 4
3 3
2 2
1 1
R5
M2
S2
B2
H2
L2
R6
C6
R8
C4
T3
T4
C5
R7

Figure B6. Water bath heater control.

B1,2: Neon bulbs; C1-6: 0.1µf; H1,2: 450 watt heaters; R1,7: 15KΩ; R2: 220Ω; R3,6: 2.2KΩ; R4,5: 120KΩ; R8,9: 100KΩ pots; S1,2: SPST; S3: Normally closed, spring return; T1,4: SK3523; T2,3: SK3508; TS1: mercury thermoswitch, closes on temp. rise; M1,2: Kurz & Root Co., FS = 1 AC mA.

APPENDIX C

CENTERING, MOUNTING, AND TESTING OF THE NOZZLE PINHOLE

One of the most difficult and also most commonly encountered operating procedures is the mounting of the laser drilled pinhole (Figure 10, Section 3.4.3) in the nozzle assembly (Figure 9, Section 3.4.3). The special punch/centering jig used for this task is shown in Figure C1. Briefly, a punch (Part 11) is used to cut out a small disk containing the pinhole and lodge it in the pinhole holder (part 5) in one clean punching motion. The pinhole holder is then clamped in place by mating nozzle assembly parts. For a successful mounting, several finish-machining steps for different parts have been found to be essential. A more detailed description of the centering/punching/mounting procedure is given below after the following subsection describing the required finish-machining.

C. 1. FINISH-MACHINING OF VARIOUS PARTS

The three parts, with important surfaces noted, that require special attention are shown in Figure C2. The end of the nozzle inlet tubing (a) which mates with the pinhole foil (see Figure 9, Section 3.4.3) must be machined to have a slight chamfer about the outer edge, a polished surface SS, and a burr-free gas exit I.D. Burrs left in the I.D. can cover the tiny pinholes after clamping. An appropriate drill bit (e.g., drill #77 or 76 for 0.51 mm I.D. tubing) will remove large metal flakes and aqua regia can be used carefully for further smoothing. At one time the entire length of tubing was clamped in a V-block so that surface SS could be polished perpendicular to the tubing axis by stroking on a flat carborundum (600 or 1000 grit) surface. The polishing procedure also removed burrs in the I.D. However, it is difficult to remove carborundum particles from within the tubing bore. More recently, Apiezon stop-cock grease has been packed in the small bore tubing ends before finish-machining (but after major machining and thorough cleaning). The grease, readily soluble in organic solvents, is removed after finish-machining and the tubing is subjected to meticulous final cleaning. The edge is chamferred on this piece for proper mating with the pinhole holder (b, Figure C2; C, Figure 9, Section 3.4.3); in some experiments a sharp, square end on the nozzle inlet tubing and a slightly tapered hole in the pinhole holder prevented clamping the pinhole foil tightly between the two parts. If the foil has been properly clamped and sealed, a polished annulus (with the inlet tubing dimensions, ~0.5 mm I.D. x ~1.5 mm O.D.) will be visible on the grained foil surface upon disassembly and inspection with a microscope.

Finish-machining of the pinhole holder is now considered. Ideally, the flat bottom hole is machined with a square end reamer so that surface S is

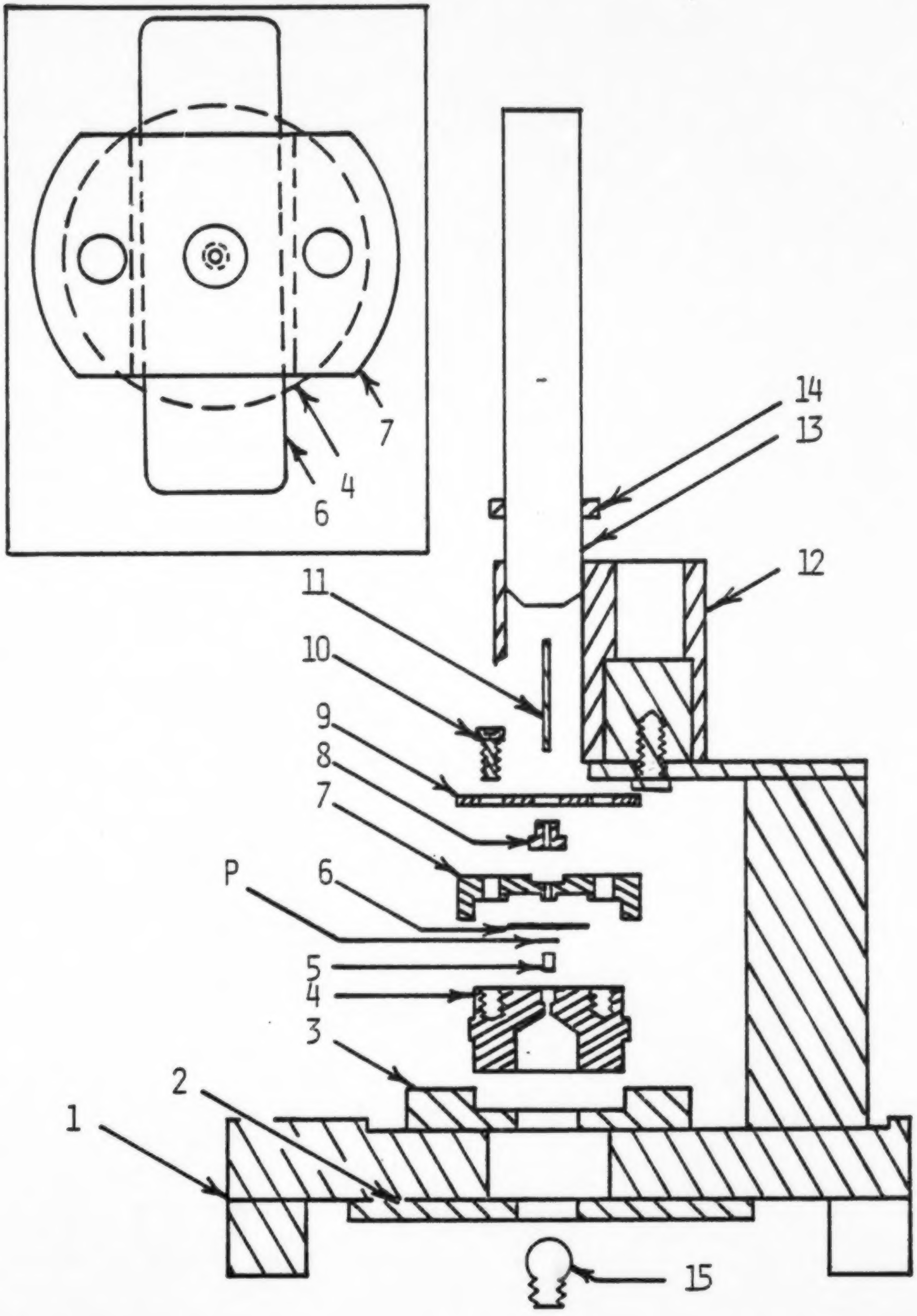
7
4
6
14
13
12
11
10
9
8
7
P
6
5
4
3
2
1
15

Figure C1. Punch/centering jig for mounting nozzle orifices.

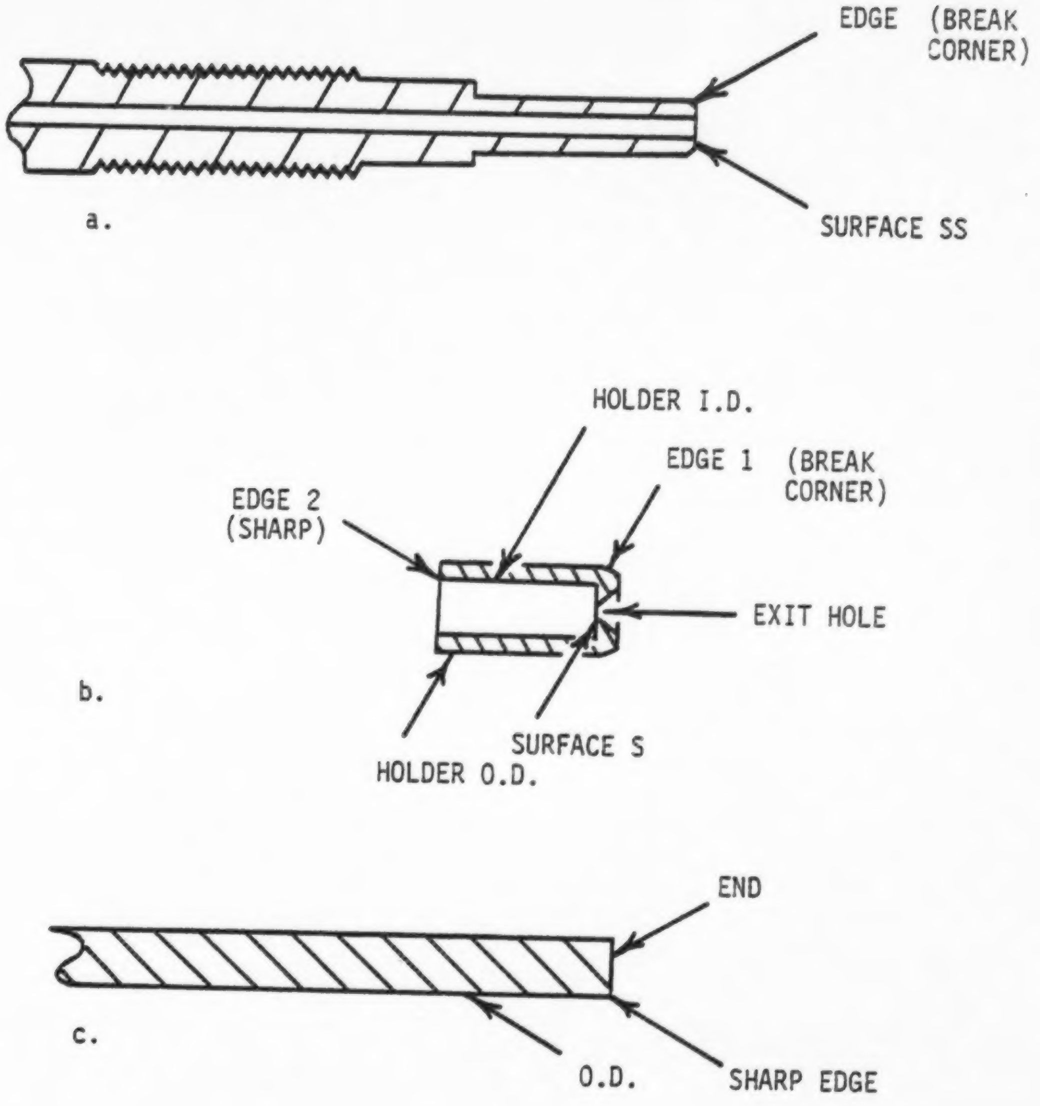
EDGE (BREAK CORNER)
SURFACE SS
a.
HOLDER I.D.
EDGE 1 (BREAK CORNER)
EDGE 2 (SHARP)
EXIT HOLE
b.
SURFACE S
HOLDER O.D.
END
c.
O.D.
SHARP EDGE

Figure C2. Parts requiring special finish-machining prior to use.

smooth and perpendicular to the hole axis. Inspection has shown that there is usually a slight taper so that surface S is conical. This imperfection must be removed by grinding with 400, 600, and 1000 grit carborundum. The grit is sprinkled into the hole and a specially prepared square-end drill bit shank is inserted. (Often the square-end of the shank wet with ethanol is touched to the grit and then inserted to avoid contaminating the hole I.D.). The shank is twisted (by hand) for several minutes to grind and polish surface S. In order to check the grinding progress the pinhole holder is rinsed with solvent, mechanically scrubbed with pipe cleaners and tight fitting twisted Kim-Wipe® tissues, dried, and inspected microscopically. A brightly reflective surface with concentric circular grain from exit hole I.D. to holder I.D. indicates the completion of grinding; otherwise, a dark ring circles the exit hole I.D. Grinding marks on the square-end of the grinding shank also indicate the grinding status. The shank may have to be ground square several times during the pinhole holder grinding. Considerable care must be taken to avoid 1) enlarging the holder I.D.--for a close fit both with the nozzle inlet tubing and, especially, with the punch (Figure C2c)-- and 2) decreasing the holder O.D.--for a close fit in the nozzle clamping piece (part D, Figure 9) and, especially, in the jig mating piece (part 4, Figure C1). It has been observed that twirling the holder between carborundum impregnated fingers about the stationary grinding shaft removes too much material from the holder O.D.

During the clean-up of surface S, the exit hole should be checked for burrs. A #80 drill bit and/or a pointed end on a wooden applicator stick (with a trace of carborundum) can be used for hole clean-up.

Edge 1 should be burr (or ridge)-free and preferably slightly chamferred for proper fit into the mating nozzle clamping piece (part D, Figure 9). It is essential to check that the holder does indeed fit squarely against the flat-bottomed exit hole surface of part D before mounting the pinhole.

For proper cutting action, edge 2 of the pinhole holder should be sharp. The holder is machined slightly too long so that after all other surfaces have been cleaned, it is placed in a special holder (snug hole of proper depth) and the extra length is ground off on a flat carborundum surface and a sharp edge 2 is produced.

Each holder should be checked before finish-machining to see that the fit of the holder with jig parts 4 and 11 is quite snug, even a small interference fit, since it is inevitable that handling in finish-machining will remove some holder material. A sloppy fit with those jig parts will make the holder useless for pinhole centering and mounting.

The final cleaning of the pinhole holder is quite important--especially since it is difficult to rinse carborundum particles off of surfaces. The usual procedure is to scrub the piece with a pipe cleaner and detergent solution, being careful not to scratch it with the pipe cleaner inner wire. After rinses with water and solvents, a Kim Wipe® tissue is twisted into a firm point and shaped to fit tightly into the flat-bottomed I.D. Turning the holder on this firm tissue shaft removes much carborundum. Fresh tissue is used until no more carborundum is removed. At times a fine syringe needle with air blowing through it has been used to scrape the corner between Surface S and the I.D. Further cleaning involves alternating between an ultrasonic bath and scouring with tissue, with the final step of a solvent rinse to eliminate any lint.

While the nozzle inlet tubing and the pinhole holder may be reassembled many times with new pinholes with no further finish-machining, they should be inspected carefully (microscopically) for deformation, burrs, and scratches before each mounting procedure. Better pinhole punching will be possible if Edge 2 of the holder is sharpened (by slight grinding) each time.

The punch shaft (c, Figure C2) should be re-ground and polished with each use. The punch shaft is a drill bit shank (1/16" D) with a squared end. (For hardness it was heated red hot and then quenched in cold water.) Before each punching it is clamped in a V-block and the end is polished so that the edge is sharp and free from nicks and the end is perpendicular to the shaft O.D. The shaft is cleaned mechanically with a soft Kim Wipe® tissue and solvent, dipped in an ultrasonic bath of ethanol, and finally inspected microscopically just before use to verify its sharp cutting edge and its clean condition (no lint, no carborundum).

C.2. CENTERING AND MOUNTING THE PINHOLE

The centering/punch jig incorporates a Bausch and Lomb microscope,* (13, Figure C1) and its modified support and clamp (12). A retaining ring (14) limits the minimum height of the microscope. A machined aluminum base (1) supports the eyepiece and the other jig components. The rest of the jig components are described in terms of their function in a typical punching procedure now presented in detail.

Screws which pass from the movable stage (3) to their tapped holes in the stage clamp (2), through (but not touching) the base (1), are loosened to permit movement. Before placing the pinhole holder die (4) in the mating ring of the stage (3), the experimenter wipes the stage, the base, and all other stationary parts with a solvent soaked tissue to remove dust. All other parts are thoroughly rinsed with solvent and placed on a lint free, clean piece of paper in such a way as to minimize contact with any surfaces. A trace of (diffusion pump) oil is applied to those surfaces of the pinhole holder die (4) which mate with the surfaces of the stage (3). Any dust or excessive oil can cock the die holder inner diameters from the punch axis. The die is placed carefully in the stage since the clearance between the parts is so small that they can be jammed in a cocked position. A small, low voltage light bulb is poked up through the stage clamp, the base, and the stage into the pinhole holder die. Taping its electrical leads (soldered directly on the bulb) to the stage clamp holds the bulb in place.

The cleaned pinhole holder is placed in its die and the die top and the cutting edge surface of the holder are inspected with the microscope for dust and/or lint. The inner cylindrical surface of the pinhole holder is inspected as the lens piece is slowly lowered to focus on the pinhole holder exit hole. The stage is moved around until the exit hole (0.0135" D, 0.343 mm D) is centered in the microscope scale (calibrated to 0.001", 0.025 mm). The three stage clamp screws are then tightened finger-tight so that the stage is firmly held in place and the exit hole centering is verified.

---

*Obtained from campus surplus stores; no model number available. Approximate magnification is 35.

The microscope is again focused on the cutting edge surface of the pinhole holder and the shim locator (6) is placed on the pinhole holder die surface about the slightly protruding O.D. of the pinhole holder. The pinhole foil (P) is placed within the shim locator I.D. with its largest I.D. up--usually the matte side vs. the shiny side. By motion of the shim locator, the pinhole is centered in the microscope scale.

The shim clamp (7), which also aligns the punch over the pinhole holder, is gently slipped into place; it rests on the shim and is recessed to permit free motion of the shim locator. Again, the clearance between this piece and the pinhole holder die (4) is minimal. Cocking of the two pieces can occur and if they are forced together the shim clamp (7) can be deformed so that the mating punch shaft guide (8) will rock on the seating surface and misdirect the punch shaft. If necessary, the pinhole is recentered using the shim locator.

Next the punch shaft guide (8), the clamping plate (9), and the clamping screws (10) are carefully put into place and the clamping screws tightened almost to finger-tightness. After a final check to insure that the point of light through the pinhole is still centered, one firmly holds the punch shaft guide between two fingers to prevent rocking and evenly tightens the clamping screws to finger tight. At this point, one should be able to wiggle the shim locator without disturbing the clamped pinhole foil.

The punch shaft (11) is slipped through the punch shaft guide (8) and the alignment piece (6) to rest on the pinhole foil. The clamped pieces (4 through 11) are removed from the stage as a unit and placed on a flat, clean surface. A light rap on the punch shaft with a small mallet cuts the center of the pinhole foil out and lodges it against the exit hole surface of the pinhole holder. Inspection of the mounted pinhole usually shows it to be centered to 0.002-0.003" (0.05 to 0.08 mm) of center; any larger deviation leads to another try with a new pinhole.

An ideal punching results in a clean-cut, securely held disk (from edges feathering) which is flat with no buckling. Most often the cut is not clean and the pinhole disk remains attached to the rest of the foil by a small tab. The disk can be broken free by repetitive bending. A drop of acetone on the punch shaft end will allow disk pick-up and placement in the pinhole holder. The resultant centering can often be as good as the 0.002 to 0.003" stated above. Another problem can be a clean-cut disk with no feathering or crimping of its O.D. Then, the disk falls out of the holder if one turns it over to inspect the centering from the exit side. However, careful handling will result in successful clamping of these loose disks. At all times, one must strive to keep the working surfaces lint-free and dust free. A combination of brass and steel tweezers is useful for handling the pinhole foils since the foil is usually slightly magnetic.

It should be noted that this jig can be used with pinhole foils of different supplied geometries. With smaller sizes, the pinholes can be moved around by using a shim locator with an appropriate center hole. However, with the 5 µm pinholes from both Ealing (supplied in a 25 mm square foil) and Optimation (0.95 cm D circle), the shim locator was dispensed with altogether. Instead scotch tape tabs were attached at the foil edges (180° from each other). These tabs extended beyond the aligning piece just as did the shim locator, so that the pinhole could be moved about. Other than the elimination of the shim locator, the punching procedure was the same as that described.

Before the punching procedure is started several milliliters of various solvents (acetone, ethanol, toluene, chloroform) are rinsed through the nozzle inlet tubing in the usual flow direction without and then with the HPLC filter units in place. Then nitrogen at about 7 atm is allowed to flow during the punching process. When it is determined that the pinhole has been properly mounted, the nitrogen flow is stopped. As soon as the flow stops at the nozzle inlet tubing tip, the pinhole holder is slipped over the nozzle inlet tubing tip. Diffusion pump oil is sparingly applied to the pinhole holder O.D. and the nozzle inlet tubing threads. Then the cleaned nozzle clamping piece (part D, Figure 9) is screwed into place and tightened using the appropriate wrenches. The clamping must be tight enough for the nozzle inlet tubing (surface SS) to seal against the soft foil; however, overtightening causes deformation of all the parts involved.

A bubble flowmeter is used to measure the volumetric flow rate through the pinhole orifice with some chosen pressure of nitrogen. If the flow rate is appropriate and no leaks are detected with a bubbling leak detector (Snoop®), the assembled parts are screwed into part E (Figure 9) of the nozzle assembly. The flow rate is again checked to make sure that no loosening of the clamped parts (held securely by set screws) occurred during the last assembling. The stainless steel surfaces of parts D and E are rinsed with solvent (avoiding the pinhole exit, through which nitrogen is still flowing) to remove any fingerprints or contamination. Then, those surfaces--particularly the cylindrical surface of part D which slips into the nozzle tip heater, threads, and the o-ring of part D are lightly coated with diffusion pump oil (for easy insertion through vacuum lock o-rings and non-galling threading). The nozzle subassembly is then ready for reassembly with the system.

C.3. TYPICAL FLOW RATES THROUGH THE NOZZLE ORIFICES IN BENCH TESTING

The flow rates measured during the work outlined in this report are summarized in Figure C3. It became standard procedure to measure the flow rate of 40 psig (3.5 atm) nitrogen into atmospheric pressure at room temperature using the same regulator to set the pressure. For all those measurements made with different gases or at different pressures or both, the equivalent nitrogen flow rates (assuming a linear volumetric flow/pressure relationship and correcting for molecular weights) are indicated in the figure legend. The most experience was with the 12.5 µm nozzle diameter where 17 measurements of flow rates were considered acceptable. The average of the 17 flow rates is 5.64 ml/min with a range of 1.52 to 10.5 ml/min. After inspection indicated that the nozzle inlet tubing on occasion may not have sealed to the pinhole foil, more care was taken to assure a seal resulting in an average for the last 12 flow rates of 5.00 ml/min with a range of 1.52 to 7.52 ml/min--the range shown in Figure C3. It is apparent from the large spread in flow rates

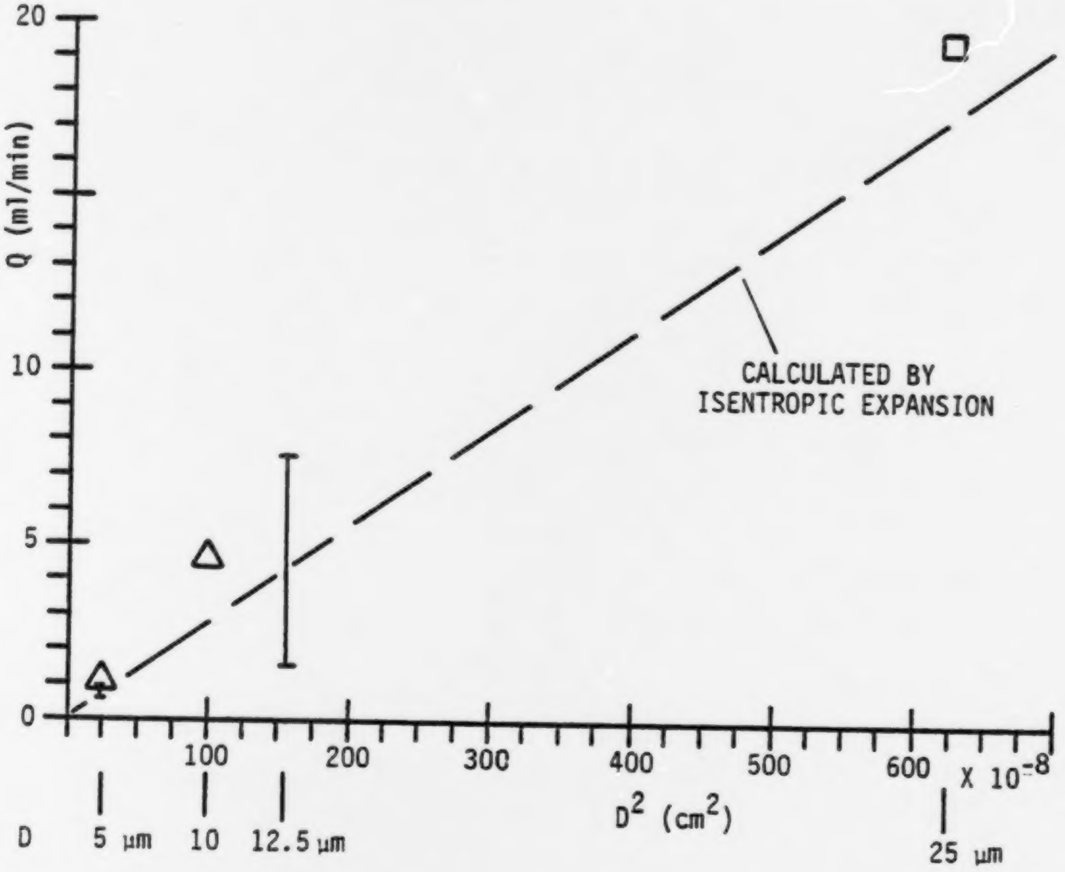

Figure C3. Volumetric flow rate (Q) vs. pinhole diameter squared (D^2) for flow equivalent to 3.5 atm N_2 expanding to 0.8 atm at ~22 °C.

△ Data obtained with equipment for the first attempt at a DGC/MS interface where the punching, mounting, and testing procedures were slightly different

□ 2.2 atm He corrected to 3.5 atm N_2

Additional data not shown on graph:
5 µm D 8.6 ml/min 57 atm CO_2 = 0.67 ml/min 3.5 atm N_2
5.4 ml/min 11 atm He = 0.65 ml/min 3.5 atm N_2
100 µm D 223 ml/min 2.8 atm N_2 = 276 ml/min 3.5 atm N_2

Dashed line indicates straight-line Q vs. D^2 behavior predicted by isentropic expansion.

that the orifice diameters and possible effects of the clamping procedure vary appreciably for the 12.5 μm pinholes; the 5 μm pinholes are stated to be more precise in diameter and the limited number of data points substantiates this.

Calculations can be made to check the order of magnitude of the measured flow rates. Two approaches will be outlined.

First, if one assumes a steady, frictionless adiabatic flow (isentropic) for a perfect gas, the following relationships hold [206] at any point (1) downstream from the stagnant reservoir condition (R):

$$\frac{P_R}{P_1} = \left(M_1^2 \frac{\gamma-1}{2} + 1\right)^{\gamma/(\gamma-1)} \quad \text{and} \quad \frac{\rho_R}{\rho_1} = \left(M_1^2 \frac{\gamma-1}{2} + 1\right)^{1/(\gamma-1)}$$

or simply, $\left(\frac{\rho_R}{\rho_1}\right) = \left(\frac{P_R}{P_1}\right)^{1/\gamma}$

where P is pressure, ρ is density, γ is the specific heat ratio, and M is the Mach number.

Under the same conditions, mass flow rate for flow through a nozzle may be obtained by calculating the flow at the nozzle throat where the velocity is sonic.[206]

$$\dot{m} = A^* P_R \cdot \left(\frac{MW \cdot \gamma}{RT_R}\right)^{\frac{1}{2}} \cdot \frac{1}{C} = A^* \cdot \rho_R \cdot \left(\frac{\gamma RT_R}{MW}\right)^{\frac{1}{2}} \cdot \frac{1}{C} = A^* \frac{v^* \rho_R}{C}$$

where $C = \left[(\gamma-1)/2 + 1\right]^{(\gamma+1)/2(\gamma-1)}$ and v^*, the sonic velocity, is $(\gamma RT_R/MW)^{\frac{1}{2}}$. Here, $\dot{m}$ is the mass flow rate, A^* is the smallest area of the nozzle throat (sonic), T is absolute temperature, MW is the molecular weight and R is the gas constant. Thus, for the experimental conditions presented above,

$P_R = 3.5$ atm or 3.55×10^3 N/m^2

$P_1 \sim 0.8$ atm

$P_R/P_1 = 4.4$

$\gamma = 1.4$

$R = 8.314 \times 10^3$ J/kmol K or 0.081 ℓ atm/mol K

$T_R = 295$°K

$MW = 28$ g/mol

and

$$\left(\frac{\rho_R}{\rho_1}\right) = \left(\frac{P_R}{P_1}\right)^{1/1.4} = 2.9$$

Then, from the perfect gas law

$$\rho_1 = \rho_R \cdot \frac{1}{2.9} = \frac{P_R \cdot MW}{RT_R} \cdot \frac{1}{2.9} = 1.4 \text{ g/ℓ}$$

Substitution into the expression for $\dot{m}$ yields

$$\dot{m} = \left[80 \text{ g/sec cm}^2\right]\left[A^*\right].$$

The mass flow is the same at all points in the flow (steady flow); the volumetric flow rate, Q_1, is

$$Q_1 = \frac{\dot{m}}{\rho_1} = \frac{\pi}{4} \frac{v^* \rho_R}{C \rho_1} D^2 = \frac{\pi}{4} \frac{v^*}{C} \left(\frac{P_R}{P_1}\right)^{1/\gamma} D^2 ,$$

where D is the nozzle throat diameter.

At point 1, where $P_1 = 0.8$ atm (laboratory atmospheric pressure)

$$Q_1 = 2.8 \times 10^6 D^2 \text{ ml/min} \qquad \text{(D in cm).}$$

The values of D for different nozzle orifices can be substituted.

The second approach to obtaining a rough estimate relies upon the assumptions of sonic velocity and reservoir density at the throat, constant mass flow, and a directly proportional density/pressure relationship.* Let A be the cross-sectional area of the flow and v be the flow velocity assumed constant over the cross section.

Then $$\dot{m} = \rho A v = \text{constant}$$

and $$\rho^* A^* v^* = \rho_1 A_1 v_1 = \rho_1 Q_1$$

(* - nozzle throat
$_1$ - point 1 where $P_1 = 0.8$ atm as before)

$$Q_1 = \frac{\rho^*}{\rho_1} (A^* v^*)$$

Assuming $\dfrac{\rho^*}{\rho_1} = \dfrac{\rho_R}{\rho_1} = \dfrac{P_R}{P_1}$, $\rho^*/\rho_1 = 4.4$.

The sonic velocity $v^* = \left(\dfrac{\gamma RT}{MW}\right)^{\frac{1}{2}} = 3.5 \times 10^4$ cm/sec for $T = 295°K$
$\gamma = 1.4$
$MW = 28$ g/mole

Combining the above, $Q_1 = 7.3 \times 10^6 D^2$ where D is the nozzle diameter (cm) and Q_1 is the volumetric flow rate in ml/min. Table C1 compares the two calculated values with the average experimental values for each of the nozzle diameters used.

TABLE C-1. EXPERIMENTAL AND CALCULATED FLOW RATES FOR SEVERAL NOZZLE DIAMETERS. (For $P_R = 3.5$ atm, $P_1 = 0.8$ atm, $T = 295°K$, and nitrogen)

D(μm)	Q_1 Experimental (ml/min)	Q_1 Isentropic flow (ml/min)	Q_1 Non-isentropic flow (ml/min)
5	0.73*	0.67	1.8
10	4.6	2.7	7.3
12.5	5 to 5.6	4.1	11
25	19.5†	17	45
100	276†	270	730

*Excludes value from first DGC/MS interface attempt.
†Approximated as discussed in the text

---

*Then the density/pressure relationship used is isothermal, but the calculation in general is not. Slow flows over long distances are isothermal, with the result that most gas flows are adiabatic--particularly here with such a fast expansion.

The calculated flow rates do indicate that the measured flow rates were reasonable. While the close agreement with the isentropic values may be fortuitous considering the various approximations made to obtain flow rates equivalent to 3.5 atm nitrogen flow, most of the flow rates measured with the 5 and 12.5 µm orifices were at the stated conditions. As noted in Figure C3, the straight dashed line is at the theoretical slope given by the equation derived on the basis of isentropic expansion, $Q_1 = 2.8 \times 10^6 D^2$ ml/min. This line is in reasonable agreement with the measured values, while the slope given by the second approach, $Q_1 = 7.3 \times 10^6 D^2$ ml/min, is clearly too large.

While the experimental points do have a large spread, their closeness to the calculated slope (isentropic expansion) indicates that the discharge coefficient (actual flow divided by theoretical flow) must be close to unity instead of the lower values expected for a flat plate orifice ($C_D \sim 0.55$ for the free molecular flow treatment[114] and $C_D \sim 0.85$ for invisid supercritical flows[207]). This large value may arise from the shape of the pinhole actually approximating a converging nozzle.

For one of the 12.5 µm pinholes, flow rates were measured at various pressures of nitrogen up to 74 atm (gauge) with a bubble flow meter. The data are presented in Figure C4 where the first three points (∇) represent bench measurements of the nozzle subassembly and the HPLC filters (2 µm/0.5 µm/0.5 µm) and all the rest (o) include flow through the DGC system at room temperature including the 50 cm Permaphase ODS column with no precolumn and the glass-bead packed sample chamber. Here, the volumetric flow rate is given in ml/min.

Figure C5 presents volumetric flow rates* (ℓ/min) as a function of gauge pressure for nitrogen flow through the DGC system (with the same column and sample chamber just described) without the nozzle subassembly. At a gauge pressure of 20 atm the flow without the nozzle orifice is ~3.4 times as high as that with it. This small ratio of flow rates appears inconsistent with the low column pressure drop plotted in Figure 37 and the lack of effect of the column on the flow shown in Figure C4, with all measurements on the same column. However, the effect of adding the nozzle to the column outlet is to increase the column outlet pressure and so decrease the mean volumetric flow

---

*The high flow rates (Δ) were measured by a Fisher and Porter flowmeter (2-F-1/4-25-5/36), factory calibrated for nitrogen flow at 0.85 atm and 26.7°C. The meter readings were not corrected since those conditions are essentially laboratory conditions. The lower flow rates were measured with a Dwyer flowmeter calibrated at unknown conditions. The meter had been obtained from military surplus and is identified only by model #592 and serial #J--numbers too old to be meaningful to the manufacturer. If one assumes that the meter was calibrated at a temperature and pressure close to our laboratory conditions using helium, the only correction necessary is the molecular weight factor. Multiplying the assumed helium flows by the factor 0.38 produces the graphed values (o) shown in Figure C5. The curve sections appear to be well-matched and the general appearance of the curve appears appropriate for flow through a packed column over a large pressure range.

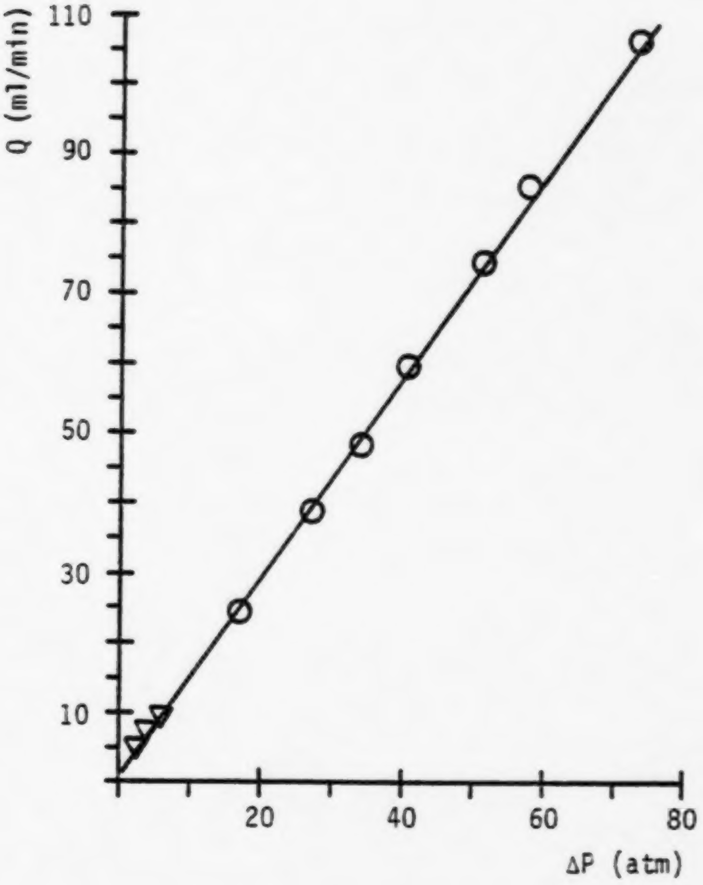

Figure C4. Volumetric flow rate (Q) vs. gauge pressure (ΔP) for N_2 flow through a typical 12.5 μm nozzle diameter.

Flow rates were measured with a bubble flow meter at ∿ 22 °C.

▽ Flow through HPLC filters and nozzle orifice only

○ Flow through DGC system including Permaphase ODS column (1.5 mm I.D. X 50 cm long, no precolumn) and glass-bead packed sample chamber in addition to HPLC filters and nozzle orifice

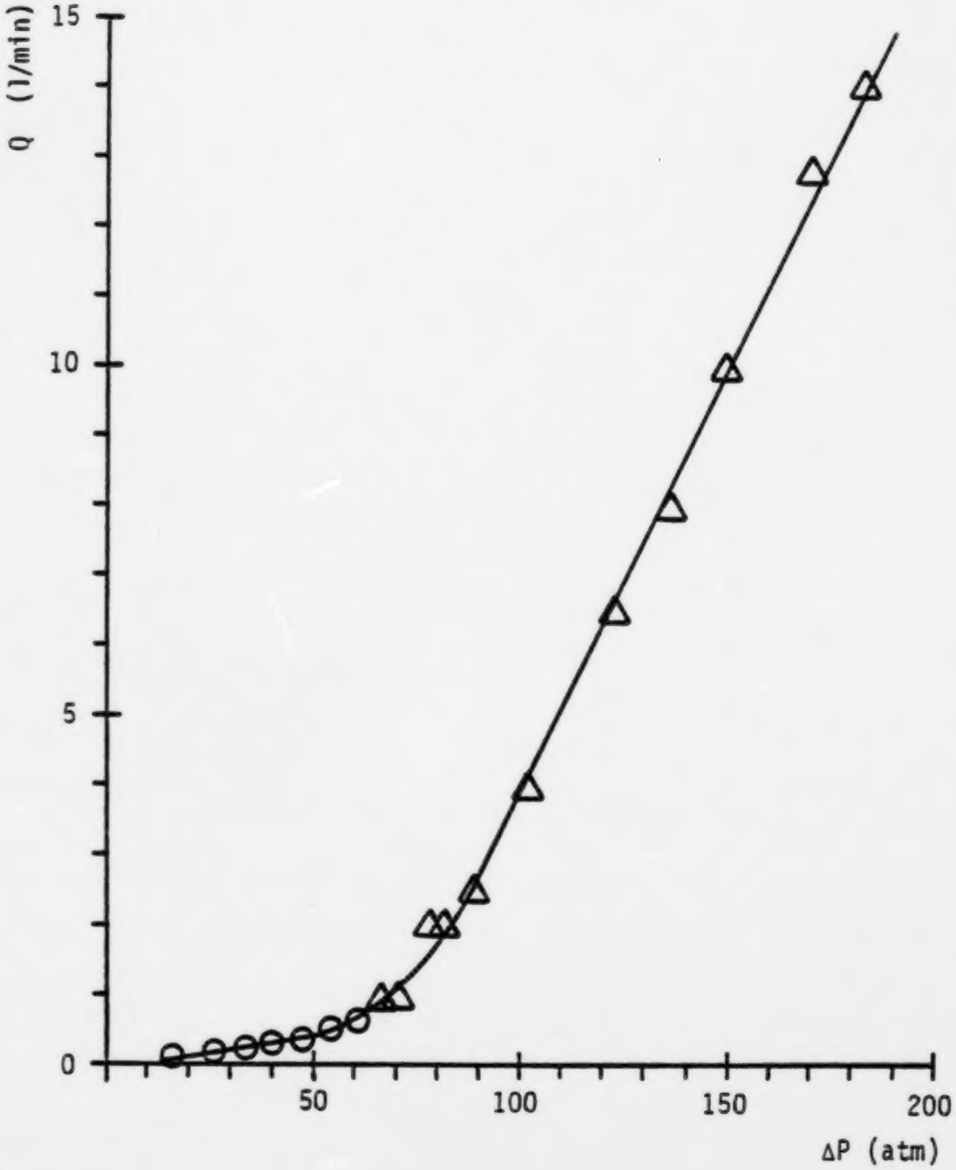

Figure C5. Volumetric flow rate (Q) vs. gauge pressure (ΔP) for N_2 flow through DGC system including Permaphase ODS column (1.5 mm I.D. X 50 cm long, no precolumn) and glass-bead packed sample chamber without the nozzle sub-assembly.

Temperature ~ 22 °C

△ Fisher and Porter flow meter

○ Dwyer flow meter (corrected)

rate at a given mass flow through the column, so that the ratio of ΔP at the nozzle to ΔP across the column is much greater than 3.4.